Netherlands Enterprise Agency

Wind Resource Assessment

IJmuiden Ver Wind Farm Zone

>> *Sustainable. Agricultural. Innovative. International.*

Netherlands Enterprise Agency

RVO Approval for Publication

Document Characteristics

Version	Title	Date of Publication	Reference Contractor	Reference RVO
1.0	Wind Resource Assessment IJmuiden Ver Wind Farm Zone	November 27th, 2023	11827690	WOZ2220015

Approval

Approval for public disclosure	Position
Daniëlle Gerritsma	Project Manager RVO Offshore Wind Energy
Matté Brijder	Programme Manager RVO Offshore Wind Energy

IJmuiden Ver Wind Farm Zone

Wind Resource Assessment

Report
Project No WOZ2220015

27 November 2023

Prepared for Rijksdienst voor Ondernemend Nederland (RVO)

The expert in **WATER ENVIRONMENTS**

IJmuiden Ver Wind Farm Zones

Wind Resource Assessment

Report
Project No WOZ2220015

Prepared for: Rijksdienst voor Ondernemend Nederland (RVO)
Represented by Mr Frank van Erp and Ms Daniëlle Gerritsma

Approved by
X Approved by

Contact person: Okan Sargin, okan.sargin@owcltd.com, +49 (0) 171 6598163
Project Manager: Ameya Sathe
Quality Supervisor: Jorge Garza from C2Wind
Author: Anna Pulo (lead author) and Okan Sargin (lead author) from OWC
Wolfgang Schlez from ProPlanEn,
Mark Stoelinga from ArcVera Renewables
Mateo Pimoult from INNOSEA

Project No.: 11827690
Approved by: Okan Sargin
Approval date: 27.11.2023
Revision: Final 1.0
Classification: **Public**

File name: O-HH-R10-0211-R001-REVE IJmuiden Ver WRA

Contents

Figures

Tables

Appendices

Acronyms

The table below lists acronyms commonly used in wind resource assessments. OWC notes that some of the acronyms listed below might not be included in this report.

Acronym	Description
AEP	Annual Energy Production
AR6	Sixth Assessment Report
BMWK	Bundesamt für Wirtschaft und Klimaschutz (Federal Ministry for Economic Affairs and Climate Action)
BSH	Bundesamt für Seeschifffahrt und Hydrographie (German Federal Maritime and Hydrographic Agency)
CDF	Cumulative distribution function
CDS	Climate Data Store
CFD	Computational Fluid Dynamics
CMIP	Coupled Model Intercomparison Project
CORDEX	Coordinated Regional Climate Downscaling Experiment
DE	Distribution Error, result of Kolmogorov-Smirnov test
DMI	Danish Meteorological Institute
DOWA	Dutch Offshore Wind Atlas
E	East
ECMWF	European Center for Medium-Range Weather Forecasts
EP	Error percentage
EPSG	European Petroleum Survey Group Geodesy
ERA5	ECMWF Reanalysis 5th Generation
ESD	Empirical statistical downscaling
ESGF	Earth System Grid Federation
ETRS	European Terrestrial Reference System
FINO	Forschungsplattformen in Nord- und Ostsee (Research Platforms in the North Sea and Baltic Sea)
FLS	Floating Lidar System
GCM	Global Climate Model
GERICS	Climate Service Center Germany
HKN	Hollandse Kust Noord
HKW	Hollandse Kust West
HKZ	Hollandse Kust Zuid

Acronym	Description
HSL	Horizontal scanning lidar
IEA	International Energy Agency
IEC	International Electrotechnical Commission
IJV	IJmuiden Ver
IPCC	The Intergovernmental Panel on Climate Change
IPSL	Institute Pierre Simon Laplace
KNMI	Koninklijk Nederlands Meteorologisch Instituut (Royal Netherlands Meteorological Institute)
KNW	KNMI North Sea Wind
KPI	Key Performance Indicator
K-S	Kolmogorov-Smirnov
LAM	Limited area model
LAT	Lowest astronomical tide
LLS	Linear least squares
LOS	Line of sight
LT	Long-term
M	Number of modelled/observed events
MBE	Mean bias error
MCP	Measure correlate predict
MEASNET	Measuring Network of Wind Energy Institutes
MERRA-2	Modern Era Retrospective Reanalysis (version 2)
Met	Meteorological
MLE	Maximum likelihood estimation
MM	Meteorological mast / met mast
MMIJ	Met mast IJmuiden
MRE	Marine Renewable Energies
MSL	Mean sea level
N	North
NASA	National Aeronautics and Space Administration
NCEP	National Center for Environmental Prediction
O_k	Observed values
OP	Overlap percentage
OT	Operation time of wind turbine generator

Acronym	Description
OWC	OWC and partners (ArcVera Renewables, ProPlanEn GmbH, Innosea)
OWEZ	Offshore windpark Egmond aan Zee
P	Percentiles
PDF	Probability density function
P_k	Projected values
Pre-FEED	Preliminary Front-End Engineering Design
RCM	Regional Climate Model
RCP	Representative Concentration Pathway
RMSE	Root mean square error
RSD	Remote Sensing Device
RVO	Rijksdienst voor Ondernemend Nederland
σ	Standard deviation
S	South
SMHI	Swedish Meteorological and Hydrological Institute
σ_n	Normalized standard deviation
SRTM	Shuttle Radar Topography Mission
SSL	Sea surface levelling
ST	Short-term
TG6	Technical Guideline Part 6, published by FGW
TLS	Total least squares
TNW	Ten noorden van de Waddeneilanden
TS	Time series
V	Wind speed
W	West
WAsP	Wind Atlas Analysis and Application Program
WCRP	World Climate Research Programme
WD	Wind direction
WFS	Wind farm site
WFZ	Wind farm zone
WPD	Wind power density
WRA	Wind resource assessment
WRF	Weather Research & Forecasting Model
WS	Wind speed

Acronym	Description
WTG	Wind turbine generator
YK	Yule-Kendall skewness measure
YSU	Yonsei University

Executive Summary

Introduction

The IJVWFZ Consortium (the Consortium) has performed a wind resource assessment for the IJmuiden Ver Wind Farm Zone (IJVWFZ, Project). The Consortium is led by DHI and consists of DHI, OWC and C2 Wind Aps. OWC, together with its partners ProPlanEn, ArcVera and Innosea, has been responsible for the development of the wind resource assessment and mesoscale modelling presented in this report. OWC together with its partners is hereforth referred to as 'OWC'.

The IJVWFZ has been designated by RVO as an area for wind energy development. The Project site is located in the Dutch Exclusive Economic Zone on the Dutch shelf in the North Sea. It lies approximately 62 km from the west mainland coast of the Netherlands. Within the IJVWFZ, RVO has identified three wind farm sites (WFS) for development, labelled as IJV Alpha WFS, IJV Beta WFS and IJV Gamma WFS. Exact information on the location and shape of the Project sites can be found through the online portal of RVO called 'Development of Offshore Wind Farms in the Netherlands'.

The aim of the study was to assess the wind resource at the IJVWFZ which may inform future development in offshore wind in the wind farm zone (WFZ). As part of this scope, the development of a mesoscale model was also requested by RVO at the proposal stage to address the imperative need to streamline and harmonize analysis processes for offshore wind sites. The challenge was to create a unified, gridded wind dataset capable of satisfying the requirements of both wind resource assessment and metocean analysis. By achieving this integration, OWC established a pre-aligned state with respect to the input wind dataset, enabling a unified approach towards the above-mentioned ultimate goal. The mesoscale model was labelled as Unified-WRF.

Wind measurements

In this wind resource assessment study, measured data from various offshore locations in the Dutch and German North Sea were thoroughly reviewed. Out of the 14 datasets considered, they were classified as either primary or secondary, based on factors such as their proximity to the Project sites, the integrity of the measurement campaign, and the duration of the measurements. The primary datasets, sourced both on-site and off-site within the Dutch North Sea, are distinctly representative of the project area. These datasets have been determined as suitable for making long-term corrections and carrying out an uncertainty analysis. They acted as the principal reference in discerning the long-term climate patterns within the IJVWFZ and in understanding the inherent uncertainties. On the other hand, secondary datasets, which were obtained from distant off-site locations in both the Dutch and German North Sea, primarily facilitated the development and validation of the mesoscale model designed for this study, together with the primary datasets.

Datasets gathered from four (4) locations have been considered as primary in this assessment. A total of five (5) measured datasets were considered, two of which were co-located. The datasets consisted of: two on-site floating lidar systems, labelled collectively as FLS IJV, a co-located pair of an on-site offshore met mast and vertical profiling lidar, labelled respectively as MM IJmuiden and lidar IJmuiden, two off-site FLS at the Hollandse Kust West WFZ, labelled collectively as FLS HKW and lastly a vertical profiling lidar located on an offshore platform, labelled as lidar K13-A. Each of these datasets was gathered by third parties and underwent a screening and post-processing. OWC has analysed these datasets and found them to be of very good quality.

Long-term climate calculation

The FLS IJV, MM IJmuiden, FLS HKW and lidar K13-A were considered suitable to correct to the long-term at the height of 160 m. The two FLS IJV datasets and two FLS HKW datasets were respectively aggregated to form a singular dataset at each of these locations. The data from MM IJmuiden and lidar K13-A were adjusted vertically to a height of 160 m using the observed wind shear coefficients. The four datasets were corrected to the long-term by means of a measure-correlate-predict (MCP) procedure. This was done by applying the ERA5 reanalysis data over a period of 13 years, from 01

January 2010 to 31 December 2022. The long-term wind speeds at the height of 160 m were found to be 10.12 m/s, 10.17 m/s, 9.89 m/s and 10.12 m/s at FLS IJV, MM IJmuiden, FLS HKW and lidar K13-A, respectively. The long-term prevailing wind direction is in the southwest for all these locations.

Unified-WRF model development and spatial analysis

The development of the Unified-WRF model was undertaken by ArcVera as part of the wind resource package consortium (OWC, ArcVera, ProPlanEn and Innosea) under the coordination of OWC and involved the creation of a bespoke mesoscale dataset utilizing the Weather Research and Forecasting (WRF) model, referred to as Unified-WRF within this report.

A primary goal of the Unified-WRF dataset was to serve as a wind input for both the met-ocean and energy yield analyses, with particular attention to surface (10-m height) extreme wind conditions for the met-ocean analysis, and to long-term hub-height wind statistics for the energy yield analysis. Note that extreme wind conditions are reported in the metocean assessment but that the entire WRF methodology, including extreme conditions, is discussed in this assessment report.

The model was driven by initial and boundary conditions sourced from the ERA5 reanalysis, developed for the entire Dutch North Sea, with the overarching goal of assessing wind potential across the IJVWFZ region. The process was initiated with a pre-configuration test of the raw WRF model, which was subsequently refined through the integration of several high-quality datasets. These enhancements were made to align the model more closely with short-term on-site measurements and the DOWA dataset. Crucially, a major aspect of this development involved the correction of biases in point measurements, an imperative task for model evaluation. This bias correction process consisted of two phases: the initial phase focused on aligning the model with in-situ measurements from 12 specific sites within a 1.7 km domain. For wind speed, a 12-month by 24-hour bias correction matrix was constructed, complemented by wind direction adjustments by sector. These corrections were then spatially averaged across the entire grid using an inverse distance weighting approach. In regions with fewer nearby measurement sites, notably the northwest quadrant, the Dutch Offshore Wind Atlas played a pivotal role as a secondary source for bias correction, enhancing the overall accuracy of the model.

Spatial analysis of Unified-WRF

The spatial analysis assessed the performance of the Unified-WRF model specifically for wind resource assessment purposes. The spatial analysis was conducted to gain insight into two specific criteria: to inspect how well the Unified-WRF model performs in comparison to other mesoscale model datasets and to verify that it is able to represent the long-term climate across IJVWFZ appropriately. These investigations were achieved in two main parts.

Firstly, by comparing the Unified-WRF with other mesoscale models over the short-term measurement period of each primary dataset. Concurrent datasets of the primary measured datasets and modelled data from nodes closest to each respective measurement location were applied. Based on these assessments the Unified-WRF model was found to have comparable or better performance than that exhibited by other mesoscale modelled datasets. These results give confidence that the Unified-WRF model is an excellent choice to represent the short-term climate at each primary location.

Secondly by verifying that the Unified-WRF long-term climate output over a select long-term period is in agreement with the long-term climates derived from the MCP procedure. The results over the long-term period verified that the Unified-WRF model is in excellent agreement with the MCP long-term climates and is able to represent the long-term climate at the observed locations for the selected long-term period. This established that the Unified-WRF model is able to represent the long-term climate across the IJVWFZ appropriately and with high associated confidence.

IJVWFZ long-term climate

Based on the Unified-WRF model selected long-term period the long-term climate was observed across the IJVWFZ and at five (5) specified nodal locations. The long-term wind speed at the height of 160 m ranges between 10.08 m/s and 10.20 m/s across the IJVWFZ. The lower wind speeds are observed in the southeast and east of the WFZ with higher wind speeds in the west and northwest area. The

IJVWFZ has a southwest prevailing wind direction. The final wind gradient map across IJVWFZ at the height of 160 m is presented in Figure 0.1 below.

Climate change assessment

A climate change assessment was also conducted for the IJVWFZ, focusing on the FLS IJV location, by utilising seven climate projections from the Climate Downscaling Experiment (CORDEX) research project, both the Representative Concentration Pathway (RCP) 4.5 and RCP8.5 scenarios were evaluated. RCP 4.5 envisions controlled global warming by mid-century through mitigation, while RCP8.5 represents a “business-as-usual” trajectory with potential significant temperature rises by the end of the century.

The results indicate reductions in wind speed and annual energy yield generation over various future periods, with the RCP8.5 scenario forecasting more substantial declines compared to the RCP4.5 scenario. The overall uncertainty in wind speed to the climate change was found to be 0.2% in wind speed for the near-term scenarios. No bias correction was applied to the Unified-WRF’s final long-term climates from the climate change analysis. This is considered outwith the scope of this analysis, and the reader is expected to evaluate and adapt any changes as necessary.

Uncertainty assessment

In the uncertainty assessment conducted for IJVWFZ, several elements were meticulously evaluated, including uncertainties in wind speed measurement, vertical extrapolation, historical wind resource, spatial variation, and implications of climate change. Data from four distinct wind resource assessments were integrated, with both dependent and independent uncertainties combined using inverse variance and distance weighting methodologies. It should be noted that the independent uncertainties included variations in the measured wind speed, vertical extrapolation, and the MCP method. On the other hand, dependent uncertainties were associated with long-term resource representation, horizontal extrapolation, and climate change evaluations. Within the assessed dependent parameters, only horizontal variations underwent combination utilizing a distance-weighting mechanism. For the remaining parameters, weighting was deemed non-applicable since they were postulated to remain consistent across each discrete WRA location.

The combined total uncertainties in the long-term wind speed at the example of N1_Alpha1 location were found to be 2.1% for the historic period, 2.7% for the 10-year projection, and 2.3% for the 25-year projection.

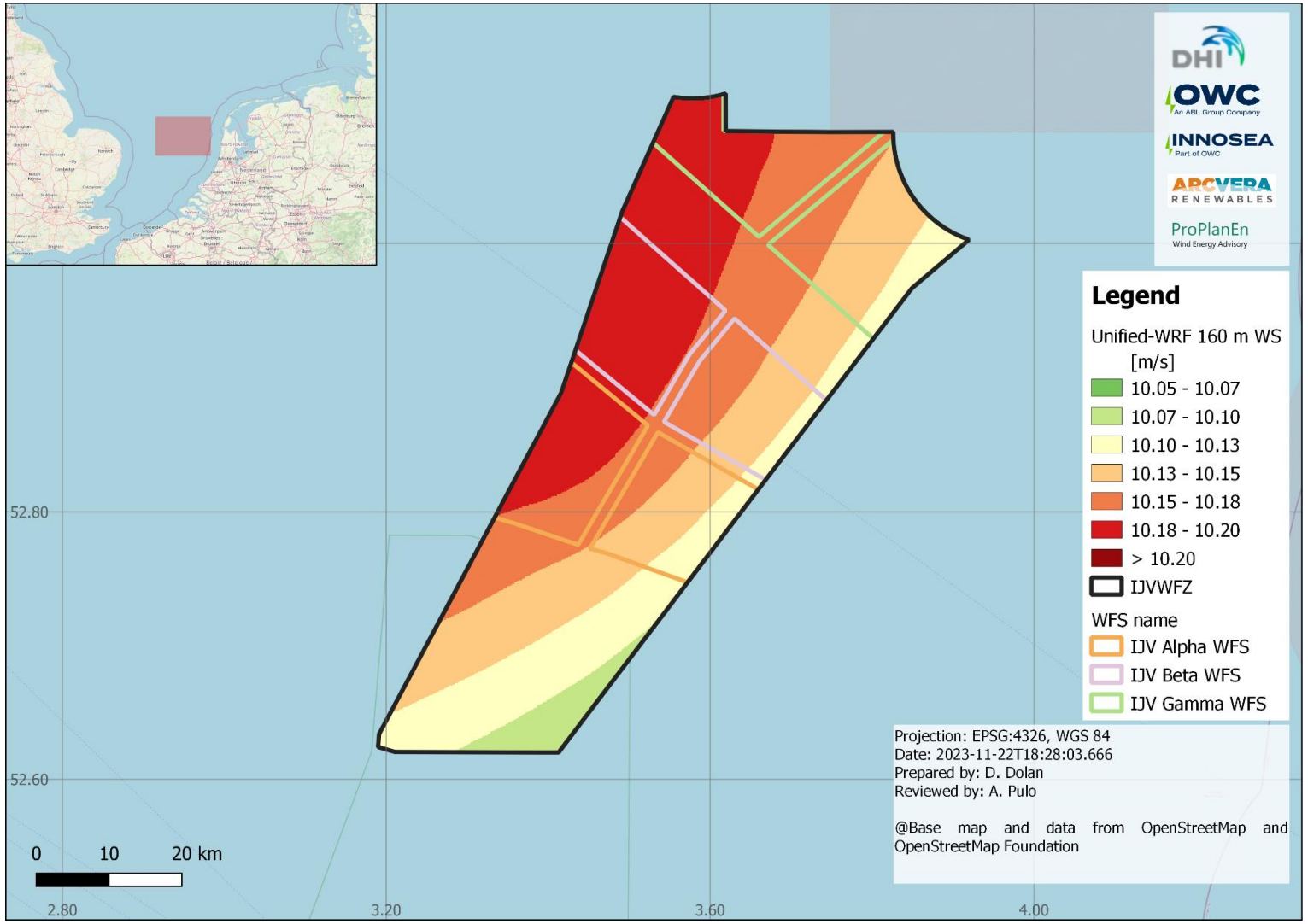

Figure 0.1 IJVWFZ wind speed gradient map at 160 m

Samenvatting

Inleiding

Het IJVWFZ Consortium (het Consortium) heeft een wind resource assessment (WRA) uitgevoerd voor het windenergiegebied IJmuiden Ver (IJVWFZ, Project). Het Consortium wordt geleid door DHI en bestaat uit DHI, OWC en C2 Wind Aps. OWC is, samen met haar partners ProPlanEn, ArcVera en Innosea, verantwoordelijk voor de ontwikkeling van de wind resource assessment en mesoschaalmodellering die in dit rapport worden gepresenteerd. OWC en haar partners worden hierna 'OWC' genoemd.

De IJVWFZ is door RVO aangewezen als gebied voor de ontwikkeling van windenergie. De projectlocatie bevindt zich in de Nederlandse Exclusieve Economische Zone op het Nederlands Continentaal Plat in de Noordzee. IJVWFZ ligt ongeveer 62 km van de westkust van het vasteland van Nederland. Binnen de IJVWFZ heeft RVO drie windparklocaties (WFS) geselecteerd voor ontwikkeling, aangeduid als IJV Alpha WFS, IJV Beta WFS en IJV Gamma WFS. Exacte informatie over de locatie en vorm van de projectlocaties is te vinden via het online portaal van RVO genaamd 'Ontwikkeling van Offshore Windparken in Nederland'.

Het doel van de studie is om toekomstige projectontwikkelaars voldoende informatie aan te bieden over de windklimatologie van IJVWFZ. Als onderdeel van dit onderzoek heeft RVO ook uitgevraagd om een mesoschaalmodel te ontwikkelen om te voorzien in de behoefte om analyseprocessen voor offshore windlocaties te stroomlijnen en te harmoniseren. De uitdaging was om een uniforme en fijnmazige winddataset te creëren die kan voldoen aan de eisen van zowel de wind resource assessment als de metocean assessment. Door beide assessments te integreren creëerde OWC met deze winddataset een gedeelde basis voor beide studies, wat een uniforme benadering van het bovengenoemde einddoel mogelijk maakt. Het mesoschaalmodel draagt de naam Unified-WRF.

Windmetingen

In deze WRA zijn de meetgegevens van verschillende offshore locaties in de Nederlandse en Duitse Noordzee grondig onderzocht. De 14 onderzochte datasets zijn geclassificeerd als primair of secundair, gebaseerd op factoren zoals de nabijheid tot de projectlocaties, de volledigheid van de meetcampagne en de duur van de metingen. De primaire datasets, die zowel binnen als buiten de Nederlandse Noordzee zijn verzameld, zijn duidelijk representatief voor het projectgebied. Deze datasets zijn geschikt bevonden voor het maken van langetermijncorrecties en het uitvoeren van een onzekerheidsanalyse. Ze dienen als belangrijkste referentie voor het onderscheiden van de klimaatpatronen op de lange termijn binnen het IJVWFZ en voor het in kaart brengen van de inherente onzekerheden van de voorgestelde aanpak. Aan de andere kant hebben secundaire datasets, die zijn verkregen van verafgelegen locaties in zowel de Nederlandse als de Duitse Noordzee, voornamelijk bijgedragen aan de ontwikkeling en validatie van het mesoschaalmodel dat voor deze studie is ontworpen, samen met de primaire datasets.

Op vier (4) locaties zijn datasets verzameld die in deze studie als primaire datasets beschouwd worden beschouwd. In totaal zijn vijf (5) datasets gebruikt, waarvan twee op dezelfde locatie hebben gemeten. De datasets bestaan uit: twee on-site drijvende lidars (FLS), gezamenlijk aangeduid als FLS IJV, een co-located paar van een on-site offshore meetmast en verticale profiling lidar, aangeduid als MM IJmuiden respectievelijk lidar IJmuiden, twee off-site drijvende lidars op de Hollandse Kust West WFZ, gezamenlijk aangeduid als FLS HKW en tot slot een verticale profiling lidar op een offshore platform, aangeduid als lidar K13-A. Elk van deze datasets is opgesteld door derden en onderging een screening en post-processing. OWC heeft deze datasets geanalyseerd en vond ze van zeer goede kwaliteit.

Correctie windklimaat naar lange termijn

De FLS IJV, MM IJmuiden, FLS HKW en lidar K13-A, op de hoogte van 160 m, zijn geschikt bevonden voor de correctie naar de lange termijn. De twee FLS IJV datasets en twee FLS HKW datasets werden respectievelijk samengevoegd tot een enkelvoudige dataset op elk van deze locaties. De gegevens van

MM IJmuiden en lidar K13-A werden verticaal gecorrigeerd naar een hoogte van 160 m met behulp van de waargenomen windscheringscoëfficiënten. De vier datasets werden gecorrigeerd naar de lange termijn door middel van een measure-correlate-predict (MCP) procedure. Dit werd gedaan door het ERA5 reanalysis-model toe te passen over een periode van 13 jaar, van 01 januari 2010 tot en met 31 december 2022. De windsnelheden op de lange termijn op 160 m hoogte zijn 10,12 m/s, 10,17 m/s, 9,89 m/s en 10,12 m/s te zijn bij FLS IJV, MM IJmuiden, FLS HKW respectievelijk lidar K13-A. Al deze locaties hebben zuidwesten als overheersende windrichting.

Unified-WRF modelontwikkeling en ruimtelijke analyse

De ontwikkeling van het Unified-WRF model werd uitgevoerd door ArcVera als onderdeel van het wind resource consortium (OWC, ArcVera, ProPlanEn en Innosea) onder coördinatie van OWC en omvatte de creatie van een op maat gemaakte mesoschaaldataset met behulp van het Weather Research and Forecasting (WRF) model, waarnaar in dit rapport wordt verwezen als Unified-WRF.

Het primaire doel van de Unified-WRF dataset is om te dienen als windinvoer voor zowel de metocean als de energieopbrengst analyses, met bijzondere aandacht voor extreme windcondities nabij het zee-oppervlak (10 m hoogte) voor de metocean assessment, en voor langetermijn-windstatistieken op ashoogte voor energieopbrengstanalyses. N.B.: de extreme windcondities die worden gerapporteerd in de metocean assessment. De gehele WRF-methodologie, inclusief extreme omstandigheden, wordt eveneens behandeld in deze studie.

Het model wordt gedreven op begin- en randvoorwaarden afkomstig van de ERA5-reanalysis, ontwikkeld voor de gehele Nederlandse Noordzee, met als overkoepelend doel het windpotentieel in de hele IJVWFZ-regio te beoordelen. De ontwikkeling van dit model is gestart met een preconfiguratietest van het ruwe WRF-model, dat vervolgens werd verfijnd door de integratie van verschillende datasets van hoge kwaliteit. Verbeteringen zijn aangebracht om het model beter af te stemmen op lokale kortetermijnmetingen en de DOWA-dataset. Cruciaal bij deze ontwikkeling was de biascorrectie in puntmetingen, een essentiële taak voor de modelevaluatie. Dit biascorrectieproces bestond uit twee fasen: Fase 1 was gericht op het afstemmen van het model op in-situ metingen van 12 specifieke locaties binnen een domein van 1,7 km. Voor de windsnelheid is een biascorrectiematrix van 12 maanden per 24 uur opgesteld, aangevuld met windrichtingcorrecties per sector. Deze correcties werden vervolgens ruimtelijk gemiddeld over het hele raster met behulp van een inverse afstandsweging. In regio's met minder nabijgelegen meetlocaties, met name het noordwestelijke kwadrant, speelde de Dutch Offshore Wind Atlas een centrale rol als secundaire bron voor biascorrectie, waardoor de algehele nauwkeurigheid van het model werd verbeterd.

Ruimtelijke analyse van Unified-WRF

De ruimtelijke analyse beoordeelde de prestaties van het Unified-WRF-model specifiek voor de beoordeling van windbronnen. De ruimtelijke analyse is uitgevoerd om inzicht te krijgen in twee specifieke criteria: inspecteren hoe goed het Unified-WRF-model presteert vergeleken met andere datasets van mesoschaalmodellen en controleren of het in staat is om het langetermijnklimaat in IJVWFZ goed weer te geven. Deze onderzoeken werden uitgevoerd in twee hoofdonderdelen.

Ten eerste is de Unified-WRF te vergelijken met andere mesoschaalmodellen over de korte meetperiode van elke primaire dataset. Er werden gelijktijdige datasets van de primaire gemeten datasets en gemodelleerde gegevens van knooppunten die het dichtst bij elke respectieve meetlocatie lagen, toegepast. Op basis van deze beoordelingen bleek dat het Unified-WRF-model vergelijkbare of betere prestaties levert dan andere mesoschaalmodellen. Deze resultaten geven aan dat het Unified-WRF-model een uitstekende keuze is om het kortetermijnklimaat op elke primaire locatie weer te geven.

Ten tweede is gecontroleerd of de uitvoer van het Unified-WRF langetermijnklimaat over een geselecteerde langetermijnperiode overeenkomt met de langetermijnklimaten die zijn afgeleid van de MCP-procedure. De resultaten over de langetermijnperiode gaven aan dat het Unified-WRF model uitstekend overeenkomt met de MCP langetermijnklimaten en in staat is het langetermijnklimaat op de waargenomen locaties voor de geselecteerde langetermijnperiode weer te geven. Hieruit bleek dat het

Unified-WRF-model in staat is om het langetermijnklimaat in de hele IJVWFZ goed en met een hoge betrouwbaarheid weer te geven.

Langetermijnklimaat IJVWFZ

Op basis van de geselecteerde langetermijnperiode van het Unified-WRF-model is het langetermijnklimaat bepaald in het hele IJVWFZ en op vijf (5) gespecificeerde knooppuntlocaties. De langetermijngemiddelde windsnelheid op 160 m hoogte varieert tussen 10,08 m/s en 10,20 m/s over de hele IJVWFZ. De lagere windsnelheden worden waargenomen in het zuidoosten en oosten van de WFZ met hogere windsnelheden in het westen en noordwesten. De IJVWFZ heeft een zuidwestelijke overheersende windrichting. De uiteindelijke windgradiëntkaart over IJVWFZ op 160 m hoogte wordt weergegeven in Figuur 0.1 hieronder.

Beoordeling klimaatverandering

Als onderdeel van de studie zijn de effecten van klimaatverandering op FLS IJV-locatie in IJVWFZ nader beschouwd. Hierbij is gebruik gemaakt van zeven klimaatprojecties van het Climate Downscaling Experiment (CORDEX) onderzoeksproject, waarbij zowel het Representative Concentration Pathway (RCP) 4.5 als het RCP8.5 scenario zijn beschouwd. RCP 4.5 gaat uit van een beheerste opwarming van de aarde halverwege deze eeuw door middel van mitigerende klimaatmaatregelen, terwijl RCP8.5 staat voor een ‘business-as-usual’ traject met mogelijk aanzienlijke temperatuurstijgingen tegen het einde van de eeuw.

De resultaten wijzen op een afname van de windsnelheid en de jaarlijkse energieproductie in verschillende toekomstprojecties, waarbij het RCP8.5-scenario een grotere afname voorspelt dan het RCP4.5-scenario. De totale onzekerheid in de windsnelheid ten gevolge van de klimaatverandering 0,2% te bedragen voor de scenario's voor de nabije toekomst. Er is geen biascorrectie toegepast op de uiteindelijke langetermijnklimaten van de Unified-WRF op basis van de analyse van de klimaatverandering. Dit valt buiten het bestek van deze analyse, van de lezer wordt verwacht dat hij eventuele wijzigingen evalueert en aanpast indien nodig.

Beoordeling van onzekerheid

In de onzekerheidsbeoordeling voor IJVWFZ zijn de onzekerheden van alle elementen van de WRA bepaald, waaronder onzekerheden in windsnelheidsmetingen, verticale extrapolatie, historische windgegevens, ruimtelijke variatie en de effecten van klimaatverandering. De data van vier verschillende WRA’s zijn geïntegreerd in één overkoepelende WRA, waarbij zowel afhankelijke als onafhankelijke onzekerheden zijn gecombineerd met behulp van de ‘inverse variantie-weegmethode’. De onafhankelijke onzekerheden omvatten met name variaties in de gemeten windsnelheid, verticale extrapolatie en de MCP-methode. De afhankelijke onzekerheden hebben betrekking op de weergave het langetermijnwindklimaat, horizontale extrapolatie en de effecten van klimaatverandering. Binnen de beoordeelde afhankelijke parameters zijn alleen horizontale variaties gecombineerd met behulp van een afstandweging. Voor de overige parameters werd weging niet van toepassing geacht, omdat ze verondersteld werden consistent te blijven voor elke afzonderlijke WRA-locatie.

De gecombineerde totale onzekerheid in de langetermijngemiddelde windsnelheid op de N1_Alpha1-locatie is bepaald op 2,1% voor de historische periode, 2,7% voor de 10-jaarsprognose en 2,3% voor de 25-jaarsprognose.

1 Introduction

IJVWFZ Consortium

This study has been developed by the IJVWFZ Consortium (the Consortium). The Consortium is led by DHI and consists of DHI, OWC and C2 Wind Aps. OWC, together with its partners ProPlanEn, ArcVera and Innosea, has been responsible for the development of the wind resource assessment and mesoscale modelling presented in this report. OWC together with its partners is hereforth referred to as 'OWC'. Information regarding OWC and Partners is provided in Appendix A.

The Dutch government has developed a Routekaart Wind op Zee, which sets out the development of offshore wind energy up to a total capacity of approximately 21 GW by 2030, enough to supply 8.5% of all the energy in the Netherlands.

The Ministry of Economic Affairs and Climate has assigned the IJmuiden Ver (IJV) Wind Farm Zone (WFZ, together IJVWFZ, Project sites) as a designated wind farm area. The Project site is located in the Dutch Exclusive Economic Zone on the Dutch shelf in the North Sea. It lies approximately 62 km from the west mainland coast of the Netherlands.

Within the IJVWFZ, RVO has identified three wind farm sites (WFS) for development, labelled as IJV Alpha WFS, IJV Beta WFS and IJV Gamma WFS. Exact information on the location and shape of the Project sites can be found through the online portal of RVO called 'Development of Offshore Wind Farms in the Netherlands'. The location of the Project sites relative to the Netherlands is presented in Figure 1.1.

RVO plays a central role in the tendering process for Dutch Offshore Wind Farm Zones. Preliminary investigations are carried out for suitable sites, and their results are published as part of the tendering process. As part of the bid calculation, the bidder needs as detailed information as possible to estimate the wind climate in the area. This wind resource assessment (WRA) study aims to provide the input required for the bidder to use in its preliminary front-end engineering design (Pre-FEED) as well as the corresponding energy yield prediction.

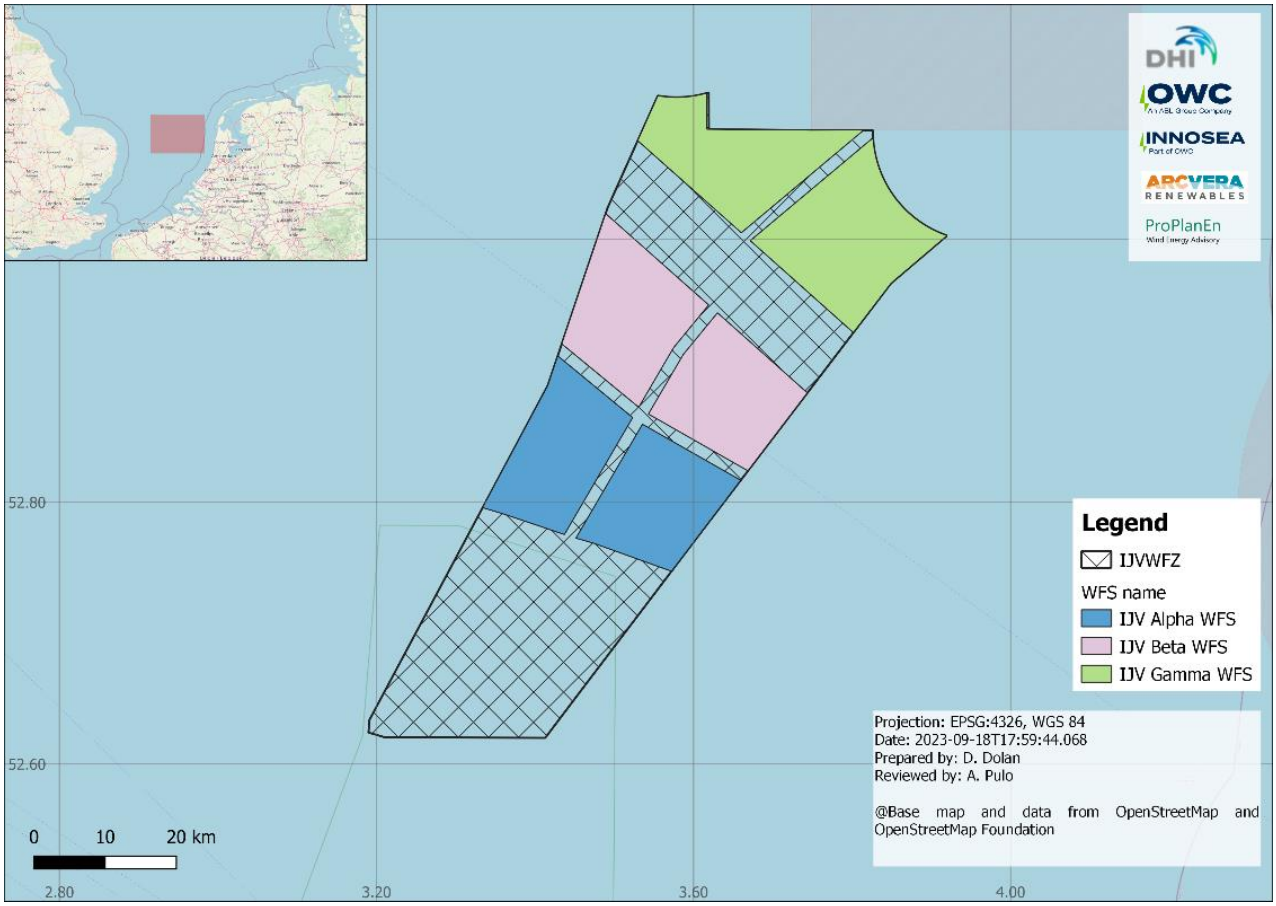

Figure 1.1 Project Sites Relative to Mainland Netherlands

1.1 Scope of the study

As part of the strategy in offshore wind energy, RVO has requested an independent investigation into the wind and meteorological conditions. The investigation is based on several short-term and long-term measurements.

The scope of this report is to present the assessment of the wind resource conducted across IJV which will form part of the information package that informs potential offshore wind developers with an interest in these Project sites.

The vertical datum of mean sea level (MSL) is being used in this report as the vertical height reference unless noted otherwise. The lowest astronomical tide (LAT) at the IJVWFZ is approximately 0.88 m below MSL [1]. It is noted that for wind speed and wind direction observations gathered on-site at IJVWFZ, the difference between MSL and LAT is considered to be negligible.

The reference coordinate system was chosen as EPSG:4326 WGS84 to accommodate the extensive geographical coverage. Correspondingly, the coordinates delineated within the associated table have been reported in this format as well.

English Style Guide of the European Commission [2] is applicable throughout the document. Point is used as a decimal separator in this study. It is noted that no thousand grouping was used in this study deviating from the same guideline.

1.2 Methodology overview

Analysis of measured data across the Dutch and German North Sea.

Datasets gathered by measurement devices at several locations across the North Sea were available for analysis and considered in this study. The primary measurements, located within the Dutch North Sea, consist of two floating lidar systems (FLS[1]), one offshore meteorological mast (met mast, MM) and two vertical profiling lidars. A total of nine (9) secondary datasets were also considered for validation purposes, located across the Dutch and German North Sea.

Long-term correction of the primary datasets.

The measured datasets were screened and analysed. Wake impact was comprehensively examined in the context of the measured data where relevant. The primary datasets were corrected to the long-term using a measure-correlate-predict (MCP) procedure.

WRF mesoscale modelling to serve both wind resource and metocean.

A mesoscale model that covers the full Dutch North Sea was developed using the numerical weather prediction Weather Research and Forecasting (WRF) model. The mesoscale model was built such that it provides a uniform output that informs both wind resource and metocean purposes. To this end, the model is referred to as the Unified-WRF model.

A primary goal of the Unified-WRF dataset was to serve as a wind input for both the met-ocean and energy yield analyses, with particular attention to surface (10-m height) extreme wind conditions for the met-ocean analysis, and to long-term hub-height wind statistics for the energy yield analysis. Note that extreme wind conditions are reported in the metocean assessment but that the entire WRF methodology, including extreme conditions, is discussed in this assessment report.

The Unified-WRF model was initiated with ERA5 reanalysis data. It was then bias corrected through a multi-stage iterative process by making use of the primary and secondary measured datasets as well as the Dutch Offshore Wind Atlas (DOWA) in locations where measurements were scarcer. The final Unified-WRF model has a resolution of 1.7 km and outputs data for multiple variables from 1979 to 2022 at a 10-minute resolution.

Spatial analysis to assess the performance of the Unified-WRF model.

A spatial analysis was conducted to ascertain the performance of the Unified-WRF. This was done in two ways: by comparing the Unified-WRF against other mesoscale modelled datasets using a number of key performance indicators (KPIs) and by assessing the long-term behaviour of the Unified-WRF model against the results from the MCP procedure. The Unified-WRF model was found to have outstanding performance and used to derive the long-term climate across the IJVWFZ.

Uncertainty assessment

The uncertainty associated with the final derived long-term climate across the Project sites is assessed and presented.

Figure 1.2 below presents a flowchart of the applied wind resource assessment methodology.

[1] The acronym FLS denotes both singular and plural forms.

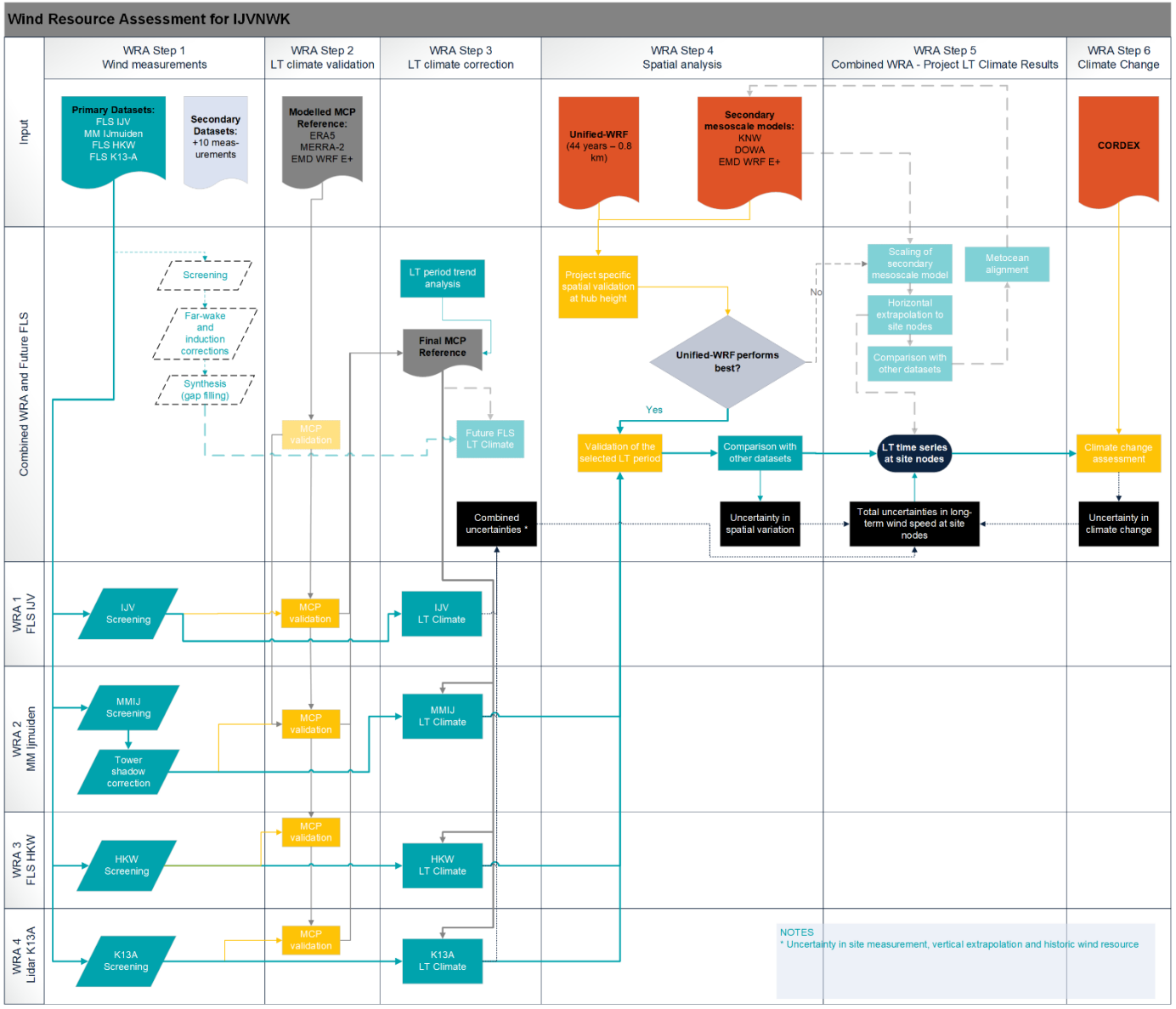

Figure 1.2 Flowchart of wind resource assessment methodology

1.3 Report structure overview

Measured data	Section 2: Presents the measured datasets considered in this assessment. It provides descriptions of each measurement location and gives insight into the data quality and screening processes applied. This is followed by a quantification of the uncertainty associated with each primary measurement campaign.
Data aggregation, vertical extrapolation, and long-term corrections	Section 2.4: Presents the selection of the hub height of interest, followed by a description of the datasets selected for long-term corrections and any adjustment applied prior to conducting an MCP. Finally, the long-term correction of the primary measured data is presented along with its associated methodology and uncertainty.
Unified-WRF mesoscale modelling	Section 4: Gives a detailed description of the Unified-WRF mesoscale model development that was conducted through a multi-stage iterative process. The mesoscale model was built such that it provides a uniform output that informs both wind resource and metocean assessments.
Spatial analysis, assessing the performance of Unified-WRF.	Section 5: Presents the spatial analysis conducted to ascertain the performance of the Unified-WRF. This was done in two ways: by comparing the Unified-WRF against other mesoscale modelled datasets using several key performance indicators (KPIs) and by assessing the long-term behaviour of the Unified-WRF model against the results from the MCP procedure. The Unified-WRF model was found to have outstanding performance and used to derive the long-term climate across the IJVWFZ.
Long-term wind climate across IJVWFZ	Section 6: Presents the long-term results from the Unified-WRF mesoscale model, including various parameters associated with the long-term wind speed and wind direction and, where possible, compared with the short-term measured corresponding values. Climatic parameters are also presented in this section from the measured data and the modelled mesoscale output.
Climate change analysis	Section 7: Presents a study that evaluated the potential impact of climate change on wind resource availability, to help inform accurate and reliable wind resource assessments in the Dutch North Sea region. The analysis offers valuable insight for stakeholders and policymakers in making informed decisions regarding the development of offshore wind farms amidst changing environmental conditions.
Uncertainty assessment	Section 8: Details an uncertainty assessment for IJVWFZ, where multiple uncertainty drivers such as wind speed measurement, vertical extrapolation, historical wind resource, spatial variation, and climate change implications were considered. Data from four unique wind resource evaluations were incorporated, merging both dependent and independent uncertainties through inverse variance and distance-weighting techniques.
Conclusions	Section 9: Presents concluding remarks on the study in this report.

2 Wind Measurements

This section presents the measured datasets considered in this assessment. It provides descriptions of each measurement location, gives insight into the data quality and screening processes applied. This is followed by a quantification of the uncertainty associated with each primary measurement campaign.

Following an exhaustive analysis by OWC of data from offshore sites in the Dutch and German North Sea, 14 datasets underwent close scrutiny. They were subsequently categorised into primary and secondary sets, taking into account their proximity to the Project sites, the integrity of the measurement (data collection) campaign, and the duration of data recording.

The primary datasets, sourced from the immediate vicinity of the Project area, hold crucial significance due to their representativeness. They are pivotal for making long-term adjustments and for delving into uncertainty assessments.

Secondary datasets, derived from more remote locations in the Dutch and German North Sea, primarily serve to support the development and verification of the mesoscale model conceived for this research.

The following sections present descriptions of the data gathered at each measurement location and the associated measurement campaign. Commentary on the data screening methodology and findings are also presented.

2.1 Wind measurement campaigns overview

The primary and secondary datasets analysed in the study have been gathered by various measurement technologies: floating lidar systems (FLS), vertical profiling lidars (referred to as lidar) and offshore meteorological (met) masts (MM).

Table 2.1 presents an overview of the measured datasets considered and their associated key properties. Figure 2.1 shows their locations within the North Sea relative to the Project sites.

Table 2.1 Overview of measured dataset

Measurement location	Measurement device type	Label	Location relative to IJVWFZ	Dataset classification
IJmuiden Ver	FLS	FLS IJV	on-site	primary
IJmuiden Ver	MM	MMIJ/ MM IJmuiden	on-site	primary
IJmuiden Ver	lidar	IJlidar/ lidar IJmuiden	on-site	primary
Hollandse Kust West OWF	FLS	FLS HKW	off-site	primary
K13-A offshore platform	lidar	lidar K13-A	off-site	primary
Lichteiland Goeree offshore platform	lidar	lidar LEG	off-site	secondary
Europlatform offshore platform	lidar	lidar EPL	off-site	secondary

Measurement location	Measurement device type	Label	Location relative to IJVWFZ	Dataset classification
Hollandse Kust Noord OWF	FLS	FLS HKN	off-site	secondary
Hollandse Kust Zuid OWF	FLS	FLS HKZ	off-site	secondary
Ten noorden van de Waddeneilanden OWF	FLS	FLS TNW	off-site	secondary
Offshore Windpark Egmond aan Zee	MM	MM OWEZ	off-site	secondary
Borssele OWF	FLS	FLS Borssele	off-site	secondary
Site N-7.2 OWF	FLS	FLS N-7.2	off-site	secondary
FINO1	MM	MM FINO1	off-site	secondary

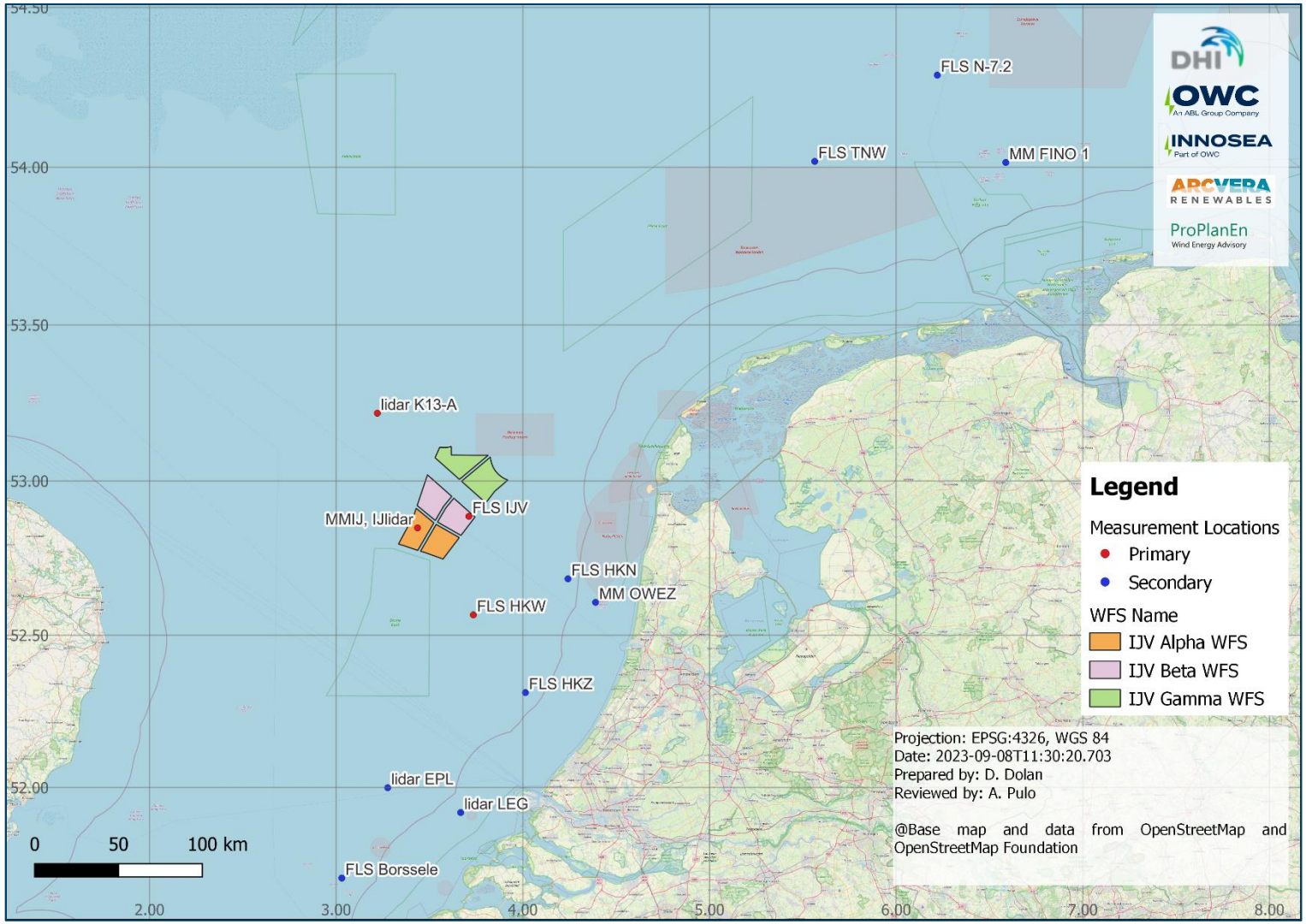

Figure 2.1 Measured datasets' locations in the North Sea

It can be observed that the primary datasets are on-site and the closest off-site measurements. The secondary datasets are spread across a large geographical area that captures the variation of the wind climate across the North Sea, particularly along the coast.

2.2 Primary measurement campaigns

Datasets gathered from four (4) locations have been considered as primary in this assessment. A total of five measured dataset were gathered, two of which were co-located. These datasets have been selected based on the reliability of their measurement campaign, data quality, duration of data and distance from the Project sites. The primary datasets gathered at the four measurement locations have been corrected to the long-term.

The primary datasets have been gathered with different measurement devices and across different measurement periods. Table 2.2 below presents further details on each of these datasets. Figure 2.2 presents a Gantt chart of the measurement periods considered in this study and Figure 2.3 presents an overview of their locations.

The following sections provide a detailed description of each of these datasets.

Table 2.2 Key parameters of primary datasets

Dataset	Distance from IJVWFZ centre [km]	Data duration considered [31pprox.. years]
FLS IJV	6	1.1
MMIJ and IJlidar	18	4
FLS HKW	41	2
Lidar K13-A	43	5

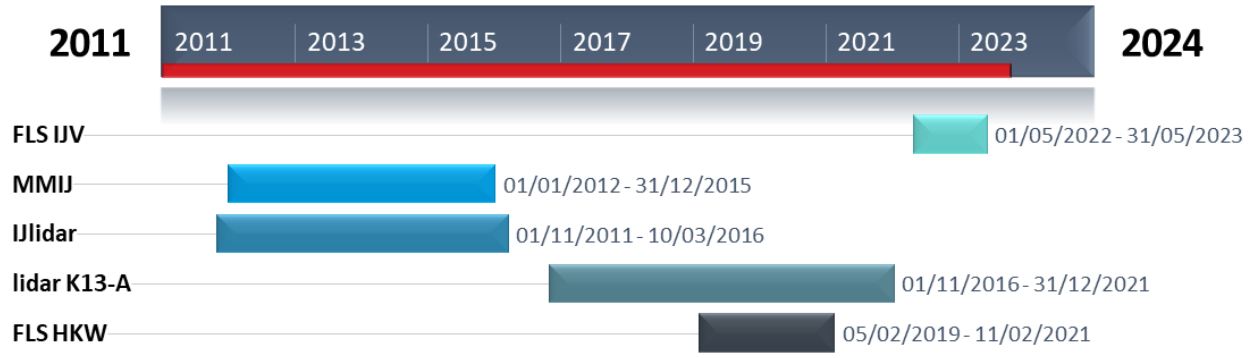

Figure 2.2 Gantt chart of measurement periods of primary datasets

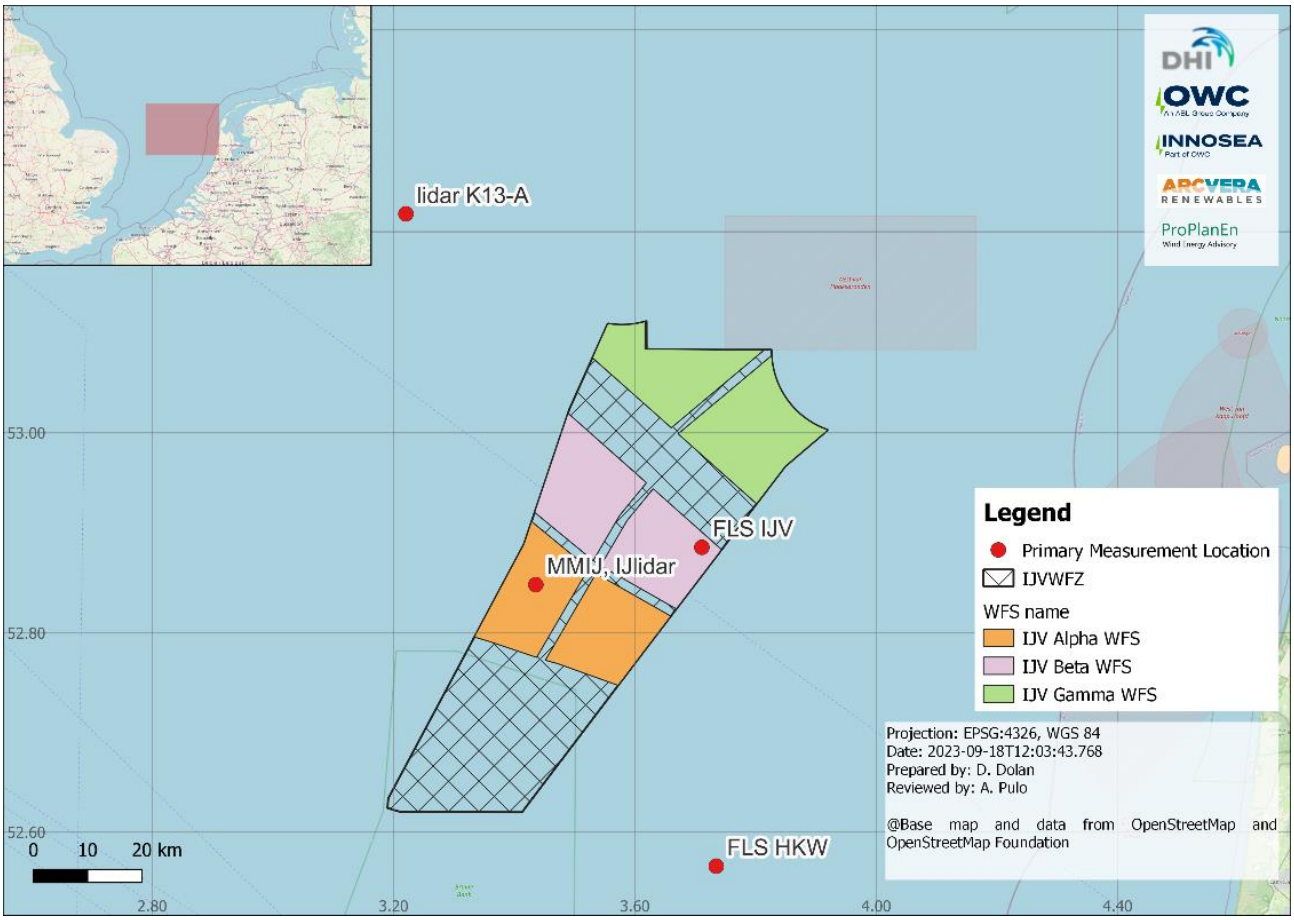

Figure 2.3 Primary measurements' locations

For this study, the measurement campaigns have been abbreviated to:

- FLS at IJVWFZ to FLS IJV
- Met mast at IJVWFZ to MMIJ or MM IJmuiden
- Lidar at IJVWFZ, co-located with the MMIJ to lidar IJmuiden or Ijlidar
- FLS at HKWWFZ to FLS HKW
- Lidar at K13-A offshore platform to lidar K13-A

2.2.1 FLS IJV

FLS IJV measurement campaign description

The FLS IJV measurement campaign was executed and monitored by RPS Group (RPS).

A measurement campaign at IJVWFZ was conducted with multiple FLSs, located within the IJV Beta WFS. The wind measurement campaign was executed and monitored by RPS Group (RPS) which also compiled the monthly reports on the measurement campaign and associated data quality. The information presented in this section is based on the publicly available monthly reports and supporting validation reports.

Two FLS buoys were used in the measurement campaign.

Two RPS lidar 4.5 buoy systems were installed at the site, approximately 1 km apart, to be referred to as FLS IJV A and FLS IJV B [2]. The FLS were deployed between 28 April 2022 and 01 May 2022. At the time of the analysis, 13 months of measured data were available from the FLS installed at the IJVWFZ, from 01 May 2022 until 31 May 2023. It is noted that the FLS IJV measurement campaign was still ongoing at the time of writing. The full FLS IJV measurement campaign will cover a period of 24 consecutive months.

The FLS IJV measurement locations are presented in Table 2.3 and depicted graphically in Figure 2.4. Note that the measurement locations in Table 2.3 are the initial installation locations. The floating nature of the buoys causes the location to change slightly within a small radius.

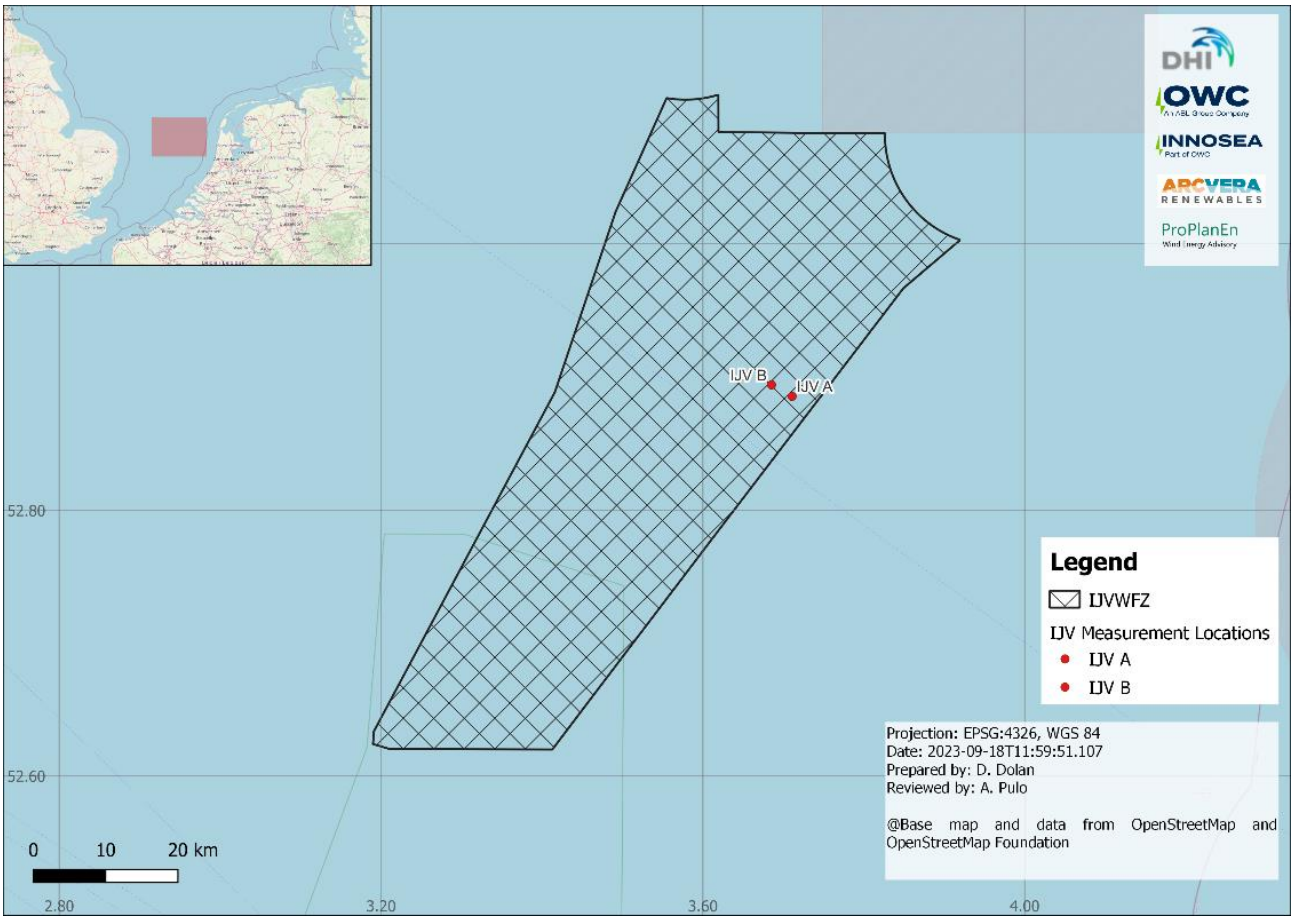

Figure 2.4 Installation locations of the FLS IJV A and FLS IJV B

At the FLS IJV A location, the RPS lidar 4.5 with number 104 was installed on 29 April 2022. This was replaced by an RPS lidar 4.5 buoy with number 103 on 01 December 2022. This had been recovered from FLS IJV B at an earlier date. The buoy with number 104 had to be recovered due to tangled mooring lines which caused some solar panels installed on the buoy to be damaged by storms. The buoy was working continuously throughout the period of mooring line entanglement. On 24 April 2023, buoy 103 went adrift due to third-party intervention. It was towed away on 26 April 2023 and replaced with buoy 104 on 03 May 2023. As a result of the drifting buoy, the FLS IJV A data in April 2023 has lower data coverage.

At the FLS IJV B location, the RPS lidar 4.5 with number 103 was installed on 01 May 2022. This was replaced by an RPS lidar 4.5 buoy with number 105 on 13 October 2022. The buoy with number 103 had to be recovered due to a faulty cable used by the ADCP metocean measurement device.

A Gantt chart indicating the timeline of the buoy installed at each of FLS IJV A and FLS IJV B is shown in Figure 2.5.

Table 2.3 FLS IJV A and FLS IJV B measurement campaign overview [2]

Parameter	FLS IJV A	FLS IJV B
Measurement type	ZephIR ZX 300M lidar	
Measurement period considered in the analysis	01 May 2022 to 31 May 2023	
RPS lidar 4.5 number	104, 103	103, 105
Location (latitude, longitude) [°]	52°53.133' North (N) 03°42.650' East €	52°53.650' N 03°41.117' E
Measurement averaging temporal interval [min]	10	
Measurement heights (MSL) [m]	300, 250, 200, 180, 160, 140, 120, 100, 70, 41, 30	
Approx. distance from the coast [km]	66	
Approx. distance from IJV centre [km]	6	

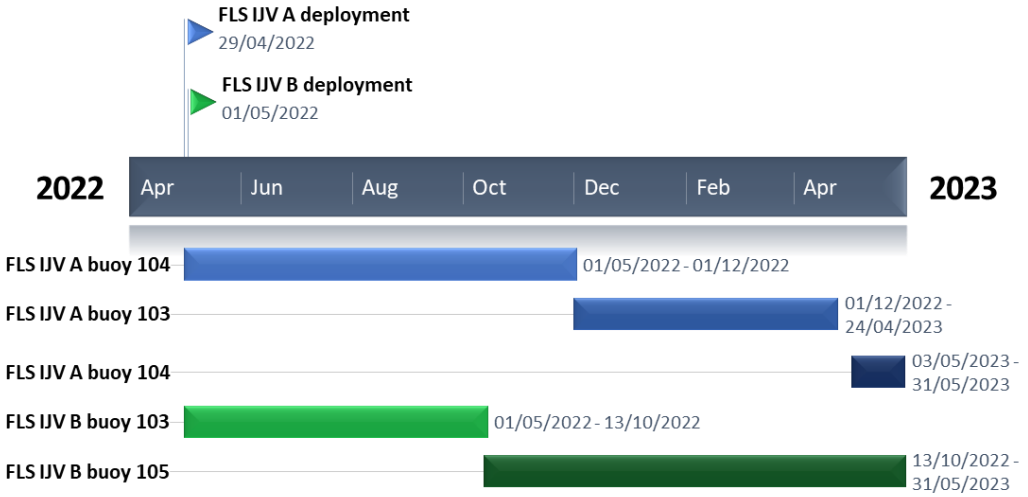

Figure 2.5 FLS IJV Gantt chart of considered measurement period

All installed FLS successfully passed pre- deployment validation.

All the RPS lidar 4.5 buoys installed on-site during the observed measurement period were equipped with a ZephIR ZX 300M vertical profiling lidar. Prior to installation on site, the RPS lidar 4.5 buoys underwent validation campaigns [3]–[5] in September and October 2019 (buoy 103 and buoy 104) and August and September 2020 (buoy 105). The buoy validations were conducted by West Wind off the coast of Perth, Western Australia, against a reference lidar installed on a fixed navigation beacon. The validation campaign met all the

'best practice' criteria KPIs specified by the OWA Roadmap [6] and was considered to be suitable for offshore wind resource assessments. It is recommended by the IEA to verify the performance of an FLS no greater than one year prior to deployment on-site [7]. The validation campaign conducted for the RPS lidar 4.5 buoys falls outwith this recommended timeframe[2].

In addition, the vertical profiling lidars installed on each buoy underwent their own verification exercise conducted by DNV against a reference met mast near Pershore/Throckmorton in the UK [8]–[10]. The ZX lidars (ZX888, ZX874, ZX914) mounted on buoys 104, 103 and 105, respectively, were found to be able to reproduce cup anemometer wind speeds and wind directions at an accurate and acceptable level [6]–[8]. The ZX914 passed all best practice criteria KPIs. The ZX888 and ZX874 passed all best practice criteria KPIs, except for the data bin averaging procedure defined in IEC [11] for the lowest three heights of validation. Note that the top height under verification, which is the main height of interest, passed all KPIs.

FLS IJV Data handling and quality checks

The data validation and quality checks were conducted each month by RPS. Monthly reports were issued by the RPS as part of the monitoring process. The validated and post-processed data was extracted from the RVO online portal.

The validation and post-processing conducted by the RPS consisted of:

- Detailed checks of real-time data during deployment.
- Instrument details were logged and noted as checked in their quality control process.
- Upon instrumentation recovery, the first and last logged instruments are compared against a reliable source, such as GPS time. Any timing errors were corrected in the post-processing.
- Time series was inspected manually for instrument faults, sensory drift, and spurious constancy.
- Each timestamp was assigned a quality index as follows;
- 0 - unknown
- 1 - good
- 2 - suspect
- 3 - bad

The data was found to be of very good quality and no further filtering of data was conducted by OWC. Following the data checks, the data coverage at each measurement height was observed.

Table 2.4 shows the data coverage and the mean values of the wind speed and wind direction for the measurement heights of 100 m, 140 m and 160 m. Appendix B presents the campaign documentation and Appendix C exhibits the mean monthly values and associated data coverage for the duration of the measurement period for all the measurement heights.

It can be observed that the wind speed data at the measurement height of 160 m has an excellent data coverage above 90% for the measurement period from 01 May 2022 to 31 May 2023.

Table 2.4 FLS IJV A and FLS IJV B mean values across the measurement period

Height above MSL [m]	Data Type	FLS IJV A		FLS IJV B	
		Mean value wind speed [m/s] wind direction [°]	Data Coverage [%]	Mean value wind speed [m/s] wind direction [°]	Data Coverage [%]
160	Wind speed	9.90	92.1	9.81	94.5
140	Wind speed	9.79	92.4	9.70	94.8
100	Wind speed	9.50	93.4	9.41	95.7
160	Wind direction	238	91.4	237	93.9
140	Wind direction	237	91.9	237	94.4
100	Wind direction	236	92.9	235	95.3

FLS IJV data usability remarks

- The data gathered by FLS IJV A and FLS IJV B was found to be of very good quality with excellent data coverage.
- The wind speed data coverage for the specified heights of 100 m, 140 m, and 160 m all exceeded or met the 95% threshold.
- The data gathered by FLS IJV A and FLS IJV B were found to be appropriate for long-term correction to determine the on-site long-term climate.

2.2.2 MM IJmuiden and Lidar IJmuiden

The vertical datum in all documentation relating to the MM IJmuiden and lidar IJmuiden measurement campaigns is LAT. The LAT at the IJVWFZ is approximately 0.88 m below MSL [1]. Therefore, for wind speed and wind direction observations gathered at this measurement location, the difference between MSL and LAT is considered negligible.

Hereafter, all heights presented in this report in relation to MM IJmuiden and lidar IJmuiden will be in reference to MSL.

MM IJmuiden measurement campaign description

MM IJmuiden measurement campaign was monitored by ECN.

A measurement campaign at the IJVWFZ was conducted with an offshore met mast the IJmuiden met mast (MMIJ/ MM IJmuiden), located within the IJV Alpha WFS. The MM IJmuiden was erected in 2011, approximately 87 km west of the IJmuiden harbour. The met mast was installed at an offshore met station that consisted of a platform with a control room and the installed met mast. The installed platform was approximately 18 m above LAT.

The wind measurement campaign was monitored by ECN (now TNO[3] Energy Transition, referred as TNO throughout the report). The information presented in this section is based on the publicly available report issued by ECN [12].

The sensors on the MM IJmuiden were mounted at three measurement heights above LAT. The MMIJ was equipped with anemometers, wind vanes, ultrasonic anemometers, thermometers, barometers, a hygrometer, and precipitation sensors.

The design of the met mast and data processing techniques were designed such as to ensure high data quality [13]. Flow distortion due to the tower was minimized by installing anemometers on three booms mounted at each height; two anemometers were installed at the top height [12].

The met mast was decommissioned in the year 2016. Therefore, the measurement period considered covers a duration of four (4) whole years from 2012 to 2016.

Key details of the IJmuiden met mast measurement campaign are summarized below in Table 2.5.

Table 2.5 MM IJmuiden measurement campaign overview [9]

Parameter	MM IJmuiden
Measurement type	Lattice met mast
Measurement period considered in the analysis	01 January 2012 to 31 December 2015
Location (latitude, longitude) [°]	52°50.89'N 03°26.14'E
Measurement averaging temporal interval [min]	10
Measurement heights (MSL) [m]	92, 85, 58 and 27
Approx. distance from the coast [km]	82
Approx. distance from IJV centre [km]	18

The report [12] states that all the sensors mounted on the MM IJmuiden were calibrated according to ISO 17025. OWC is not in possession of the sensors' calibration certificates. It is unclear if the instruments were replaced or recalibrated during the measurement period at the MM IJmuiden. The MEASNET association recommends in [14] that anemometers should be re-calibrated after 12 months of measurements. If this is not conducted the anemometers can be tested to ensure that the calibration has been maintained throughout the measurement campaign. In [15], ECN presents a comparison of the lidar and MM data gathered at the IJmuiden platform covering the period 01 January 2012 to 01 January 2014. The two datasets were found to have excellent agreement with an R^2 value greater than 0.99.

[3] Nederlandse Organisatie voor Toegepast Natuurwetenschappelijk Onderzoek" (TNO) is an independent research organization in the Netherlands that focuses on applied science.

MM IJmuiden data handling and quality checks

ECN was responsible for checking the data and did this in several ways. The measurement computer checked the sensor connection and if recordings exceeded minimum and maximum thresholds. Subsequently, the data was checked manually. Only valid data was kept in the provided raw data files. Missing values were indicated with blanks.

Single undisturbed wind speeds from the measurements at each height were derived based on the methodology defined by ECN [12], with a slight modification by OWC to include a period with only a single undisturbed wind vane. This methodology was applied to the measurement heights with three anemometers.

No information regarding recommended filters for the top measurement height was defined by ECN, where there are two anemometers. OWC defined its own methodology by interpolation based on disturbed sectors. An intercomparison of the two measured wind speeds confirmed the flow disturbances in the expected sectors, based on the mast configuration. The directional filters were then defined based on these sectors [13].

Following the post-processing exercise, the final wind speed value for the top measurement heights is shown in Table 2.6. Appendix B presents the campaign documentation and Appendix C exhibits the mean monthly values and associated data coverage for the duration of the measurement period for all the measurement heights.

Table 2.6 MM IJmuiden mean values across measurement period

Height above MSL [m]	Data Type	MM IJmuiden Mean value wind speed [m/s] wind direction [°]	Data Coverage [%]*
92	Wind speed	9.98	99.1
87	Wind direction	230	96.7

Lidar IJmuiden measurement campaign description

The Lidar IJmuiden measurement campaign was monitored by ECN.

A measurement campaign at IJVWFZ was conducted with a vertical profiling lidar system, referred to as the lidar at IJmuiden (IJlidar/ lidar IJmuiden). The lidar IJmuiden was installed at the IJmuiden offshore met station consisting of a platform, a control room and an offshore met mast. The lidar IJmuiden was installed on the platform, to the southwest of the MM IJmuiden. One ZephIR 300 vertical profiling lidar system was installed at the IJmuiden platform at a height of 20.88 m LAT. The lidar was configured to gather measurements between the heights of 90 m and 315 m above MSL.

One vertical profiling lidar was installed at the IJmuiden offshore met station platform.

At the IJmuiden site, the Lidar and MM IJmuiden were co-located for data acquisition. It's pertinent to mention that the Lidar has been integrated into the met-mast (see Figure B.6 in Appendix B), causing potential interference due to obstacles during its operation. Leveraging continuous wave lidar technology, the unit is capable to identify instances when the laser beam encounters obstacles, subsequently filtering out these measurement points from the results. The top measurement height of the MM IJmuiden is 92 m, which indicates that the majority of the lidar IJmuiden measurements lie well above the influence of the MM IJmuiden top measurement height. [12] states that the

lidar has been installed in such a way that it has enough ‘free sight to perform wind speed measurements’.

The wind measurement campaign was monitored by ECN (now TNO) which also monitored the data gathering and data quality. The information presented in this section is based on the publicly available report issued by ECN [12]. It is unclear to OWC whether the lidar installed at the IJmuiden platform underwent a verification test prior to installation on site. However, in [15], ECN presents a comparison of the lidar and MM data gathered at the IJmuiden platform covering the period 01 January 2012 to 01 January 2014. The two datasets were found to have excellent agreement. [11] also recommends using the lidar IJmuiden data for any vertical extrapolation to be performed on the MM IJmuiden data as the lidar data is more representative of the wind climate at higher heights. Figure 2.6 presents the location of the lidar IJmuiden and the MM IJmuiden relative to the OWFZ.

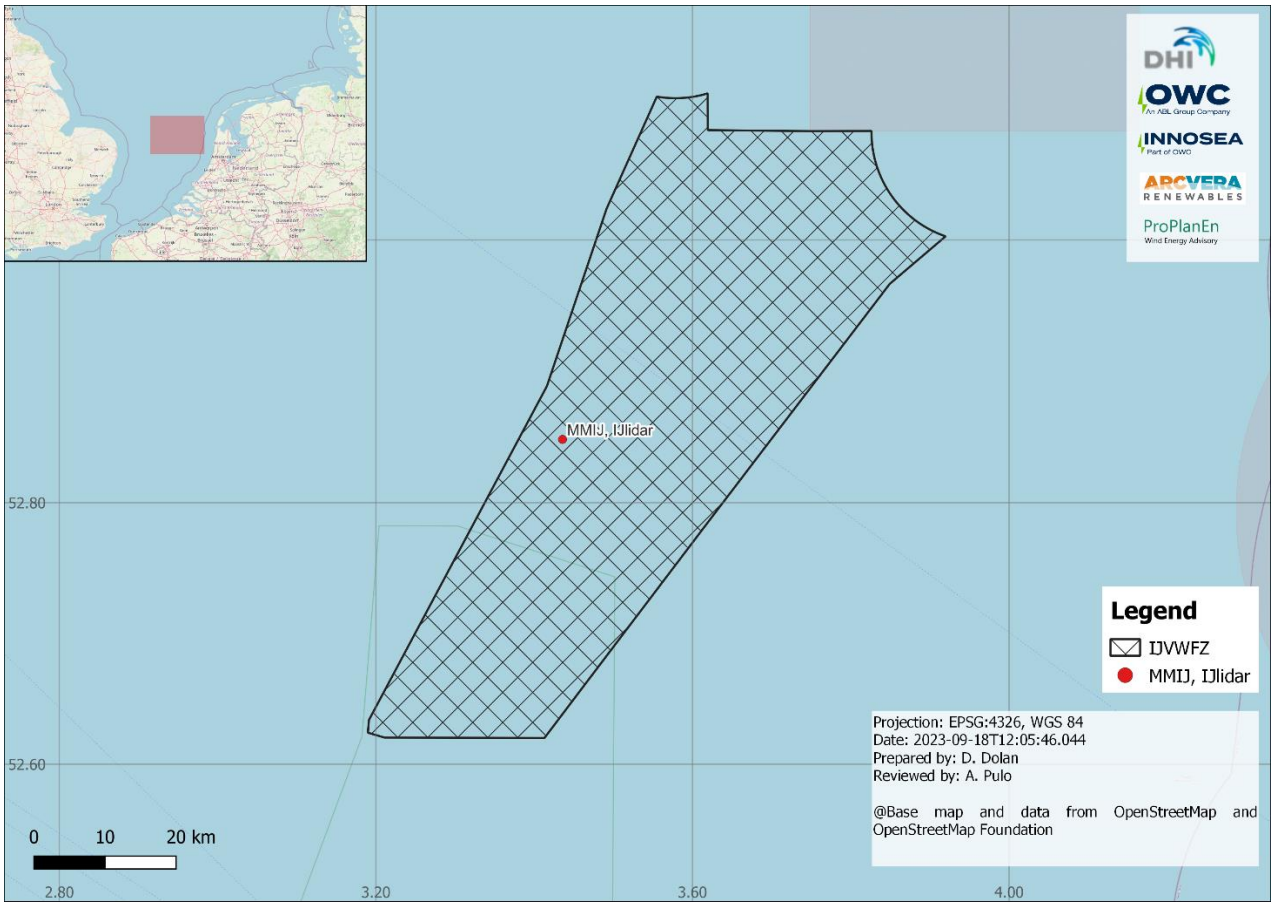

Figure 2.6 Installation location of the lidar IJmuiden and MM IJmuiden

Key details of the lidar IJmuiden measurement campaign are summarized below in Table 2.7.

Table 2.7 Lidar IJmuiden measurement campaign overview [12]

Parameter	MM IJmuiden
Measurement type	ZephIR ZX 300
Unit number	unknown

Parameter	MM IJmuiden
Measurement period considered in the analysis	01 November 2011 to 10 March 2016
Location (latitude, longitude) [°]	52°50.89'N 03°26.14'E
Measurement averaging temporal interval [min]	10
Measurement heights (MSL) [m]	315, 290, 265, 240, 215, 190, 165, 140, 115 and 90
Approx. distance from the coast [km]	82
Approx. distance from IJV centre [km]	18

Lidar IJmuiden data handling and quality checks

ECN was responsible for checking the data and did this in several ways. The measurement computer checked the sensor connection and if recordings exceeded minimum and maximum thresholds. Subsequently, the data was checked manually. Only valid data was kept in the provided raw data files. Missing values were indicated with blanks. No further information regarding the filtering conducted was defined by ECN in [12].

OWC applied filtering for range checks on all the data gathered by IJmuiden lidar. Wind speed values below 0 m/s and above 50 m/s and wind direction data outwith 0° and 360° were considered out of range. The direction data was also checked for the Doppler shift where the ZX 300 lidar may have a 180°ambiguity. The data was compared to the data gathered by the wind vanes of the MM IJmuiden and used to correct any offset. A quality check flag was also run on the data based on the "packets in average" (PiA) data column provided in the data. The PiA indicates the number of fit-derived wind measurements that are used to produce the 10-minute wind data and is an indicator of the system availability. A minimum threshold PiA of 21 was applied to the data[4].

Following the post-processing exercise, the final wind speed value for the heights of interest is shown in Table 2.5. Appendix B presents the campaign documentation and Appendix C exhibits the mean monthly values and associated data coverage for the duration of the measurement period for all the measurement heights.

Table 2.8 Lidar IJmuiden mean values across the measurement period

Height above MSL [m]	Data Type	Mean value wind speed [m/s] wind direction [°]	Data Coverage [%]

165	Wind speed	10.66	94.2
140	Wind speed	10.53	94.2
115	Wind speed	10.38	94.3
165	Wind direction	236	93.4
140	Wind direction	235	93.5

MM IJmuiden and Lidar IJmuiden data usability remarks

- The MMIJ was installed in November 2011 and decommissioned in March 2016. In the context of the analysis, full years were considered, therefore the data period considered in this study is from 01 January 2012 to 31 December 2015, covering a period of four (4) whole calendar years.
- The data quality of lidar IJmuiden was found to be very good, with data coverage being above 90% at all the measurement heights.
- The data quality of MMIJ was found to be excellent, with data coverage being excellent at 99% at the top measurement height for the measurement period being considered.
- The data collected by the lidar IJmuiden was deemed appropriate for long-term correction. However, given the superior quality of the MM IJmuiden dataset, the lidar IJmuiden dataset was excluded from the long-term analysis.
- MM IJmuiden data is considered suitable for long-term correction. Given that the top measurement height is 92 m, the data required vertical extrapolation to the height of interest of 160 m prior to applying the long-term correction. As the MM IJmuiden and lidar IJmuiden are co-located, the lidar IJmuiden data was used to vertically extrapolate the MM IJmuiden top measured data to the heights of interest. The lidar IJmuiden data reflects the wind shear expected at these higher heights closer to the hub height of interest. Further details are presented in Section 3.3.2.

2.2.3 FLS HKW

FLS HKW measurement campaign description

FLS HKW measurement campaign was executed and monitored by Fugro.

A measurement campaign was completed at the planned offshore wind farm zone Hollandse Kust West (HKW, HKWWFZ) with several FLS. This measurement location is considered to be off-site with respect to the Project OWFZ IJmuiden Ver. The wind measurement campaign was executed and monitored by Fugro. The post-processing was conducted by Fugro while Deltares was commissioned by Fugro to do the data validation. The information presented in this section is based on the publicly available reports and supporting validation/verification reports.

Two FLS locations were utilized in the measurement campaign.

Three Seawatch Wind lidar buoy (SWLB) systems were installed simultaneously at the HKW OWFZ. Initially, two SWLBs were installed, FLS HKW A and FLS HKW B. However, a third location, FLS HKW C was temporarily added to facilitate in-situ validations. At a later date another measurement location was added, approximately 150 m from FLS HKW A,

labelled as FLS HKW A-2. This measurement location was added as the original HKW A mooring lines became unusable [16].

FLS HKW A was deployed on 05 February 2019, FLS HKW B was deployed on 10 February 2019 and FLS HKW C was deployed on 01 August 2019. The alternative FLS HKW A-2 was deployed on 09 May 2020. The measurement campaign at OWFZ HKW covered a period of 24 consecutive months [16].

The FLS HKW measurement locations are presented in Table 2.9 and depicted graphically in Figure 2.7. Note that the measurement locations in Table 2.9 are the initial installation locations. The floating nature of the buoys causes the location to change slightly within a small radius.

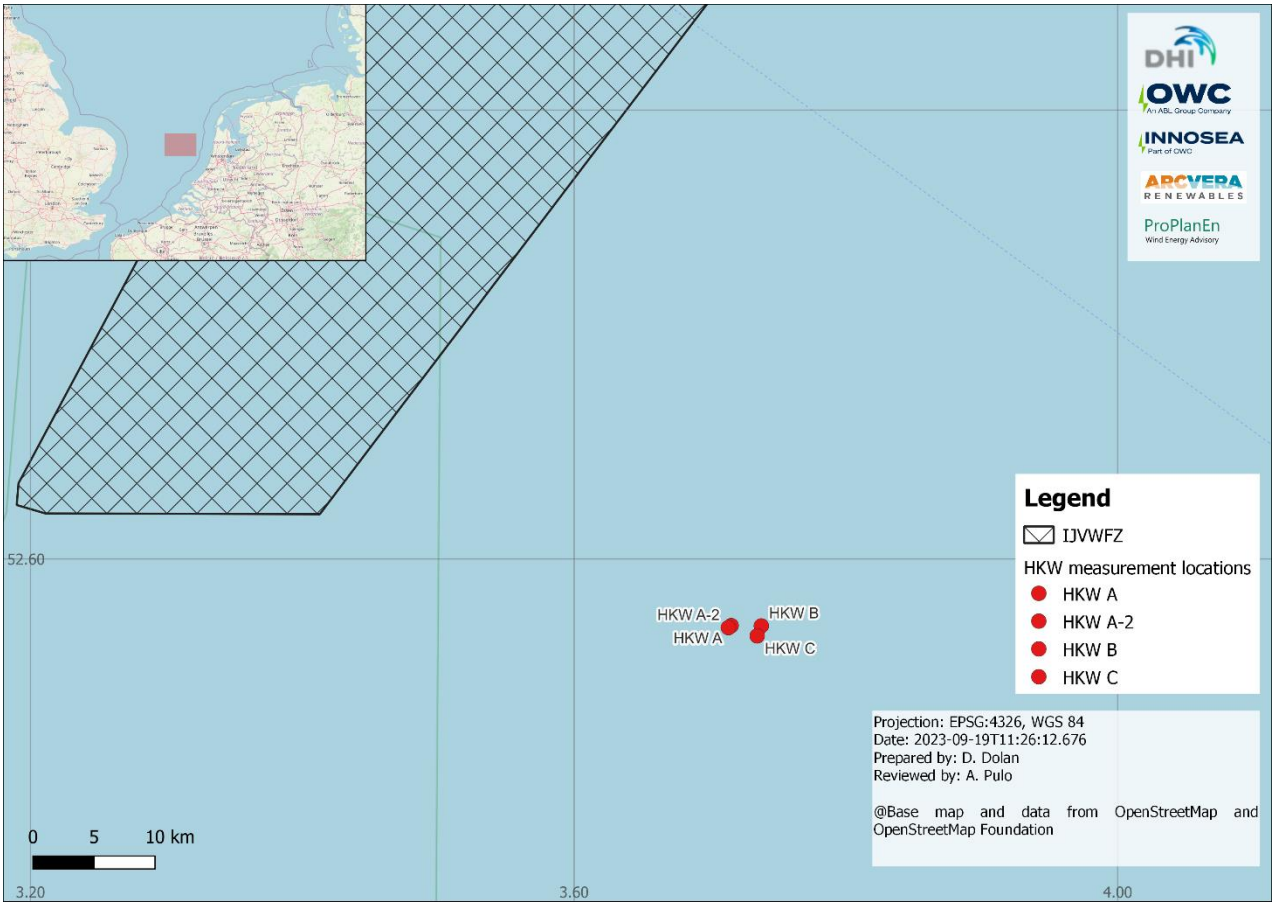

Figure 2.7 Installation locations of the FLS HKW A FLS HKW B and FLS HKW C

Throughout the measurement campaign, 3 different SWLBs were used and rotated between the FLS HKW A/A-2, FLS HKW B and FLS HKW C locations. A buoy was deployed at all times during the 24 months except for the period from 24 April 2020 to 09 May 2020. A detailed description of the cause for each replacement and the maintenance conducted at each site and to each SWLB can be found in [16].

A Gantt chart indicating the timeline of the buoy installed at each of the HKW measurement locations is shown in Figure 2.8.

Table 2.9 FLS HKW A, FLS HKW A-2, FLS HKW B and FLS HKW C measurement campaign overview [16]

Parameter	FLS HKW A	FLS HKW A-2	FLS HKW B	FLS HKW C
Measurement type	ZephIR ZX300 CW			
Measurement period considered in the analysis	05 February 2019 to 24 April 2020	09 May 2020 to 11 February 2021	10 February 2019 to 11 February 2021	01 August 2019 to 07 February 2020
SWLB number	WS187, WS188	WS187, WS188	WS188, WS170, WS187	WS170, WS188
Location (latitude, longitude) [°]	52°34.211'N 3°42.937' E	52°34.156'N 3°42.812' E	52°34.203'N 3°44.264' E	52°33.935'N 3°44.083' E
Measurement averaging temporal interval [min]	10			
Measurement heights (MSL) [m]	250, 200, 180, 160, 140, 120, 100, 80, 60, 40, 30			
Approx. distance from the coast [km]	58			
Approx. distance from IJV centre [km]	41			

All installed FLS successfully passed pre- deployment validation.

Figure 2.8 FLS HKW Gantt chart of the measurement period

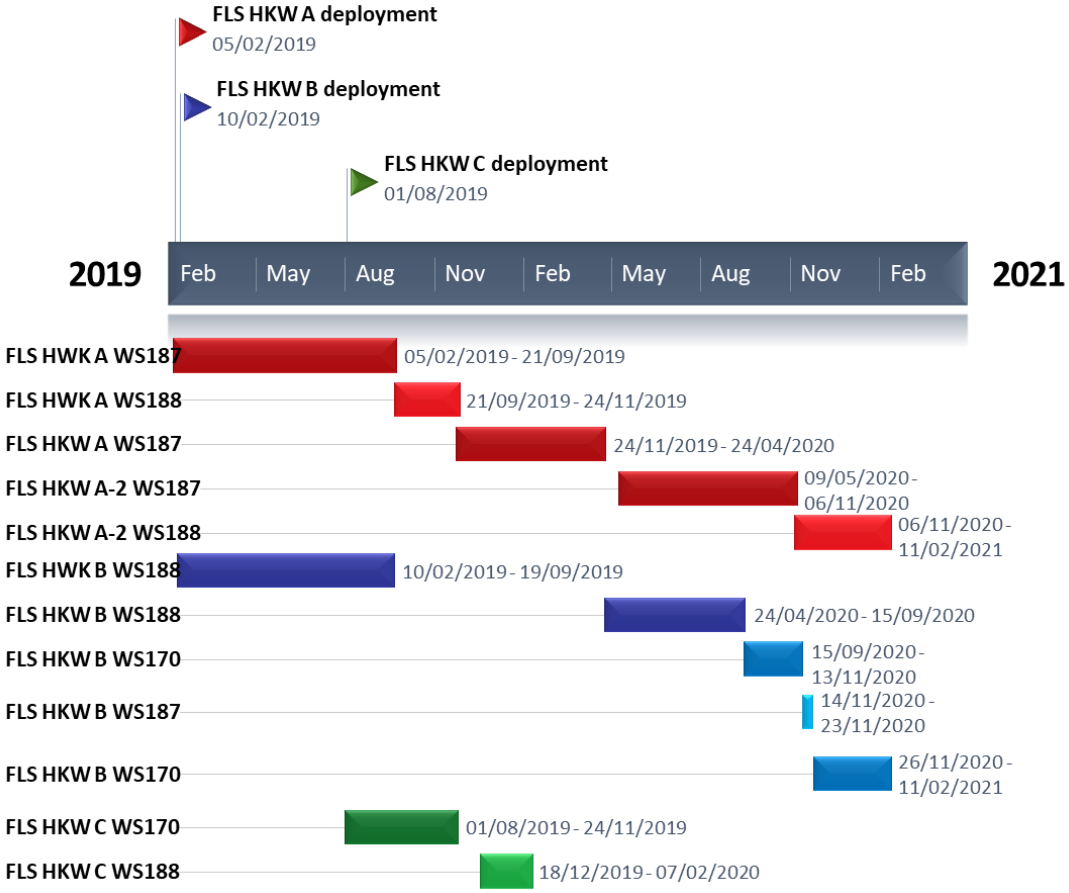

All the SWLB installed at HKW during the observed measurement period were equipped with a ZephIR ZX300M vertical profiling lidar which is a marinized version of the ZX300 lidar type. Prior to installation, the SWLBs WS188 and WS 187 underwent validation campaigns [17], [18]. The buoy validations were conducted by DNV GL (now DNV), next to the Island of Frøya in the Norwegian Sea against a fixed/land-based industry-accepted lidar. DNV has assessed the pre-deployment validation conducted and concluded that the WS187 and WS188 buoys have demonstrated the capability to accurately measure wind speed and direction across a range of sea states and meteorological conditions.

The SWLB WS170 was validated in situ at the FLS HKW C location against the WS187 installed at FLS HKW A and WS 188 installed at FLS HKW B. The validation was conducted by DNV GL. The SWLB WS170 was found to be capable of producing accurate wind speed and direction data across the range of meteorological conditions experienced in the validation period [19]. The SWLB WS170 also underwent a post-deployment validation in May 2021 and was found to be capable of producing accurate wind speed and wind direction data [20].

In addition, the vertical profiling lidars installed in each buoy underwent their own verification exercise conducted by DNV against a reference met mast near Pershore/Throckmorton in the UK. The ZX lidars (ZX818, ZX802, ZP585) mounted on buoys WS187, WS188 and WS170, respectively, were found to be able to reproduce cup anemometer wind speeds and wind directions at an accurate and acceptable level [21]–[23].

FLS HKW data handling and quality checks

Deltares, which was commissioned by Fugro, conducted the data validation, and produced monthly reports based on the assessments conducted. The post-processing was conducted by Fugro which is detailed in the monthly reports issued by Fugro as part of the monitoring process. The validated and post-processed data was then provided to RVO. The data sourced by OWC via the RVO portal is this aforementioned post-processed data.

The post-processing conducted on the data by Fugro consisted of [16]

- Marking any missing timesteps with NaN
- Removing any values that are:
- outside the times that the system is deployed
- duplicated transmission values
- out-of-range values which are replaced by NaN
- applying parameter/instrument-specific quality control
- Manual inspection and assessment

Based on the post-processing described above, quality flags were assigned to each datapoint, as indicated in Table 2.10.

Table 2.10 FLS HKW QA filter/flags applied in post-processing [16]

Flag value	Text code	Description
0	Good data	Passed all tests
1	Duplicated set	Duplicated set of values from 1 sensory found and removed
2	Consecutive duplicate	Consecutive duplicate values found and removed
3	Out of bounds	Value outside of the valid range, found and removed
4	Outlier	Outlier found and removed
5	Low signal strength	Signal strength below threshold and value removed
6	Flipped 180°	180° ambiguity found and lidar wind direction flipped 180°
7	Low packet count	Number of valid lidar wind measurements below threshold lidar
8	Missed transmissions	No data was saved for this 10-minute interval
9	Not evaluated/failed	Not evaluated (currents) or failed

Following the post-processing by Fugro, the dataset was validated by Deltares. The validation checks for consistency within the dataset, data files and whether any outliers were present. Based on feedback provided by Deltares, the data is checked again by Fugro. Further details on this process are presented in [16].

Table 2.11 shows the data coverage and the mean values of the wind speed and wind direction and the corresponding data coverage for the measurement heights of 100 m, 140 m and 160 m. Appendix B presents the campaign documentation and Appendix C exhibits the mean monthly values and associated data coverage for the duration of the measurement period for all the measurement heights.

It can be observed that the wind speed data at the measurement height of 160 m has a reasonable data coverage of 85% at FLS HKW A and 71% at FLS HKW A-2. A lower data coverage is observed at FLS HKW B and FLS HKW C.

Table 2.11 FLS HKW mean values across the measurement period

Height above MSL [m]	Data Type	FLS HKW A		FLS HKW A-2		FLS HKW B		FLS HKW C	
		Mean value WS [m/s] WD* [°]	Data Coverage [%]*	Mean value WS [m/s] WD* [°]	Data Coverage [%]*	Mean value WS [m/s] WD* [°]	Data Coverage [%]*	Mean value WS [m/s] WD* [°]	Data Coverage [%]*
160	Wind speed	10.91	85.3	9.83	71.0	9.71	58.3	10.13	66.0
140	Wind speed	10.78	85.4	9.73	71.0	9.61	58.4	10.05	66.1
100	Wind speed	10.43	85.6	9.48	71.1	9.34	58.5	9.82	66.1
160	Wind direction	234	85.3	235	71.0	236	58.3	228	66.0
140	Wind direction	234	85.4	235	71.0	235	58.4	228	66.1
100	Wind direction	233	85.6	235	71.1	234	58.5	227	66.1

FLS HKW data usability remarks

- The data gathered by the FLS HKW measurement campaign was found to be of very good quality with good data coverage at FLS HKW A and FLS HKW A-2.
- The data gathered at each of FLS HKW A, HKW A-2, HKW B and HKW C does not cover the full measurement period of the consecutive 24 months. However, combining the measurements results in excellent data coverage across the full period. Further details on this are provided in Section 3.3.3.
- The data gathered by FLS HKW were found to be appropriate for long-term correction to determine the long-term climate at this measurement location. As aforementioned, for a dataset that is more suitable for long-term correction, the measurements gathered at each of FLS HKW A, HKW A-2, HKW B and HKW C were combined for a single measured dataset with increased data coverage.

2.2.4 Lidar K13-A

The vertical datum in all documentation relating to the lidar K13-A measurement campaign is MSL.

Lidar K13-A measurement campaign description

Lidar K13-A measurement campaign was executed and monitored by TNO.

A measurement campaign at an offshore platform in the Dutch North Sea was conducted with a vertical profiling lidar. This lidar was installed at the K13-A offshore platform owned by Wintershall Nordzee B.V. K13-A is a production platform for natural gas commissioned in 1975 and situated approximately 110 km to the northwest of Den Helder. Whilst it has historically served as a gas production platform and central hub, at present, it is no longer in production, but rather functions as a bypass platform. K13-A has transitioned to an unmanned platform starting from January 2019 [24].

One ZX300M lidar was installed on this platform at a height of 36.2 m LAT and started gathering data on 01 November 2016. The lidar was installed to the east of a helicopter deck that is at a height of 37.7 m MSL [25]. According to [19], although the lidar was installed at a lower height than the helicopter deck, it was still installed high enough to have a 'clear view' and is free of obstacles. The lidar was configured to gather measurements between the heights of 63 m and 291 m above MSL.

The wind measurement campaign was managed and monitored by TNO, which also compiled the reports on the measurement campaign and associated data quality every couple of years. The information presented in this section is based on the publicly available reports.

Two consecutive ZX lidars were installed at this measurement location. The lidar with serial number ZX563 was installed on 01 November 2016 and gathered data until 11 November 2022. This was then replaced on 11 November 2022 with another lidar unit with serial number ZX1525. It is noted that data up to 01 January 2022 was considered in this study as no further data was available at the time the study was conducted.

A vertical profiling lidar was deployed in this measurement campaign.

The measurement location is presented in Table 2.12 and depicted graphically in Figure 2.9.

The initial lidar installed at the measurement location, ZX563, underwent a validation exercise prior to installation at the site. The validation was conducted by ECN, which is part of the "TNO LiDAR Calibration" facility, against an onshore met mast. The validation exercise indicated that the ZX563 lidar unit was suitable for offshore application at the K13-A platform [26]. It is noted that according to the TG6 guidelines [27], the maximum interval between pre-verification and post-verification (another verification) should not exceed 30 consecutive months. The ZX563 gathered data for six consecutive years, exceeding the 30-month threshold. According to [28], the lidar still produced plausible data.

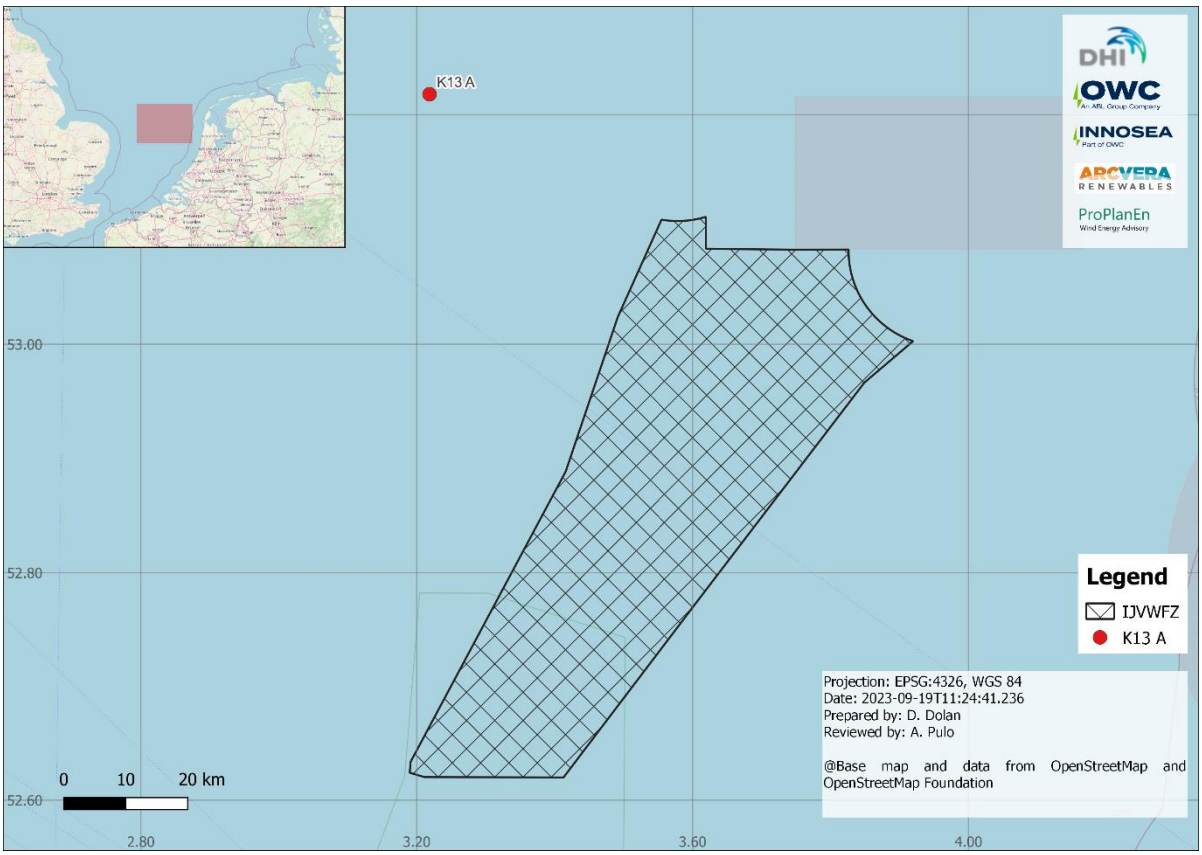

Figure 2.9 Installation locations of the lidar K13-A

Table 2.12 Lidar K13-A measurement campaign overview [25]

Parameter	Lidar K13-A
Measurement type	ZephIR ZX 300M lidar
Unit number	ZX563
Measurement period considered in the analysis	01 November 2016 to 31 December 2021
Location (latitude, longitude) [°]	53°13.062' N 03°13.216' E
Measurement averaging temporal interval [min]	10
Measurement heights (MSL) [m]	291, 266, 241, 216, 191, 166, 141, 116, 91, 63
Approx. distance from the coast [km]	102
Approx. distance from IJV centre [km]	43

Lidar K13-A data handling and quality checks

TNO was responsible for checking the data and did this in several ways. The quality checks by TNO were done on a daily basis using daily plots. The signals were checked for deviation or failures. Where needed, data was marked as invalid and is not part of the downloadable data package. During these initial checks, no data filtering was applied to the data. The direction data was also checked for the Doppler shift where the ZX 300M lidar may have a 180°ambiguity. The data was compared to the data gathered by the met station of the lidar unit and used to correct any offset. No further filtering was applied by TNO in [29].

OWC applied filtering for range checks on all the data gathered by lidar K13-A. Wind speed values below 0 m/s and above 50 m/s and wind direction data outwith 0° and 360° were considered out of range. A quality check flag was also run on the data based on the packets in average (PiA) data column provided in the data. The PiA indicates the number of fit-derived wind measurements used to produce the 10-minute wind data and is an indication of the quality of the data within the observed 10-minute interval. A minimum threshold PiA of 21 was applied to the data.

Following the post-processing exercise, the final wind speed values for the heights closest to the heights of interest are shown in Table 2.5. The mean monthly values for the heights of 91 m, 140 m and 166 m are shown in Table 2.13. Appendix B presents the campaign documentation and Appendix C exhibits the mean monthly values and associated data coverage for the duration of the measurement period for select measurement heights.

Table 2.13 Lidar K13-A mean values across the measurement period

Height above MSL [m]	Data Type	Lidar K13-A	
		Mean value wind speed [m/s] wind direction [°]	Data Coverage [%]
166	Wind speed	10.21	98.9
141	Wind speed	10.10	98.9
91	Wind speed	9.95	98.9
166	Wind direction	241	98.9
141	Wind direction	240	98.9
91	Wind direction	239	98.9

Lidar K13-A data usability remarks

- The data gathered by lidar K13-A was found to be of very good quality with excellent data coverage.
- The overall wind speed data coverage at the heights of 91 m, 141 m and 166 m were excellent, each exceeding 95%.
- The data gathered by lidar K13-A were found to be appropriate for long-term correction to determine the long-term climate at this measurement location.

2.2.5 Remarks on compliance with best practices

FLS IJV

Three different RPS lidar 4.5 buoys (buoys 103, 104, 105) were installed during this measurement campaign to date. Prior to installation on site, the RPS lidar 4.5 buoys underwent validation campaigns [3]–[5] in September and October 2019 (buoy 103 and buoy 104) and August and September 2020 (buoy 105). The buoy validations were conducted by West Wind off the coast of Perth, Western Australia, against a reference lidar installed on a fixed navigation beacon. The validation campaign met all the KPIs specified by the OWA Roadmap [6] and was considered to be suitable for offshore wind resource assessments. It is recommended by the IEA to verify the performance of an FLS not more than a year prior to deployment on-site [7]. The validation campaign conducted for the RPS lidar 4.5 buoys falls outwith this recommended timeframe. This is considered to be a minor deviation from best practices.

The IEA recommends conducting a post-deployment check of the FLS unit only in cases where doubt arises through an accident or any impact that may have affected the FLS during deployment. No such incidents were recorded during the Project measurement campaign. However, as the pre-validation was conducted outwith the recommended timeframe prior to deployment, OWC recommends that post-verifications be conducted in accordance with best practises.

The vertical profiling lidars installed on each buoy underwent their own verification exercise conducted by DNV against a reference met mast near Pershore/Throckmorton in the UK [8]–[10]. The ZX lidars (ZX888, ZX874, ZX914) mounted on buoys 104, 103 and 105, respectively, were found to be able to reproduce cup anemometer wind speeds and wind directions at an accurate and acceptable level [6]–[8]. The ZX lidar914 passed all best practice criteria KPIs. The ZX lidars ZX888 and AX874 passed all best practice criteria KPIs with the exception of the IEC 61400-12-1 Edition 2 data bin averaging procedure for the lowest three heights of validation. The top height under verification passed this KPI as well. This is considered to be a very minor deviation with negligible impact on the associated uncertainty.

MM IJmuiden

The report [12] states that all relevant sensors mounted on the MM IJmuiden were calibrated according to ISO 17025 and signals were found to be in accordance with IEC61400-12. OWC is not in possession of the sensors' calibration certificates and was unable to source them online. It is unclear if the instruments were replaced or recalibrated during the measurement period at the MM IJmuiden. The MEASNET cooperation recommends in [14] that anemometers should be re-calibrated after 12 months of measurements. If this is not conducted the anemometer measurements can be tested to ensure that the calibration has been maintained throughout the measurement campaign.

In [15], ECN presents a comparison of the lidar and MM data gathered at the IJmuiden platform covering the period 01 January 2012 to 01 January 2014. The two datasets were found to have excellent agreement with an R^2 value greater than 0.99. This provides confidence in the MM IJmuiden measured wind data.

IJmuiden lidar

The documentation related to the IJmuiden lidar measurement campaign does not indicate whether the lidar was verified prior to installation at this measurement location. However, note that the IJmuiden lidar was deployed on the IJmuiden platform in 2012, prior to the publication of several recommended guidelines and standards. For instance, the IEA documentation on ground-based vertically profiling lidars was first published in 2013 and the TG6 guidelines started to incorporate recommendations on the application of lidars in their 9th revision which was issued in 2015. The recommended guidelines and standards on best practice for the deployment of lidars, which are now considered as industry-standard practices, has improved significantly since 2012.

In [15], ECN presents a comparison of the lidar and MM data gathered at the IJmuiden platform covering the period 01 January 2012 to 01 January 2014. The two datasets were found to have excellent agreement with an R^2 value greater than 0.99.

FLS HKW

At FLS HKW the initial buoys installed were the SWLBs WS188 and WS 187. These SWLBs underwent validation campaigns [17], [18] which were conducted by DNV GL (now DNV), next to the Island of Frøya in the Norwegian Sea against a fixed/ground-based industry-accepted lidar. The SWLBs were found to be able to demonstrate the capability to accurately measure wind speed and direction across a range of sea states and meteorological conditions.

A third SWLB measured intermittently at FLS HWK, the SWLB WS170. The SWLB WS170 was validated in situ at the FLS HKW C location against the WS187 installed at FLS HKW A and WS 188 installed at FLS HKW B. The validation, which was conducted by DNV GL showed that the SWLB WS170 was capable of producing accurate wind speed and direction data across the range of meteorological conditions experienced in the validation period [19]. The SWLB WS170 also underwent a post-deployment validation in May 2021 and was found to be capable of producing accurate wind speed and wind direction data [20].

Lidar K13-A

The lidar K13-A was installed on a production platform for natural gas. Offshore platforms are sizeable structures that may impact the free flow wind. According to [19], the lidar was installed at a location that has a ‘clear view’ and is free of obstacles. Whilst it is noted that natural gas production platforms may emit heat during operation that may impact the local wind climate, it is understood that the platform was not in production during the measurement campaign.

The lidar ZX563 installed at this measurement location, underwent a validation exercise against an onshore met mast prior to installation at the site and was found to be suitable to gather wind data [26]. The ZX563 gathered data for six consecutive years at this measurement location, exceeding the 30-month threshold recommended by the TG6 guidelines [27] as the maximum interval between pre-verification and post-verification (another verification).

Conclusions regarding best practices

During the comprehensive review, no deviations from established best practices were identified within the scope of the investigation. In the evaluation of uncertainty, the performance and quality of each primary dataset from the measurement campaigns were appropriately taken into account.

2.3 Secondary measurement campaigns

Secondary datasets are measured datasets gathered in the Dutch and German North Sea and have been mainly used to support the development and validation of the WRF mesoscale model created for this study.

A total of nine (9) secondary datasets gathered at various locations across the North Sea were considered. These data were gathered by met masts, FLS and vertical profiling lidars. Each of these datasets and their associated documentation are publicly available.

It is noted that FINO1 data from the FINO database were amongst the secondary datasets. The data was made available by the FINO initiative (research platforms in the North Sea and Baltic Sea), which was organized by the Federal Ministry for Economic Affairs and Energy (BMWi) on the basis of a resolution by the German Bundestag, the Jülich project management organization (PTJ) [5].

Each of the datasets was sourced by OWC. The data sourced was most often already analysed and post-processed by third parties. For each of the datasets, OWC observed their plausibility and ran high-level range checks on the wind speed and wind direction data. Data was screened out where necessary.

Following the post-processing, the datasets were observed for their data coverage and data quality. All datasets were considered suitable to support the mesoscale modelling validation process. Where necessary, co-located measurements taken for redundancy purposes were combined to create a single dataset with maximised data coverage.

Table 2.14 below presents an overview of the datasets considered and some key parameters. Figure 2.10 presents a Gantt chart of the secondary measured datasets. Appendix D presents an overview of each measurement campaign.

[6] The second edition of the standard was utilized in this study, even though a third edition is now available. The third edition of IEC 61400-12-1 has been introduced as part of a structural revision, replacing the performance standards IEC 61400-12-1:2017 and IEC 61400-12-2:2013. No technical alterations were introduced in this revision compared to IEC 61400-12-1:2017 and IEC 61400-12-2:2013 [45].

Table 2.14 Overview of secondary measurement campaigns

The start and end date indicate the measurement period considered in the study and not necessarily the start and end date of the measurement campaign.

Label	Type	Start date considered	End date considered	Range of measurement heights (MSL/LAT) [m]	Data coverage at WS 100 m	Reference
lidar LEG	lidar	17/11/2014	01/01/2022	62 m to 290 m MSL	83%	[30], [31]
lidar EPL	lidar	01/07/2016	01/01/2022	63 m to 291 m MSL	83%	[26] [33]
FLS HKN	FLS	10/04/2017	11/04/2019	30 m to 200 m MSL	88%	[34] [35]
FLS HKZ	FLS	05/06/2016	05/06/2018	30 m to 200 m MSL*	88%	[13], [36]
FLS TNW	FLS	19/06/2019	20/06/2021	30 m to 250 m LAT	90%	[37], [38]
FLS Borssele	FLS	12/02/2016	27/02/2017	40 m to 250 m MSL*	96%	[39]–[41]
FLS N-7.2	FLS	20/05/2020	04/05/2021	42 m to 250 m LAT	87%	[42]
MM OWEZ	MM	01/07/2005	02/07/2006	21 m to 116 m MSL	86%	[13], [43]
MM FINO1	MM	01/02/2004	31/12/2008	34 m to 103 m LAT	96%	[44]

* It is unclear from the documentation whether the reference height is MSL or LAT. It is assumed to be MSL for the purpose of this study.

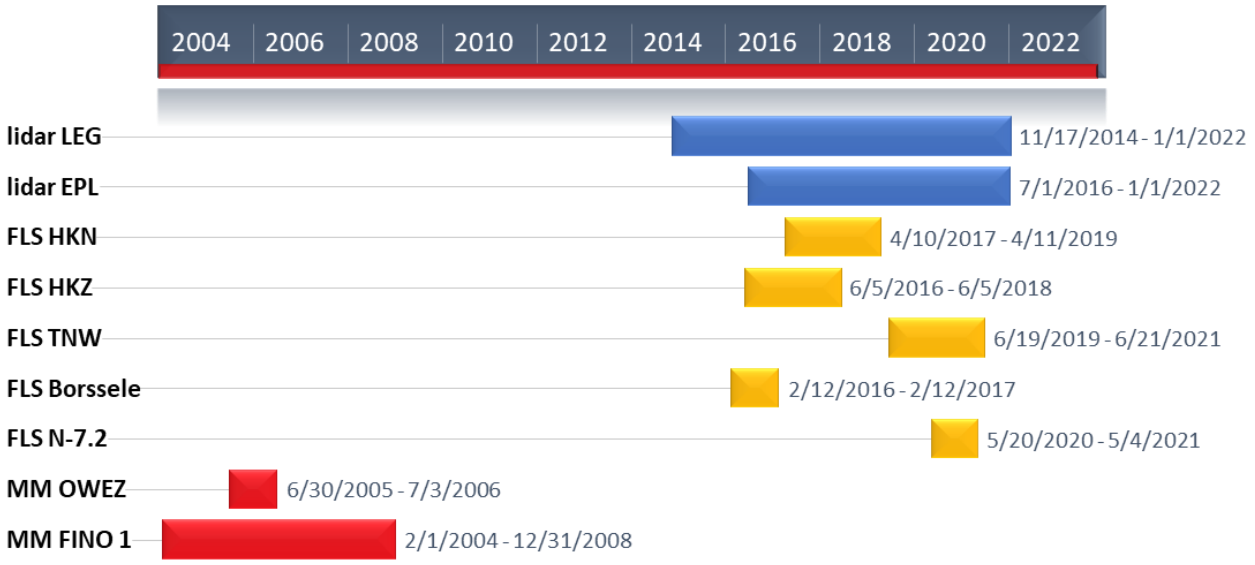

Figure 2.10 Gantt chart of measurement periods of secondary datasets

2.4 Uncertainty of measured wind speed

OWC has reviewed the uncertainty associated with the wind speed measured data in terms of instrument accuracy, mounting, the homogeneity of the surrounding wind flow as well as data quality and processing.

The second edition of IEC 61400-12-1:2017[6] specifies the use of lidar, with a detailed procedure (Annex L) that ensures the traceability of the measurements and evaluates associated uncertainty components, which can be applied in wind resource assessments [11]. This method is typically considered in verification reports of FLS.

The pre-deployment validation reports of IJVA and IJVB wind measurements did not include an analysis of the uncertainties in line with the above-mentioned IEC standard. However, prior to their deployment, the RPS lidar 4.5 buoys underwent validation campaigns as documented in references [3]–[5] and all buoys met best-practice criteria of OWA roadmap [6]. Since a comprehensive verification study for the FLS was lacking, along with a full uncertainty assessment, uncertainty of measured wind speed was estimated for each FLS unit based on available error metrics within the pre-deployment reports. The derived combined verification and classification uncertainties are summarized in Table 2.15. Subsequently, these unit-specific uncertainties were weighted according to measurement duration and availability to determine the uncertainty in measured wind speed at the IJVA and IJVB locations.

Variation in flow, data acquisition and post-processing uncertainty for the buoys are considered to be negligible due to the fact that the performance validation tests of the FLS units were conducted offshore. Furthermore, the vertical profiling lidars installed on each buoy underwent their own verification exercise conducted by DNV against a reference met mast [8]–[10] were found to be able to reproduce cup anemometer wind speeds and wind directions at an accurate and acceptable level [6]–[8].

The uncertainty related to the inhomogeneity in the wind flow was assumed to be 0% for all FLS units. The mounting uncertainty is regarded as negligible for the FLS, and it is further noted that it is partly concealed by its sensitivity to sea motions, which is already encompassed by the classification uncertainty [6].

[6] The second edition of the standard was utilized in this study, even though a third edition is now available. The third edition of IEC 61400-12-1 has been introduced as part of a structural revision, replacing the performance standards IEC 61400-12-1:2017 and IEC 61400-12-2:2013. No technical alterations were introduced in this revision compared to IEC 61400-12-1:2017 and IEC 61400-12-2:2013 [45].

Table 2.15 Uncertainty in measured wind speed (wind statistics) for the FLS units used at IJVWFZ

ID	FLS uncertainty description	Corresponding generic uncertainty per Table 2.17	buoy 103	buoy 104	buoy 105
F1	Calibration of lidar (from performance verification test)	G1, G3	3.4%*	4.6%*	3.1%*
F2	FLS classification	G1, G3, G4			
F3	Non-homogenous flow uncertainty	G1, G4	0.0%	0.0%	0.0%
F4	Mounting uncertainty	G2	0.0%	0.0%	0.0%
F5	Uncertainty in variation in flow, data acquisition and post processing	G1, G3, G4	0.0%	0.0%	0.0%
F0	**Uncertainty in measurements (instrument)**	**G0**	**3.4%**	**4.6%**	**3.1%**

* Approximation based on available error metrics

Finally, the given values were analysed and informed the weighted uncertainties for the IJVA and IJVB locations associated with the measurement uncertainty of the FLS, as shown in Table 2.16. It should be acknowledged that the determination of the sum total of uncertainties in measured wind speed was not feasible through binwise calculations, primarily because of the absence of verification analysis. It is further noted that the IJVA and IJVB have been aggregated into a single dataset prior to long-term correction, as discussed in the subsequent Section 3.3.1. The weighted total uncertainty of the IJV is 3.2% and further presented in Section 3.3.5.

Table 2.16 Uncertainty in measured wind speed (wind statistics) for IJVA and IJVB prior to data-aggregation

ID	FLS uncertainty description	Corresponding generic uncertainty per Table 2.17	FLS IJVA	FLS IJVB
F0	**Uncertainty in measurements (instrument)**	**G0**	**4.1%**	**3.2%**

No wakes and induction effects from nearby existing wind farms were applicable to the IJV measurements at the time of this analysis.

It is noted that no classification trial results have yet been published for the RPS at the time of this study, and the current type is understood to be stage 2 as per Carbon Trust roadmap. It is noted that a typical assumed class rating for an FLS, along with an anticipated verification uncertainty FLS based on historical performance and past verifications of similar units from other manufacturers, reinforces the estimated combined uncertainties (F1 and F2) presented in Table 2.15.

- The uncertainty in measurement accuracy has been assessed for each of the following primary datasets in terms of instrument accuracy and mounting, as well as data quality and processing as shown in Table 2.7.
- The lidar K-13A underwent validation at the ECN part of the TNO LiDAR Calibration Facility, where Meteorological Mast 4 measurements were conducted in compliance with IEC 61400-12-1:2005, Annex G, and LiDAR verification aligned with IEC 61400-12-1:2017, Annex L.

The validation process involved the assessment of Key Performance Indicators. Subsequent to the evaluation, the ECN section of TNO certified this LiDAR unit as suitable for offshore application at the K13-A production platform. The site-specific uncertainty in measured wind speed for lidar K13-A was determined based on the pre-deployment verification outcomes, the unit's classification, in addition to mounting uncertainties of 0.5%, and a modest uncertainty allocation of 0.2% to account for potential platform-related effects.

- Regarding MM IJmuiden it is noted that there is a previous WRA for Hollandse Kust (zuid) wind farm zone (HKZWFZ), issued in 2017 [13]. In light of the most recent validation studies carried out by TNO subsequent to the year of this evaluation, the assessment from 2017 is regarded as outdated. An extensively documented uncertainty assessment is available for review in the document [46]. TNO affirms that the configuration of the MM IJmuiden, along with its specific instrumentation, adheres to the criteria established in the IEC 61400-12-1 standard and MEASNET protocols. The uncertainty analysis outlined in this document aligns with the same standard and delineates the following components of uncertainty: calibration-related uncertainty, operational characteristics, mounting effects, and data acquisition.
- TNO estimated the combined uncertainty in measurement accuracy of the top anemometer to be 1.8% and 1.2% in the wind speed range 4 m/s and 16 m/s, respectively. For the purpose of this analysis 1.8% has been adapted as a conservative value for the combination of instrument accuracy and instrument mounting. Detailed information about the specific instrumentation can be found in [12]. Uncertainty in data quality and data processing have been kept as in [13].
- The uncertainties FLS HKW have been incorporated from the previous certified studies in the Dutch North Sea from the WRA for Hollandse Kust (west) wind farm zone (HKWWFZ), issued in 2020 [47].

Table 2.17 Uncertainty in measured wind speed (wind statistics) of the other primary datasets

ID	Generic (mast) uncertainty description	MM Ijmuiden	FLS HKW	Lidar K13-A
G1	Instrument accuracy	1.8%	2.6%	2.9%
G2	Instrument mounting		0.0%[7]	
G3	Data quality	0.5%	1.0%	
G4	Data processing	1.0%	1.0%	
G0	**Uncertainty in measured wind speed (wind statistics)**	**2.1%**	**2.9%**	**2.9%**

Each uncertainty in measurement wind speed is assumed to be independent and represented as a Gaussian distribution, so the subtotal uncertainty is calculated as the root-sum-square of all uncertainties.

3 Long-Term Wind Climate Calculation

This section presents the selection of the hub height of interest, followed by remarks on the wake impact from nearby operational wind farms on the primary measured datasets. This is followed by a description of the datasets selected for long-term corrections and any adjustment applied prior to conducting an MCP. Finally, the long-term correction of the primary measured data is presented along with its associated methodology and uncertainty.

3.1 Selection of representative height

The height of 160 m was selected as the height of interest for this assessment. The historic development of offshore wind turbine generators (WTG) shows an increase in hub heights for new turbines, while the average installed turbine hub height is growing with a time delay of several years [48], [49]. RVO is forward-looking and aims to install modern and state-of-the-art WTGs in the IJVWFZ development. It is noted that the opted hub height of 160 m is consistent with the recent North Sea recommendations stipulated by the Netherlands Wind Energy Association (NWEA) [50]. Therefore, a height of 160 m was selected as the appropriate choice.

3.2 Remarks on wake impact on measured data

The FLS HKW measurement campaign took place approximately 31 km west of the Prinses Amalia operational wind farm. Given that the measurements are a considerable distance away from the operational wind farm and any wake impact would lie within the non-prevailing wind directions, the wake impact of Prinses Amalia wind farm on the measurements at FLS HKW was considered to be negligible.

It is noted that a wind resource assessment for the HKWWFZ was presented in [47] based on the FLS HKW data. The study in [47] was certified by DNV that the wind climate at HKWWFZ has been derived in line with the requirements stated in Section 2.3.3 of the DNVGL-SE-0190 for site conditions and can be used for the design of the HKWWFZ [36]. In this study, it was assumed that the wind measurements gathered at the FLS HKW were free flow and the operational Prinses Amalia wind farm did not have any wake impact on the measurements.

The other primary datasets did not lie within the wake impact radius of any operational wind farm during their respective measurement periods.

3.3 Data selection for long-term correction

The primary datasets gathered at the four measurement locations were corrected to the long-term. The data from each of these measurement locations have good quality data with more than 12 months of consecutive measurements that cover all seasonal variations.

Prior to correcting to the long-term, the datasets were adjusted in the following way:

- The FLS IJV data at the height of 160 m was combined into a single dataset.
- The MM IJmuiden data at the height of 92 m was vertically extrapolated to the height of 160 m by applying wind shear measurement gathered by the lidar IJmuiden.
- The FLS HKW data at the height of 160 m was combined into a single dataset.
- The lidar K13-A data at the height of 166 m was vertically extrapolated to the height of 160 m.

The following sections describe the methodology applied for each of the above adjustments.

3.3.1 FLS IJV: combining FLS IJV A and FLS IJV B

The FLS IJV A and FLS IJV B datasets were combined to form a single dataset that is representative of the short-term measurements at the site that maximises the data coverage.

As observed in Section 2.2.1, the data coverage at the height of 160 m is 92.1% and 94.5% at FLS IJV A and FLS IJV B, respectively. Given that the data at both locations is of excellent quality, the FLS IJV B dataset was selected as the primary dataset since it has higher data coverage. Therefore, FLS IJV A was used as the backup dataset to fill the minimal gaps within the FLS IJV B dataset. This combined dataset will be referred to as FLS IJV.

Prior to selecting the combination method, the following key performance indicators (KPIs) were observed:

- Wind speed and wind direction correlation[8].
- Data coverage and data quality.
- Mean bias error in mean wind speed for the concurrent data.
- Measurement uncertainty associated with each measured dataset.

FLS IJV: wind speed and wind direction correlations

The wind speed and wind direction correlations of the FLS IJV A and FLS IJV B concurrent datasets were investigated at the height of 160 m.

The coefficient of determination (R^2) was found to be 0.99 for wind speed and wind direction for the FLS IJV A and FLS IJV B data at the height of 160 m. The almost unity R^2 is an expected outcome from a correlation analysis between two FLS in close proximity offshore. A scatter plot of the wind direction data and a sectorwise scatter plot of the wind speed data are shown in Figure 3.1 and Figure 3.2, respectively.

8

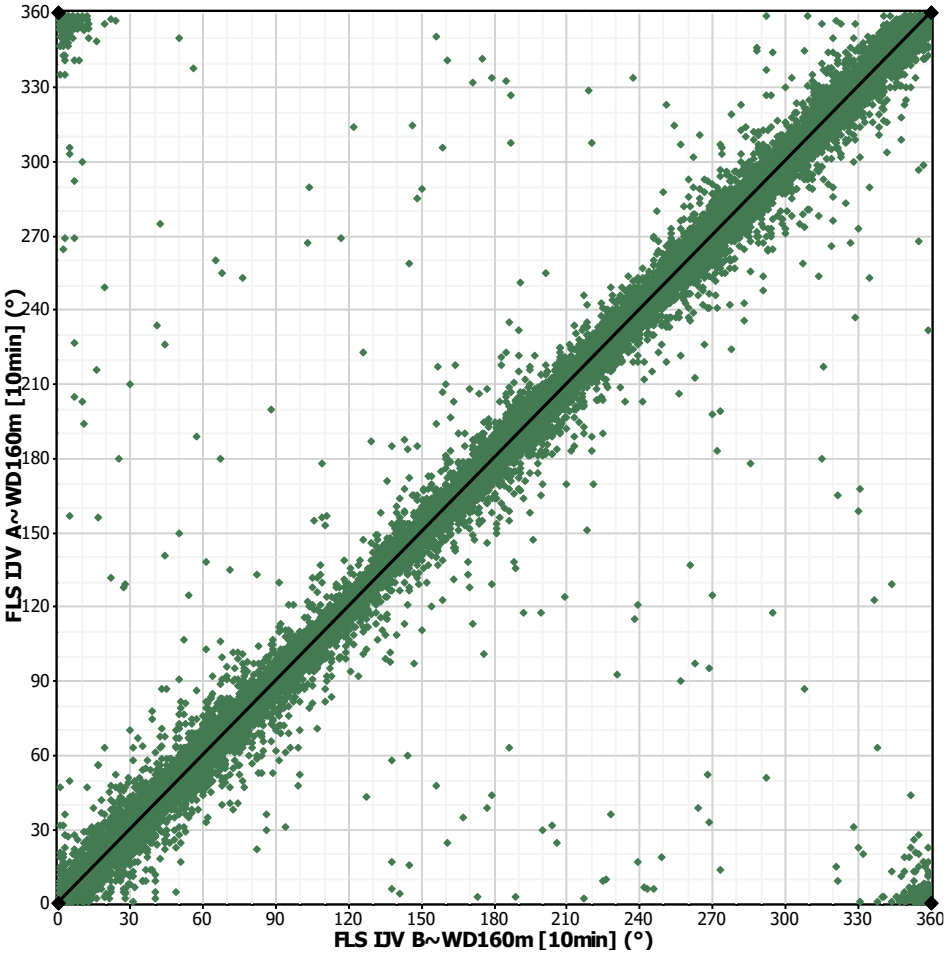

Figure 3.1 Scatter plot of FLS IJV A vs FLS IJV B 160 m wind direction

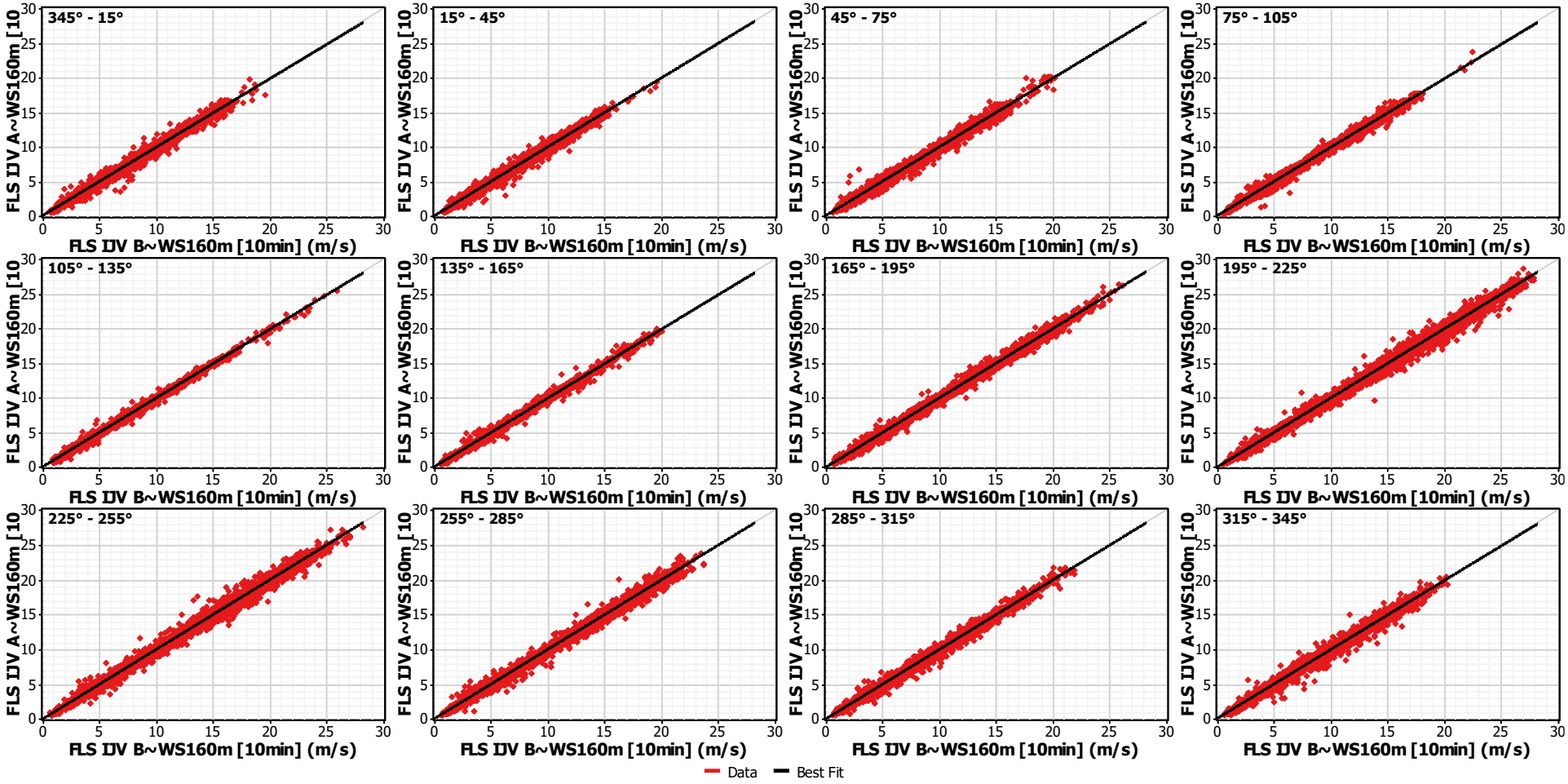

Figure 3.2 Sectorwise scatter plots of FLS IJV A vs FLS IJV B 160 m wind speed

The sectorwise correlations for the wind speed data are presented in Table 3.1. It can be observed that the R^2 value is 0.99 across all sectors, indicating a very strong relationship between the two datasets.

Table 3.1 FLS IJV A vs FLS IJV B sectorwise 160 m wind speed R^2 values

Sector	160 m WS R^2 value
345° - 15°	0.99
15° - 45°	0.99
45° - 75°	0.99
75° - 105°	0.99
105° - 135°	0.99
135° - 165°	0.99
165° - 195°	1.00
195° - 225°	0.99
225° - 255°	0.99
255° - 285°	0.99
285° - 315°	0.99
315° - 345°	0.99
All	**0.99**

FLS IJV: mean wind speed bias for concurrent data

The exact concurrent period between FLS IJV A and FLS IJV B was used to assess the mean wind speed values measured by the two locations. The results of these are presented in Table 3.2. As can be observed the concurrent mean wind speed at the two locations is identical when observed to two decimal places. The mean bias error between the two datasets is very small at 0.06%. This, once again, indicates the strong relationship between the two datasets.

Table 3.2 FLS IJV A vs FLS IJV B 160 m mean wind speed and bias error

Parameter	FLS IJV A 160 m	FLS IJV B 160 m
Concurrent mean wind speed [m/s]	9.92	9.92
Mean bias error [m/s]	0.006	
Mean bias error [%]	0.06	

FLS IJV: data combination

The FLS IJV A and FLS IJV B were combined to derive a single FLS IJV dataset with maximised data coverage. The following observations are made:

- The wind speed correlations between FLS IJV A and FLS IJV B are excellent with R^2 values of 0.99 in each direction sector.
- The coefficient of determination of wind direction between FLS IJV A and FLS IJV B is excellent with an R^2 value of 0.99.
- For the same measurement period, FLS IJV B has a marginally higher data coverage at 94.5% while FLS IJV A has a corresponding value of 92.1%.
- The measurement uncertainties associated with FLS IJV A and FLS IJV B are in good alignment, as shown in Section 2.4
- For concurrent data, the wind speed bias between the two datasets if 0.06% which is well within the uncertainty associated with the measured data.

Based on the above points, FLS IJV A and FLS IJV B exhibit excellent alignment in measurements and can be combined into a single dataset with a high associated confidence. Therefore, given that FLS IJV B has the higher data coverage and the lower uncertainty in the measurements, this dataset was considered primary and FLS IJV A was used as a back-up to fill any gaps in the FLS IJV B data.

The final combined dataset had an increased data coverage of 96.6% for the period 01 May 2022 to 01 June 2023, with a final wind speed value of 9.79 m/s at 160 m. It is noted that the data coverage of the combined FLS IJV data at the height of 160 m has improved the data coverage in each month within the measurement period. This is particularly true for April 2023 and May 2023 (increased to 92% and 88%, respectively) where lower data coverage is observed at both FLS IJV A and FLS IJV B.

As most of the combined dataset is comprised of the FLS IJV B data, the reference location for the FLS IJV dataset is considered to be at the FLS IJV B location.

Table 3.3 Combined FLS IJV dataset overview

Parameter	FLS IJV 160 m
Location [latitude, longitude]	52°53’39” N 3°41’07” E
Measurement period available for analysis	01/05/2022 to 01/06/2023,
Measurement averaging interval [min]	10
Mean wind speed at 160 m [m/s]	9.79
Data coverage of 160 m wind speed [%]	96.6
Mean wind direction at 160 m [°]	247.5
Data coverage of 160 m wind direction [%]	96.5

3.3.2 MMIJ: vertical extrapolation

The MM IJmuiden top wind speed measured data at the height of 92 m was vertically extrapolated to the 160 m height of interest. For this purpose, the wind shear measured by the co-located lidar IJmuiden was applied.

The lidar IJmuiden wind speed data at the height of 115 m, 140 m, 165 m, and 190 m were used to observe the wind shear. The data was seasonally

balanced to have an equal representation of summer and winter months and avoid any seasonal bias. The overall omni-directional measured wind shear coefficient[9] at the lidar IJmuiden was found to be 0.07.

The wind shear coefficients were obtained through the vertical wind shear profile and by analysing the monthly and diurnal variations. These can be observed in Figure 3.3 and Table 3.4.

The lidar IJmuiden wind shear on a monthly versus diurnal basis was applied for the vertical extrapolation to the MM IJmuiden 92 m wind speed data. The final wind speed at the height of 160 m at MM IJmuiden is 10.36 m/s.

It is noted that wind shear coefficients obtained at the MM IJmuiden were not applied for vertical extrapolation, as the MM IJmuiden measurement heights are not high enough to provide a reliable understanding of the vertical wind profile at the higher heights. As the lidar dataset is not concurrent with the measurement at MM IJmuiden, a statistical matrix approach rather than a time-series approach was chosen.

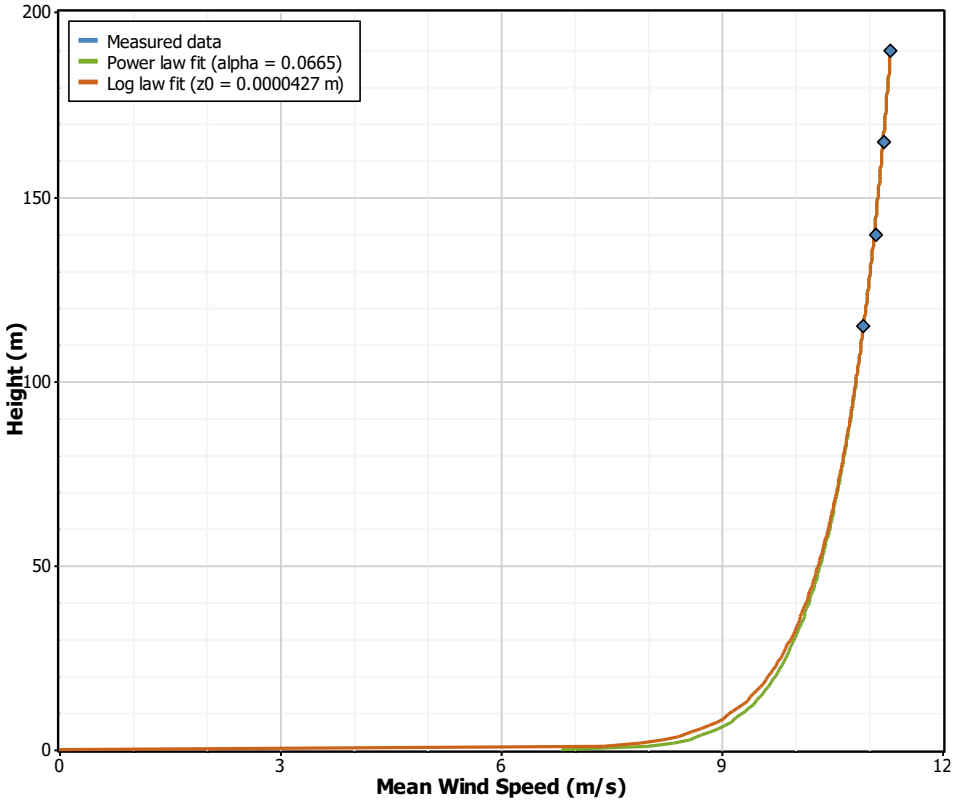

Figure 3.3 Lidar IJmuiden vertical wind profile

[9] Obtained from the power law

Table 3.4 Lidar IJmuiden monthly versus diurnal wind shear coefficients

Hour (UTC+1)	Jan	Feb	Mar	Apr	May	Jun	Jul	Aug	Sep	Oct	Nov	Dec	All
00:00 - 01:00	0.09	0.08	0.06	0.09	0.06	0.09	0.05	0.07	0.02	0.05	0.06	0.08	0.07
01:00 - 02:00	0.09	0.08	0.07	0.09	0.06	0.08	0.09	0.08	0.02	0.05	0.06	0.08	0.07
02:00 - 03:00	0.09	0.09	0.06	0.06	0.06	0.07	0.08	0.08	0.02	0.04	0.06	0.08	0.07
03:00 - 04:00	0.10	0.09	0.04	0.06	0.07	0.08	0.07	0.06	0.02	0.06	0.06	0.09	0.07
04:00 - 05:00	0.09	0.08	0.05	0.05	0.07	0.08	0.04	0.06	0.04	0.05	0.06	0.08	0.07
05:00 - 06:00	0.09	0.08	0.04	0.05	0.06	0.07	0.03	0.05	0.03	0.06	0.06	0.08	0.06
06:00 - 07:00	0.09	0.08	0.05	0.04	0.06	0.07	0.02	0.05	0.03	0.06	0.05	0.08	0.06
07:00 - 08:00	0.09	0.09	0.05	0.05	0.06	0.06	0.02	0.05	0.02	0.06	0.05	0.08	0.06
08:00 - 09:00	0.09	0.09	0.06	0.06	0.06	0.06	0.03	0.05	0.02	0.05	0.04	0.08	0.06
09:00 - 10:00	0.09	0.08	0.07	0.07	0.07	0.05	0.04	0.06	0.01	0.06	0.04	0.08	0.06
10:00 - 11:00	0.09	0.06	0.07	0.08	0.08	0.07	0.03	0.05	0.02	0.05	0.05	0.08	0.06
11:00 - 12:00	0.09	0.06	0.07	0.08	0.07	0.09	0.03	0.06	0.02	0.05	0.05	0.08	0.06
12:00 - 13:00	0.07	0.07	0.07	0.08	0.07	0.09	0.04	0.06	0.02	0.06	0.05	0.09	0.07
13:00 - 14:00	0.08	0.08	0.07	0.09	0.06	0.08	0.04	0.07	0.02	0.06	0.06	0.09	0.07
14:00 - 15:00	0.08	0.08	0.07	0.10	0.07	0.07	0.04	0.08	0.02	0.06	0.06	0.09	0.07
15:00 - 16:00	0.08	0.08	0.08	0.10	0.09	0.08	0.04	0.08	0.03	0.06	0.07	0.09	0.08
16:00 - 17:00	0.08	0.08	0.08	0.10	0.07	0.06	0.08	0.08	0.04	0.06	0.07	0.08	0.07
17:00 - 18:00	0.07	0.07	0.07	0.09	0.07	0.06	0.07	0.07	0.04	0.07	0.06	0.10	0.07
18:00 - 19:00	0.08	0.09	0.08	0.08	0.07	0.06	0.06	0.08	0.04	0.06	0.07	0.09	0.07
19:00 - 20:00	0.08	0.10	0.08	0.09	0.08	0.09	0.06	0.08	0.04	0.06	0.07	0.08	0.08
20:00 - 21:00	0.08	0.10	0.08	0.10	0.09	0.08	0.06	0.08	0.04	0.06	0.07	0.08	0.08
21:00 - 22:00	0.09	0.09	0.07	0.11	0.08	0.08	0.02	0.10	0.05	0.06	0.07	0.08	0.08
22:00 - 23:00	0.08	0.09	0.06	0.08	0.07	0.08	0.04	0.08	0.04	0.06	0.06	0.09	0.07
23:00 - 24:00	0.09	0.09	0.06	0.10	0.06	0.08	0.04	0.07	0.04	0.05	0.06	0.09	0.07
All Hours	0.09	0.08	0.07	0.08	0.07	0.07	0.05	0.07	0.03	0.06	0.06	0.08	0.07

3.3.3 FLS HKW: combining FLS HKW A, FLS HKW A02, FLS HKW B, FLS HKW C

The FLS HKW datasets were combined to form a single dataset that is representative of the short-term measurements at the site that maximises the data coverage.

The methodology applied to combine the datasets was thoroughly investigated in the wind resource assessment conducted for the HKWWFZ and is reported in [26], which is a certified report by DNV. Therefore, the same method is replicated in this analysis and briefly described below.

As observed in Section 2.2.3, the data coverage at the height of 160 m is poor at the FLS HKW A-2, FLS HKW B and FLS HKW C locations. The highest data coverage is at the FLS HKW A location at 84%. None of the measurement locations covers the full measurement period, as described in Section 2.2.3. Therefore, to maximise the data coverage as much as possible the datasets were combined such that FLS HKW A and FLS HKW A-2, which cover consecutive measurement periods and are quasi-co-located, were considered primary while FLS HKW B and FLS HKW C were used as back up to fill in any existing gaps. This combined dataset will be referred to as FLS HKW.

In [26] the following key performance indicators (KPIs) were investigated;

- Distance between the measurement locations.
- Data coverage and data quality.
- Wind speed and wind direction correlation.
- Mean bias error in mean wind speed for the concurrent data.

To ensure a comprehensive review, correlations between wind speed and direction, as well as the mean wind speed bias for concurrent data, will be detailed for the targeted height of 160 m in the ensuing sections.

FLS HKW: wind speed and wind direction correlations

The wind speed and wind direction coefficient of determination factors of the FLS HKW A, FLS HKW A-2, FLS HKW B and FLS HKW C pairs of concurrent datasets were observed at the height of 160 m. It is noted that concurrency across datasets could not be observed due to low periods of overlap between the measurements.

It can be observed in Table 3.5 and Table 3.6 that there are excellent coefficients of determination for the concurrent measured dataset pairs, indicating a strong correlation between them.

Table 3.5 FLS HKW A, FLS HKW A-2, FLS HKW B, FLS HKW C 160 m wind speed R^2 values

160 m WS	FLS HKW A	FLS HKW A-2	FLS HKW B	FLS HKW C
FLS HKW A	-	No concurrency	0.99	0.99
FLS HKW A-2	No concurrency	-	0.99	No concurrency
FLS HKW B	0.99	0.99	-	0.99
FLS HKW C	0.99	No concurrency	0.99	-

Table 3.6 FLS HKW A, FLS HKW A-2, FLS HKW B, FLS HKW C 160 m wind direction R^2 values

160 m WS	FLS HKW A	FLS HKW A-2	FLS HKW B	FLS HKW C
FLS HKW A	-	No concurrency	0.98	0.99
FLS HKW A-2	No concurrency	-	0.98	No concurrency
FLS HKW B	0.98	0.98	-	0.99
FLS HKW C	0.99	No concurrency	0.99	-

FLS HKW: mean wind speed bias for pairs of concurrent data

The concurrent pairs of data between FLS HKW A, FLS HKW A-2, FLS HKW B and FLS HKW C were used to assess the mean wind speed values measured by these locations.

It is noted that there is no concurrency between FLS HKW A and FLS HKW A-2, FLS HKW A-2 and FLS HKW B and FLS HKW A-2 and FLS HKW C.

The results of these are presented in Table 3.7. As can be observed the concurrent mean wind speed at the locations is very similar with low mean bias error. It is noted that all the mean bias error values observed are within the measured uncertainty margin and in line with what was observed in [26]. This, once again, indicates the strong relationship between the datasets.

Table 3.7 FLS HKW A, FLS HKW A-2, FLS HKW B, FLS HKW C 160 m mean wind speed and bias error

Parameter	FLS HKW A 160 m	FLS HKW B 160 m
Concurrent mean wind speed [m/s]	9.41	9.44
Mean bias error [m/s]	0.03	
Mean bias error [%]	0.32%	
Parameter	**FLS HKW A 160 m**	**FLS HKW C 160 m**
Concurrent mean wind speed [m/s]	10.31	10.32
Mean bias error [m/s]	0.01	
Mean bias error [%]	0.10%	
Parameter	**FLS HKW A-2 160 m**	**FLS HKW B 160 m**
Concurrent mean wind speed [m/s]	9.77	9.77
Mean bias error [m/s]	0.00	
Mean bias error [%]	0.00%	

Parameter	FLS HKW B 160 m	FLS HKW C 160 m
Concurrent mean wind speed [m/s]	11.16	11.18
Mean bias error [m/s]	0.02	
Mean bias error [%]	0.18%	

FLS HKW: data combination

The FLS HKW datasets were combined to derive a single FLS HKW dataset with maximised data coverage. The following observations are made:

- The distance between the respective measurement locations at FLS HKW is less than 2 km. The small distance between the measurement locations implies that there is negligible discrepancy in wind climate observed at the different measurement locations.
- The squared correlation coefficients (coefficient of determination, R^2) between FLS HKW A, FLS HKW A-2, FLS HKW B and FLS HKW C are excellent with R^2 values of 0.98 and higher across the pairs of datasets.
- FLS HKW A has the highest data coverage, followed by FLS HKW A-2.
- For concurrent pairs of data, the wind speed bias error is well within the uncertainty associated with the measured data.

Based on the above points, FLS HKW A, FLS HKW A-2, FLS IJV B and FLS HKW C have a strong behavioural relationship and can be combined into a single dataset with a high associated confidence. Therefore, FLS HKW A and FLS HKW A-2 were considered primary and FLS IJV B and FLS HKW C were used as a back-up to fill any remaining gaps.

The final combined dataset had an increased data coverage of 94.4% for the period 05 February 2019 to 12 February 2021, with a final wind speed value of 10.43 m/s.

The reference location for the FLS HKW dataset is considered to be the same as that derived in [26] and presented in the Table 3.8 below.

Table 3.8 Combined FLS HKW dataset overview

Parameter	FLS HKW 160 m
Location [latitude, longitude]	52°34’11.75” N, 3°43’36.05” E
Measurement period available for analysis	05/02/2019 to 12/02/2021
Measurement averaging interval [min]	10
Mean wind speed at 160 m [m/s]	10.43
Data coverage of 160 m wind speed [%]	94.4
Mean wind direction at 160 m [°]	238
Data coverage of 160 m wind direction [%]	94.4

3.3.4 Lidar K13-A: vertical extrapolation

The lidar K13-A wind speed measured data at the height of 166 m was vertically extrapolated to the 160 m height of interest.

The lidar K13-A wind speed data at the height of 116 m, 141 m, 166 m, and 191 m were used to observe the wind shear. The overall measured wind shear coefficient at the lidar IJmuiden was found to be 0.07.

Following a wind shear analysis, the power law wind shear exponents were evaluated from the vertical profile shown in Figure 3.4.

The vertical extrapolation was conducted by vertically extrapolating the wind speed data at the height of 166 m by using the power law wind shear exponents obtained from the measurement heights of 116 m, 141 m, 166 m, and 191 m on a timestep basis. The final wind speed at the height of 160 m at lidar K13-A is 10.19 m/s.

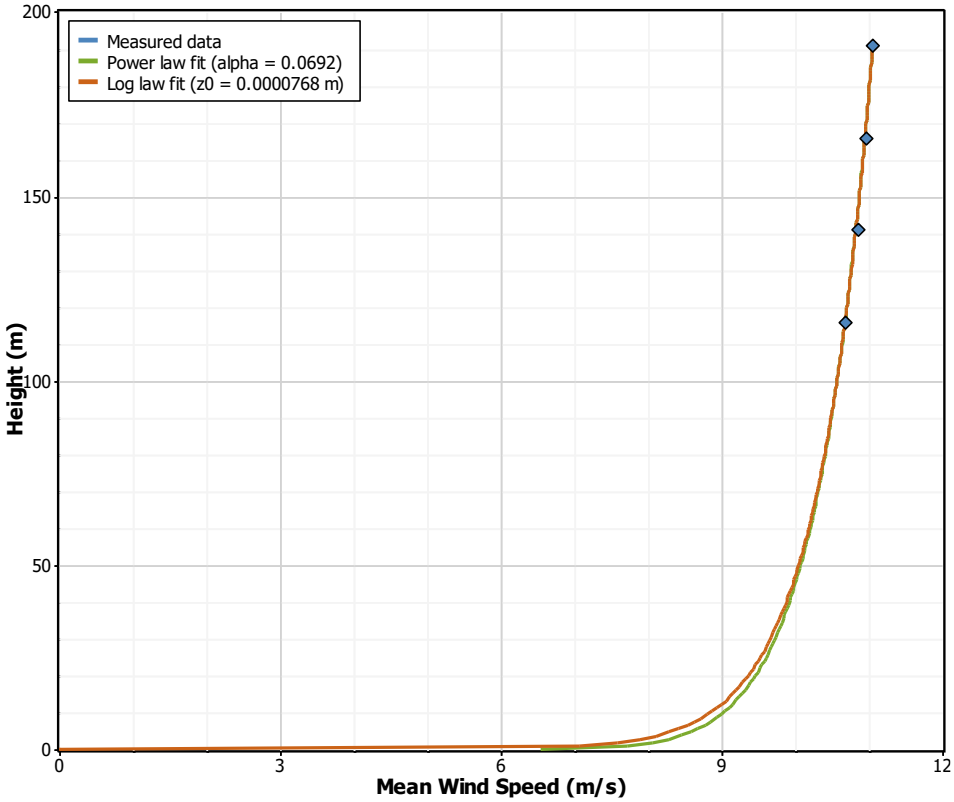

Figure 3.4 Lidar K13-A vertical wind profile

3.3.5 Uncertainty in IJVWFZ wind speed measurements

The uncertainty in measurement accuracy for the aggregated IJW dataset is presented in Table 3.9.

Table 3.9 Uncertainty in measured wind speed (wind statistics) for IJV

Uncertainty Description	IJV
Instrument accuracy	3.2%
Instrument mounting	
Data quality	

Uncertainty Description	IJV
Data processing	
Data aggregation	negligible
Wake and induction corrections	not applicable
Uncertainty in measured wind speed (wind statistics)	**3.2%**

The uncertainty in the data aggregation was estimated to be negligible, as the mean bias error is near null, as presented in Table 3.2. At the time of the assessment no wake and induction corrections are applicable to IJV measurements.

A vertical wind speed profile was derived at the primary dataset locations to represent the variation of the wind speed over the rotor, and hub heights other than the target height (160 m) of this report. The vertical wind profiles of the short-term measured wind speed at the datasets and the long-term modelled data is shown in Section 6.5 in Figure 6.3 for IJV.

The vertical profile was determined from:

- The long-term data for different heights
- Measurements of the vertical wind speed profile

A wind speed profile was fitted to the data above. The deviations of the data from the model can be used as an indicator of the vertical extrapolation uncertainty. In the case of the primary datasets and the specific IJVWFZ, measured shear was utilized for the purpose of wind speed interpolation on a timestep basis, which is commonly referred to as vertical extrapolation within the industry. Given the characteristics of the RSD technology and the extensive coverage of higher measurement heights, uncertainty in the vertical extrapolation is deemed to be negligible for IJV, FLS HKW, and Lidar K13-A. For MM Ijmuiden the uncertainty in vertical extrapolation was estimated from the use of measured power law wind shear exponents.

Finally, the uncertainty in measured wind speed and vertical extrapolation for all datasets are shown in Table 3.10.

Table 3.10 Uncertainty in measured wind speed (wind statistics) and vertical extrapolation, including IJV (combined)

Uncertainty Description	IJV	MM Ijmuiden	FLS HKW	Lidar K13-A
Uncertainty in measured wind speed (wind statistics)	3.2%	2.7%	2.9%	2.9%
Vertical extrapolation	-	0.4%	-	-

3.4 Long-term climate calculation

The calculation of the long-term climate at each of the four primary measurement locations was based on the 160 m measured datasets. The long-term calculation was done by applying ERA5 reanalysis data as a reference using a measure-correlate-predict (MCP) procedure. The MCP method analyses the statistical relationship between the short-term measured data and the concurrent data from the reference. The statistical relationship between the two datasets is then used to predict and synthesise the short-term data to the

long-term. The synthesis method extends the measured data but does not replace it.

The short-term measured datasets were seasonally balanced prior to conducting the MCP procedure. This avoids any seasonal bias in the long-term correction. This was done by ensuring an equal number of timesteps in the summer and winter months, whereby summer is from 21 March to 20 September and winter is from 21 September to 20 March.

3.4.1 Long-term reference data selection

Several long-term model data sources were considered as long-term reference data. The suitability of each of these sources was assessed based on the thorough validation procedure described below.

- **ERA5** is a continuously updated reanalysis dataset, which is provided by the European Centre for Medium-Range Weather Forecasts (ECMWF). A broad range of meteorological parameters is available, for the time from 1950 up until near real-time (with an approximately five-day delay). ERA5 data is provided with a spatial resolution of approximately 30 km (0.25°) and a temporal resolution of one hour [51]
- **EMD WRF Europe+** is a mesoscale modelled data generated by EMD using the WRF numerical weather prediction model. It is only available via EMD WindPRO software, METEO module. The EMD WRF Europe+ data is initiated using ERA5 reanalysis data developed by ECMWF. The mesoscale model is run with a spatial resolution of 3 km by 3 km with hourly temporal resolution. This data is available at multiple heights [52].
- **MERRA-2** reanalysis data is the second version of the Modern-Era Retrospective analysis for Research and Application (MERRA), provided by NASA. MERRA-2 data is available for the period since 1980 at a temporal resolution of one hour and a spatial resolution of 50 km in the latitudinal direction [53].

All the reference datasets were sourced for the most recent 20 years, concurrently with the measured datasets. The selection of the reference dataset was based on a validation procedure that considered the following parameters:

- Coefficient of determination with measured wind speed data (R^2).
- Coefficient of determination with measured wind direction data (R^2).
- Height of reference dataset.
- Distance between the data node and measurement location.
- Data availability.
- Acceptance within the industry.

Table 3.11 below shows the comparison of the above parameters for each reference source and the short-term correlation (R^2) values of each reference dataset against the respective measured wind speed datasets. A depiction of the long-term trend across the selected period is shown in Appendix E.

It is noted that there are other publicly available reference datasets considered to be reliable and well accepted within the industry, such as the Dutch Offshore Wind Atlas (DOWA) mesoscale dataset. However, the other sources available

do not overlap with all the primary measured datasets, particularly FLS IJV and FLS HKW which are the most recently gathered data.

Table 3.11 MCP reference datasets comparison

Parameter	Reference data source	FLS IJV	MMIJ	FLS HKW	Lidar K13-A
No. of concurrent hourly timesteps		8,668	33,949	16,516	43,437
Reference dataset location [latitude, longitude]	ERA5	53.000°N, 3.750°E	52.750°N, 3.500°E	52.500°N, 3.750°E	53.250°N, 3.250°E
	EMD-WRF Europe+	52.883°N, 3.683°E	52.851°N, 3.418°E	51.557°N, 3.743°E	53.213°N, 3.204°E
	MERRA2	53.000°N, 3.750°E	53.000°N, 3.125°E	52.500°N, 3.750°E	53.000°N, 3.125°E
Height [m]	ERA5	100			
	EMD-WRF Europe+	100			
	MERRA2	50			
R^2 wind speed	ERA5	**0.91**	**0.92**	**0.93**	**0.92**
	EMD-WRF Europe+	0.89	0.91	0.91	0.90
	MERRA2	0.88	0.90	0.91	0.88
R^2 wind direction	ERA5	**0.95**	**0.97**	**0.96**	**0.96**
	EMD-WRF Europe+	0.94	0.96	0.95	0.96
	MERRA2	0.95	0.96	0.95	0.95
Distance from site [km]	ERA5	12.7	12.0	7.8	4.2
	EMD-WRF Europe+	1.2	1.3	1.8	1.2
	MERRA2	12.7	27.0	7.8	25.6
Data availability [%]	ERA5	100			
	EMD-WRF Europe+	100			
	MERRA2	100			
Grid resolution [km]	ERA5	31			
	EMD-WRF Europe+	3			
	MERRA2	38			

Based on the sources presented in Table 3.11, ERA5 shows the best correlation to the measured dataset. It is a well-known and accepted dataset within the industry and was therefore chosen as the reference dataset for the MCP.

A long-term trend analysis on the ERA5 reference datasets was conducted to select the most suitable long-term period with the lowest bias. Different long-term periods ranging from 10 years to 20 years were observed. A period was selected that minimises the effect of a possible trend while remaining representative of the long-term today. The selected long-term period was from 01 January 2010 to 31 December 2022, a period of 13 years.

It is noted that the FLS IJV measured data ends on 31 May 2023 and hence extends further than the selected reference long-term period. However, the correlation between the measured and reference datasets was based on the full overlap between the two datasets.

3.4.2 MCP method selection

The measure correlate predict (MCP) methods typically analyse the statistical relationship between the short-term measured dataset and concurrent data from the long-term reference dataset. Applying this relationship to long-term data allows extending the short-term measured time series to include the long-term period. The new time series acquires the statistical properties of the long-term reference data while reproducing the measured data. Note that this method is commonly, but somewhat misleading, referred to as carrying out a long-term correction of the short-term data.

An MCP algorithm can be defined as the combination of a method, sub-method, model and concept [54]. Linear regression is the method used, the sub-methods linear least squares (LLS) and total least squares (TLS) describe how the model is optimised to get a linear fit, whilst the model choices concentrate on the specifics of model selections. Lastly, the model may be fitted numerous times for various sectors, or it can be based on multiple data such as with a high temporal resolution (hourly) or fewer values such as with a monthly resolution. As an example of a monthly resolution, one may evaluate the relative weights of each month. The final MCP algorithm is defined by these circumstances, as illustrated in Figure 3.5 [54].

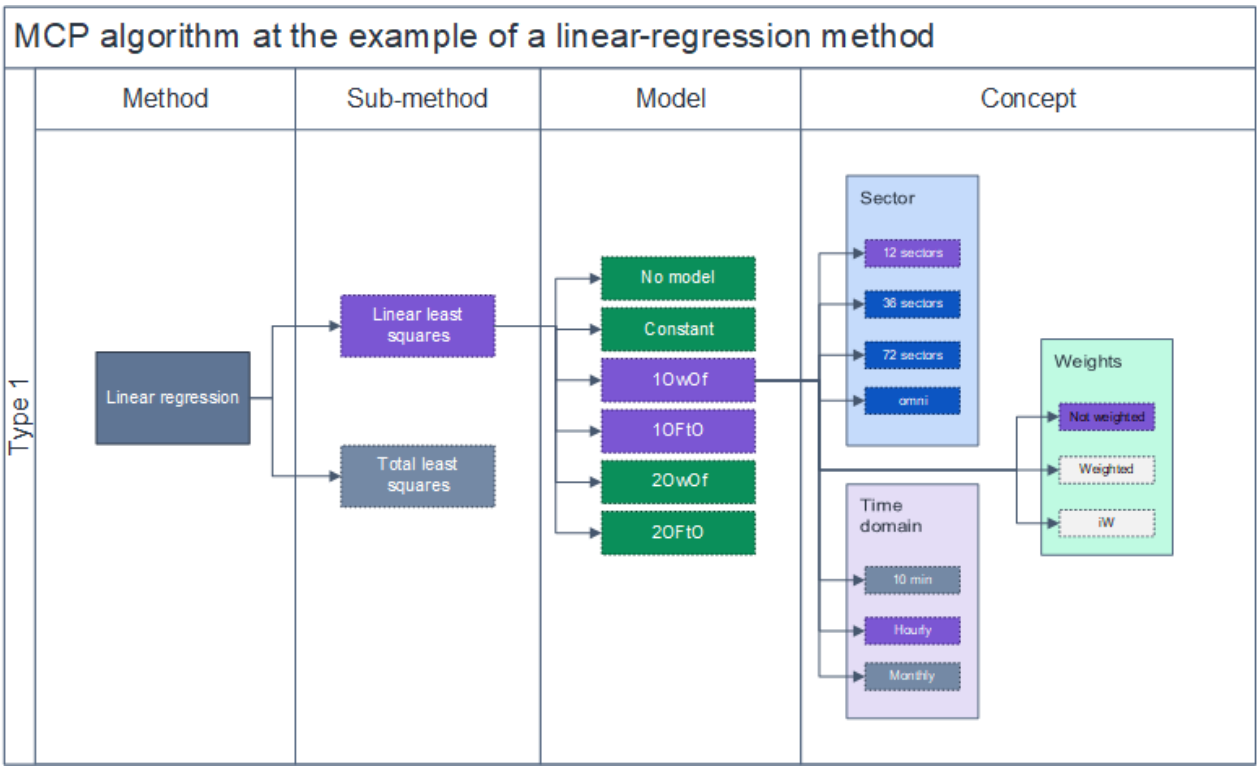

Figure 3.5 Definition of an MCP algorithm at the example of linear regression [54]

Different MCP algorithms implementing sub-methods were tested and results observed for different statistical KPIs. Following the testing of each of the MCP algorithms, their statistical KPIs were observed and scored, depending on the outcome. The MCP algorithm with the highest score was selected as the best performing. Given the excellent correlation results and OWC's familiarity with the regional climate, the linear regression method was chosen as a starting point by OWC in advance. The MCP algorithms (short: Algo) that were tested are presented in Table 3.12.

The MCP methods were tested with the FLS IJV and MM IJmuiden datasets are presented below.

Table 3.12 Different MCP algorithms tested

Parameters	Algo 1	Algo 2	Algo 3	Algo 4
Method	Linear regression			
Sub-method	LLS*	TLS	LLS	TLS**
Model	Linear first-order polynomial with offset			
Concept parameters				
Number of sectors	12	12	16	16
Temporal resolution	1 day	1 hour	1 hour	1 hour
Weighting	-	-	-	-

*Linear least square (LLS)

**Total least square (TLS)

Each of these MCP algorithms was observed for the following KPIs:

- Mean bias error (MBE)
- Mean absolute error (MAE)
- Distribution error (DE) of Kolmogorov Smirnov
- Long-term climatic adjustment factor for wind speed (LCA)
- Bootstrapping statistical procedure for relative standard deviation

The LCA is the factor by which the measured short-term dataset would need to be scaled to reflect the expected long-term mean conditions.

The MBE, MAE and DE were determined by randomly dividing the short-term measurements and using one-half of the data as input and the other half as a reference to compare the MCP output. This operation was carried out 100 times with different randomised data divisions. As a result of the performance test, the mean bias error (MBE), mean absolute error (MAE) and distribution error (DE) intrinsic to each MCP estimator were quantified.

The bootstrapping simulation was run with 3000 iterations to create a distribution of results and observe the associated relative standard deviation. This exercise indicates the confidence associated with the correlation between the two datasets and informs the correlation uncertainty associated with the MCP procedure applied.

The results of the KPIs for each of the MCP algorithms are presented in Table 3.13 and Table 3.14 when tested with FLS IJV and MM IJmuiden and their respective ERA5 dataset. Based on these results the following is observed:

- The MBE value is quasi-identical across all algorithms for both measured datasets.
- The MAE value is marginally lower for the LLS method than the TLS method for both pairs of datasets.
- The DE method is slightly lower for the TLS method than the LLS method for both pairs of datasets.
- Similar LCA values are observed across all algorithms for each respective pair of datasets.
- The LLS method shows a marginally lower bootstrapping uncertainty at the MMIJ than the TLS method. The bootstrapping uncertainty at FLS IJV is identical across all algorithms.

As all algorithms present very similar statistical outputs, some further observations were made:

- The LLS method intrinsically assumes that one variable (measured data) is free of error and forces the reduction of error in the other variable (reference data), therefore having a higher reliance on the measured dataset.
- The TLS method intrinsically assumes that both variables (measured and reference data) are subject to error.
- High confidence is associated with the measured data as it has high data coverage and is of excellent quality. Moreover, all of the primary measured datasets cover a minimum of 12 consecutive months, providing a solid understanding of the short-term climate.

- Given the high volume of wind development occurring in the North Sea, the directional sectorwise understanding of the wind distribution becomes even more critical. Therefore, a higher sectorwise resolution is preferred.

Based on the above points and discussion the LLS method with 16 sectors was considered to be the more appropriate selection.

Table 3.13 FLS IJV: KPIs of tested MCP algorithms

Parameters	Algo 1	Algo 2	Algo 3	Algo 4
Method	LLS	TLS	**LLS**	TLS
Number of sectors	12	12	**16**	16
Yearly divisions	1	1	**1**	1
Temporal resolution	1 hour	1 hour	**1 hour**	1 hour
KPI	**Algo 1**	**Algo 2**	**Algo 3**	**Algo 4**
MBE [%]	-0.01	0.00	-0.02	0.00
MAE [%]	11.4	11.6	11.4	11.6
DE [%]	2.26	1.85	2.16	1.97
LCA factor	1.026	1.029	1.026	1.029
Bootstrapping relative std. dev. [%]	0.16	0.16	0.16	0.16

Table 3.14 MMIJ: KPIs of tested MCP algorithms

Parameters	Algo 1	Algo 2	Algo 3	Algo 4
Method	LLS	TLS	**LLS**	TLS
Number of sectors	12	12	**16**	16
Yearly divisions	1	1	**1**	1
Temporal resolution	1 hour	1 hour	**1 hour**	1 hour
KPI	**Algo 1**	**Algo 2**	**Algo 3**	**Algo 4**
MBE [%]	-0.02	-0.03	-0.03	-0.03
MAE [%]	9.73	9.84	9.73	9.85
DE [%]	0.51	0.18	0.49	0.17
LCA factor	0.984	0.983	0.984	0.983
Bootstrapping relative std. dev. [%]	0.05	0.06	0.05	0.06

3.4.3 Long-term correction

The long-term adjustment of the short-term datasets was conducted with the ERA5 reference data. The ERA5 reference node closest to each respective

primary dataset was used for optimal correlations and resulting long-term correction.

The short-term measured datasets were seasonally balanced (50% winter, 50% summer) prior to conducting the MCP procedure. This avoids any seasonal bias in the long-term correction.

It is noted that the FLS IJV measured data ends on 31 May 2023 and hence extends further than the selected reference long-term period. However, the correlation between the measured and reference datasets was based on the full overlap between the reference and measurement datasets.

The correlation scatter plots showing the sectorwise wind speed and wind direction are presented in Appendix F.

The resulting long-term wind speeds at each of the primary locations are presented in Table 3.15 below. It can be observed that the long-term wind speeds range from 9.89 m/s at FLS HKW to 10.17 m/s at MM IJmuiden.

A comparison of the short-term and long-term wind frequency roses is provided in Figure 3.6 to Figure 3.9.

It is noted that a sensitivity check of the MCP was conducted with a 15-year long-term reference period from 2008 to 2022. This 15-year long-term period also exhibited low trends in the reference data. The result from this sensitivity check has long-term wind speeds at each primary location well within the uncertainty margin associated with the MCP results presented in Table 3.15 below.

Table 3.15 MCP details and results

Dataset characteristics	Value			
Input dataset (short-term)	FLS IJV	MMIJ	FLS HKW	Lidar K13-A
Measurement height [m MSL]	160	160	160	160
Measurement period	01/05/2022 to 31/05/2023	01/01/2012 to 31/12/2015	05/02/2019 to 11/02/2021	01/11/2016 to 31/12/2021
Short-term measured wind speed [m/s]	9.89	10.37	10.43	10.17
ERA5 reference dataset (long-term)	53.000°N, 3.750°E	52.750°N, 3.500°E	52.500°N, 3.750°E	53.250°N, 3.250°E
Reference height [m]	100	100	100	100
Reference period	01/01/2010 to 31/12/2022			
Mean wind speed concurrent period [m/s]	9.14	9.51	9.67	9.53
Mean wind speed total period [m/s]	9.40	9.32	9.19	9.50
Output extended dataset (long-term)	FLS IJV	MMIJ	FLS HKW	lidar K13-A
Height [m MSL]	160	160	160	160
Long-term period	01/01/2010 to 31/12/2022			

Dataset characteristics	Value			
Input dataset (short-term)	FLS IJV	MMIJ	FLS HKW	Lidar K13-A
Long-term mean wind speed [m/s]	10.12	10.17	9.89	10.12
Short-term to the long-term difference [%]	+2.3	-2.0	-5.5	-0.5

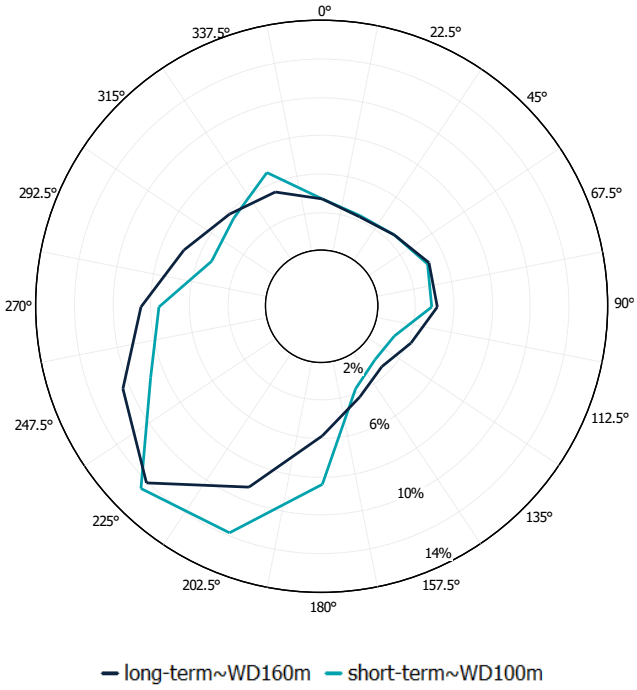

Figure 3.6 FLS IJV 160 m short-term and long-term wind roses

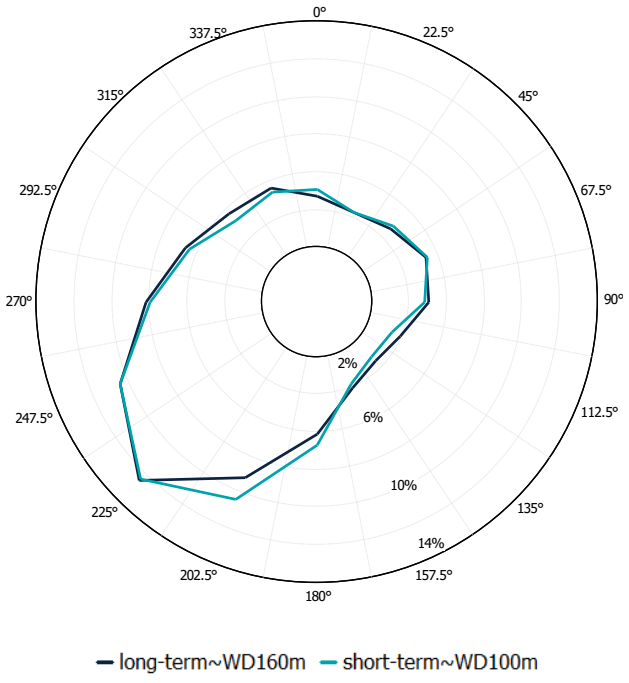

Figure 3.7 MMIJ 160 m short-term and long-term wind roses

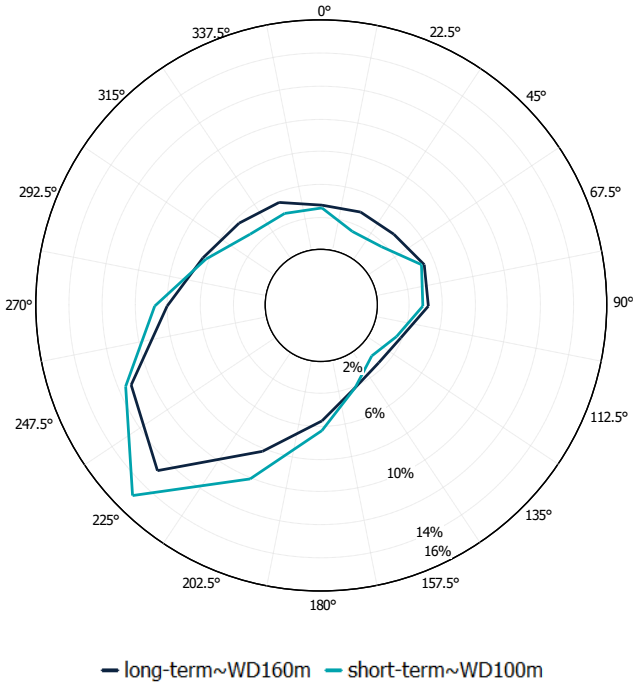

Figure 3.8 FLS HKW 160 m short-term and long-term wind roses

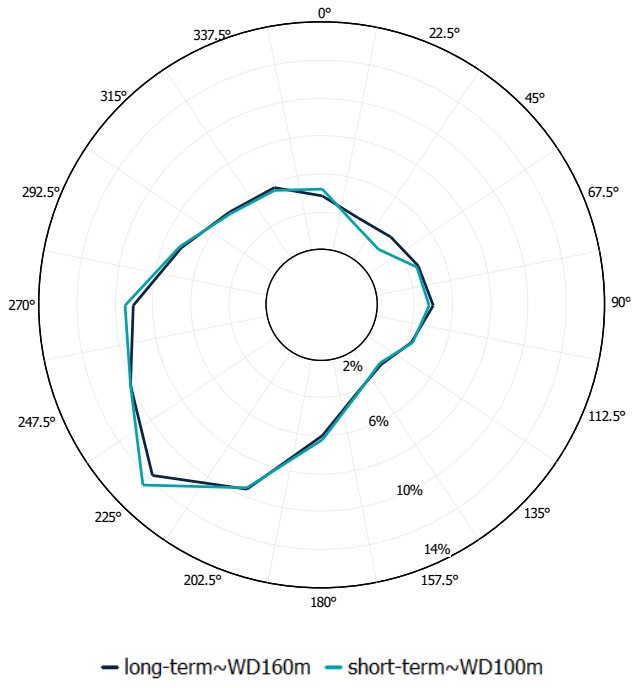

Figure 3.9 Lidar K13-A 160 m short-term and long-term wind roses

3.4.4 Uncertainty in long-term correction

The uncertainty intrinsic to the MCP method was calculated by considering the quality of the reference dataset, the correlation between the reference dataset and the measurements, and the representativeness of the reference long-term data on the local wind conditions. On this basis the estimated uncertainty in the

MCP method uncertainty (long-term correction) is 1.2% and 1.1% in terms of wind speed for IJW and the remaining primary datasets MM IJmuiden, FLS HKW and lidar K13-A respectively.

3.5 Total uncertainty in long-term wind climate

The combined uncertainty in the long-term wind speed at the primary measurement locations at 160 m height above MSL is shown in Table 3.16. Brief descriptions are also provided below.

Table 3.16 Total uncertainty in long-term wind speed

Uncertainty description	FLS IJV	MM Ijmuiden	FLS HKW	Lidar K13-A
Total uncertainty in measured wind speed (wind statistics)	3.2%	2.1%	2.9%	2.9%
MCP method uncertainty (long-term correction)	1.2%	1.1%	1.1%	1.1%
Long-term representation	1.4%	1.4%	1.4%	1.4%
Total uncertainty in long-term wind climate	**3.4%**	**2.4%**	**3.1%**	**3.1%**

The uncertainty in measured wind speed is the value of the respective uncertainty associated with the wind speed measurements of each dataset, presented in Section 3.3.5.

The uncertainty intrinsic to the MCP method was calculated by considering the quality of the reference dataset, the correlation between the reference dataset and the measurements, and the representativeness of the reference long-term data for the local wind conditions. It is noted that the MCP method uncertainty of FLS IJV is marginally higher than the remaining datasets due to slight increase in the uncertainties related to correlation uncertainty derived from bootstrapping analysis during the MCP process.

The uncertainty related to the long-term representation (variability) is based on the length of the long-term extended measurements of 13 years at all locations.

4 Unified-WRF Model Development

This section presents a detailed description of the development of the Unified-WRF mesoscale model for the purpose of IJVWFZ wind resource and metocean assessments.

The development of the Unified-WRF dataset was requested by RVO at the proposal stage to address the imperative need to streamline and harmonize analysis processes for offshore wind sites. Historically, wind resource assessment and metocean analysis were operated as distinct endeavours, each pursuing its own course with unique methodologies, models, and input wind datasets. Convergence occurred only upon completion of their individual analyses, necessitating a subsequent alignment check to ensure consistency between the wind data employed in both assessments.

The challenge was to create a unified, gridded wind dataset capable of satisfying the requirements of both wind resource assessment and metocean analysis. By achieving this integration, OWC & partners aimed to establish a pre-aligned state with respect to the input wind dataset, enabling a unified approach towards the above-mentioned ultimate goal.

However, this objective presented a significant challenge due to the inherent disparities in the requirements of the wind dataset for metocean analysis and wind resource assessment. Metocean analysis demanded extensive spatial coverage, particularly over oceanic and sea areas, with a focus on 10-meter wind speeds and a need for accuracy during extreme conditions. In contrast, wind resource assessment prioritized high resolution to capture wind climate, gradients, and the influence of coastal features on wind patterns. Attention was centred on WTG rotor layer winds at hub heights of 160 meters, requiring precision in terms of long-term mean and wind speed distribution for accurate long-term evaluations.

4.1 Methodology

The development of the Unified-WRF model was undertaken by ArcVera as part of the wind resource package consortium (OWC, ArcVera, ProPlanEn and Innosea) under the coordination of OWC and involved the creation of a bespoke mesoscale dataset utilizing the Weather Research and Forecasting (WRF) model, referred to as Unified-WRF within this report. The model was driven by initial and boundary conditions sourced from the ERA5 reanalysis, with the overarching goal of assessing wind potential across the IJVWFZ region.

Balancing these distinct requirements to create a unified WRF dataset posed a formidable technical challenge, necessitating innovative and practical solutions to accommodate the divergent needs of wind resource assessment and metocean analysis while maintaining accuracy and consistency throughout. The process was initiated with a pre-configuration test of the raw WRF model, which was subsequently refined through the integration of several high-quality datasets. These enhancements were made to align the model more closely with short-term on-site measurements and the DOWA dataset. Crucially, a major aspect of this development involved the correction of biases in point measurements, an imperative task for model evaluation. This bias correction process consisted of two phases: the initial phase focused on aligning the

model with in-situ measurements from 12 specific sites within a 1.7 km domain. For wind speed, a 12-month by 24-hour bias correction matrix was constructed, complemented by wind direction adjustments by sector. These corrections were then spatially averaged across the entire grid using an inverse distance weighting approach. In regions with fewer nearby measurement sites, notably the northwest quadrant, the Dutch Offshore Wind Atlas played a pivotal role as a secondary source for bias correction, enhancing the overall accuracy of the model.

The Unified-WRF model represents a significant advancement in meteorological and oceanographic modelling, tailored to simulate the intricate spatial patterns of wind climate in the Dutch North Sea. Its development adheres to a systematic iterative process outlined in the accompanying methodology flow chart. This model serves as the fundamental tool for conducting metocean assessments for design purposes and resource assessments in the region. From the project's inception, a deliberate decision was made to adopt a single WRF modelling domain encompassing a 44-year time span, with a horizontal resolution of 1.7 kilometres. This high-resolution approach was selected to enhance precision and reliability in capturing the dynamic atmospheric conditions of the Dutch North Sea. This modelling methodology promises to advance our understanding of the wind climate in this maritime area and its implications for various applications, facilitating more informed decision-making.

Figure 4.1 below presents a flowchart of the methodology employed in this study.

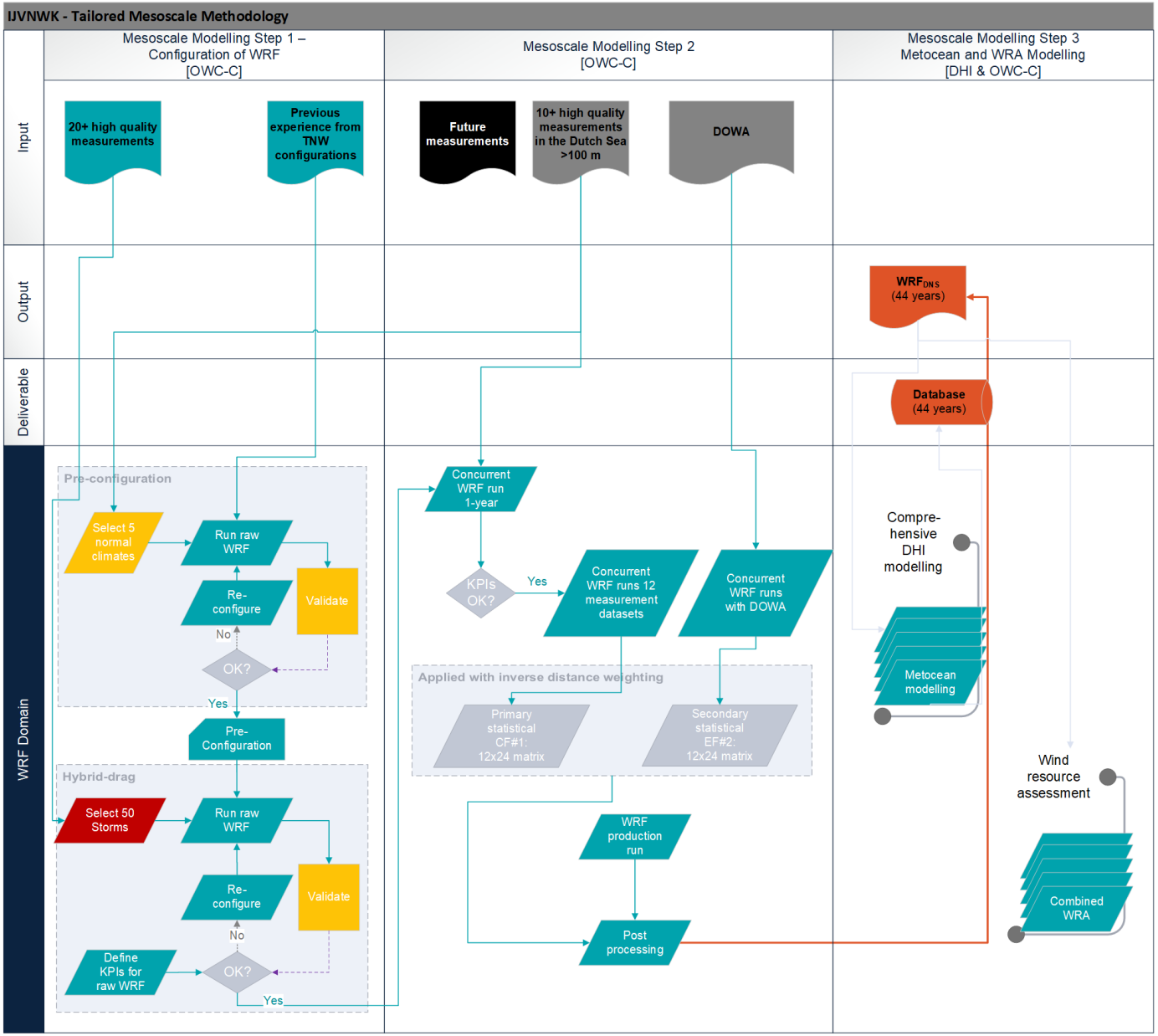

Figure 4.1 Mesoscale modelling methodology

4.2 Pre-configuration

The first stage of development was to test for the best configuration of the Weather Research and Forecasting Model (WRF) for the Dutch North Sea (DNS) offshore domain. Many aspects of the model could be configured to potentially affect its accuracy for a particular application, but the main motivator was the desire for near-surface wind speed accuracy and hence the testing of planetary boundary layer (PBL) representations. The PBL is the model physics option that is most likely to have an impact on the near-surface wind flow patterns.

Three (3) commonly used PBL schemes were tested initially by OWC & partners during the previous project done at TNW [37]: the Yonsei University Scheme (YSU), the Mellor-Yamada-Nakanishi-Niino (MYNN) scheme and the Total energy-mass flux (TEMF) scheme. Based on the findings from that analysis the following schemes were compared as the starting point for this exercise:

- ERA5-driven with YSU PBL scheme
- ERA5-driven with MYNN PBL scheme
- CFSR-driven with YSU PBL scheme

Through the utilization of these schemes, configuration tests were conducted to assess the performance of the three candidate PBL schemes. The configuration tests were executed as follows:

- Simulations encompassed a span of 30 randomly selected days, distributed evenly across all seasons within a single year.
- Four sets of 30 random days were chosen to ensure overlap with periods of unwaked observations from one or more of the five sites: FLS TNW (June 2019 – June 2020), MM FINO1, and MM OWEZ (July 2005 – June 2006), FLS HKN (April 2017 – March 2018), and MM IJmuiden (January – December 2015), totalling 120 days in all.
- Based on the 30 simulated days overlapping with each respective measurement site, the following metrics were employed to determine the final mesoscale modelled dataset:
- Hourly correlation coefficient R^2 values for wind speed and wind direction.
- Mean absolute error of wind speed.
- Kolmogorov-Smirnov (K-S) test for equality of the wind speed distribution.
- Additionally, the spatial pattern of mean wind speed was evaluated by calculating the root mean square error (RMSE) across these measurement locations. However, it's worth noting that RMSE is influenced by both overall bias and variability across the five measurement locations. Therefore, the bias-corrected RMSE (bc-RMSE) was computed, providing a more accurate indication of which model source effectively captures the spatial variability across the different modelled measurement locations.

The outcomes of this assessment are presented in Table 4.1 with the best-performing scheme result being highlighted in green according to a traffic light system.

Table 4.1 Statistical test results for the different PBL schemes

Location	Parameter	YSU PBL (ERA5)	MYNN PBL (ERA5)	YSU PBL (CSFR)
FLS TNW	Wind speed R^2	0.955	0.938	0.923
MM FINO1		0.905	0.915	0.823
FLS HKN		0.881	0.866	0.821
MM OWEZ		0.921	0.924	0.837
MM IJmuiden		0.931	0.91	0.892
FLS TNW	MAE	0.661	1.037	1.109
MM FINO1		1.026	0.944	1.412
FLS HKN		1.041	1.175	1.401
MM OWEZ		0.992	0.965	1.438
MM IJmuiden		0.980	1.085	1.167
FLS TNW	K-S test	0.026	0.068	0.047
MM FINO1		0.034	0.042	0.052
FLS HKN		0.075	0.097	0.076
MM OWEZ		0.047	0.064	0.068
MM IJmuiden		0.052	0.081	0.045
FLS TNW	Wind direction R^2	0.979	0.981	0.977
MM FINO1		0.963	0.961	0.905
FLS HKN		0.974	0.972	0.955
MM OWEZ		0.914	0.912	0.870
MM IJmuiden		0.973	0.971	0.943
Spatial RMSE of long-term mean wind speed [m/s]		0.16	0.16	0.29
Spatial bc-RMSE of long-term mean wind speed [m/s]		**0.11**	**0.11**	**0.11**

As discernible from the data presented in Table 4.1, upon a thorough evaluation of all the metrics across the five measurement sites, it became evident that the YSU scheme coupled with ERA5 exhibited superior performance compared to the MYNN scheme and significantly outperformed the YSU scheme coupled with CFSR.

Further, a 10-minute time series of 10-m wind speed from the WRF production run for FLS TNW was produced, which used ERA5 and the YSU PBL scheme (as in Configuration 1 in Table 4.1). Conventional metocean modelling typically employs CFSR datasets; accordingly, DHI independently evaluated WRF-ERA5 and WRF-CFSR, applying their distinct shear parametrisation (for 10 m level) before OWC's further WRF model configuration (refer to Section 4.3). OWC subsequently performed a concurrent KPI analysis, comparing WRF driven by both CFSR and ERA5 against actual measurements. This rigorous assessment determined that the WRF configured with ERA5 demonstrated superior performance, in line with the criteria detailed in Section 4.4.

This time series was provided to DHI, and DHI also produced a raw hourly CFSR time series of 10-m wind speed. Both time series covered a 1-year period from mid-2019 to mid-2020, coincident with the first full year of measurements at the FLS TNW floating lidar pair, allowing for direct comparison of each to the observed 10-m wind speed at FLS TNW. Scatter plots of each source versus the observed winds are shown in Figure 4.2.

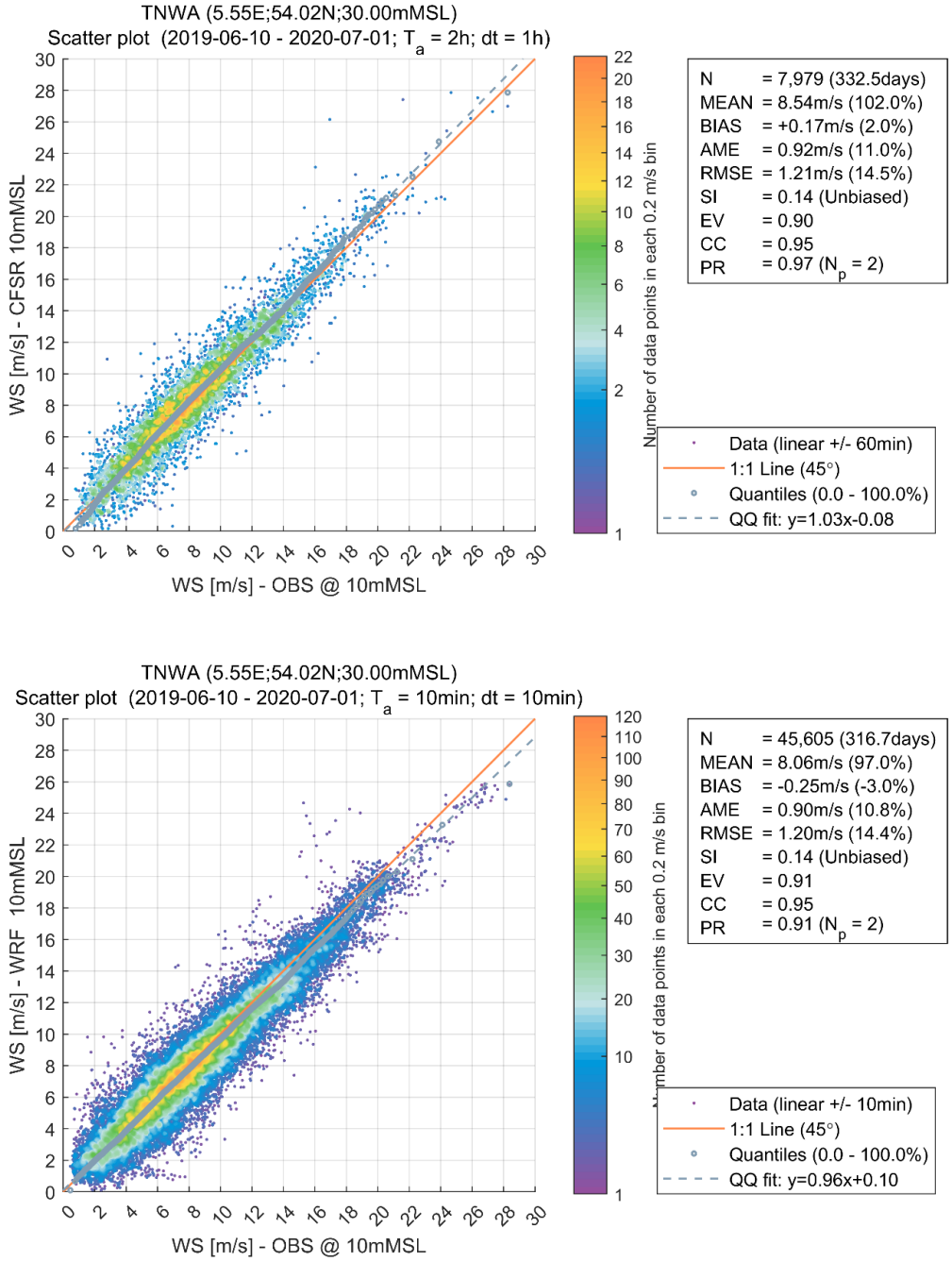

Figure 4.2 Scatter plots of 10-m wind speed from CFSR (top, y-axis), and WRF with ERA5 and YSU PBL (bottom, y-axis), versus observed (x-axis in both)
Note, that hourly data is shown for CFSR, whereas 10-minute data is shown for WRF-ERA5.

Both scatter plots depict a clear linear relationship and exhibit a robust correlation coefficient of 0.95 (excellent correlation with R^2 higher than 0.9) when compared to the observed wind data. The mean wind speed derived from

CFSR is higher by approximately half a meter per second than the ERA5 based mean wind and non-conservative from a wind resource point of view.

The primary distinction between the two plots is evident at the highest wind speeds, notably the grey quantile dots corresponding to a 20 m/s observed wind speed. In this regard, it is noteworthy that CFSR tends to exhibit a bias towards high wind speeds, while ERA5-WRF displays a bias in the opposite direction, registering a bias towards low wind speeds of roughly the same magnitude. It's important to note that the year under consideration did not witness any extreme storms, making it uncertain whether either dataset accurately represents wind speeds exceeding 25 m/s based solely on these plots.

The conclusions outlined below are derived from the preceding results and a subsequent detailed evaluation of Key Performance Indicators (KPIs) (For criteria specifics, refer to Section 4.4.2). This retrospective analysis reaffirmed the initial decision, indicating ERA5's outperformance relative to CSFR. These findings will inform further analysis and the next stages of the project:

- In terms of hub-height wind speed at FLS TNW, it is determined that the utilization of CFSR to drive WRF for the simulations cannot be justified. This decision is primarily based on the reduced performance observed in key metrics crucial for hub-height wind resource assessment when compared to ERA5-driven WRF.
- Comparisons between ERA5-driven WRF and CFSR at FLS TNW, specifically regarding 10-meter wind speed, reveal indications of a potential low bias in wind speed, particularly at high wind speeds. This observation raised concerns by DHI, particularly if the model output is intended for metocean modelling and analysis.
- Nonetheless, it is worth noting that the relationship between ERA5-driven WRF and the measurements at 10 meters exhibits linearity and very good correlation. Furthermore, the observed low bias is relatively small, suggesting the possibility of correction through a straightforward bias correction process. This corrective approach would be deemed valid if it can be established that the bias is systematic and consistent across multiple validation sites.
- The next step in the process involves conducting a test involving 50 storms, incorporating a greater number of observation sites for validation purposes. This step is anticipated to provide further insights into the nature of ERA5-driven WRF's bias characteristics, particularly at extreme wind speeds.

Consequently, the decision was made to select the YSU scheme in conjunction with ERA5 for implementation in further testing and validation.

The final model parameters are shown in Table 4.2 and the grid boundaries are visualised in Figure 4.3. It is noted that a spectral nudging was applied using a low-pass spatial filter to the continuous nudging toward the reanalysis, which keeps the WRF model aligned with ERA5 throughout the simulation at spatial scales resolved by the ERA5 grid (28 km) but allows it to freely develop smaller-scale meteorological features on its much higher resolution grid (1.7 km)

Table 4.2 Final model parameter for the selected mesoscale model

Parameter	Setting
WRF model version	4.2.1
Land-use data	MODIS land-cover data (~450 m grid)
Atmospheric boundary conditions	ERA5
Sea surface conditions	ERA5
Grid nudging to reanalysis	Yes
Horizontal resolution	1.7 km (outer nests of 5.0 and 15.0 km)
Vertical resolution	37 levels from surface to 100 hPa
Model output interval	10 minutes
Planetary boundary layer scheme	YSU
Surface layer scheme	Monin-Obukhov similarity scheme
Grid-resolved clouds and precipitation	Thompson scheme
Atmospheric radiation	RRTM (long wave) and Dudhia (short wave)

The pre-configuration phase extends its scope through comprehensive evaluation, as elaborated in the ensuing chapters. It is worth emphasizing that a pivotal decision has been made to introduce a key performance indicator (KPI) system, aimed at rendering the validation process more objective and pragmatic. Further details regarding the KPI system are expounded upon in the forthcoming section.

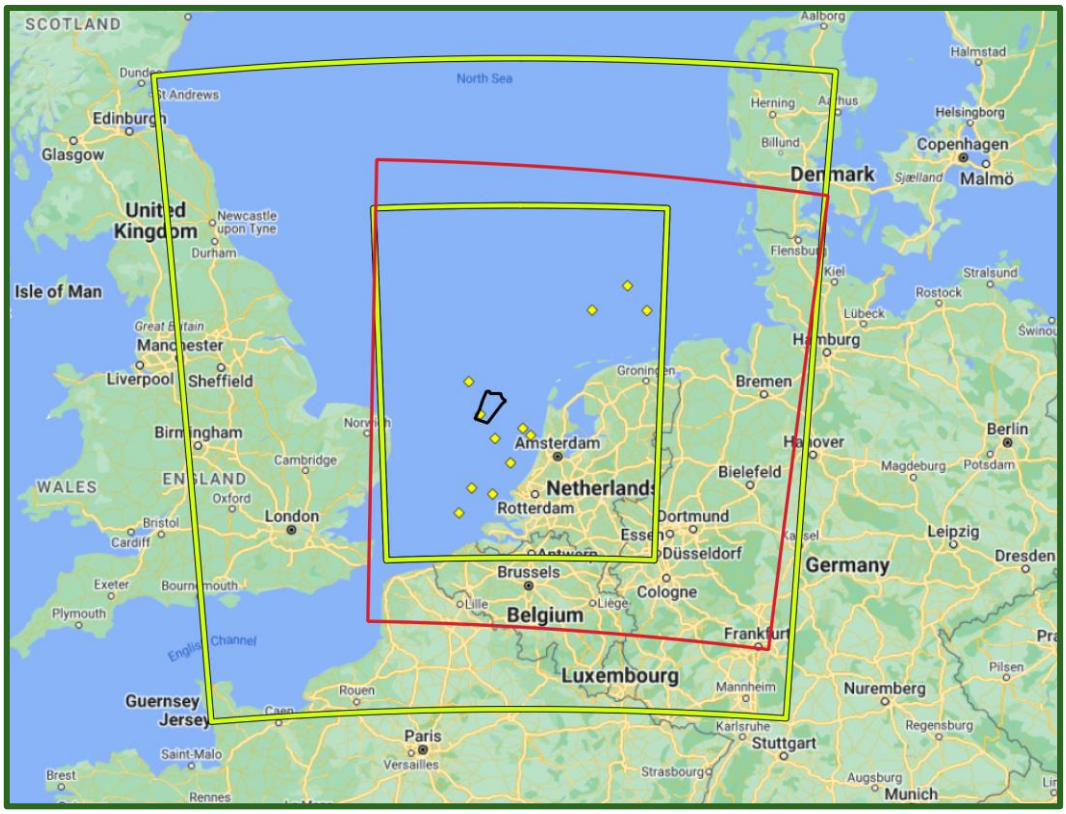

Figure 4.3 Unified-WRF model domain configuration. The inner green box and outer green box are the 1.7-km and 5-km grids, respectively. The red box is the DOWA domain, for reference.

4.3 Hybrid-drag

A key controlling parameter of wind speed over water is the drag coefficient of the water surface, and the consortium focused its efforts on refining the determination of this parameter in the Unified-WRF model so that, when driven with the ERA5 reanalysis, the model would produce more accurate (i.e., higher) wind speed peaks in extreme conditions then it does with its standard settings, but without adding a high bias to the model's near-surface winds under non-extreme conditions.

Over water, the WRF model assumes that surface roughness is a function of surface wind speed (at a reference height typically taken as 10 m), arising from the increase of surface wave amplitude with wind speed. Early versions of WRF used the long-established relationship of Charnock (1955) [55], which is expressed in the model as:

$$z_0 = \alpha_c u_*^2 / g \,,$$

where z_0 is the roughness length, u_* is the friction velocity, g is acceleration due to gravity, and α_c is the Charnock parameter. Under neutral conditions, u_* is related to both z_0 and u_{10}, the wind speed at 10 m, by the relationship:

$$u_{10} = u_* / \kappa \ \ln (z_{ref} / z_0),$$

where κ is the Von Karman constant and z_{ref} is 10 m. Therefore, z_0 can be alternatively expressed as a function of u_{10}, the surface wind speed. Finally, the

surface drag coefficient, C_D, is often shown and discussed instead of the roughness length, with the two related by:

$$C_D = \kappa^2 / \ln (z_{ref} / z_0)^2.$$

The Charnock relationship (expressed as C_D versus u_{10}) is shown as the blue curve in Figure 4.4. Except at very low wind speeds, the drag increases nearly linearly with wind speed. The drag curve in the graph is capped at a value of 2.4×10^3, which will be discussed shortly.

During the early 2000s, several observational studies of surface drag versus wind speed over water found that at extreme wind speeds, the steady increase of drag with wind speed no longer applies. In roughly the 20 – 30 m/s range of surface wind speed, the drag versus speed curve flattens, or even begins to decrease with further increase of wind speed (see groups of dots, from observational studies, in Figure 4.5). In response to this finding, a number of alternative functions to Charnock were introduced, which reflected this behaviour. See, for example, the red curves, or the dark green [56] curve in Figure 4.5. In response to these findings, the WRF model developers made two adjustments to the drag formula configuration options. The Charnock relationship was capped at a value of 2.4×10^3 (as in Figure 4.4), and the Davis et al. (2008) relationship was also provided as an optional alternative to Charnock, also with a cap at 2.4×10^3 (the orange curve in Figure 4.4). The Davis curve is lower than the Charnock curve at all wind speeds, except at very high speeds where they both have reached the capped value.

Following testing of the Davis curve, it was observed that it did produce higher peak winds during storms, but also raised the mean wind speed under non-extreme conditions to produce an unacceptable positive long-term mean wind speed bias. To gain the benefit of the Davis curve at high wind speeds, but not the undesirable speed increases at non-extreme wind speeds the “hybrid” drag relationship was formulated, which follows the higher-drag Charnock curve from 0.0 to 12.5 m/s, but then transitions to values closer to the Davis curve at higher wind speeds, exactly equalling the Davis curve value at 26 m/s (dashed green curve in Figure 4.4).

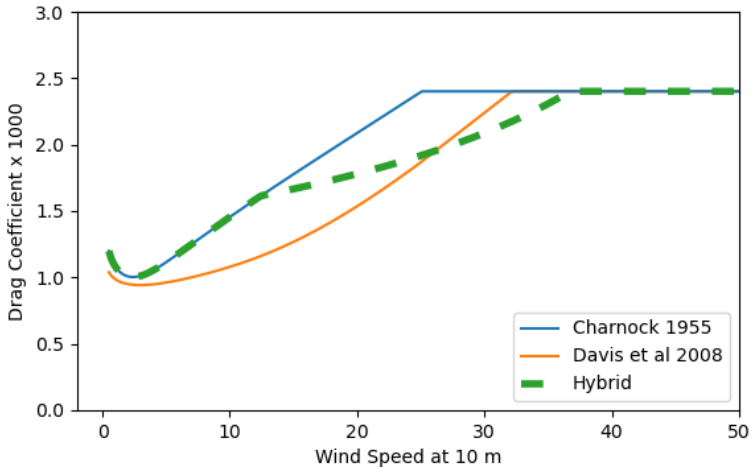

Figure 4.4 Drag coefficient (CD) versus wind speed at 10-m in the WRF model

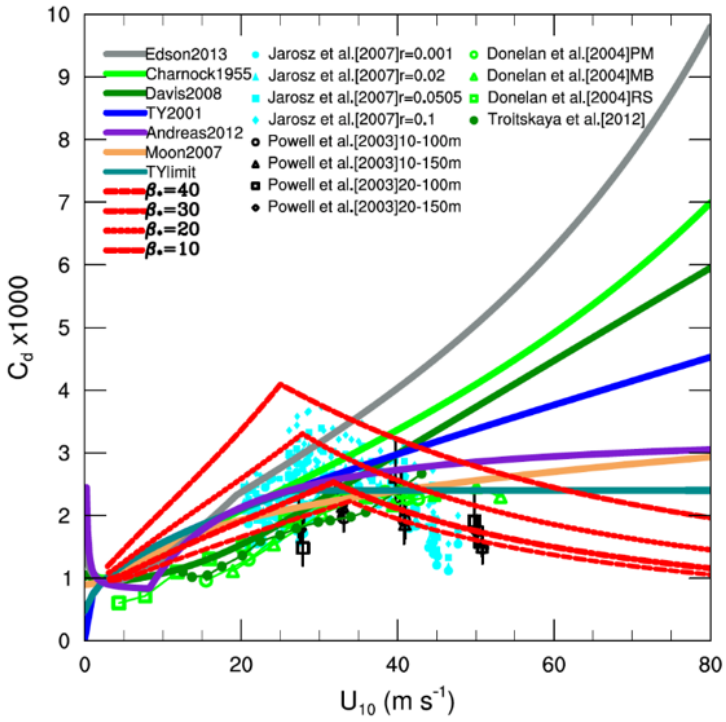

Figure 4.5 Drag coefficient (CD) versus wind speed at 10-m from observational studies (dots), and functional curve fits based on those studies (solid curves) [57]

In the WRF model, the three drag curves were tested in several storm cases. It was found that the winds responded as expected. In non-extreme winds (u10 < 15 m/s), the hybrid and Charnock formulas were observed to perform similarly, and were found to produce slightly lower wind speeds than Davis. In extreme winds (u10 > 20 m/s), the hybrid and Davis formulas were seen to perform similarly and were found to produce slightly higher wind speeds than Charnock.

The WRF model, configured with the hybrid drag and informed by ERA5 initial and boundary conditions, serves as an exemplar of its capability to precisely simulate winds across both typical and extreme speeds. Figure 4.6 presents several time series comparing measured and modelled winds. From the WRF model, time series data were extracted at identical horizontal locations, at a height of 30-m, and concurrent with the measurements for each specified location. The selection of the 30 m height is due to it being the most commonly accessible height at a majority of the measurement sites. While this is higher than 10 m, it remains sufficiently proximate to the surface to be significantly affected by the surface drag differences.

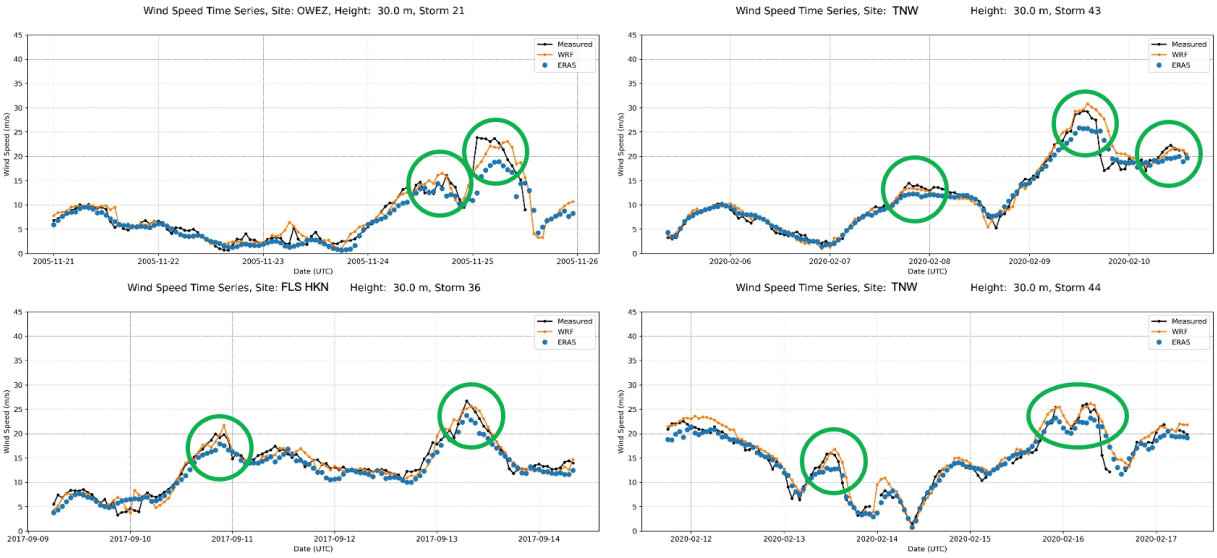

Figure 4.6 Time series of 30-m wind speeds for four different storm cases

The measurement site is indicated in the title above each time series. Hourly wind speeds from the measurements, the Unified-WRF with hybrid drag, and the ERA5 reanalysis are shown. Green circles highlight peak wind events.

In general, the Unified-WRF (with hybrid drag) and ERA5 perform similarly in capturing the measured time series outside of the high wind peaks. However, Unified-WRF performs better at capturing the peak values accurately, compared to the generally low-biased ERA5. Based on these tests and results, the consortium moved ahead with adopting the hybrid drag in the Unified-WRF for the further testing and finally post-processing.

4.4 WRF model performance

Following the pre-configuration and the implementation of the hybrid-drag configuration in the raw model, Key Performance Indicators (KPIs) were defined to rigorously evaluate the model's performance in relation to both test cases and results, encompassing both extreme and normal wind climates (relevant for wind resource assessment). This assessment was conducted within the first modelling step, as depicted in the methodology illustrated in Figure 4.1. Subsequent to this initial assessment, the raw model performance of the Unified-WRF was scrutinized based on these established criteria before the commencement of post-processing, as highlighted in Step 2 of Figure 4.1.

4.4.1 Definition of key performance indicators

In general, the verification is expected to demonstrate whether or not the Unified-WRF model meets a minimum level of performance deemed necessary by RVO and its expert advisors for use in metocean modelling and wind resource assessment at IJVWFZ. This objective will be measured via KPIs, which are a measure of performance over time for a specific objective.

The KPIs for the WRF model performance are tested in an iterative process as shown in Figure 4.7.

It is noted that the 49 storm events were prioritized during the production runs to enable an additional quality assurance (QA) layer, to ensure that the WRF model is performing in line with the KPIs.

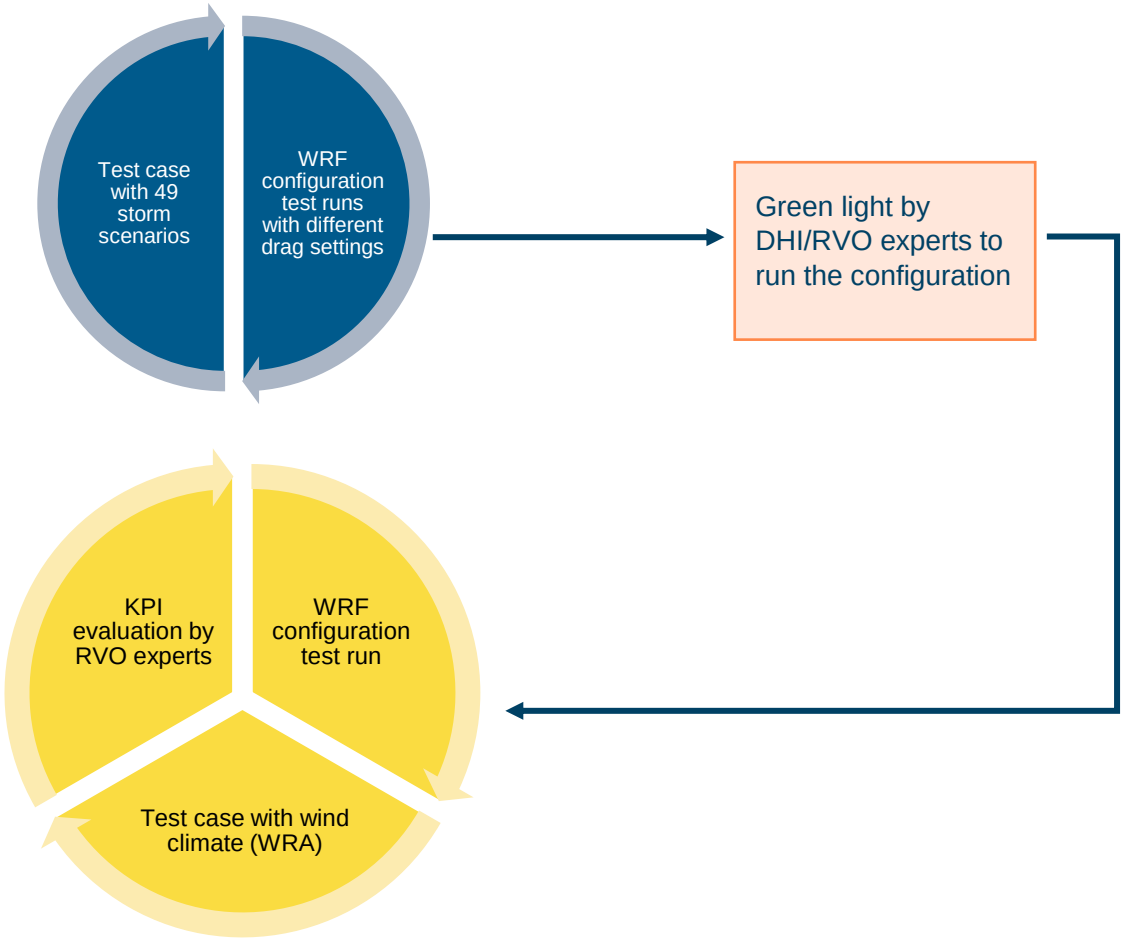

Figure 4.7 Iterative process to validate the WRF configuration before the WRF production run

The test case is a WRF configuration run for a set of defined simulation periods in the complete WRF domain. The simulation periods consist of 49 distinctive short time periods (storm scenarios) for the test case with storms and one (1) continuous year for the test case with the wind climate. Storm periods were typically 5 days in length, though a small number were up to 10 days. The continuous year was chosen as January-December 2019, as that period had temporal overlap with the largest number of measurement site periods of record.

Definition of a storm (peak) scenario:

In the pursuit of defining storm (peaks) scenarios, some tolerance was incorporated to accommodate potential misalignment in the model's timing of peak occurrence. This approach facilitated a comparison between the model's peak value and the observed peak value, rather than aligning the model's value with the time of the observed peak value. A deliberate intent was to limit the number of peak values under consideration, thereby excluding every local maximum from being classified as a "peak." The adopted procedure was as follows:

1) The highest observed measured value throughout the entire storm simulation was identified. Only speeds exceeding 20 m/s were categorized as a "storm peak".

2) The model's highest value within a timeframe of ±3 hours of the observed peak wind time was sought, serving as the model's corresponding peak.

3) The disparity between these values was computed, designating the "error" for that particular storm peak.

4) All observed values within a contextually reasonable time span (ranging from ±6 hours to 2 days) surrounding that storm peak were excluded from subsequent scrutiny, ensuring not every local maximum was labelled as a "peak".

5) The procedure reverted to the initial step to assess any further peaks within the storm simulation.

Definition of scenarios and test cases is summarized in Table 4.3.

Table 4.3 Definition of test cases and scenarios

Definition	Storms	Wind Climate (WRA)
Test case	49 storm scenarios.	1 wind climate scenario.
Scenario	WRF simulation period with 3-5 days.	WRF simulation period with 365 days.
Validation dataset	Measurement (observation) dataset at a single location and a single height.	

It is noted that KPIs need to be fulfilled for a minimum of 90% of the validation datasets.

Table 4.4 KPI for WRF validation – test cases

Test Cases	ID	Storms		ID	Wind Climate (WRA)	
		Minimum criteria	Notes		Minimum criteria	Notes
Simulation period	TC-S1	49 storm scenarios, with a total of +200 days of WRF simulation.	Ideally including winter 13/14 for storms simulation.	TC-W1	1 wind climate scenario with a single consecutive year, 365 days of WRF simulation.	2019 is a representative year.[10]
Horizontal distribution	TC-S2	10 measurement locations, ensuring reasonable horizontal distribution across the horizontal domain, also visualised in a GIS map.	No further changes.	TC-W2	3 measurement locations, ensuring reasonable horizontal distribution across the horizontal domain, also visualised in a GIS map.	K13, LEG, EPL, HKW
Vertical distribution	TC-S3	Minimum two heights at each measurement location.	Lower section of the rotor plane from lower tip height up to the hub height.	TC-W3	Minimum two heights at each measurement location.	Lower section of the rotor plane from lower tip height up to the hub height.
Selection of technology for measurements	TC-S4	Anemometers (preferred), supplemented with a mix of floating lidar and lidar datasets.	-	TC-W4	A mix of lidar and floating lidar systems.	-
Screening criteria	TC-S5	Wake influence accepted, and validation plots to include wind direction to enable a qualitative assessment of the storm event.	We assume that FINO1 is wake-free for storms.	TC-W5	Wake-free periods only.	-

[10] The continuous year was chosen as January-December 2019, as that period had temporal overlap with the largest number of measurement site periods of record.

Table 4.5 KPI for WRF validation – KPI criteria

Key Performance Indicators (KPI)	ID	Storms		ID	Wind Climate (WRA)	
		Minimum criteria	Notes		Minimum criteria	Notes
Relative mean bias error of wind speed [%]	-	N/A	-	KPI-W1	<2 x measurement uncertainty	1-year simulation, for a minimum of 75% of validation datasets.
Standard deviation[11] of rel. mean speed bias error [%] (spatial)	-	N/A	-	KPI-W2	<2%	Between validation datasets 80% of data below the threshold.
Distribution error	-	N/A	-	KPI-W3	<0.06	Kolmogorov Smirnov test statistic (D). For a minimum of 80% of validation datasets.
Hourly averaged wind speed correlations– R^2	KPI-S1	>0.8	90% of validation datasets above threshold.	KPI-W4	>0.8	90% of validation datasets above the threshold.
Wind profile in the rotor plane – difference in alpha (omnidirectional)	KPI-S2	Deviation of modelled alpha from measured alpha within 30% of measured alpha, with a qualitative assessment[12].	Power law from measurement vs model. 80% of measurement locations. Lower section of the rotor plane from lower tip height up to the hub height.	KPI-W5	Deviation of modelled alpha from measured alpha within 30% of measured alpha, with a qualitative assessment	Power law from measurement vs model. 80% of measurement locations. Lower section of the rotor plane from lower tip height up to the hub height.

[11] Standard deviation of all samples

[12] The qualitative assessment should ideally include wind profile comparisons with:
- omnidirectional & per wind sector
- storm profiles (especially strongest storm peaks).

Key Performance Indicators (KPI)	ID	Storms		ID	Wind Climate (WRA)	
		Minimum criteria	Notes		Minimum criteria	Notes
RMSE in mean wind speed [m/s]	KPI-S3	<x2 measurement accuracy, obtained from the wind speed measurement uncertainty (ideally cup anemometer).	Model vs storm periods.	'	N/A	-
Storm peaks: mean bias error [m/s]	KPI-S4	<0.2 m/s	See the below definition, +-3 hours around the maximum	'	N/A	-

4.4.2 KPI criterion and performance

Upon a comprehensive review of the Unified-WRF's raw model performance, as delineated in Table 4.6 and Table 4.7, several observations can be made. The results were color-coded using a traffic light system to provide clarity on the model's performance: green indicated scenarios where all criteria were met, amber highlighted instances with some deviations, and red was used in cases where the criteria were not satisfied.

For the test cases outlined in Table 4.4, the majority of the criteria were met. Specifically, in terms of simulation periods and horizontal distribution, the criteria were successfully satisfied. For vertical distribution, while most cases met the criteria, three out of the thirteen sites only considered one height. When assessing the technology selected for measurements, a combination of anemometers and advanced remote sensing technologies such as lidar and FLS were observed. The screening criteria ensured that sites with minimal wake impact were utilized.

Table 4.6 Criterion for test cases

Test Cases	ID	Storms Performance	ID	Wind Climate (WRA) Performance
Simulation period	TC-S1	Criterion met.	TC-W1	Criterion met.
Horizontal distribution	TC-S2	13 total, but 2 are close to others.	TC-W2	Criterion met.
Vertical distribution	TC-S3	True for 10 of them, 3 of 13 have only one height (FLS Borssele, FINO1, N-7.2)	TC-W3	Criterion met.
Selection of technology for measurements	TC-S4	4 anemometer, 6 remote sensing technology (lidar and FLS).	TC-W4	2 anemometer, 6 remote sensing technology (lidar and FLS).
Screening criteria	TC-S5	Site without wake impact, or with negligible impact used. Direction scatter plots provided.	TC-W5	Site without wake impact, or with negligible impact used.

The KPI results are discussed in Table 4.7, based on criteria as defined in Table 4.5. The relative mean bias error of wind speed was observed to comply with the required criterion across all sites. The standard deviation of the relative mean speed bias error presented a performance of 0.87%. Additionally, all distribution errors were found to be less than 0.03, and the hourly averaged wind speed correlations exhibited very good R^2 values, all exceeding 0.88. An important note in the wind profile for the rotor plane pertained to the bias in shear. The Unified-WRF consistently showcased a low bias, particularly at elevated wind speeds greater than 20 m/s. In contrast, ERA5 depicted a high

bias with a more considerable spatial scatter of errors. Nevertheless, when comparing shear by direction, Unified-WRF was noted to outperform ERA5 significantly. The RMSE in mean wind speed criterion was achieved for 11 out of the 13 sites during the 50-storm validation. However, for storm peaks, only seven out of thirteen sites adhered to the strict tolerance of an MBE less than 0.2 m/s.

Table 4.7 KPI results

Key Performance Indicators (KPI)	ID	Storms	ID	Wind Climate (WRA)
		Performance		Performance
Relative mean bias error of wind speed [%]	-	-	KPI-W1	Criterion is met at all sites.
Standard deviation[13] of rel. mean speed bias error [%] (spatial)	-	-	KPI-W2	0.87%
Distribution error	-	-	KPI-W3	All <0.03
Hourly averaged wind speed correlations– R^2	KPI-S1	All > 0.88	KPI-W4	All >0.89
Wind profile in the rotor plane – difference in alpha (omnidirectional)	KPI-S2	All within 25%. However, WRF is consistently low-biased on shear, especially at higher (> 20 m/s) wind speeds. ERA5 is consistently high-biased on shear, and has greater scatter of errors spatially.	KPI-W5	WRF is 6.4% too low on average. Max error is 7.8% too low. Criterion met. Note, WRF shears are very low (by 18-27%) when wind is >20 m/s. ERA5 has lower overall bias but greater scatter of errors among sites. WRF performs significantly better at shear by direction than ERA5.
RMSE in mean wind speed [m/s]	KPI-S3	Criterion met for 11 of 13 sites in 50-storm validation.	-	-
Storm peaks: mean bias error [m/s]	KPI-S4	Only 7 of 13 individual sites have MBE < 0.2 m/s. Criterion is not met. 0.2 m/s is a tight tolerance for hourly RMSE of hourly winds.	-	-

Based on this assessment, the raw performance of the Unified-WRF model is considered appropriate for the goals of this study. The variations observed in storm peaks can be ascribed to the stringent tolerance for hourly RMSE of

[13] Standard deviation of all samples

hourly winds. However, these deviations did not undermine the overall commendable performance of the raw Unified-WRF model. Consequently, the study progressed, emphasizing post-processing as detailed in the following stages.

4.5 Post-processing

In the post-processing of the Unified-WRF model, a two-pronged approach was employed. Firstly, bias correction in relation to point measurements was prioritized. Such in-situ measurements serve as the benchmark for model evaluations, and therefore it was imperative for the model to align closely with these measurements. However, since these measurements do not span the entirety of the domain, a supplementary bias correction method was integrated using another reputable dataset, the Dutch Offshore Wind Atlas (DOWA).

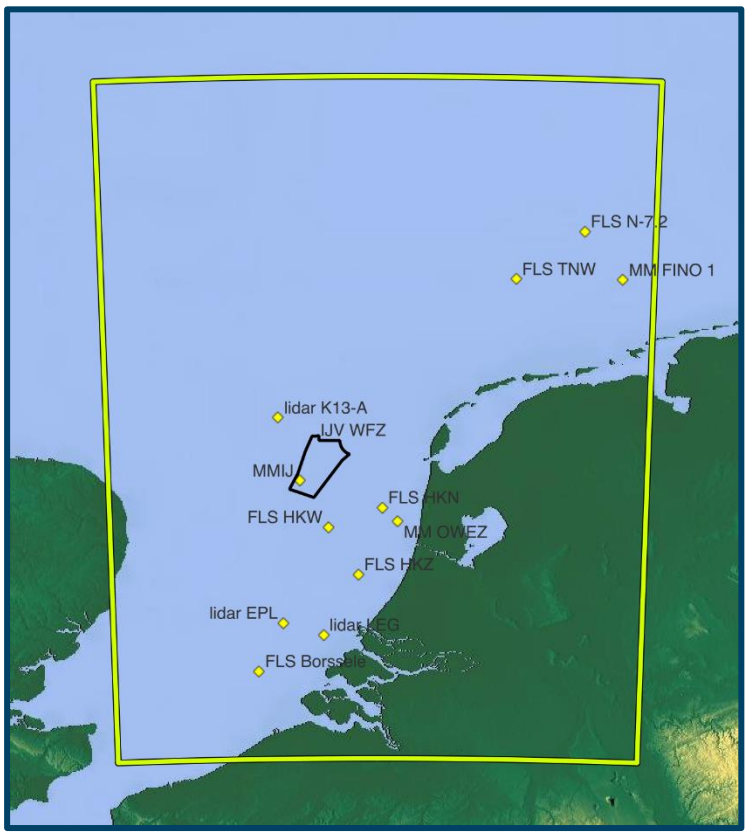

Figure 4.8 1.67 km Unified-WRF domain (yellow boundary) and measurement datasets used in the post-processing

For the measurement-based bias correction, twelve specific sites, all within the 1.67-kilometer domain, were chosen. The time periods from each site, displayed in a Gantt chart, were used as shown in Figure 4.9, providing at least nearly a year of data from all sites. Some sites offered multiple years of data. Direct comparisons between the measured wind speeds and directions, and the time series extracted from the Unified-WRF model at corresponding locations and heights, were performed. Based on these concurrent time series, a 12-month by 24-hour bias correction matrix was developed (see Figure 4.10 as an example), encompassing correction factors for wind speed. As for wind direction, an offset in wind direction by sector was deemed the most logical bias correction. These correction factors and offsets were formulated for every

measurement location and height. To apply them across the entire domain, an inverse distance weighting method was adopted to spatially average the correction factors and offsets, considering the closeness of the nearest measurement sites.

		Year --->	2004	2005	2006	2007	2008	2009	2010	2011	2012	2013	2014	2015	2016	2017	2018	2019	2020	2021	2022
Site	Start Date	End Date																			
MM FINO 1	2004-02-01	2008-12-31																			
MM OWEZ	2005-07-01	2006-07-02																			
MMIJ	2012-01-01	2016-01-01																			
FLS Borssele	2016-02-12	2017-02-12																			
lidar LEG	2016-01-01	2018-12-31																			
FLS HKZ	2016-06-05	2018-06-04																			
lidar EPL	2016-07-01	2018-12-31																			
lidar K13-A	2016-11-02	2022-01-01																			
FLS HKN	2017-04-10	2019-04-10																			
FLS HKW	2019-02-05	2021-02-12																			
FLS TNW	2019-06-19	2021-06-20																			
FLS N-7.2	2020-05-20	2021-05-04																			

Figure 4.9 Gantt chart of measurement datasets used in the post-processing

It is noted that such corrections were particularly effective in the coastal zone, due to the dense concentration of measurement sites. However, certain areas in the model domain, especially the northwest quadrant, lacked close proximity to measurement sites. In these areas, DOWA was utilized as a secondary bias correction method. Despite its shorter duration of ten years and slightly coarser grid, DOWA was chosen due to its incorporation of a comprehensive set of local measurements, both onshore and over the ocean.

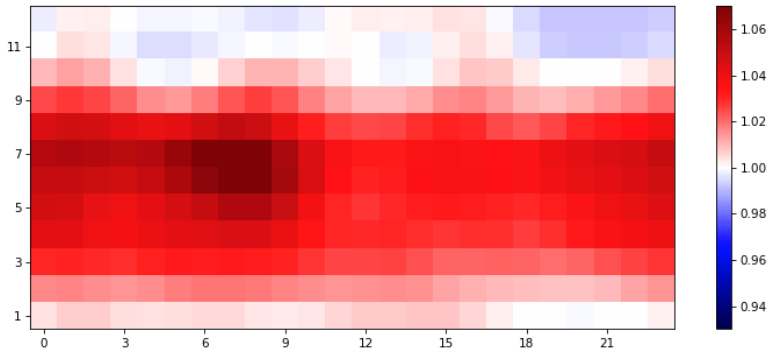

Figure 4.10 Example of 12x24 correction factor matrix for MMIJ at 100 m

By incorporating DOWA, it was assumed that the model would be able to achieve an almost bias-free mean wind speed across its domain. Primarily in the northwest quadrant and predominantly at lower altitudes, the correction factor generally increased wind speeds by a few percentage points.

4.6 Performance of Unified-WRF at the bias correction measurement sites

In the process of evaluating the effectiveness of the implemented techniques and ensuring alignment with key metrics, various metrics were assessed both for storm situations and the complete duration for which site measurements were available following the bias correction (post-processing).

Specifically, for storm periods, by pinpointing peak wind moments from the measurements, the peak wind bias error was determined as shown in Figure

4.11. The green line represents the error in Unified-WRF model after post-processing, the blue depicts the Unified-WRF model before bias correction, and the orange line signifies the performance of ERA5. Only sites with at least 4 peak wind events were included. The number of peak wind events among the sites ranged from 4 to 28. It should be highlighted that the same sites used for model evaluation were also employed for the bias correction. As a result, it was anticipated that the errors would consistently align with ideal values. However, due to the provided weight functions, there was no guarantee of an exact match between model values and measured ones. This process, however, validated the effectiveness of the weighted average.

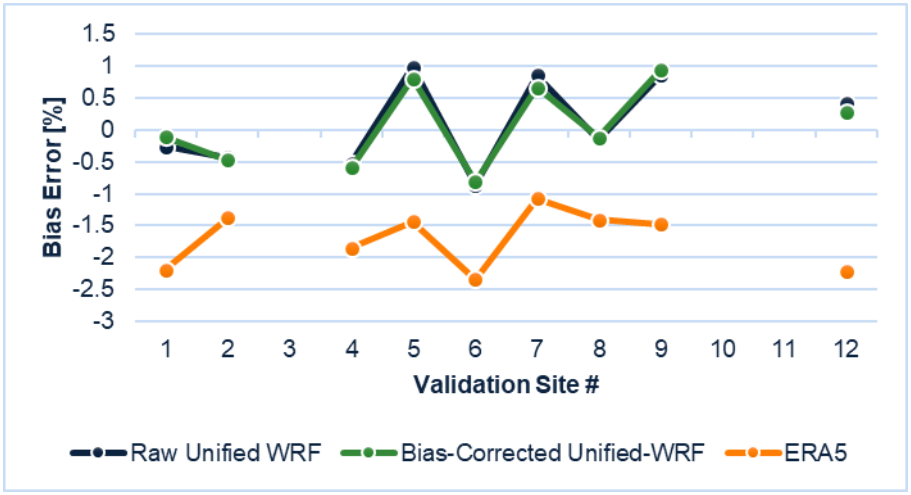

Figure 4.11 Storm-peak wind bias error

In the context of storm peak winds, the raw Unified-WRF model exhibited a near-zero bias. Notably, the bias correction had a minimal effect on the Unified-WRF model's results as the correction was rooted in long-term mean statistics, not solely peak wind figures.

The primary objective of the long-term wind mean bias error validation shown in Figure 4.12 was to verify that the performance of the Unified-WRF model was not degrading, and this appeared to be upheld. Upon analysing the entire dataset, it was discerned that the Unified-WRF model, on average, had a low bias of about 1% across the 12 measurement sites. After bias correction, as expected, this bias was substantially reduced, as evident in Figure 4.12.

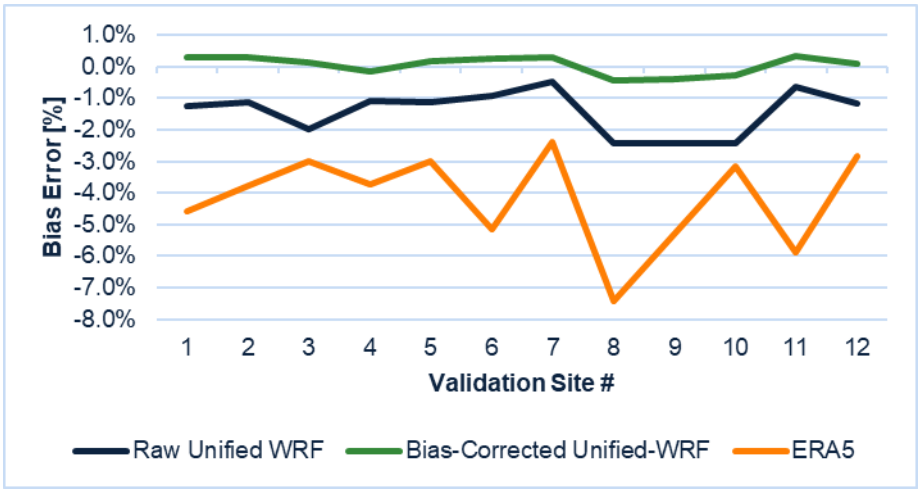

Figure 4.12 Long-term mean wind speed bias error

The correlation performance of the model (R^2 values) is shown in Figure 4.13. Despite excellent hourly R-squared results of the Unified-WRF model, ERA5 outperformed in this category, though the difference was marginal.

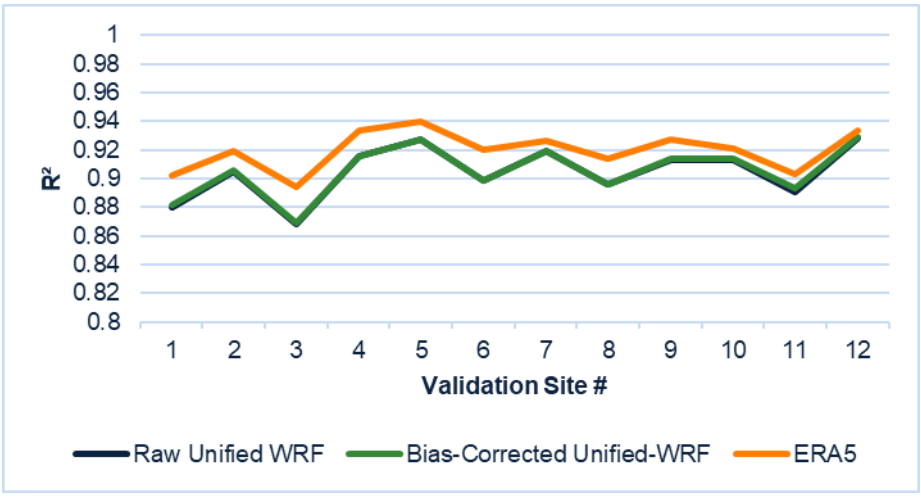

Figure 4.13 Hourly coefficient of determination

The shear parameter was also scrutinized to ensure the raw model and bias correction didn't adversely affect it. Post-bias correction, the Unified-WRF model exhibited near-zero shear bias with minor site-specific variations as shown in Figure 4.14.

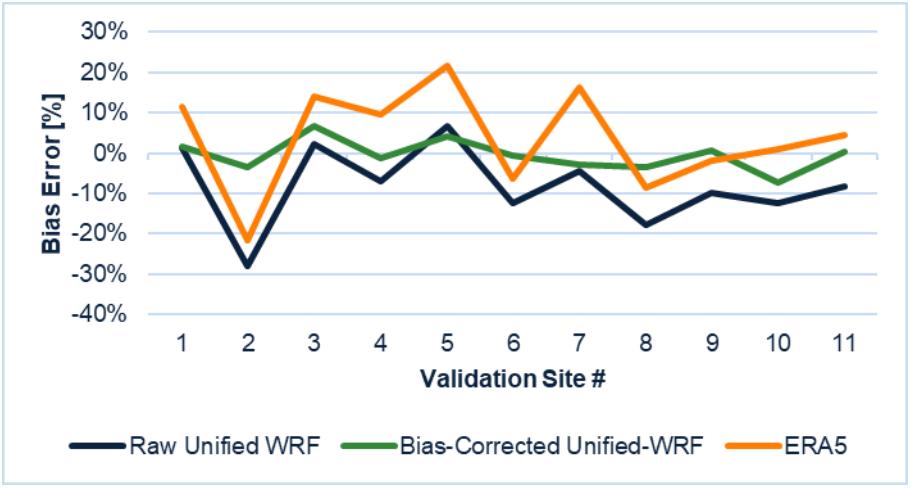

Figure 4.14 Mean shear parameter bias error

The Kolmogorov-Smirnov statistic, a measure of the distribution's goodness of fit, was another area of focus. The results shown in Figure 4.15 further solidified the Unified-WRF model's robustness, showing marked improvements, especially after bias corrections.

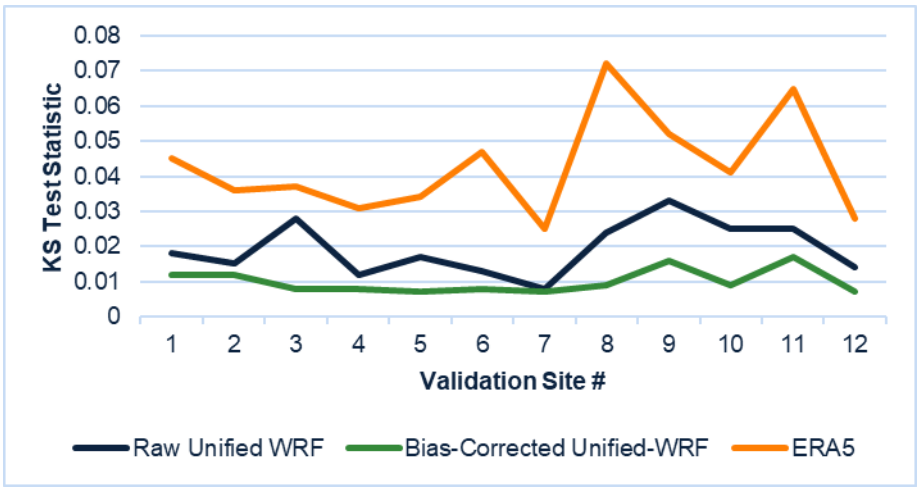

Figure 4.15 Long-term KS Statistic

4.7 Model output

In the comprehensive analysis covering 44 years, a detailed output at 10-minute intervals was generated, emphasizing crucial variables vital to wind energy analysis. These included wind speed, direction, air temperature, and humidity, represented across ten different heights within the rotor layer. Additionally, a range of meteorological parameters such as surface pressure, temperature, boundary layer height, downward irradiance, and rain rate were documented. Furthermore, air pressure and density were presented at the same ten heights, albeit at a 60-minute output frequency. Conclusively, the study of the Unified-WRF model yielded notable insights. The primary objective was to curate a dataset that would adeptly support both metocean analysis and wind resource assessment, and this was successfully realized. The dataset, with a granularity of 1.67 km, captures 44 years of information with a 10-minute output cadence. Importantly, the Unified-WRF, with its integrated hybrid drag

formulation, accurately reflects extreme wind peaks, a critical aspect for metocean modelling. Moreover, by leveraging both the hybrid drag formulation and the astute post-processing bias correction, the data exhibited near-zero bias. This dataset also showcases a very good hourly correlation and is closely aligned with the wind speed distribution of long-term measured winds offshore, underscoring its value for wind resource assessment.

5 Spatial Analysis of Unified-WRF

This section provides an insight into the performance of the Unified-WRF model developed for the Dutch North Sea for wind resource assessment purposes. It presents a comparison of the Unified-WRF model against other mesoscale models to ascertain its quality of performance. This section also presents a comparison of the long-term climate from the Unified-WRF and the MCP procedure. The Unified-WRF model is found to provide an outstanding representation of the wind resource assessment at the primary measurement locations.

The Unified-WRF model was developed for the entire Dutch North Sea, with the overarching goal of assessing wind potential across the IJVWFZ region by using the primary and secondary measured datasets for the development and validation of the model as described in Section 4. The spatial analysis presented in this section assessed the performance of the model specifically for wind resource assessment. The spatial analysis was conducted to gain insight into two specific criteria:

- To inspect how well the Unified-WRF model performs in comparison to other mesoscale model datasets.
- To verify that it is able to represent the long-term climate across IJVWFZ appropriately.

The above investigations were achieved in two main parts:

- Applying short-term data: comparing the Unified-WRF with other mesoscale models over the short-term measurement period of each primary dataset. Concurrent datasets of the primary measured datasets and modelled data from nodes closest to each respective measurement location were applied.
- Applying long-term data: verifying that the Unified-WRF long-term climate output over a select long-term period is in agreement with the long-term climates derived from the MCP procedure.

The above analyses were conducted for specified KPIs, as described in the following sections.

5.1 Spatial analysis over the short-term measurement periods

The aim of the spatial analysis with the short-term data is to inspect how well the Unified-WRF model performs in comparison to the other observed mesoscale modelled datasets.

The performance of the Unified-WRF model was compared with that of other mesoscale models for pairs of concurrent data of measured and modelled datasets. A set of KPIs were observed for each of these dataset pairs. The KPIs give an insight into the performance of the Unified-WRF model on its associated modelling properties and characteristics, representativeness of the measured data and associated biases.

5.1.1 Modelled data selection for spatial analysis

Several modelled data sources were considered to assist in the spatial analysis. These data sources are shown below in Table 5.1. It is noted that the DOWA data is a successor of the KNW data, as an improved version that is forced with the more recently issued ERA5 reanalysis data.

The Unified-WRF model is available up to and including the year 2022, at the time of writing and will be updated later to include the years up to 2025 at the next stages of the project[14].

A detailed description of each modelled data source is presented in Appendix G.

Table 5.1 Modelled datasets for spatial analysis

Parameter	EMD-WRF E+	DOWA	KNW	Unified-WRF
Scale	Mesoscale	Mesoscale	Mesoscale	Mesoscale
Forcing	ERA5	ERA5	ERA-Interim	ERA5
Centre / Provider	EMD	DOWA Project/ Royal Netherlands Meteorological Institute	Royal Netherlands Meteorological Institute	Developed by ArcVera Renewables
Model	WRF	HARMONIE	HARMONIE	WRF
Vertical levels in the final public dataset	13	17	8	10
Output frequency	1 hourly	1 hourly	1 hourly	10 min
Spatial resolution	3 km	2.5 km	2.5 km	1.7 km
Period available	From 1980	2008 – 2018*	1979 – 2019**	1979 - 2022

*up to and including 2018
** up to August 2019

5.1.2 Overview of the measured and modelled datasets

Hourly time series were acquired for each modelled data source for the nearest grid point to the primary measurement locations as defined in Table 5.1. It is noted that the Unified-WRF modelled datasets were generated at the exact location of each of the primary modelled datasets and not from the closest grid point. The details of the selected modelled dataset heights and locations are presented in Table 5.2. The exact nodal locations of the modelled datasets considered are presented in Appendix H.

For the MMIJ and lidar K13-A datasets the measured data was vertically extrapolated to the height of 100 m in the same method described in Section 3.3. Meanwhile, the FLS IJV data used in this analysis covered the measurement period from 01 May 2022 to 31 December 2022 as no further data was available at the time of the analysis.

Table 5.2 Modelled and measured dataset heights for spatial analysis

Dataset	Type (measured/modelled)	Height [m]
FLS IJV	measured	100
MMIJ	measured	100
FLS HKW	measured	100
lidar K13-A	measured	100
EMD-WRF Europe+	mesoscale modelled	100
DOWA	mesoscale modelled	100
KNW	mesoscale modelled	100
Unified-WRF	mesoscale modelled	100

The spatial analysis with short-term data was conducted by observing multiple KPIs to assess the performance of the Unified-WRF model against the measured data and the other mesoscale modelled data sources. The analysis was conducted in three main steps:

1. Firstly, the modelled datasets were observed to assess whether they have full concurrency with the measured datasets. This would allow an exact like-with-like comparison across all the data sources.
2. Secondly, the modelled datasets that had full concurrency with the measured data were correlated against the measured data for both wind speed and wind direction.
3. Lastly, the mean wind speed bias and distribution tests between the measured and modelled datasets were conducted.

The above assessments were carried out with each pair of measured and respective modelled datasets (a total of 16 pairs of datasets). Two other parameters related to each modelled dataset were also observed: the temporal and spatial resolution of each modelled dataset.

Each KPI was classified according to the traffic light classification criteria shown in Table 5.3. Green, amber and red represent outstanding, average, and poor performance, respectively.

It is noted that the FLS IJV data was not used in the development of the Unified-WRF model and therefore acts as a blind test when observing these KPIs.

Table 5.3 Classification criteria for KPIs

Evaluation Criteria	Green	Amber	Red
Months of concurrency	Full	Partial	None
Temporal resolution (minutes)	<60	=60	>60
Spatial resolution	<1 km	1 – 6 km	>6 km
Hourly wind speed correlations (R^2)	>0.80	0.80 – 0.60	<0.60
Hourly wind direction correlations (R^2)	>0.80	0.80 – 0.60	<0.60
Mean absolute difference in wind speed	<1%	1 – 2%	>2%

Evaluation Criteria	Green	Amber	Red
Kolmogorov-Smirnov (K-S) test for wind speed distribution	<=2%	2 – 6%	>6%
Earth mover's distance	<=0.1m/s	0.1 – 0.5 m/s	>0.5 m/s

5.1.3 Results of spatial analysis over short-term

Concurrency of data

The concurrency of each pair of modelled and measured datasets was observed and is presented in Figure 5.1. It can be observed that EMD-WRF Europe+ and Unified-WRF fully overlap with the measured data. Meanwhile, KNW exhibits full overlap with MMIJ and partial overlap with lidar K13-A and FLS HKW. DOWA exhibits full overlap with MMIJ, partial overlap with lidar K13-A and no overlap with FLS HKW. Neither KNW nor DOWA has any concurrency with FLS IJV.

Based on these observations DOWA and KNW could only be observed in the next steps at the MMIJ location.

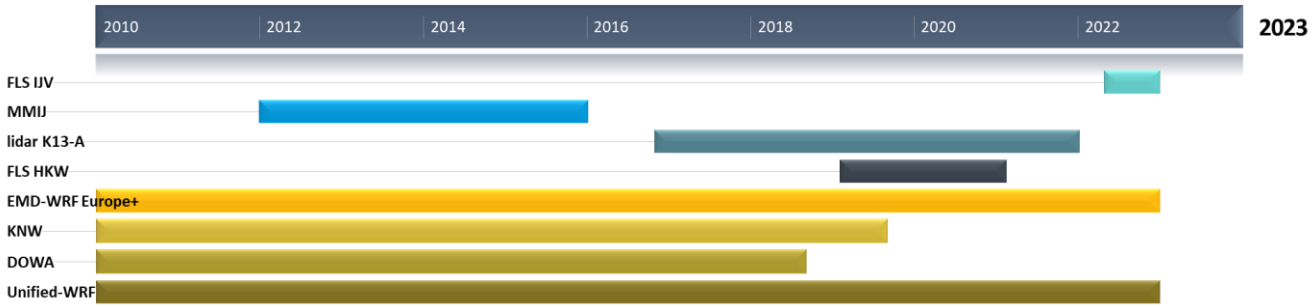

Figure 5.1 Gantt chart of measured and mesoscale modelled datasets

Correlation values

In this step of the analysis, the correlation value between the pairs of primary measured and modelled datasets that have full concurrency was calculated. The correlation coefficient R (Pearson) is a measure of the linear dependence between the measured and modelled wind speed. A correlation coefficient of +1 indicates that two values can be perfectly described by a linear equation. A high correlation in wind speeds indicates that the two time series are largely in sync. This was done for both wind speed and wind direction. The correlation coefficient (R) directly informs the coefficient of determination (R^2) values used in this study, as R^2 represents the proportion of variance in the dependent variable that can be explained by the independent variable, calculated as the square of the correlation coefficient (R).

Table 5.4 below presents the correlation values (coefficient of determination, R^2) of the modelled versus measured datasets, with values above 0.85. All the modelled datasets observed have outstanding R^2 values at all the measurement locations considered for both wind speed and wind direction. This indicates that the Unified-WRF model performs in line with other mesoscale modelled datasets.

Mean wind speed bias and distribution tests

In the final step of assessments, three tests were performed to evaluate any bias in the modelled data and the magnitude associated with that. Three main tests were conducted:

- Mean absolute difference in wind speed: this shows the variation of the modelled wind speed against the measured wind speed in absolute percentage (%). This test is used to assess the performance of each modelled data in absolute mean wind speed values across the short-term.
- Kolmogorov-Smirnov test statistic: A two-sample Kolmogorov-Smirnov test compares the cumulative distribution of two datasets. The Kolmogorov-Smirnov test statistic quantifies the largest distance between the empirical distribution functions of both samples. The test is sensitive to differences in both the location and shape of the empirical cumulative distribution functions of the two samples and thus can indicate the goodness of fit curve. Two datasets with identical cumulative distributions will yield a test statistic of zero.
- Earth mover's distance test: the earth mover's distance is a way to assess the dissimilarity between two probability distributions over a defined region, where a distance measure between single features is given, see [58].

The results of these tests are presented graphically in Figure 5.2, Figure 5.3 and Figure 5.4 and numerically in Table 5.4. As can be observed, the Unified-WRF model exhibits a notably lower mean absolute difference in wind speed than the EMD-WRF Europe+ dataset at all the measurement locations. Meanwhile, at MMIJ, Unified-WRF has comparable performance to that of KNW and DOWA, with a marginally higher difference than DOWA and slightly better performance than KNW.

A similar distribution of performance can also be observed in the Kolmogorov-Smirnov and Earth mover's distance tests. Across these two tests, the Unified-WRF model outperforms the EMD-WRF Europe+ notably well at all the locations observed. At the MMIJ location, the Unified-WRF has comparable performance to that of KNW and DOWA, albeit slightly outperforming KNW as well.

It is reiterated, that the FLS IJV data was not used in the development of the Unified-WRF model and therefore acts as an independent test when observing these KPIs. At the FLS IJV location, the Unified-WRF model exhibits outstanding performance, albeit with slightly higher errors than at the other observed locations. This was expected as the FLS IJV observed period covered approximately seven months, as opposed to the +24 months at the other locations. Therefore, when observing wind speed distribution, a larger volume of data would yield a more stable result.

These results indicate that the Unified-WRF model can represent the mean wind speed and wind speed distribution at the primary measurement locations across the observed short-term period very well. It also has very similar performance to KNW and DOWA which are trusted mesoscale modelled datasets available across the Netherlands and the Dutch North Sea.

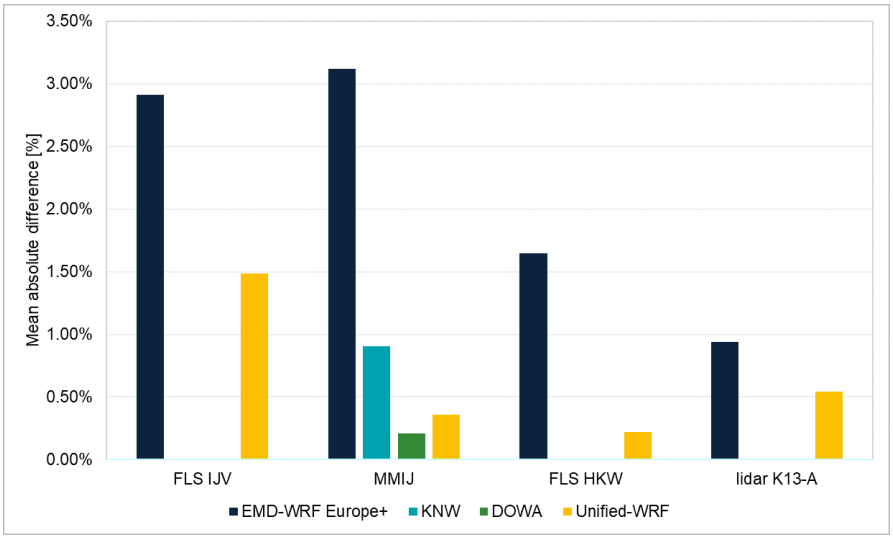

Figure 5.2 Mean absolute difference in wind speed

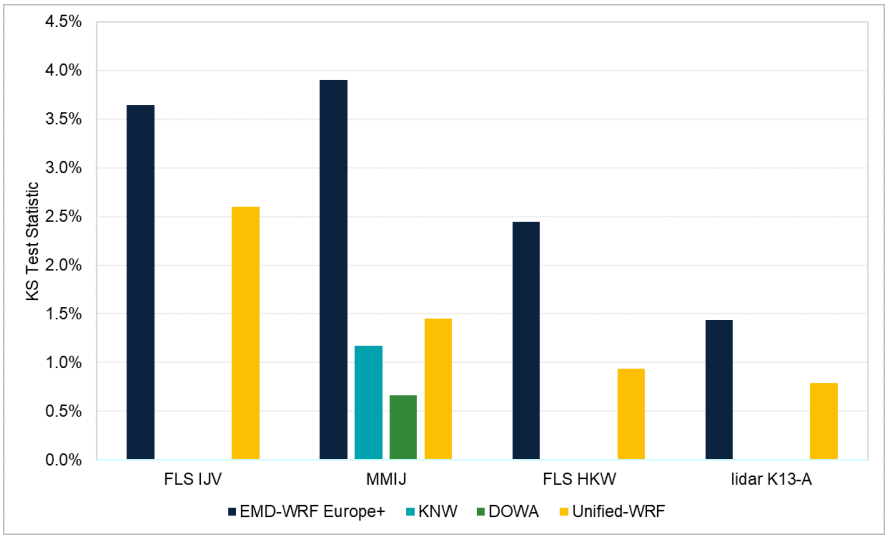

Figure 5.3 Two-sample Kolmogorov-Smirnov test

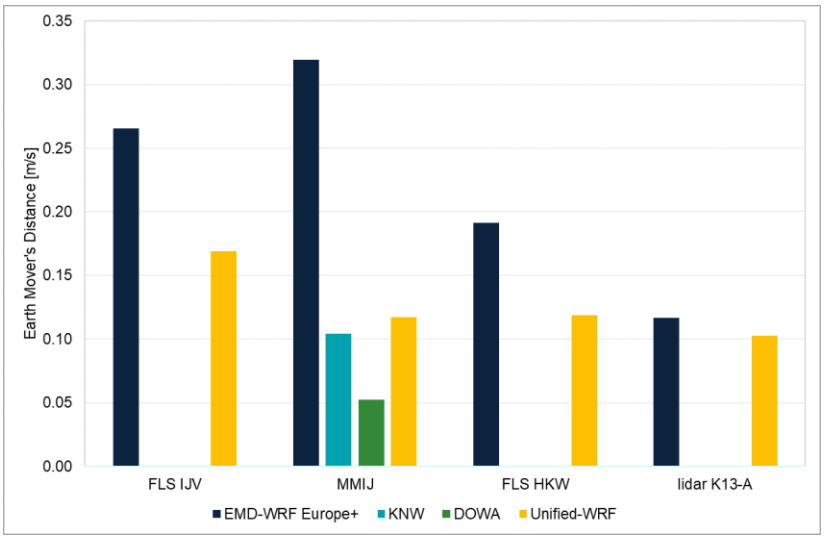

Figure 5.4 Earth mover's distance test

Final classification of results

The results for each of the KPIs were classified according to the criteria in Table 5.3. These results are shown in Table 5.4. The following remarks are made on the results obtained:

- The Unified-WRF model exhibits outstanding or average performance for all the KPIs observed.
- The Unified-WRF shows better or equally good performance as the other mesoscale modelled data sources.
- The DOWA and KNW mesoscale datasets are widely accepted and trusted datasets in the wind industry for the Dutch North Sea. The Unified-WRF model exhibits performance aligned with that of DOWA and KNW at MMIJ, giving high confidence in the Unified-WRF modelled outputs.
- It is noted the DOWA and KNW datasets do not encompass the period from 2019 to 2023 due to their discontinuation, which has implications for their inclusion in the comprehensive spatial validation exercise.
- The EMD-WRF Europe+ data, which was also available concurrently with all the measured data, is outperformed by the Unified-WRF model for the majority of the KPIs investigated.
- The mean distribution bias and distribution test show good performance by the Unified-WRF model which indicates that it is well aligned with the behaviour exhibited by the measured data.
- The Unified-WRF model was developed to inform not just wind resource assessment but also metocean purposes which the other mesoscale datasets are unable to do.

Based on the above remarks, it is concluded that the Unified-WRF model has outstanding performance and surpass the results demonstrated by other mesoscale model datasets. These results give confidence that the Unified-WRF model is able to represent the short-term climate at each primary measurement location outstandingly.

Table 5.4 KPI results of mesoscale modelled datasets

Parameter	Measured dataset	EMD-WRF Europe+	DOWA	KNW	Unified-WRF
Temporal resolution [minutes]		60 mins	60 mins	60 mins	10 mins
Spatial resolution [km]		3	2.5	2.5	1.7
Months of concurrency	FLS IJV	8	0	0	8
	MMIJ	48	48	48	48
	FLS HKW	23	0	7	23
	lidar K13-A	62	26	34	62
Hourly wind speed correlations (R^2)	FLS IJV	0.86	-	-	0.89
	MMIJ	0.91	0.92	0.90	0.92
	FLS HKW	0.91	-	-	0.92
	lidar K13-A	0.91	-	-	0.92
Hourly wind direction correlations (R^2)	FLS IJV	0.93	-	-	0.93
	MMIJ	0.96	0.97	0.96	0.96
	FLS HKW	0.95	-	-	0.95
	lidar K13-A	0.96	-	-	0.96
Mean absolute difference in wind speed [%]	FLS IJV	2.9	-	-	1.5
	MMIJ	3.1	0.2	0.9	0.3
	FLS HKW	1.6	-	-	0.2
	lidar K13-A	0.9	-	-	0.5
K-S test [%]	FLS IJV	3.6	-	-	2.6
	MMIJ	3.9	0.7	1.2	1.5
	FLS HKW	2.4	-	-	0.9
	lidar K13-A	1.4	-	-	0.8
Earth mover's distance [m/s]	FLS IJV	0.27			0.17
	MMIJ	0.32	0.05	0.1	0.12
	FLS HKW	0.19			0.12
	lidar K13-A	0.12			0.10

5.1.4 Uncertainty in spatial variation

In the preceding analysis, average wind speeds at 100 m, both primary and secondary measurements, were utilized. The speed up factors derived from the raw Unified-WRF model were incorporated into this evaluation. For investigating the horizontal gradient, a cross prediction exercise was undertaken.

By calculating the average wind speeds at measurement locations using the raw Unified-WRF model, the modelled speed up effect between the respective sites was ascertained. This procedure can alternatively be regarded as a quantification of the modelled wind gradient. The short-term wind speeds were multiplied by the modelled speed up values to cross-predict wind speeds at each measurement location. The differential wind speeds between the predicted and actual values at the corresponding sites were then computed, where the pairwise distances are shown in Table 5.5 and the results are exhibited in Table 5.6.

Table 5.5 Pairwise cross-prediction distances in km

Predicted site --> Known site	FLS Borss-ele	lidar EPL	MM FINO 1	FLS HKN	FLS HKW	FLS HKZ	lidar K13-A	lidar LEG	MMIJ	FLS N-7.2	MM OWEZ	FLS TNW
FLS Borssele	-	36.3	350.8	136.7	106.7	93.1	168.5	50.1	129.8	358.0	136.4	308.0
lidar EPL		-	315.8	101.0	70.4	59.8	135.7	28.3	95.2	322.1	101.8	271.8
MM FINO 1			-	215.0	250.0	258.1	239.8	303.9	246.4	38.8	214.5	68.0
FLS HKN				-	37.9	47.0	90.6	93.1	57.3	221.4	13.4	172.0
FLS HKW					-	37.1	79.4	71.6	36.2	253.5	45.8	202.4
FLS HKZ						-	116.2	46.5	73.3	266.9	43.8	218.4
lidar K13-A							-	146.8	43.6	231.0	104.0	178.1
lidar LEG								-	103.7	313.4	90.2	264.9
MMIJ									-	244.4	69.8	191.6
FLS N-7.2										-	223.2	53.0
MM OWEZ											-	175.3
FLS TNW												-

Table 5.6 Cross-predicted differential wind speeds

Predicted site --> Known site	FLS Borss-ele	lidar EPL	MM FINO 1	FLS HKN	FLS HKW	FLS HKZ	lidar K13-A	lidar LEG	MMIJ	FLS N-7.2	MM OWEZ	FLS TNW
FLS Borssele	-	-0.10%	-0.40%	0.02%	0.48%	-0.07%	0.77%	-1.03%	-0.72%	-0.75%	0.94%	0.58%
lidar EPL		-	-0.29%	0.12%	0.59%	0.03%	0.88%	-0.93%	-0.62%	-0.64%	1.05%	0.68%
MM FINO 1			-	0.42%	0.89%	0.33%	1.18%	-0.64%	-0.32%	-0.35%	1.35%	0.98%
FLS HKN				-	0.46%	-0.09%	0.75%	-1.05%	-0.74%	-0.77%	0.92%	0.56%

Predicted site --> Known site	FLS Borss-ele	lidar EPL	MM FINO 1	FLS HKN	FLS HKW	FLS HKZ	lidar K13-A	lidar LEG	MMIJ	FLS N-7.2	MM OWEZ	FLS TNW
FLS HKW					-	-0.55%	0.29%	-1.51%	-1.20%	-1.23%	0.46%	0.09%
FLS HKZ						-	0.85%	-0.96%	-0.65%	-0.67%	1.02%	0.65%
lidar K13-A							-	-1.79%	-1.48%	-1.51%	0.17%	-0.19%
lidar LEG								-	0.32%	0.29%	2.00%	1.63%
MMIJ									-	-0.03%	1.67%	1.31%
FLS N-7.2										-	1.70%	1.34%
MM OWEZ											-	-0.36%
FLS TNW												-

It should be highlighted that cross-prediction error often represents a blend of measurement uncertainty and spatial modelling uncertainty.

Drawing from the work of [59], an attempt was made to numerically ascertain the RMS of cross-prediction errors, recognizing them as an combination of measurement uncertainty and spatial modelling uncertainty. Pursuant to [59], equation 10, it was postulated that modelling uncertainty operates as a function of distance.

The measurement uncertainty introduces cross-prediction variability at both the known and predicted sites. Consequently, this uncertainty is manifested twice and in a squared manner due to its presumed independence. Yet, when the site measurement uncertainty is dissected into a universal bias across all locations and a stochastic site-specific component, only the latter remains independent. The relative bias, in contrast, nullifies itself with every cross prediction. Therefore, it is a plausible assumption that the measurement uncertainty, when isolated to its random component, is marginally less than the conventionally posited total measurement uncertainty, approximately around 2%.

It is noted that an average uncertainty of 2% including FLS is considered reasonable, as there are studies indicating that uncertainty in FLS might be less than the current industry practice. This is discussed in the study “Lidar Uncertainty Standard Review Methodology Review and Recommendations” of Carbon Trust, suggesting a revised uncertainty approach for floating lidar systems [60], with further detail is provided in Section 5.5 of a representative calculation for FLS calibration uncertainty, where the revised approach resulted in the equivalent calibration uncertainty of 2.5%, which is notably in line with the previously mentioned average uncertainty of 2%, indicating a close correlation between the proposed revised approaches and the actual findings in this analysis. The binned RMS of the cross-prediction error is presented in Table 5.7.

It can be observed from Figure 5.5 that the random part of the average measurement uncertainty of 0.6% (shown in amber colour) is considerably less than the expected average uncertainty of 2%. This is further discussed at the end of this Section.

Table 5.7 Binned RMS of the cross-prediction error

From distance [km]	To distance [km]	Mean bin distance [km]	Actual RMSE	Count
0	50	25	0.83%	12
50	100	75	1.04%	15
100	150	125	0.83%	11
150	200	175	0.75%	5
200	250	225	0.98%	11
250	300	275	1.02%	5

The formulation employed to approximate cross-prediction uncertainty is described as follows:

$$\sigma^2_{crosspred} = 2 * \sigma^2_{avg_{meas_{random}}} + \sigma^2_{spatial_{model}}$$

This poses a dilemma as the equation is unconstrained, entailing more variables than mathematical expressions. Nevertheless, by incorporating values that prompt the hypothetical cross-prediction error versus distance graph, depicted in cyan in Figure 5.5, to most congruently align with the genuine RMS of cross-prediction errors against distance graph (illustrated in navy blue), an informed estimation of modelling uncertainty in relation to distance can be achieved, resonating with the Clerc et al equation provided in [59], as shown in green in Figure 5.5. The actual RMSE of the cross-prediction error is detailed in Table 5.7 and shown in Figure 5.5 together with spatial modelling uncertainty and hypothetical combined uncertainty.

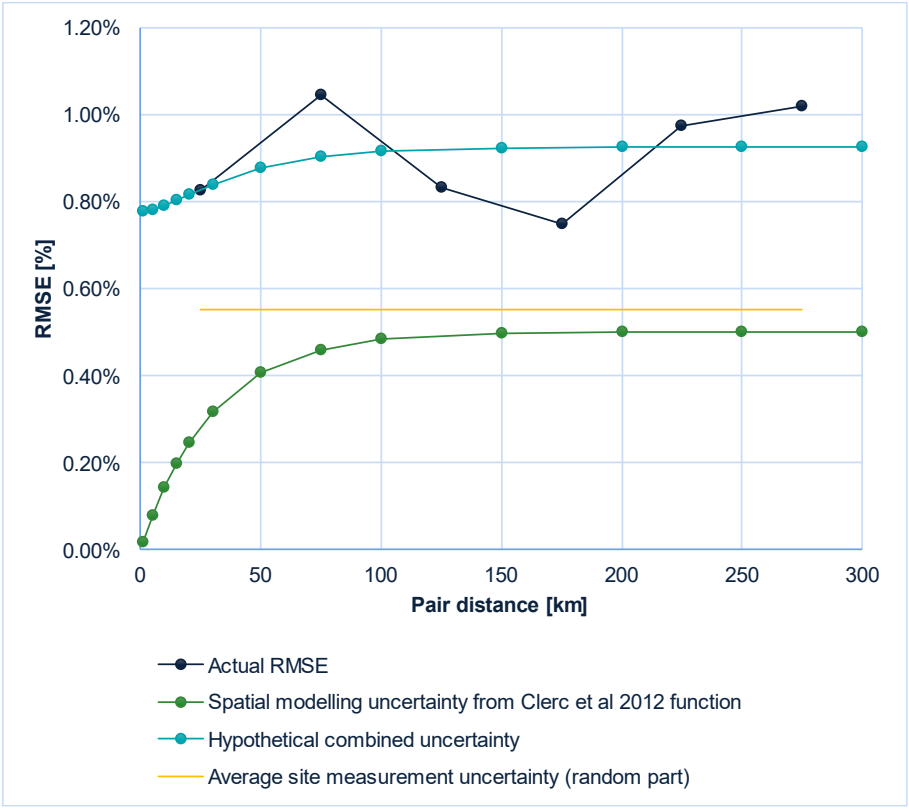

Figure 5.5 Uncertainty in horizontal extrapolation versus distance

As can be seen in Figure 5.5 the maximum cross prediction error is estimated to be ±1.0% and in its magnitude aligned with the approximate mean wind speed bias of 1% observed in Section 4.6 and shown in Figure 4.12.

Based on the configuration tests and cross-prediction exercise, the individual uncertainties in horizontal extrapolation from the relative primary datasets are estimated to range from ±0.0% to ±0.4% at the difference locations across the IJVWFZ. This is further described in Section 8.

Discussion

A systematic error or universal bias is, by definition, consistent across all sites. During cross-prediction, this error is introduced at both the known and predicted sites. However, since it's consistent, such a bias cancels itself out during the cross-prediction process.

On the other hand, random errors or stochastic site-specific components remain and don't cancel out because they're unique to each site and independent. In a cross-prediction, the random component of the measurement uncertainty remains, while the systematic error is averaged out.

However, each measurement instance will also feature specific systematic bias errors that vary between the measurements and show up in a cross prediction. Such biases may for example be caused by differences in:

- **Data filtering:** Outliers and erroneous data have been efficiently filtered out, leading to a lower random measurement error.
- **Temporal and spatial averaging:** The datasets are averaged over time and over multiple sites, which can reduce random uncertainties.

- **Underestimation of systematic errors:** While random errors seem low, there might be systematic errors that aren't accounted for. These could arise from instrument biases, environmental factors, or modelling assumptions.

In conclusion, whilst the actual RMSE and the hypothetical combined uncertainties exhibit variations with pair distances, the spatial modelling and random measurement uncertainties show distinct patterns. The offshore environment is relatively invariant in terms of wind speed, leading to lower variability and hence low spatial uncertainty.

Understanding these patterns and the reasons behind the observed lower random measurement uncertainty can guide improvements in mesoscale modelling and offshore wind speed measurements. A detailed investigation of these phenomena is outside the scope of this study and requires further research.

5.2 Spatial analysis over the long-term periods

The Unified-WRF long-term climate output over a select long-term period was compared with the long-term climates derived from the MCP procedure at each of the primary measurement locations. This was done to verify that the Unified-WRF model output is able to represent the long-term climate across IJVWFZ appropriately.

5.2.1 Unified-WRF long-term trend analysis

A long-term trend analysis on the Unified-WRF datasets generated at each respective primary measurement location was conducted to select the most suitable long-term period with the lowest bias. Different long-term periods ranging from 10 years to 20 years were observed for the most recent years. A period was selected that minimises the effect of a possible trend while remaining representative of the long-term today. The selected long-term period was from 01 January 2010 to 31 December 2022, a period of 13 years. A depiction of the long-term trend across the selected period is shown in Appendix I.

5.2.2 Overview of the datasets

Time series were prepared for each of the MCP and the corresponding Unified-WRF long-term time series at the height of 160 m. It is noted that the Unified-WRF modelled datasets were generated at the exact location of each of the primary modelled datasets. The details of the selected datasets' heights and locations are presented in Table 5.8.

Table 5.8 Modelled and measured dataset heights for spatial analysis

Dataset	Type [measured/modelled]	Long-term period	No. years	Height [m]
FLS IJV	MCP long-term corrected	01/01/2010 to 31/12/2022	13	160
MMIJ				
FLS HKW				
lidar K13-A				

Unified-WRF	mesoscale modelled	01/01/2010 to 31/12/2022	13	160

5.2.3 Results of spatial analysis over long-term

The long-term mean wind speeds from the MCP results and the long-term period selected from the Unified-WRF were compared at each of the primary measurement locations. The datasets are described in Table 5.8 above.

For each of these dataset pairs, the following are observed:

- Long-term mean absolute difference in wind speed.
- Long-term frequency wind roses.
- Long-term monthly mean profile.

Long-term mean absolute difference in wind speed

The mean absolute difference in wind speed shows the variation of the modelled wind speed against the long-term corrected measured wind speed in absolute percentage. This test is used to assess the performance of each modelled data in absolute mean wind speed values across the observed period.

The results of this assessment are presented in Table 5.9 below. The comparison is done against the MCP results for the 13-year (2010-2022) period. It can be observed that the mean absolute difference when comparing the Unified-WRF against the MCP results is highest at FLS HKW at 0.91% and the lowest at MMIJ with 0.17%. The mean absolute difference values observed are well within the uncertainty margin associated with both the MCP results and the Unified-WRF model datasets.

It is reiterated, that the FLS IJV data was not used in the development of the Unified-WRF model and therefore acts as an independent test when observing these results. At the FLS IJV location, the Unified-WRF model exhibits outstanding performance, with very low mean absolute difference values.

Table 5.9 Unified-WRF and MCP long-term wind speeds mean absolute difference

Label	MCP LT WS 13 years [m/s]	Unified-WRF LT WS 13 years [m/s]	Mean abs. difference [%]
Height [m]	**160**	**160**	**160**
Base case	-	-	MCP 13 years
FLS IJV	10.12	10.14	0.28
MMIJ	10.17	10.19	0.17
Lidar K13-A	10.12	10.18	0.62
FLS HKW	9.89	9.98	0.91

Long-term frequency wind roses

A long-term frequency wind rose presents the frequency distribution of wind speed from each direction sector, based on the selected sectorwise binning. The comparison of the long-term frequency rose at each of the primary locations from the MCP procedure and the Unified-WRF are presented in Figure 5.6 to Figure 5.9.

It can be observed that the wind roses from the MCP and Unified-WRF exhibit excellent alignment, indicating the Unified-WRF sectorwise wind frequency is representative of the long-term.

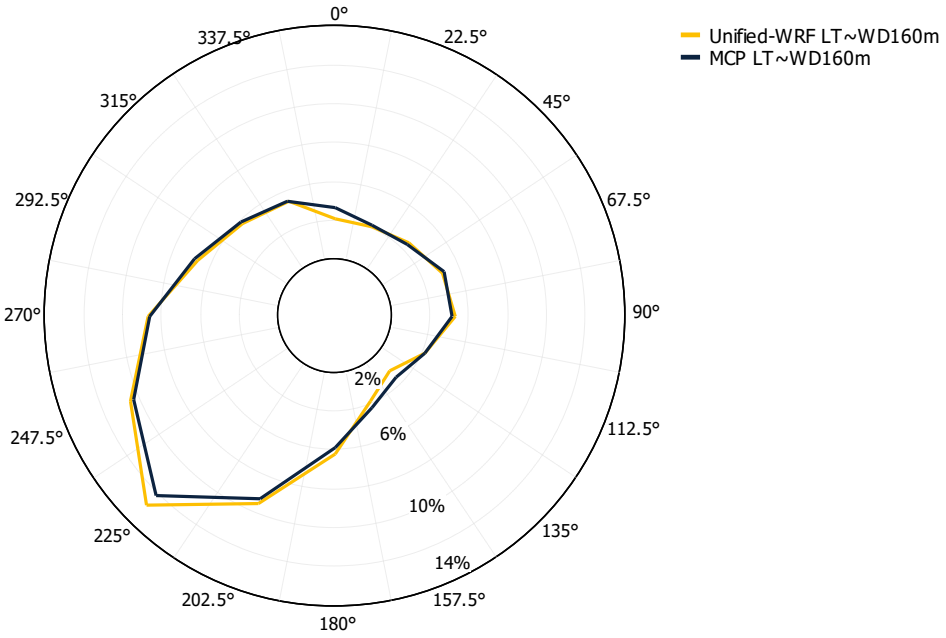

Figure 5.6 FLS IJV LT MCP and Unified-WRF 160 m wind rose

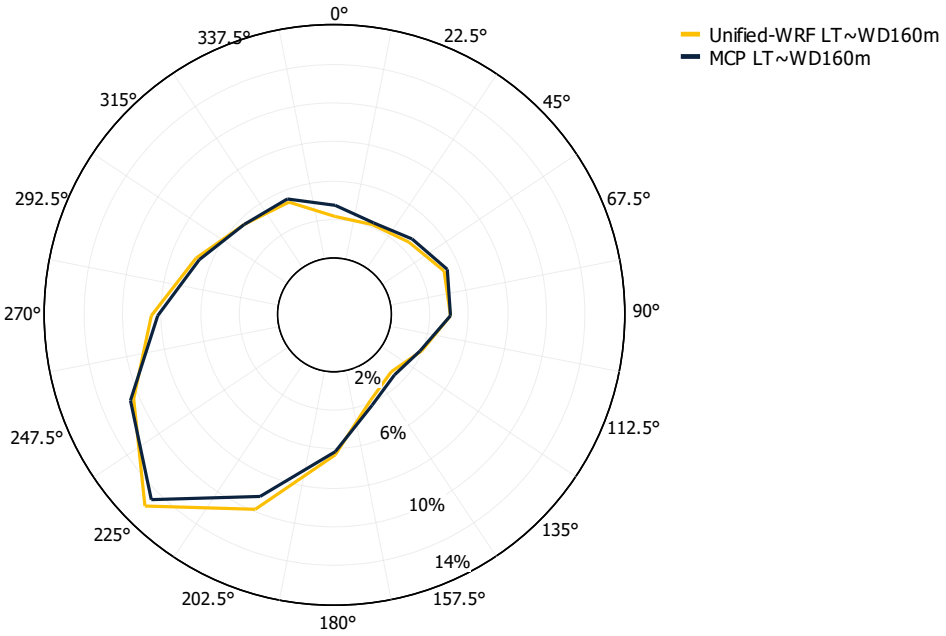

Figure 5.7 MMIJ LT MCP and Unified-WRF 160 m wind rose

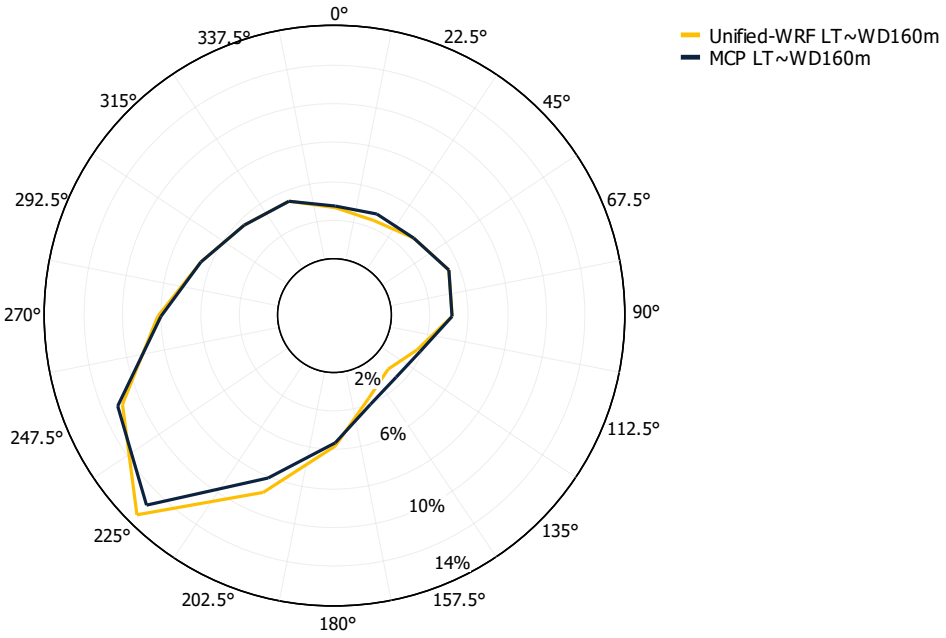

Figure 5.8 FLS HKW LT MCP and Unified-WRF 160 m wind rose

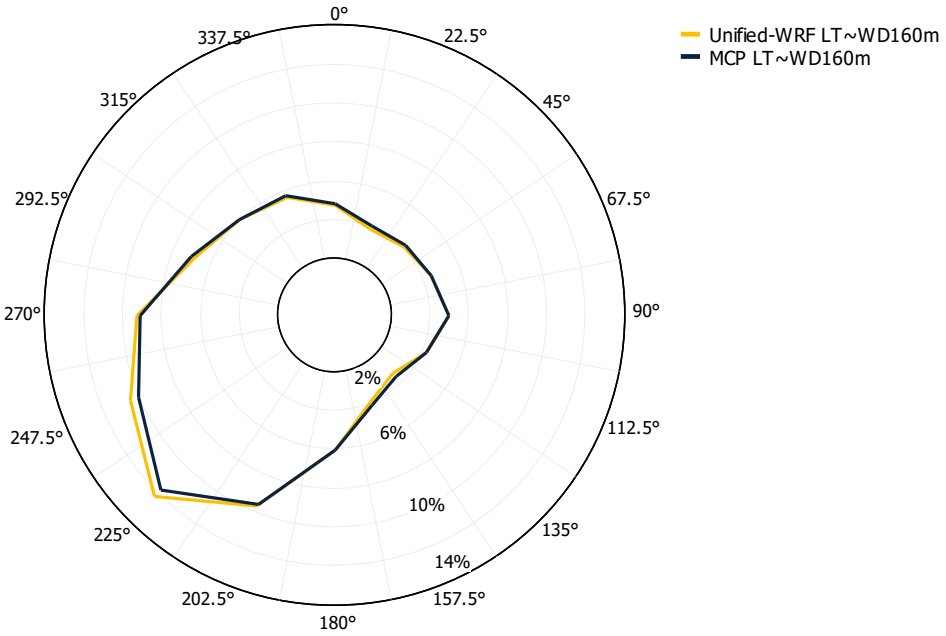

Figure 5.9 Lidar K13-A LT MCP and Unified-WRF 160 m wind rose

Long-term monthly mean profile

The long-term monthly mean profile from the MCP procedures and Unified-WRF at each of the primary measurement locations were observed. These are presented in Figure 5.10 to Figure 5.13.

It can be observed that the MCP and Unified-WRF have excellent alignment in their monthly mean distribution across the respective selected long-term periods. This indicates that the Unified-WRF is able to represent the seasonal variation across the calendar year very well.

These results indicate that the Unified-WRF model exhibits outstanding performance at all the observed locations for the long-term period. The Unified-

WRF model is able to represent the long-term climate at the IJVWFZ excellently for the selected long-term period of 13 years (2010-2022).

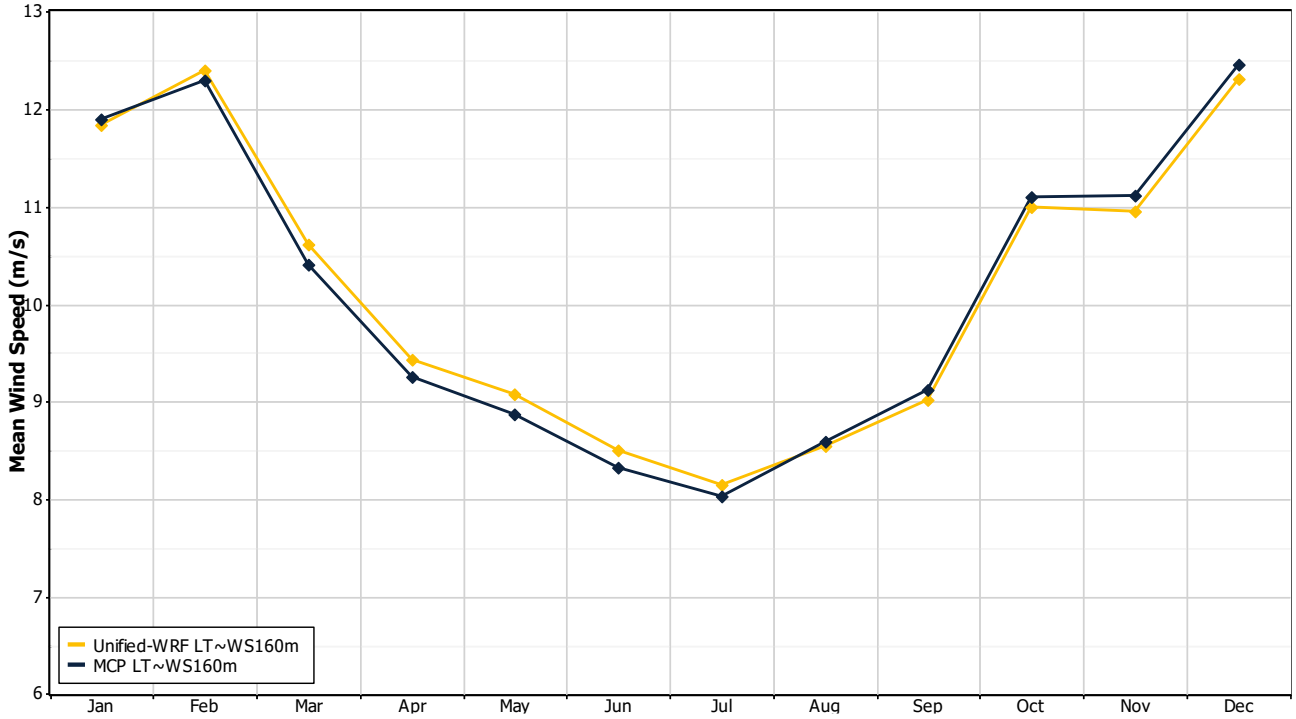

Figure 5.10 FLS IJV LT MCP and Unified-WRF 160 m monthly mean WS

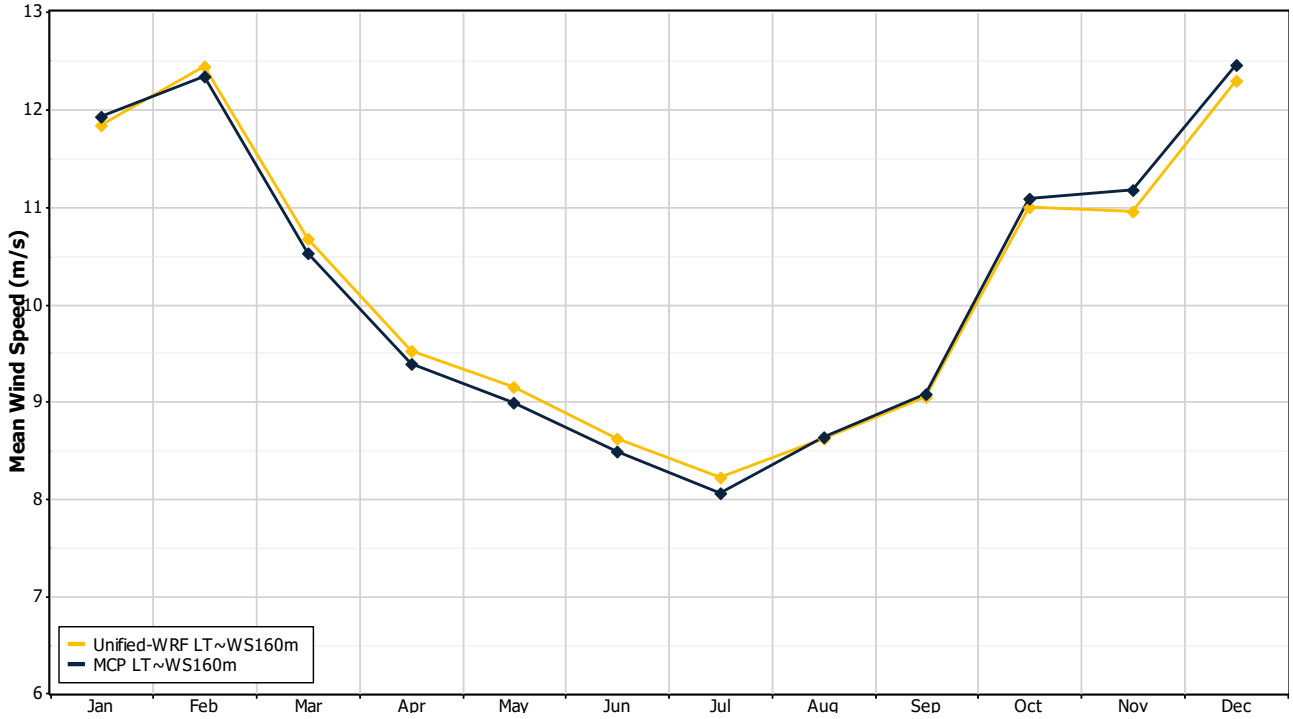

Figure 5.11 MMIJ LT MCP and Unified-WRF 160 m monthly mean WS

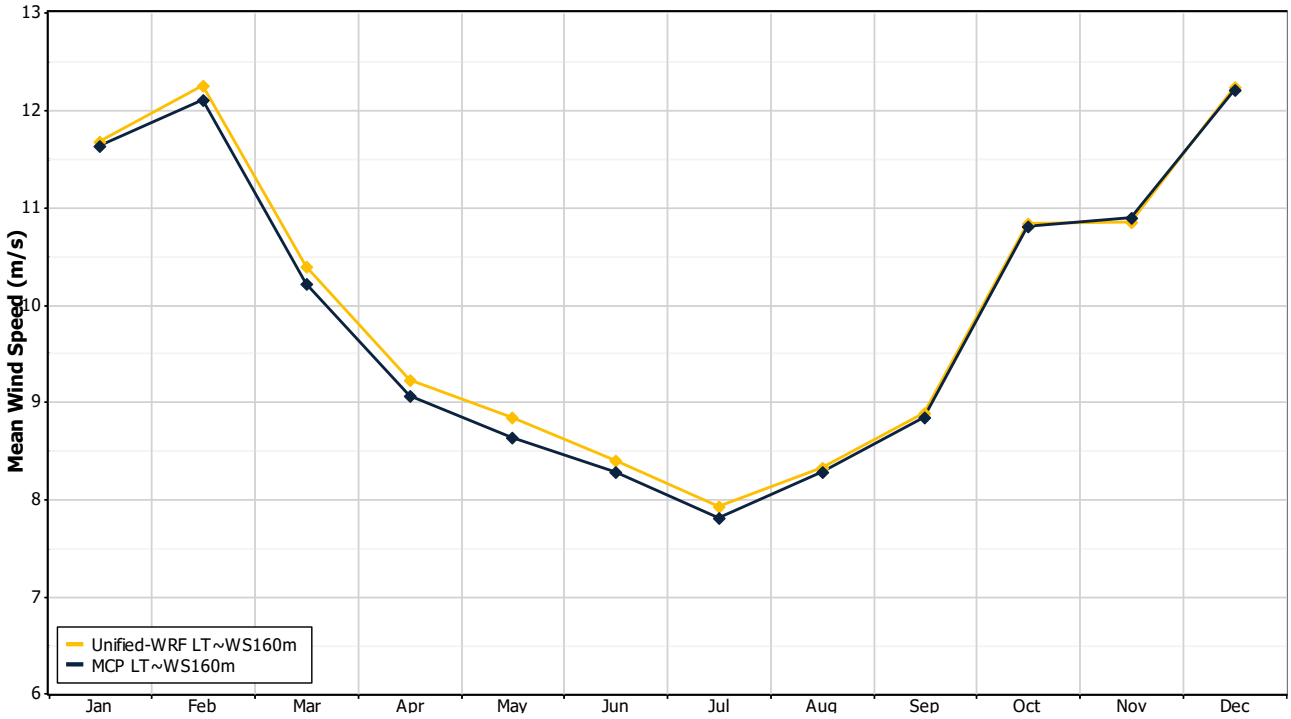

Figure 5.12 FLS HKW LT MCP and Unified-WRF 160 m monthly mean WS

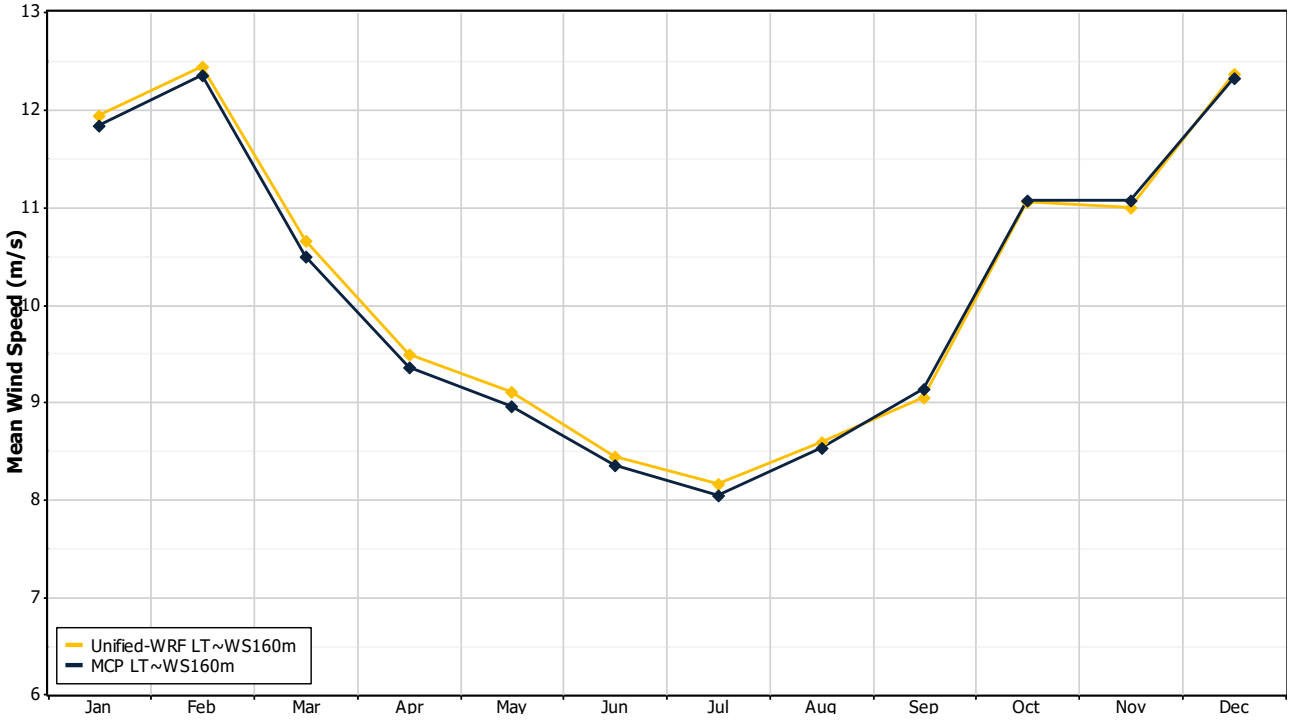

Figure 5.13 Lidar K13-A LT MCP and Unified-WRF 160 m monthly mean WS

Remarks on the spatial analysis over long-term

The following remarks are made with respect to the results obtained in the spatial analysis over long-term:

- The mean absolute difference values observed between the long-term Unified-WRF and MCP outputs are well within the uncertainty margin associated with both the MCP results and the Unified-WRF model datasets. This indicates that the Unified-WRF model mean wind speed over the selected long-term is representative of the long-term climate at each of the observed locations.
- The wind roses from the long-term MCP and Unified-WRF exhibit excellent alignment, indicating the Unified-WRF sectorwise wind frequency is representative of the long-term.
- The long-term MCP and Unified-WRF have excellent alignment in their monthly mean distribution across the selected 13-year long-term period.

The results verify that the Unified-WRF model is able to represent the long-term climate at the observed locations for the selected long-term period. This establishes that the Unified-WRF model is able to represent the long-term climate across the IJVWFZ appropriately and with high associated confidence.

6 IJVWFZ Long-Term Climate

The long-term climate results from the Unified-WRF model are presented in this section. The wind gradient across the IJWFZ is presented along with a closer look at specified locations within each of the IJV WFS.

Based on the development of the Unified-WRF model described in Section 4 and the spatial analysis assessment presented in Section 4.4.2, the Unified-WRF model was deemed appropriate to represent the long-term climate across the IJVWFZ.

As described in Section 5.2.1, a long-term trend analysis on the Unified-WRF time series output was conducted to select the most suitable long-term period with the lowest bias. A 13-year period from 01 January 2010 to 31 December 2022 was selected. A depiction of the long-term trend across the selected period is shown in Appendix I.

All the long-term representative results from the Unified-WRF model presented in this section are based on the selected 13-year period.

6.1 IJVWFZ wind gradient map

A wind speed gradient map representative of the long-term wind speed at the height of 160 m was developed for the IJVWFZ. This is presented in Figure 6.1. It can be observed that the wind gradient ranges from 10.08 m/s to 10.20 m/s across the WFZ. The lower wind speeds are observed in the southeast and east of the WFZ with higher wind speeds in the west and northwest area.

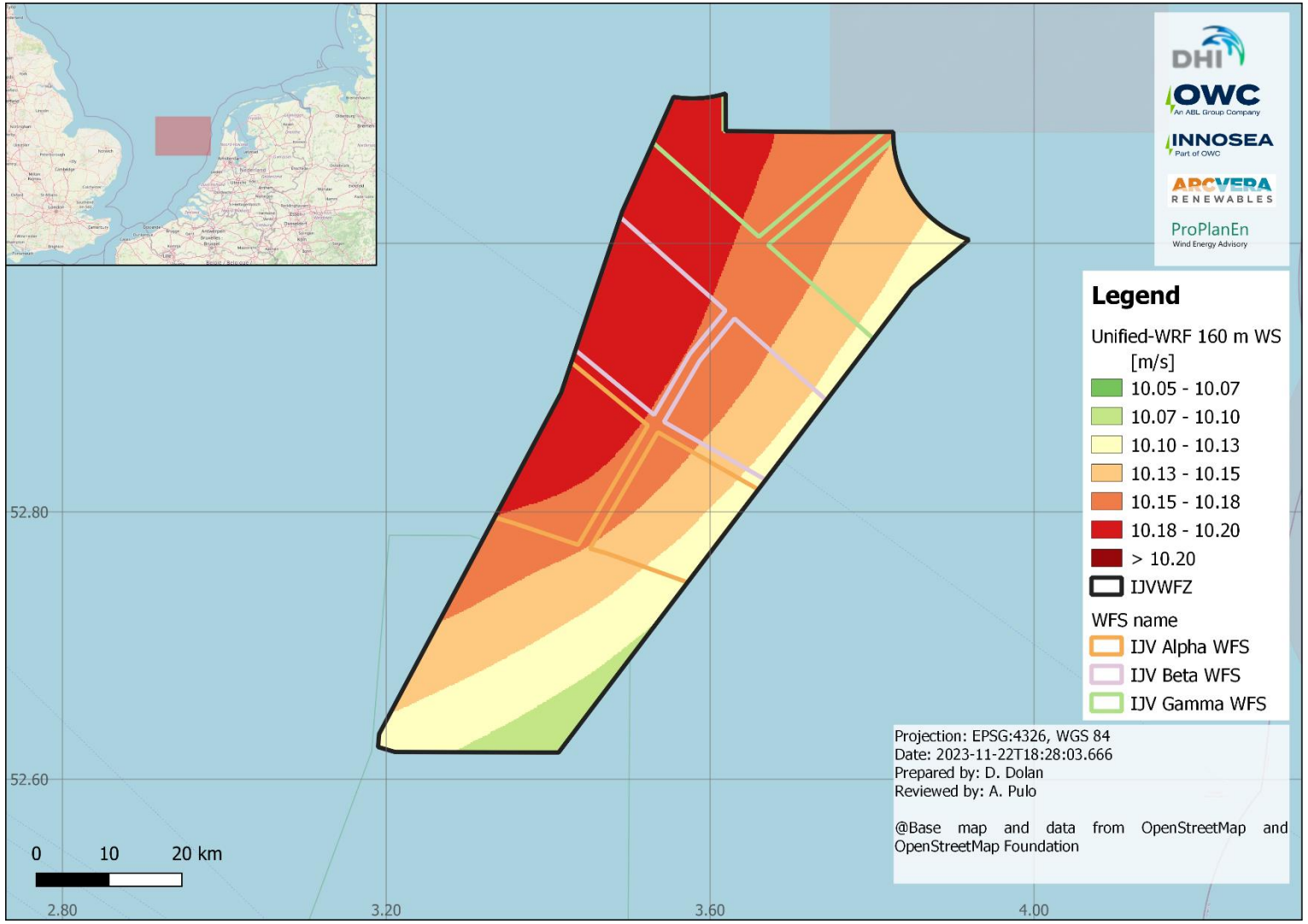

Figure 6.1 IJVWFZ wind speed gradient map at 160 m

6.2 IJVWFZ selected nodal locations mean wind speeds

Six nodal locations (two in each WFS) were selected for a closer observation of the long-term representative wind climate at specified locations. These locations are marked graphically in Figure 6.2 and presented in Table 6.1. The following sections will provide a closer look at these locations.

It is noted that N2_Alpha2 is at the MM IJmuiden location while N3_Beta1 is at the FLS IJV location.

Table 6.1 IJVWFZ nodal location coordinates

Label	Latitude	Longitude	ETRS89 UTM 31N	
			Easting [m]	Northing [m]
N1_Alpha1	52°47.9783' N	3°34.0581' E	538270	5850133
N2_Alpha2	52°50.8898' N	3°26.1399' E	529340	5855468
N3_Beta1	52°53.6500' N	3°41.1167' E	546101	5860717
N4_Beta2	52°56.6263' N	3°31.2499' E	534998	5866142
N5_Gamma1	52°59.6856' N	3°47.9871' E	553679	5871986
N6_Gamma2	53°03.4616' N	3°38.3977' E	542890	5878879

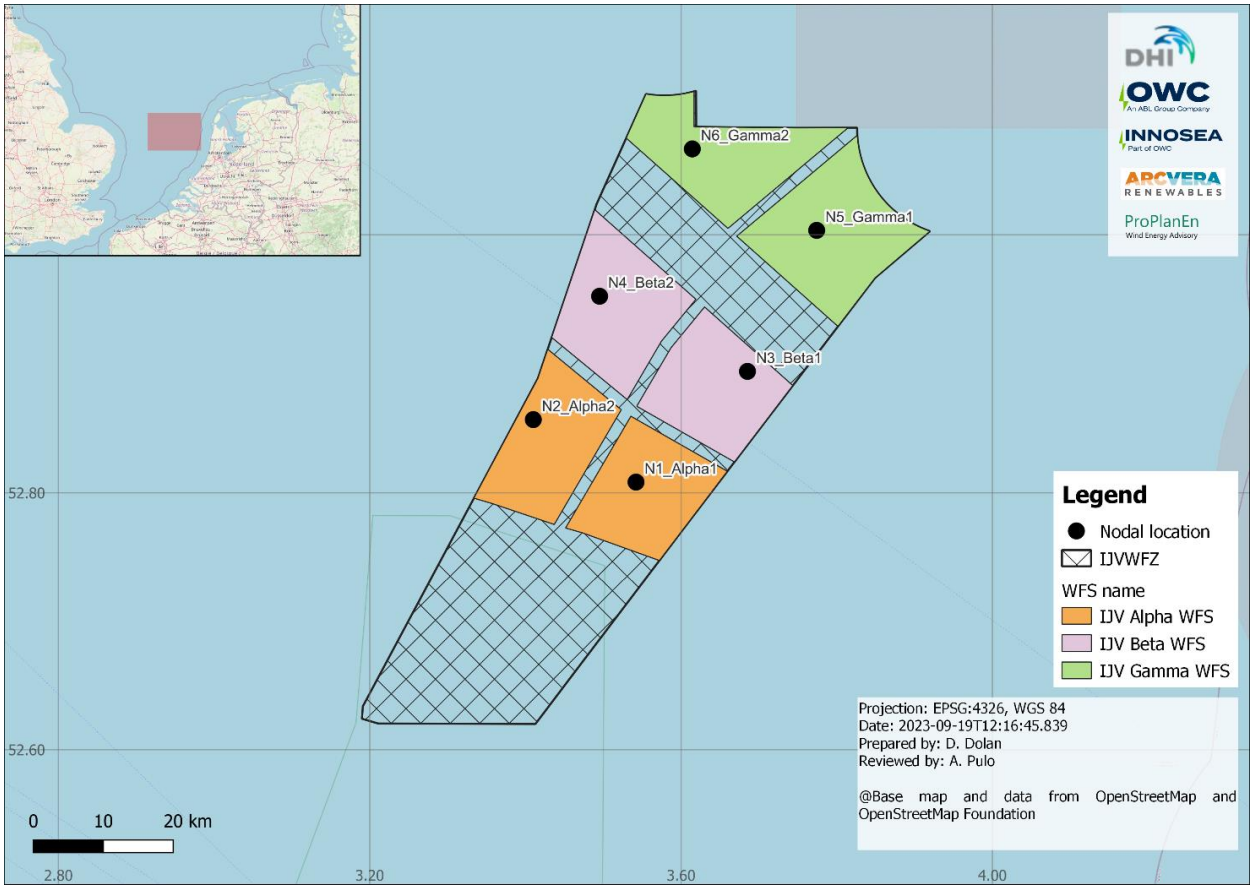

Figure 6.2 IJVWFZ nodal locations

6.3 Alignment with previous studies

The long-term mean wind speeds derived from the Unified-WRF model were compared with those derived from previous wind resource assessment studies commissioned by RVO. The offshore wind resource studies considered in this comparison exercise are listed below, together with a citation of each relevant study;

- Hollandse Kust (zuid) wind farm zone (HKZWFZ), issued in 2017 [13].
- Hollandse Kust (noord) wind farm zone (HKNWFZ), issued in 2019 [34].
- Hollandse Kust (west) wind farm zone (HKWWFZ), issued in 2020 [47].
- Ten noorden van de Waddeneilanden wind farm zone (TNWWFZ), study issued in 2022 [37].

A comparison of wind speeds at the centre of each site at the height of 100 m is presented in Table 6.2. It is noted that for the IJVWFZ the MM IJmuiden location is used as reference. The IJVWFZ exhibits minimal wind gradient and therefore this location can be considered representative for the purpose of this comparison exercise.

It can be observed that the wind speed increases with distance from the coastline which is also noted in [47] and [37]. As the IJVWFZ lies significantly further away from the coastline than the Hollandse Kust WFZs a higher wind speed at this location is expected.

Note that IJVWFZ MM IJmuiden and TNWWFZ centre are at very similar distances from the coastline however have differing mean wind speeds. This is expected as IJVWFZ which lies to the west of the western coastline as opposed to TNWWFZ which lies to the north of the northern coast of the Netherlands. Therefore, these two locations, which are more than 180 km apart, are exposed to different local wind climates.

Table 6.2 Comparison of wind speeds at 100 m at various WFZs

Reference location	Wind speed 100 m[/s]	Distance from coast [km]
N2_Alpha2[15]	9.80 ± 0.20 m/s	Approximately 80 km
HKZWFZ centre	9.44 ± 0.38 m/s	Approximately 25 km
HKNWFZ centre	9.53 ± 0.38 m/s	Approximately 25 km
HKWWFZ centre	9.72 ± 0.31 m/s	Approximately 62 km
TNWWFZ centre	9.99 ± 0.35 m/s	Approximately 80 km

6.4 Mean wind speed

The long-term mean wind speed at each nodal location is presented in Table 6.3 at multiple heights. Similar wind speeds can be observed across the nodal locations.

[15] IJVWFZ MM IJmuiden location

Table 6.4 and Table 6.5 present the long-term sectorwise frequency distribution of the 160 m wind speed at the N2_Alpha2 and the N3_Beta1 nodal locations.

Table 6.3 IJVWFZ nodal location mean wind speeds

Height [m]	Mean wind speed [m/s]					
	N1_ Alpha1	N2_ Alpha2	N3_ Beta1	N4_ Beta2	N5_ Gamma1	N6_ Gamma2
300	10.50	10.54	10.51	10.54	10.51	10.54
250	10.42	10.47	10.43	10.47	10.43	10.46
200	10.29	10.34	10.30	10.35	10.30	10.34
160	10.14	10.19	10.14	10.19	10.14	10.18
140	10.04	10.10	10.05	10.10	10.05	10.09
120	9.92	9.97	9.93	9.98	9.93	9.97
100	9.75	9.80	9.76	9.80	9.76	9.80
60	9.31	9.34	9.31	9.34	9.32	9.33
30	8.75	8.78	8.76	8.78	8.77	8.78
10	7.97	7.99	7.98	8.00	7.99	8.00

Table 6.4 Sectorwise annual frequency distribution of wind speed at N2_Alpha2
The N2_Alpha2 location is at the MMIJ location.

160 m wind speed	0°	30°	60°	90°	120°	150°	180°	210°	240°	270°	300°	330°	All
0-1	0.02	0.04	0.05	0.05	0.05	0.06	0.05	0.06	0.06	0.05	0.05	0.04	0.57
1-2	0.10	0.13	0.13	0.14	0.13	0.16	0.18	0.19	0.16	0.18	0.17	0.16	1.81
2-3	0.26	0.24	0.24	0.22	0.22	0.21	0.32	0.31	0.30	0.31	0.28	0.30	3.22
3-4	0.35	0.37	0.35	0.32	0.29	0.31	0.37	0.44	0.44	0.41	0.40	0.36	4.40
4-5	0.41	0.44	0.43	0.40	0.37	0.35	0.48	0.58	0.58	0.58	0.50	0.44	5.56
5-6	0.49	0.51	0.54	0.47	0.38	0.37	0.56	0.64	0.70	0.64	0.64	0.60	6.53
6-7	0.56	0.61	0.61	0.58	0.42	0.36	0.61	0.82	0.79	0.71	0.73	0.68	7.47
7-8	0.56	0.64	0.59	0.65	0.41	0.37	0.63	0.85	0.92	0.83	0.78	0.70	7.93
8-9	0.55	0.60	0.53	0.62	0.43	0.40	0.57	0.98	0.97	0.86	0.72	0.66	7.89
9-10	0.47	0.50	0.59	0.55	0.39	0.39	0.52	1.04	0.96	0.81	0.72	0.63	7.59
10-11	0.43	0.42	0.57	0.57	0.37	0.33	0.54	1.03	1.01	0.80	0.68	0.57	7.31
11-12	0.40	0.35	0.50	0.47	0.27	0.32	0.50	1.02	1.10	0.76	0.58	0.48	6.73
12-13	0.32	0.26	0.35	0.38	0.27	0.28	0.46	0.97	1.04	0.72	0.50	0.38	5.93
13-14	0.25	0.18	0.33	0.33	0.24	0.24	0.47	0.90	0.99	0.70	0.39	0.33	5.32
14-15	0.16	0.12	0.27	0.29	0.15	0.17	0.40	0.88	0.91	0.58	0.34	0.28	4.55
15-16	0.12	0.07	0.17	0.20	0.14	0.12	0.34	0.76	0.79	0.51	0.26	0.25	3.72
16-17	0.09	0.06	0.11	0.15	0.08	0.08	0.28	0.74	0.68	0.46	0.22	0.17	3.11
17-18	0.07	0.03	0.05	0.11	0.06	0.05	0.25	0.63	0.58	0.36	0.15	0.11	2.46
18-19	0.04	0.02	0.04	0.09	0.04	0.05	0.20	0.56	0.47	0.27	0.12	0.08	1.99
19-20	0.03	0.02	0.04	0.06	0.02	0.04	0.18	0.42	0.37	0.18	0.09	0.06	1.50
20-21	0.01	0.01	0.03	0.04	0.02	0.02	0.12	0.33	0.32	0.15	0.06	0.05	1.16
21-22	0.01	0.00	0.01	0.03	0.00	0.02	0.09	0.27	0.24	0.13	0.06	0.03	0.90
22-23	0.01	0.00	0.01	0.02	0.00	0.01	0.07	0.22	0.22	0.10	0.05	0.02	0.72
23-24	0.01	0.01	0.00	0.02	0.00	0.00	0.05	0.17	0.17	0.08	0.04	0.02	0.55
24-25	0.00	0.00	0.00	0.00	0.00	0.00	0.02	0.12	0.12	0.05	0.02	0.02	0.37
25-26	0.00	0.00	0.00	0.00	0.00	0.00	0.02	0.09	0.08	0.04	0.01	0.01	0.26
26-27	0.00	0.00	0.00	0.00	0.00	0.00	0.01	0.06	0.05	0.03	0.01	0.01	0.16
27-28	0.00	0.00	0.00	0.00	0.00	0.00	0.01	0.03	0.04	0.01	0.01	0.00	0.10
28 - 29	0.00	0.00	0.00	0.00	0.00	0.00	0.01	0.02	0.02	0.01	0.00	0.00	0.07
29 - 30	0.00	0.00	0.00	0.00	0.00	0.00	0.00	0.02	0.01	0.01	0.00	0.00	0.04
30 - 31	0.00	0.00	0.00	0.00	0.00	0.00	0.00	0.01	0.01	0.01	0.00	0.00	0.03
31 - 32	0.00	0.00	0.00	0.00	0.00	0.00	0.00	0.02	0.00	0.00	0.00	0.00	0.02
32 - 33	0.00	0.00	0.00	0.00	0.00	0.00	0.00	0.01	0.00	0.00	0.00	0.00	0.01
33 - 34	0.00	0.00	0.00	0.00	0.00	0.00	0.00	0.00	0.00	0.00	0.00	0.00	0.00
34 - 35	0.00	0.00	0.00	0.00	0.00	0.00	0.00	0.00	0.00	0.00	0.00	0.00	0.00
Total	**5.73**	**5.61**	**6.52**	**6.76**	**4.77**	**4.71**	**8.28**	**15.20**	**15.08**	**11.37**	**8.56**	**7.43**	100.0

Table 6.5 Sectorwise annual frequency distribution of wind speed at N3_Beta1
The N3_Beta1 location is at the FLS IJV location.

160 m wind speed	0°	30°	60°	90°	120°	150°	180°	210°	240°	270°	300°	330°	All
0-1	0.02	0.04	0.05	0.05	0.04	0.05	0.06	0.06	0.05	0.05	0.05	0.04	0.55
1-2	0.11	0.14	0.14	0.16	0.12	0.14	0.18	0.18	0.18	0.18	0.15	0.16	1.84
2-3	0.25	0.26	0.23	0.23	0.21	0.23	0.30	0.31	0.32	0.31	0.30	0.30	3.25
3-4	0.36	0.37	0.32	0.34	0.28	0.29	0.39	0.44	0.42	0.42	0.40	0.35	4.38
4-5	0.41	0.48	0.45	0.42	0.40	0.32	0.50	0.55	0.61	0.57	0.52	0.47	5.69
5-6	0.50	0.52	0.53	0.48	0.35	0.36	0.55	0.67	0.68	0.68	0.62	0.59	6.54
6-7	0.55	0.59	0.60	0.62	0.42	0.36	0.60	0.78	0.83	0.74	0.74	0.72	7.55
7-8	0.58	0.64	0.60	0.67	0.41	0.37	0.61	0.87	0.92	0.83	0.79	0.70	7.98
8-9	0.57	0.59	0.55	0.65	0.46	0.40	0.55	0.99	1.00	0.89	0.71	0.68	8.02
9-10	0.48	0.50	0.59	0.57	0.40	0.38	0.54	0.99	0.98	0.83	0.74	0.62	7.60
10-11	0.43	0.40	0.57	0.59	0.39	0.33	0.54	1.04	1.03	0.82	0.69	0.57	7.39
11-12	0.37	0.33	0.48	0.47	0.28	0.31	0.50	0.96	1.11	0.77	0.60	0.49	6.66
12-13	0.30	0.27	0.34	0.38	0.29	0.29	0.48	0.92	1.07	0.73	0.47	0.39	5.92
13-14	0.23	0.17	0.34	0.34	0.24	0.23	0.46	0.86	1.03	0.70	0.38	0.33	5.29
14-15	0.15	0.10	0.26	0.29	0.15	0.16	0.38	0.85	0.90	0.61	0.33	0.29	4.46
15-16	0.13	0.07	0.16	0.21	0.14	0.11	0.34	0.76	0.83	0.51	0.27	0.25	3.76
16-17	0.08	0.05	0.08	0.15	0.08	0.08	0.28	0.70	0.67	0.45	0.22	0.18	3.02
17-18	0.07	0.03	0.05	0.11	0.07	0.06	0.25	0.59	0.55	0.36	0.15	0.12	2.40
18-19	0.05	0.03	0.03	0.08	0.04	0.06	0.21	0.52	0.48	0.27	0.12	0.07	1.95
19-20	0.02	0.02	0.03	0.05	0.02	0.04	0.16	0.41	0.36	0.18	0.08	0.07	1.44
20-21	0.02	0.01	0.02	0.04	0.01	0.02	0.10	0.31	0.33	0.16	0.07	0.04	1.13
21-22	0.01	0.00	0.01	0.04	0.00	0.02	0.09	0.25	0.25	0.14	0.06	0.03	0.90
22-23	0.01	0.00	0.01	0.02	0.00	0.01	0.06	0.20	0.21	0.10	0.05	0.02	0.68
23-24	0.00	0.00	0.00	0.01	0.00	0.00	0.04	0.15	0.18	0.08	0.04	0.02	0.55
24-25	0.00	0.00	0.00	0.00	0.00	0.00	0.02	0.10	0.11	0.06	0.02	0.02	0.35
25-26	0.00	0.00	0.00	0.00	0.00	0.00	0.01	0.09	0.08	0.04	0.01	0.01	0.25
26-27	0.00	0.00	0.00	0.00	0.00	0.00	0.01	0.07	0.05	0.02	0.01	0.01	0.17
27-28	0.00	0.00	0.00	0.00	0.00	0.00	0.01	0.03	0.04	0.01	0.00	0.00	0.10
28 - 29	0.00	0.00	0.00	0.00	0.00	0.00	0.01	0.02	0.02	0.01	0.00	0.00	0.06
29 - 30	0.00	0.00	0.00	0.00	0.00	0.00	0.01	0.02	0.01	0.01	0.00	0.00	0.05
30 - 31	0.00	0.00	0.00	0.00	0.00	0.00	0.00	0.02	0.01	0.01	0.00	0.00	0.03
31 - 32	0.00	0.00	0.00	0.00	0.00	0.00	0.00	0.01	0.00	0.00	0.00	0.00	0.02
32 - 33	0.00	0.00	0.00	0.00	0.00	0.00	0.00	0.01	0.00	0.00	0.00	0.00	0.01
33 - 34	0.00	0.00	0.00	0.00	0.00	0.00	0.00	0.00	0.00	0.00	0.00	0.00	0.00
34 - 35	0.00	0.00	0.00	0.00	0.00	0.00	0.00	0.00	0.00	0.00	0.00	0.00	0.00
Total	**5.68**	**5.60**	**6.45**	**6.96**	**4.78**	**4.63**	**8.22**	**14.75**	**15.29**	**11.55**	**8.56**	**7.53**	**100.0**

6.4.1 Mean wind speed at various probability levels

The long-term mean wind speed at the height of 160 m at each nodal location is shown in Table 6.6 for various probability levels.

Table 6.6 IJVWFZ nodal location mean wind speed for various probability values

Probability level	Mean wind speed at 160 m [m/s]					
	N1_ Alpha1	N2_ Alpha2	N3_ Beta1	N4_ Beta2	N5_ Gamma1	N6_ Gamma2
P10	10.41	10.46	10.41	10.46	10.41	10.45
P25	10.28	10.33	10.28	10.33	10.28	10.32
P50	10.14	10.19	10.14	10.19	10.14	10.18
P75	10.00	10.05	10.00	10.05	10.00	10.04
P90	9.87	9.92	9.87	9.92	9.87	9.91

6.5 Wind shear

The vertical wind shear profile is observed for the IJVWFZ. The observation is done with short-term data concurrent with measured data and corresponding Unified-WRF modelled data and with Unified-WRF long-term data.

The wind shear exhibited by the following plots can be characterized by the power law exponent (α) in the power law equation:

$$U_2 = U_1 \times \left(\frac{z_2}{z_1}\right)^{\alpha}$$

U is horizontal wind speed in m/s, z is measurement height in m and α is the power law exponent.

The power law exponent is calculated to represent the best fit of the vertical wind speed profile of the power law profile by means of linear least squares regression.

Figure 6.3 presents the concurrent FLS IJV B and Unified-WRF modelled data vertical wind profile for heights between 30 m and 300 m. It can be observed that there is excellent agreement between the measured and the modelled data given a resultant wind shear coefficient of 0.075 and 0.073, respectively, over the observed short-term period.

Figure 6.4 presents the concurrent lidar IJmuiden and corresponding Unified-WRF modelled data on a sectorwise basis for the heights between 90 m and 300 m. These results are also presented in Table 6.7. It can be observed that there are some deviations between the measured and modelled data, with the Unified-WRF overpredicting in the south to southwest sectors. However, overall, there is general agreement between the two and the variation is within the expected margin of uncertainty.

Figure 6.5 presents the long-term vertical wind profile from the Unified-WRF output at all the N2_Alpha2 and N3_Beta1 locations between the heights of 60 m and 100 m. The vertical wind profile at these locations is representative of that at all the nodal locations. The long-term wind shear observed at these locations between the heights of 60 m and 300 m is 0.075, which is

characteristic of offshore locations. The corresponding sectorwise wind shear values are presented in Figure 6.6 and Table 6.8.

Table 6.9 presents the long-term wind shear exponents with different height combinations for the N2_Alpha2 and N3_Beta1 locations.

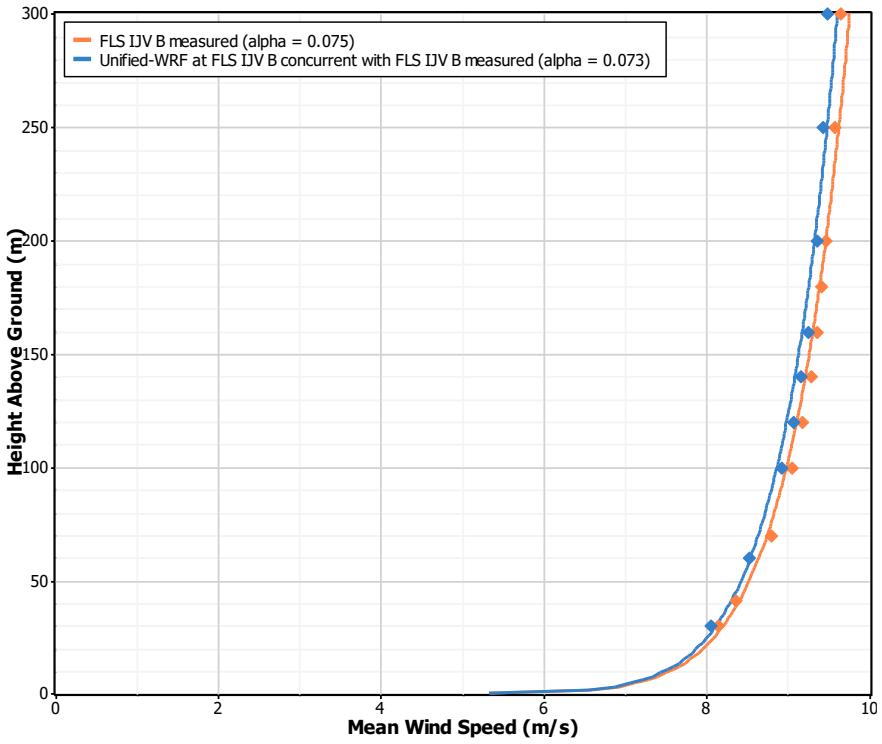

Figure 6.3 Concurrent measured and modelled vertical wind profile at FLS IJV B

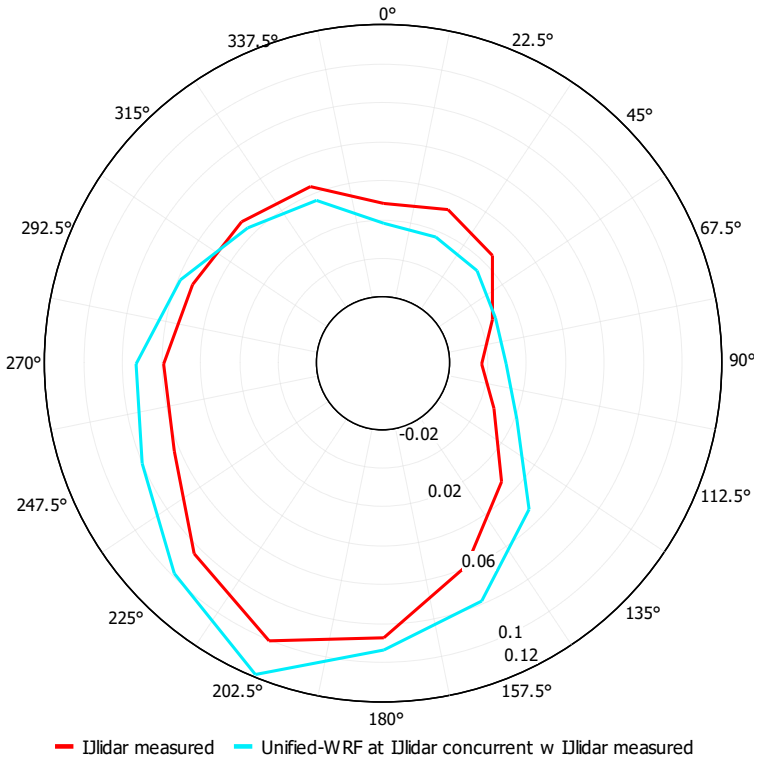

Figure 6.4 Concurrent measured and modelled wind shear rose at IJlidar

Table 6.7 Concurrent measured and modelled wind shear values at IJlidar

Sector	Wind shear coefficient (300 m, 250 m, 200 m, 160 m, 140 m, 120 m, 100 m, 60 m)	
	IJlidar measured	Unified-WRF at IJlidar *concurrent with IJlidar measured*
0°	0.027	0.028
22.5°	0.027	0.017
45°	0.022	0.012
67.5°	0.005	0.006
90°	-0.008	0.009
112.5°	0.003	0.015
135°	0.033	0.040
157.5°	0.062	0.071
180°	0.087	0.095
202.5°	0.100	0.114
225°	0.080	0.100
247.5°	0.063	0.083
270°	0.065	0.077
292.5°	0.055	0.059
315°	0.047	0.043
337.5°	0.041	0.037
All sectors	**0.058**	**0.066**

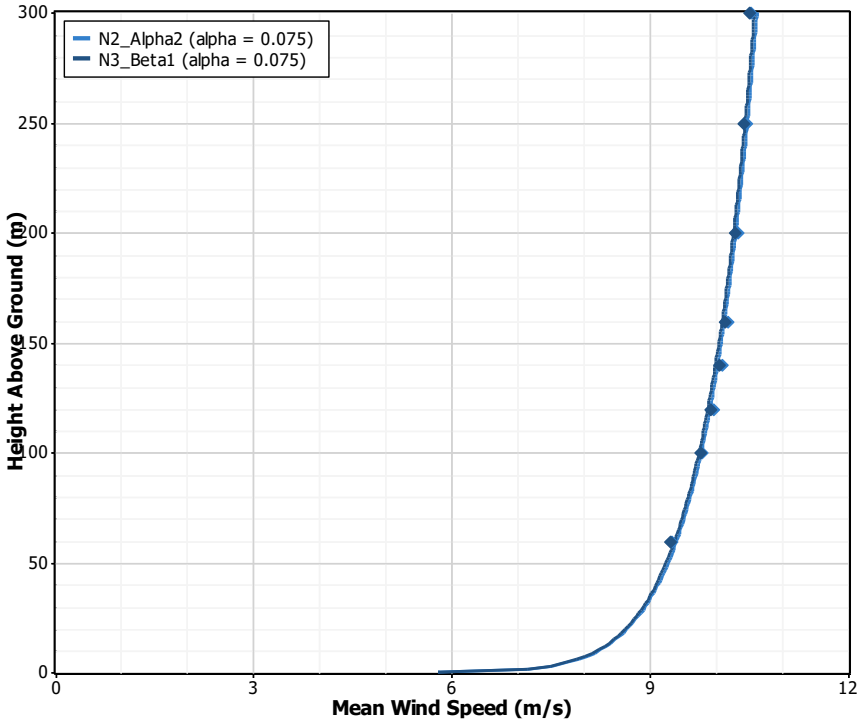

Figure 6.5 Long-term vertical wind profile at N2_Alpha2 and N3_Beta1

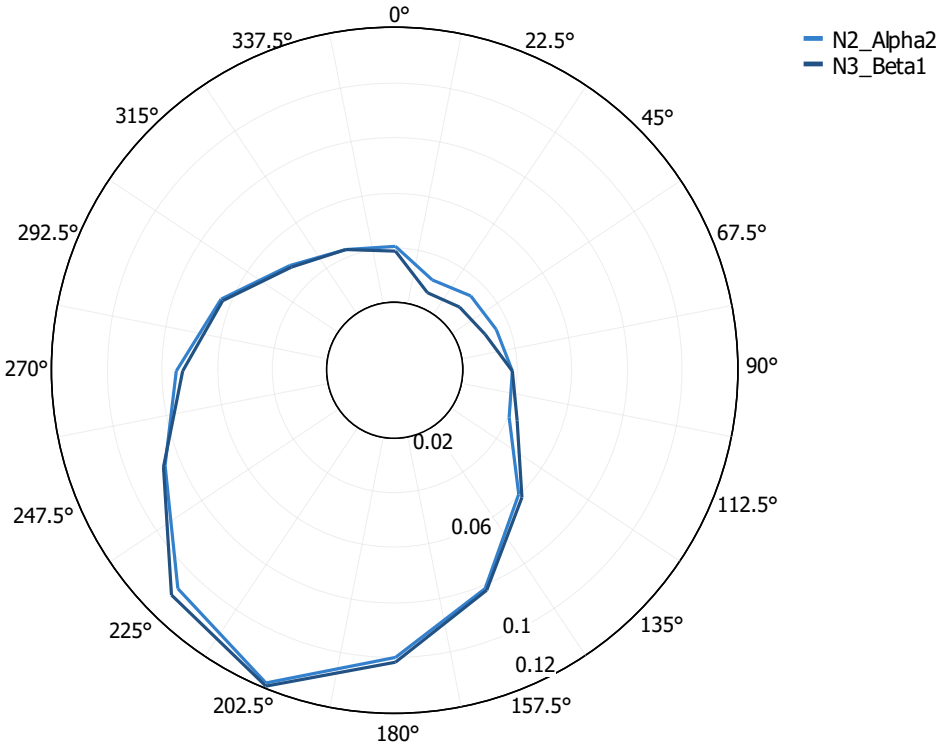

Figure 6.6 Long-term wind shear rose at N2_Alpha2 and N3_Beta1

This is representative of the wind shear between the heights of 60 m and 300 m.

Table 6.8 Long-term sectorwise wind shear at N2_Alpha2 and N3_Beta1

Sector	Wind shear coefficient (300 m, 250 m, 200 m, 160 m, 140 m, 120 m, 100 m, 60 m)	
	N2_Alpha2 long-term	N3_Beta1 long-term
0°	0.041	0.039
30°	0.032	0.027
60°	0.034	0.028
90°	0.035	0.031
120°	0.038	0.038
150°	0.040	0.043
180°	0.059	0.061
210°	0.081	0.082
240°	0.100	0.101
270°	0.119	0.119
300°	0.107	0.111
330°	0.086	0.087
All sectors	**0.075**	**0.072**

Table 6.9 Long-term wind shear at various heights at N2_Alpha2 and N3_Beta1

Heights [m]	N2_Alpha2	N3_Beta1
300 & 60	0.075	0.075
300 & 200	0.052	0.050
250 & 160	0.060	0.063
200 & 160	0.067	0.068
200 & 100	0.078	0.078
100 & 60	0.095	0.092

6.6 Turbulence intensity

The current industry best practice is to measure turbulent intensity (TI) using cup anemometers. Therefore, the TI was estimated using the MM IJmuiden measured wind data at the top measurement height of 92 m.

It is noted that the measurement period at this location is four consecutive years. Although four years is not considered to be long-term from a wind resource perspective, it is still suitably lengthy enough to give a reliable understanding of the ambient TI at this location.

The ambient mean TI at the height of 92 m at the IJmuiden MM was found to be 5.8% while the mean TI at the 15 m/s wind speed bin was found to be 5.5%. The ambient mean TI for each wind speed bin can be observed in Table 6.10 and Figure 6.7 and in Figure 6.8 per wind direction sector. It is noted that the higher wind speed bins have insufficient data points to represent the ambient mean TI appropriately.

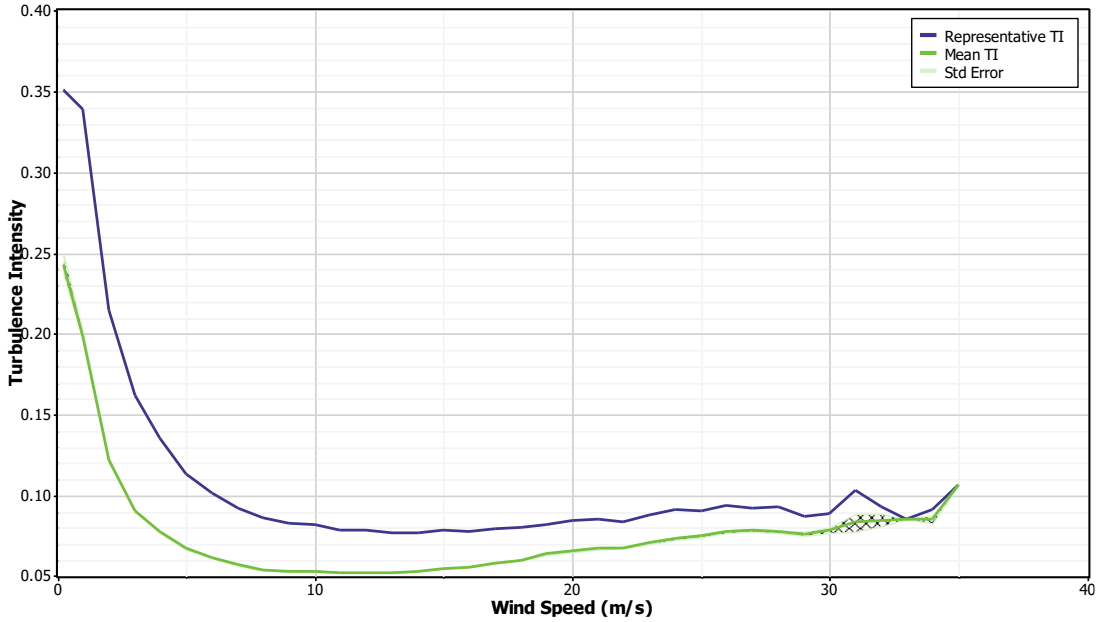

Figure 6.7 MMIJ ambient TI and representative TI (TI90) at 92 m per wind speed bin

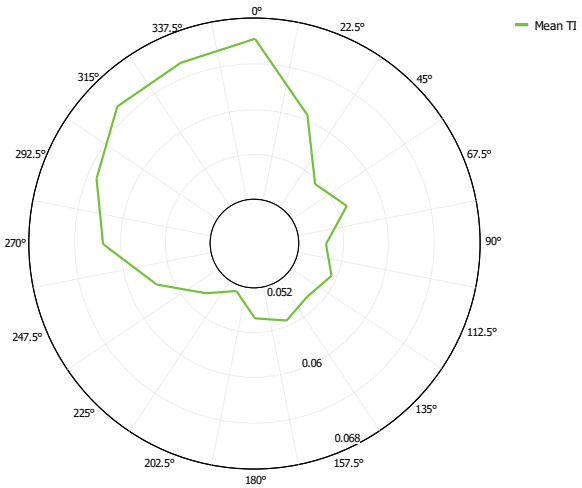

Figure 6.8 MMIJ ambient TI at 92 m per wind direction sector

Table 6.10 MMIJ mean ambient TI at 92 m

Bin midpoint	Bin endpoints		Data point in bin	Mean ambient TI [%]
	Lower [m/s]	Upper [m/s]		
0.2	0	0.5	193	24.3
1	0.5	1.5	2582	19.9
2	1.5	2.5	5110	12.2
3	2.5	3.5	7843	9.1
4	3.5	4.5	9959	7.7
5	4.5	5.5	12304	6.7
6	5.5	6.5	14999	6.2
7	6.5	7.5	16730	5.7
8	7.5	8.5	16924	5.4
9	8.5	9.5	16641	5.3
10	9.5	10.5	15286	5.3
11	10.5	11.5	14474	5.2
12	11.5	12.5	12744	5.1
13	12.5	13.5	11711	5.2
14	13.5	14.5	10161	5.3
15	14.5	15.5	8626	5.5
16	15.5	16.5	6642	5.6
17	16.5	17.5	5054	5.8
18	17.5	18.5	4004	6.0
19	18.5	19.5	3170	6.4
20	19.5	20.5	2609	6.6
21	20.5	21.5	1919	6.7
22	21.5	22.5	1236	6.8
23	22.5	23.5	728	7.1
24	23.5	24.5	365	7.4
25	24.5	25.5	206	7.6
26	25.5	26.5	127	7.8
27	26.5	27.5	124	7.9
28	27.5	28.5	106	7.8
29	28.5	29.5	39	7.6
30	29.5	30.5	23	7.8
31	30.5	31.5	7	8.3
32	31.5	32.5	3	8.5
33	32.5	33.5	1	8.5
34	33.5	34.5	3	8.6
35	34.5	35.5	1	10.7
36	35.5	36.5	0	0.0
37	36.5	37.5	0	0.0
38	37.5	38.5	1	7.5
39	38.5	39.5	193	0.0

6.7 Temporal variation in wind speed

The images below present the diurnal, monthly and interannual variation in the long-term wind climate at each nodal location, presented together with the MM IJmuiden and FLS IJV measured data.

Figure 6.9 presents the diurnal wind speed pattern at the height of 160 m. It presents the long-term output at each nodal location and the MM IJmuiden and FLS IJV measured data. It can be observed that all the data exhibits similar patterns albeit with different magnitudes. The MM IJmuiden data has a very similar pattern to the long-term output which is expected as the measurement period is four consecutive years. The FLS IJV measured data exhibits a larger variation from the long-term output, which is also expected given the significantly shorter measurement period. The long-term wind speeds across all nodes range from about 10.0 m/s to 10.4 m/s, indicating small wind speed variation throughout.

Figure 6.10 presents the monthly mean wind speed variation at the height of 160 m. It presents the long-term output at each nodal location and the MM IJmuiden and FLS IJV measured data. It can be observed that the data exhibit very similar behaviour across all months, with lower wind speeds in the summer months and higher wind speeds in the winter months. Similarly, to the diurnal plot the FLS IJV data exhibits a larger variation from the long-term output, which is expected given the shorter measurement period. At the nodal locations, wind speeds range between 8.0 m/s and 12.5 m/s.

Figure 6.11 presents the annual mean wind speeds at each nodal location and the measured MM IJmuiden data. It can be observed that the annual mean wind speeds are very similar across all the nodal locations. The minimal deviation between the measured MM IJmuiden and the N2_Alpha2 (at MM IJmuiden location) data are well within the associated uncertainty. It is also noted that the MM IJmuiden data had a data coverage of 90% and higher for the observed years. It is noted that the FLS IJV measured data has not been included in this depiction as this measured data does not have a full calendar year of measurements.

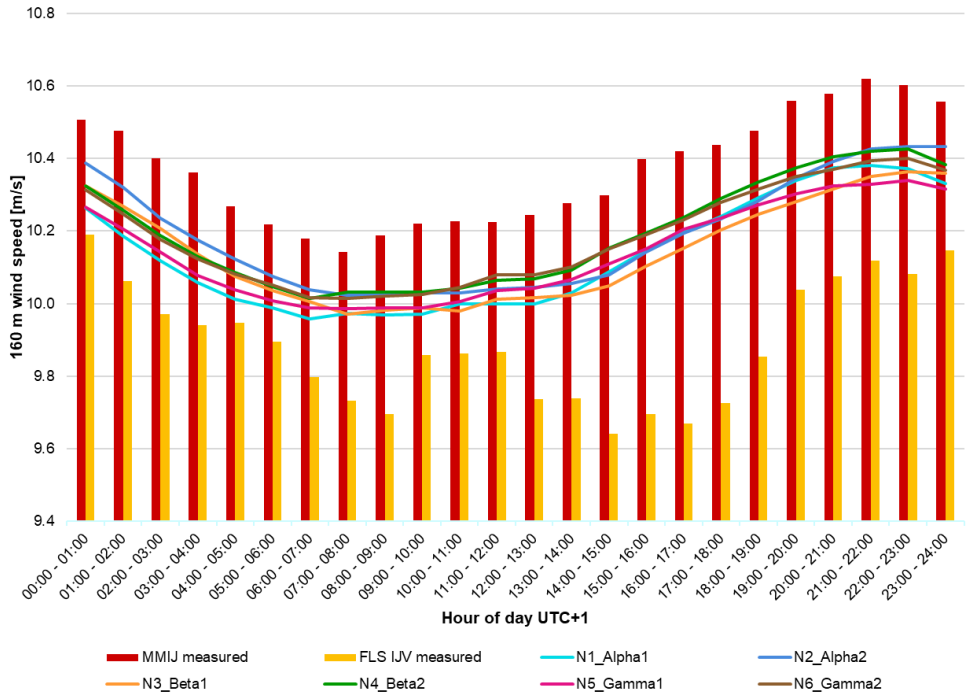

Figure 6.9 Diurnal 160 m wind speed pattern (UTC+1)

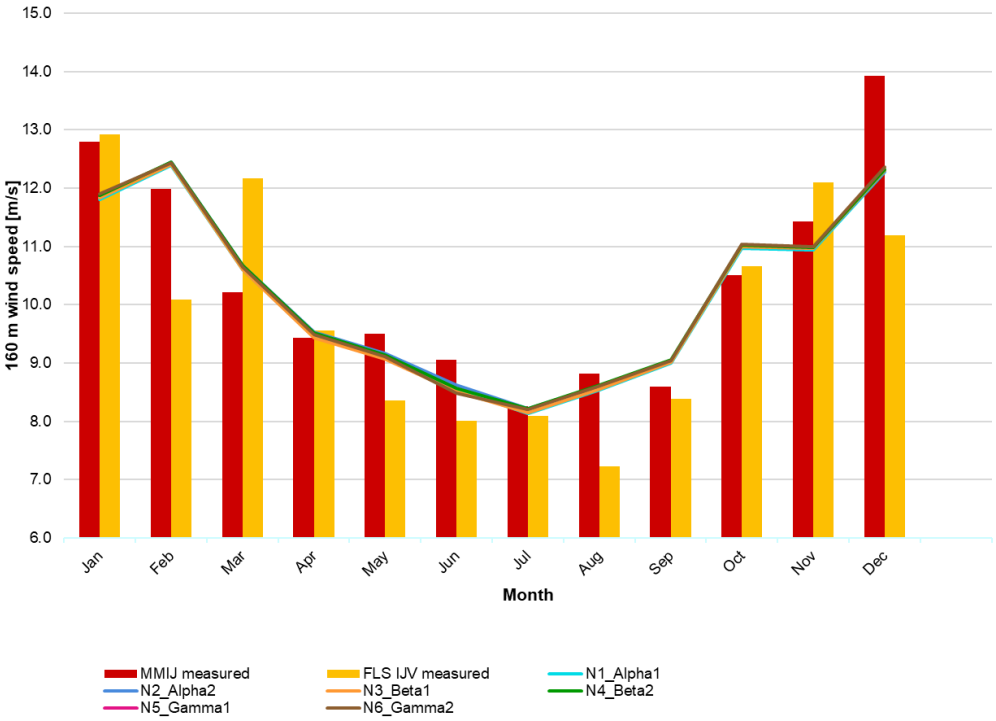

Figure 6.10 Monthly 160 m mean wind speeds

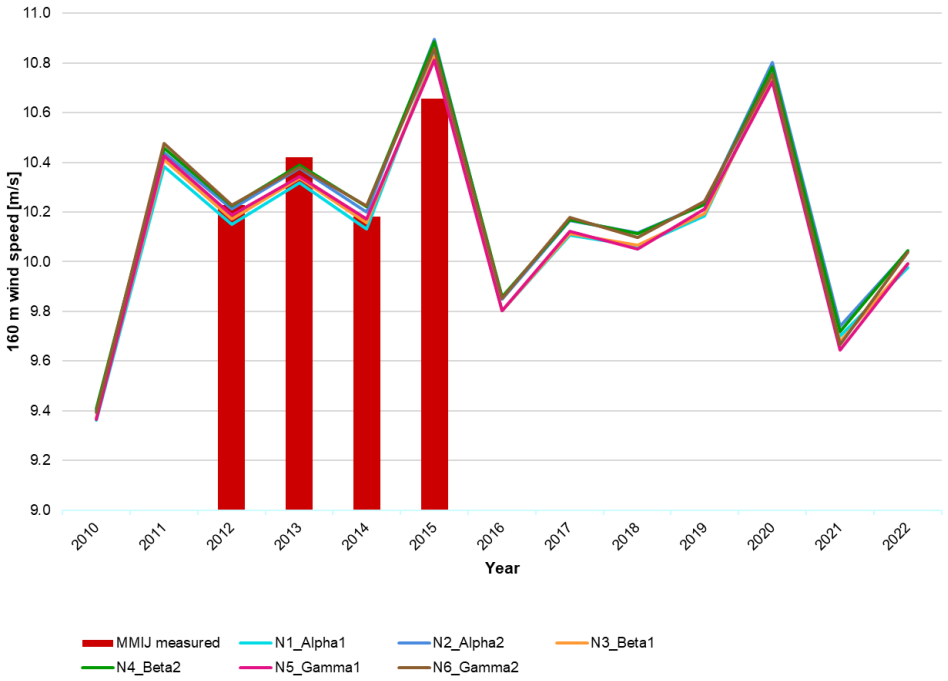

Figure 6.11 Annual 160 m mean wind speeds

6.8 Frequency distribution

The long-term wind speed frequency distribution with a Weibull fitting can be observed in Figure 6.12 for the N2_Alpha2 location. It can be observed that the wind speed distribution has a reasonable fit to a Weibull distribution with the highest percentage of events occurring around the 7 m/s to 10 m/s bins.

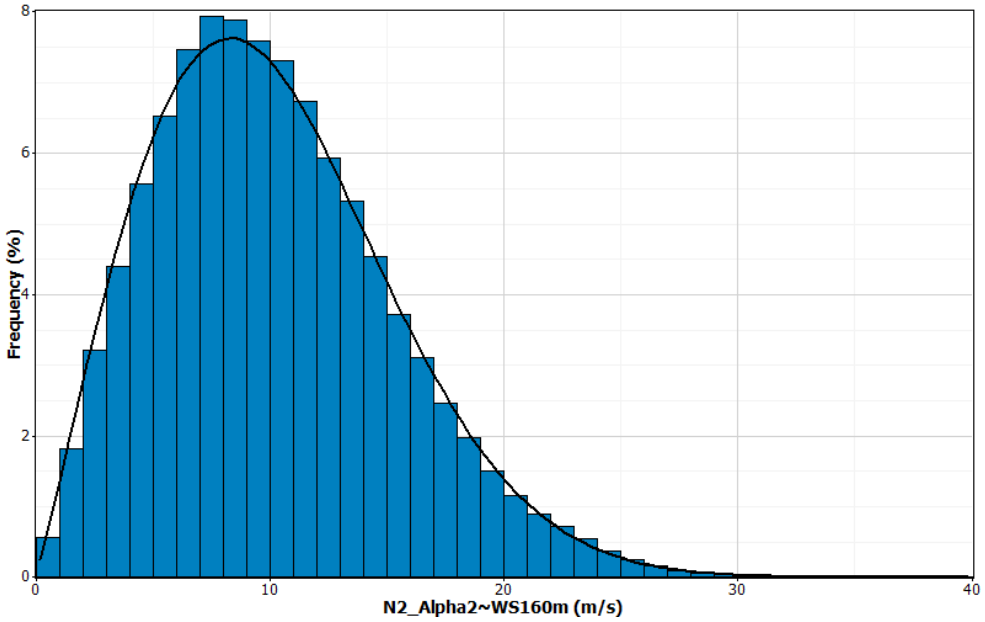

Figure 6.12 N2_Alpha2 long-term 160 m wind speed frequency distribution with Weibull fit

6.9 Weibull parameters

The long-term Weibull scale and shape parameters (A and k), are presented in Table 6.11 for the heights between 10 m and 300 m. The sectorwise Weibull values for each of the heights are in Appendix J.

Table 6.11 Weibull parameters at nodal locations

Location	Height [m] Variable	300	250	200	160	140	120	100	60	30	10
N1_ Alpha1	Weibull k	1.977	2.014	2.055	2.086	2.104	2.12	2.134	2.151	2.163	2.205
	Weibull A (m/s)	11.85	11.77	11.62	11.45	11.34	11.20	11.01	10.51	9.89	9.01
N2_ Alpha2	Weibull k	1.919	1.968	2.02	2.058	2.079	2.092	2.102	2.096	2.079	2.112
	Weibull A (m/s)	11.79	11.73	11.62	11.46	11.36	11.22	11.02	10.48	9.82	8.94
N3_ Beta1	Weibull k	1.908	1.958	2.011	2.05	2.069	2.084	2.094	2.097	2.088	2.125
	Weibull A (m/s)	11.74	11.68	11.56	11.40	11.30	11.16	10.97	10.45	9.80	8.93
N4_ Beta2	Weibull k	1.987	2.024	2.065	2.096	2.115	2.13	2.143	2.16	2.171	2.213
	Weibull A (m/s)	11.91	11.82	11.69	11.51	11.41	11.27	11.07	10.55	9.92	9.04

Location	Height [m] Variable	300	250	200	160	140	120	100	60	30	10
N5_ Gamma1	Weibull k	1.986	2.022	2.063	2.094	2.114	2.129	2.142	2.163	2.18	2.224
	Weibull A (m/s)	11.87	11.78	11.63	11.45	11.35	11.21	11.02	10.52	9.90	9.02
N6_ Gamma2	Weibull k	1.988	2.026	2.067	2.099	2.119	2.135	2.149	2.169	2.183	2.226
	Weibull A (m/s)	11.90	11.81	11.68	11.50	11.40	11.26	11.07	10.54	9.92	9.04

6.10 Wind rose

The long-term wind roses at each of the nodal locations for the height of 160 m are presented in Figure 6.13 to Figure 6.18. It can be observed that all the locations have a prevailing wind direction ranging from south-southwest to west directions.

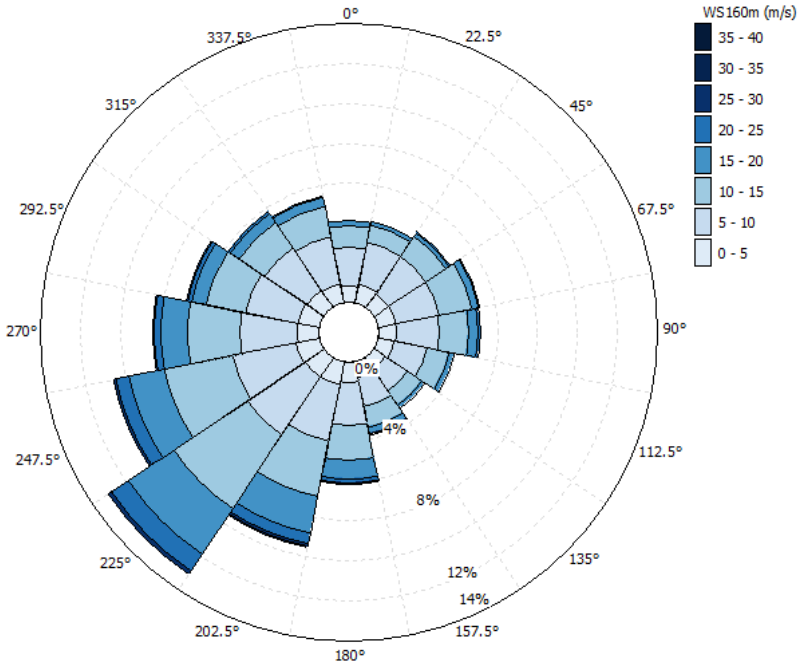

Figure 6.13 N1_Alpha1 160 m frequency wind rose

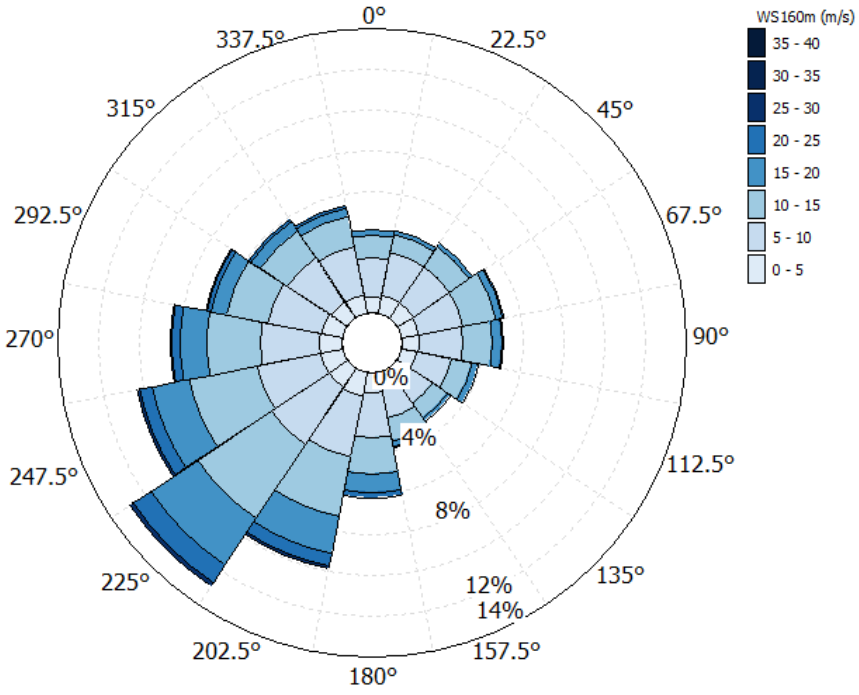

Figure 6.14 N2_Alpha2 160 m frequency wind rose

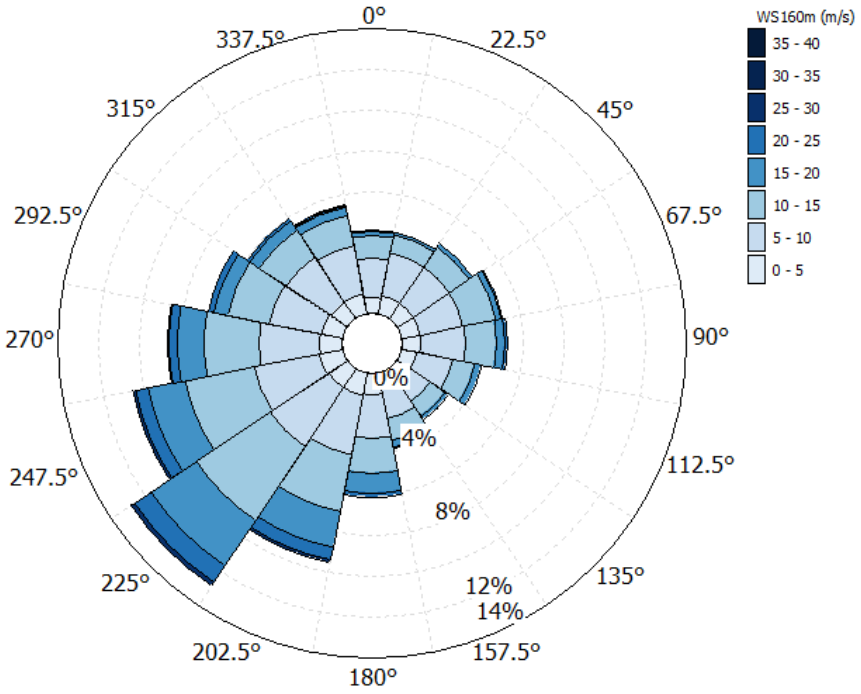

Figure 6.15 N3_Beta1 160 m frequency wind rose

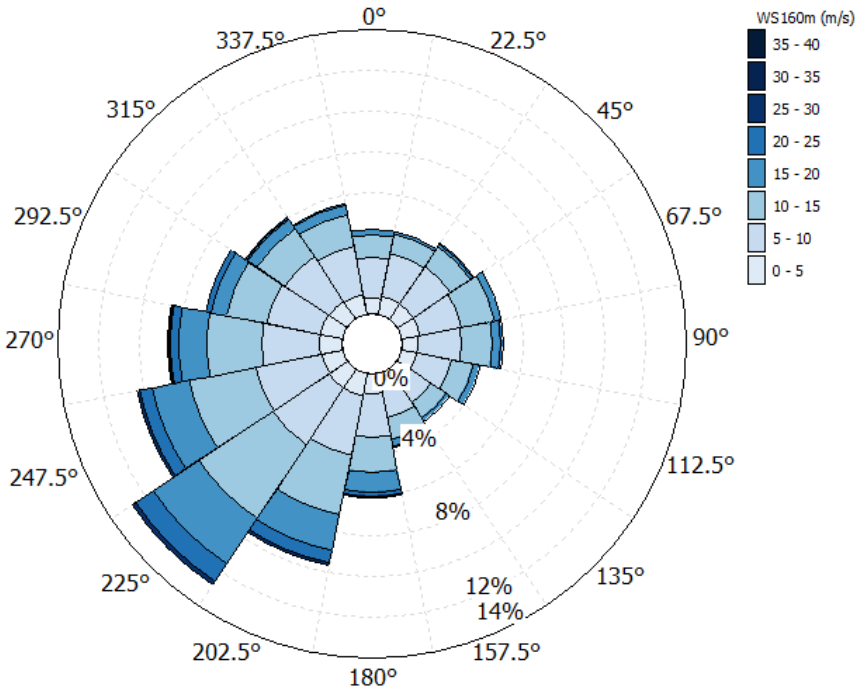

Figure 6.16 N4_Beta2 160 m frequency wind rose

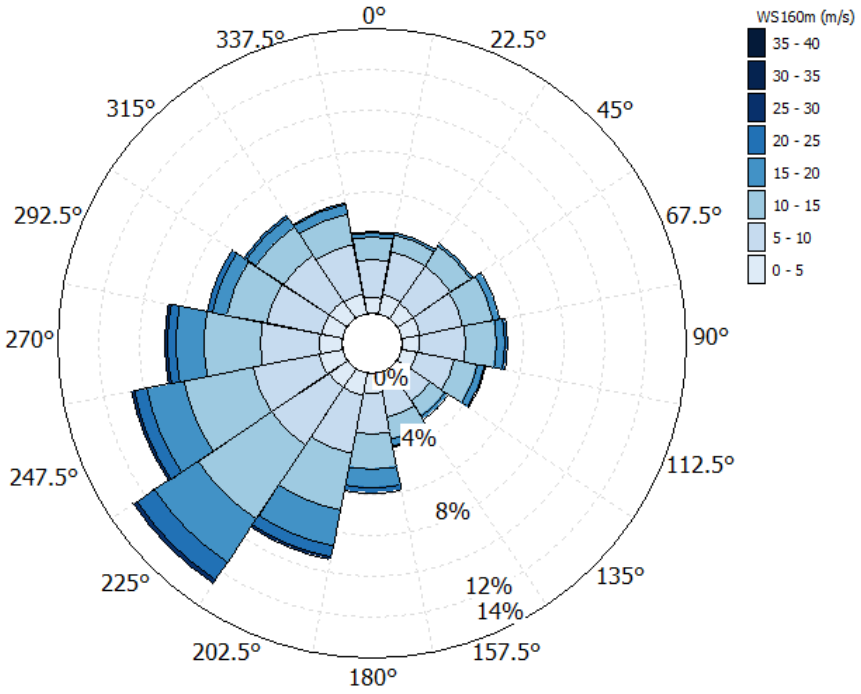

Figure 6.17 N5_Gamma1 160 m frequency wind rose

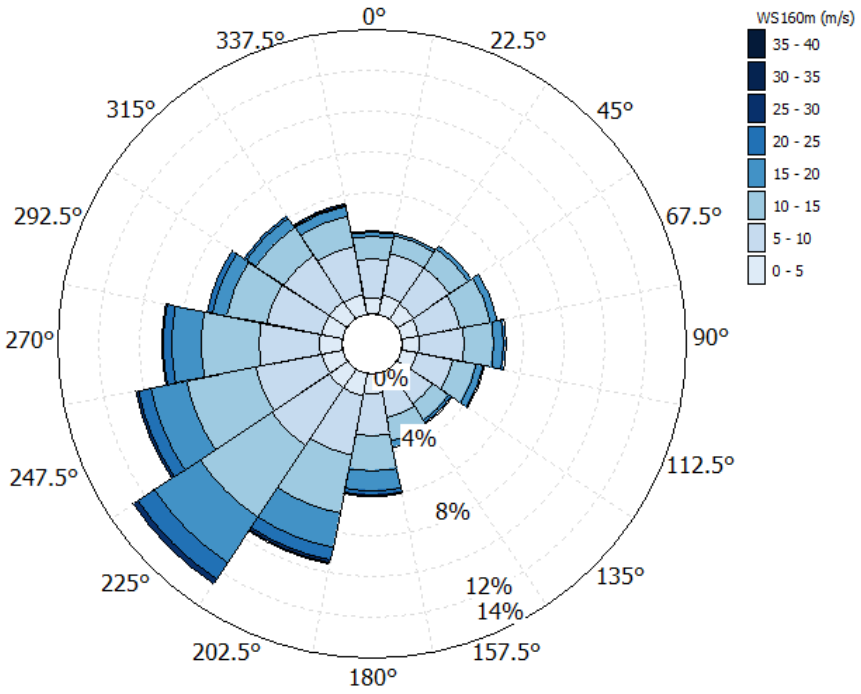

Figure 6.18 N6_Gamma2 160 m frequency wind rose

6.11 Other climatological parameters

The following sections present the thermodynamic meteorological parameters from the measured on-site datasets at MM IJmuiden and FLS IJV B, along with the long-term values at each of the nodal locations.

It is noted that the FLS IJV B data covers a period from 01 May 2022 to 31 May 2023 and MM IJmuiden data covers a period from 01 January 2012 to 31 December 2015.

6.11.1 Air temperature

The measured data at the two observed locations and long-term air temperature at each nodal location are presented below.

Table 6.12 Air temperature mean, minimum, maximum

Dataset	Height MSL [m]	Air temperature [°C]		
		Mean	Minimum	Maximum
Short-term data				
FLS IJV B	3.7	11.7	1.4	25.2
MMIJ	90	10.5	-5.9	29.6
MMIJ	21	10.9	-4.9	27.8
Long-term data				
N1_Alpha1	10	10.9	-5.5	25.0
N2_Alpha2	10	10.9	-5.2	25.0
N3_Beta1	10	10.9	-5.6	25.0
N4_Beta2	10	10.9	-5.4	24.3
N5_Gamma1	10	10.9	-5.6	25.0
N6_Gamma2	10	10.8	-5.3	23.9
N1_Alpha1	160	10.1	-7.8	34.4
N2_Alpha2	160	10.1	-7.5	34.3
N3_Beta1	160	10.1	-7.9	34.5
N4_Beta2	160	10.1	-7.7	34.4
N5_Gamma1	160	10.0	-7.9	35.0
N6_Gamma2	160	10.0	-7.6	34.3

6.11.2 Air pressure

The measured data at the two observed locations and long-term air pressure at each nodal location are presented below.

Table 6.13 Air pressure mean, minimum, maximum

Dataset	Height MSL [m]	Air pressure [hPa]		
		Mean	Minimum	Maximum
Short-term data				
FLS IJV B	3.7	1016	978	1045
MMIJ	90	1004	962	1034

Dataset	Height MSL [m]	Air pressure [hPa]		
		Mean	Minimum	Maximum
MMIJ	21	1012	967	1042
Long-term data				
N1_Alpha1	10	1013	970	1046
N2_Alpha2	10	1013	970	1046
N3_Beta1	10	1013	970	1046
N4_Beta2	10	1013	970	1046
N5_Gamma1	10	1013	970	1046
N6_Gamma2	10	1013	970	1046
N1_Alpha1	160	995	952	1027
N2_Alpha2	160	995	952	1027
N3_Beta1	160	995	952	1027
N4_Beta2	160	995	952	1027
N5_Gamma1	160	995	952	1027
N6_Gamma2	160	995	952	1027

6.11.3 Relative humidity

The measured data at the MM IJmuiden location and long-term air pressure at each nodal location are presented below.

It is noted that relative humidity measurements were not gathered at the FLS IJV B location.

Table 6.14 Relative humidity mean, minimum, maximum

Dataset	Height MSL [m]	Relative Humidity [%]		
		Mean	Minimum	Maximum
Short-term data				
MMIJ	90	78.8	12.6	101.1
MMIJ	21	80.3	34.7	101.9
Long-term data				
N1_Alpha1	10	81.7	34.7	101.7
N2_Alpha2	10	81.9	33.3	101.7
N3_Beta1	10	81.7	34.3	101.6
N4_Beta2	10	81.9	32.9	101.6
N5_Gamma1	10	81.8	34.8	101.5
N6_Gamma2	10	82.0	34.5	101.6
N1_Alpha1	160	78.0	11.2	100.1
N2_Alpha2	160	78.1	11.2	100.1

N3_Beta1	160	78.1	11.5	100.1
N4_Beta2	160	78.3	11.7	100.1
N5_Gamma1	160	78.3	11.5	100.1
N6_Gamma2	160	78.4	11.5	100.1

6.11.4 Air density

The measured data at the two observed locations and long-term air pressure at each nodal location are presented below.

Table 6.15 Air density mean, minimum, maximum

Dataset	Height MSL [m]	Air density [kg/m^3]		
		Mean	Minimum	Maximum
Short-term data				
FLS IJV B	3.7	1.243	1.183	1.311
MMIJ	90	1.233	1.148	1.345
MMIJ	21	1.243	1.175	1.351
Long-term data				
N1_Alpha1	10	1.238	1.171	1.348
N2_Alpha2	10	1.238	1.171	1.346
N3_Beta1	10	1.238	1.168	1.349
N4_Beta2	10	1.238	1.171	1.347
N5_Gamma1	10	1.238	1.170	1.350
N6_Gamma2	10	1.238	1.171	1.347
N1_Alpha1	160	1.220	1.117	1.333
N2_Alpha2	160	1.220	1.118	1.331
N3_Beta1	160	1.220	1.118	1.333
N4_Beta2	160	1.220	1.118	1.331
N5_Gamma1	160	1.220	1.117	1.334
N6_Gamma2	160	1.220	1.119	1.331

7 Climate Change Analysis

This subsection of the report investigates the potential impacts of climate change on offshore wind energy, with a particular focus on the FLS IJV measurement point.

The analysis employs seven climate projections from the Coordinated Regional Climate Downscaling Experiment (CORDEX) research project, considering both the Representative Concentration Pathway (RCP) 4.5 and RCP8.5 climate change scenarios. The RCP scenarios play pivotal roles in climate modeling and research. RCP 4.5 contemplates a scenario where global warming is controlled by the mid-century due to specific mitigation actions. In contrast, RCP 8.5 delineates a starker "business-as-usual" path, highlighting consequences in the absence of significant emission control efforts, which could lead to a marked increase in global temperatures by century's end.

The subsequent sections detail the data and methods used, present the results, and conclude with an analysis of the implications for climate change on wind energy projects.

7.1 Introduction and section summary

The development of offshore wind energy is a major alternative to produce low carbon electricity and mitigate the climate change issue. However, offshore wind energy is highly dependent on weather and climate and those projects may face climate change stimuli during their lifetime (about 30 years). It is thus important, to ensure they fully play their mitigating role and reduce the risks, to assess the potential impacts of climate change on the projects.

The impact of climate change on the wind resource was analysed at a site in the North Sea near the IJmuiden Ver measurement point using seven (7) climate projections of a research project called CORDEX. The RCP4.5 and RCP8.5 climate change scenarios were used for the purpose of the study to explore two pathways inherently linked to two different future socio-economic development.

The seven (7) models have been evaluated with respect to their ability to match key aspects of observed climate. As stated by the Intergovernmental Panel on Climate Change (IPPC) Sixth Assessment Report (AR6), there is ‘no universal, robust method for weighting a multi-model projection ensemble, […], and expert judgement must be included’. Therefore, a methodology developed by climate experts assessing the impact of climate change on the wind resource has been used in this analysis to evaluate climate models’ performances against a 26-year dataset considered representative of the site. Three ensembles are built to perform the climate change assessment based on the individual performance of each climate model. Three future periods of approximately 25 years between 2022 and 2099 were analysed: near future (**2022-2045**), mid future (**2046-2074**) and far future (**2075-2099**).

The main findings with respect to wind resource are:

- One of the three ensembles analysed (ensemble F) projects a decrease of 0.6% in mean wind speed and decrease of 1.5% in annual energy yield generation for the near future period (2022-2045) under the RCP8.5 scenario.

- In the far future (2075-2099), the decrease in wind resource and energy generation is more pronounced, reaching 1% and 3% for the mean wind speed and energy yield generation respectively, on average for the three ensembles analysed.
- The magnitude of the changes is smaller for the RCP4.5 scenario compared to RCP8.5. The mean change projected by the three ensembles analysed is a decrease of 0.7% in mean wind speed and 1.7% in annual energy produced for the far future period.
- Two (2) ensembles project a decrease in summer wind power density of about 5%, 10% and 20% under RCP8.5 for the near, mid and far future periods respectively, compared to historical levels. This reduction in the wind resource leads to a decrease in summer energy yield generation of around 25% in the long term.

An overall decrease in energy yield generation and operation hours is expected. The decrease in wind speed within the operating range of the WTG (cut-in; cut-out) and the trend towards more severe wind speeds are drivers of this overall decrease. There is a high confidence for increase of frequency for extreme wind speed events in the far future under the RCP8.5 scenario (five models out of seven projecting this trend) while the model consensus is less certain under the RCP4.5 scenario.

The changes in the parameters for the near-future, mid-future and far-future scenarios for the ensemble F under the RCP8.5 scenario are shown in Table 7.1 and the corresponding seasonal variation in normalized wind power density is shown in Figure 7.1.

Table 7.1 Results for the ensemble F under the RCP8.5 scenario

Parameter	Historical	Near-future	Mid-future	Far-future
Mean annual wind speed	100.0%	**99.45%**	98.75%	99.14%
99 percentile wind speed	100.0%	**100.30%**	100.41%	101.36%
Wind power density	100.0%	**98.74%**	97.76%	99.93%
Operating time of WTG	100.0%	**99.93%**	99.79%	99.41%
Annual energy production	100.0%	**98.50%**	96.57%	96.80%

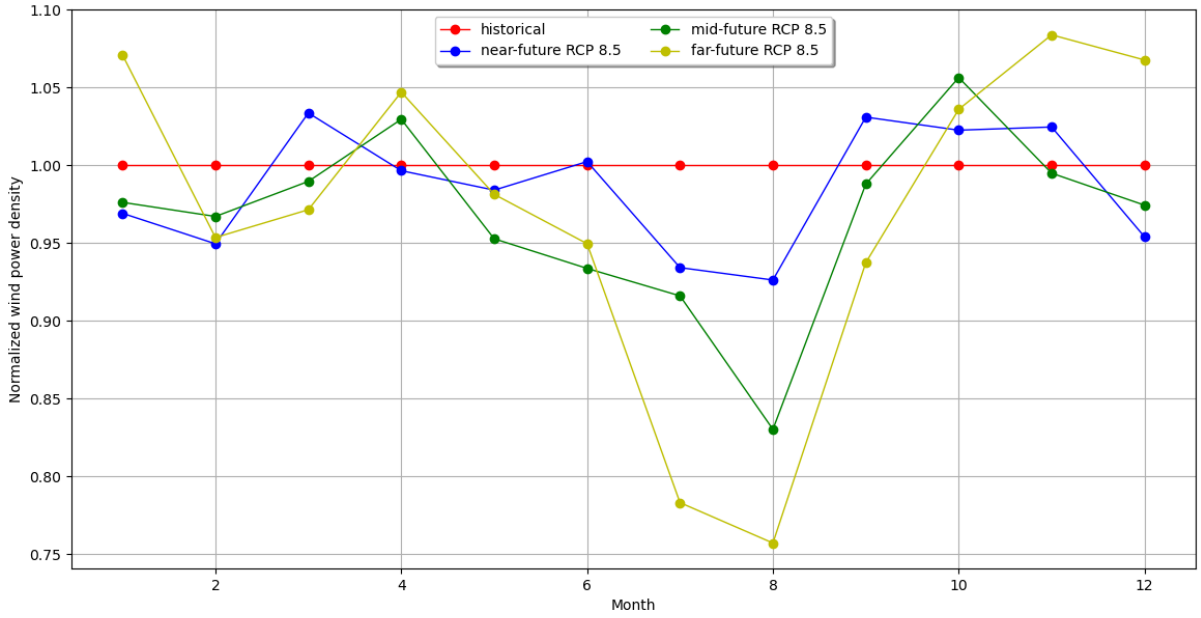

Figure 7.1 Normalized wind power density on average months

Pessimistic scenario RCP8.5 – Ensemble F

The primary constraint inherent in this study pertains to its utilization of a single grid point approach. Consideration of a larger region adjacent to the IJmuiden Ver site would increase the reliability of the results and include a broader view of the regional changes. However the findings are supported by similar results for this region found in the scientific literature which is reassuring [61], [62].

The methodology applied in this study to assess CORDEX capabilities gives an understanding of the bias of climate models to perform such climate change analysis. The availability of long-term reference data of the site under study was a major requirement to perform this study.

7.2 Data and methods

7.2.1 Data

3-hourly 10-meter wind speed data were retrieved from the European **CORDEX** domain through the Climate Data Store (CDS)[16], at the nearest location to the primary measurement dataset of FLS IJV measurements as detailed in Table 7.3.

CORDEX is the state-of-the-art scientific community and reference for the dynamical downscaling of Global Climate Models (GCMs) using Regional Climate Models (RCMs). More information on CORDEX and dynamical downscaling can be found in [63]). All regional climate projections with available 3-hourly wind speed data for the historical and future period under both Representative Concentration Pathway (RCP) RCP 4.5 and RCP 8.5 scenarios was considered (more information on climate scenarios can be found in Section K.3.1). Table 7.2 summarizes the considered climate models in this study. All simulations have a spatial resolution of 0.11°x0.11° (approximately 12x12 km) and cover the same time span described below.

[16] https://cds.climate.copernicus.eu

Wind speed data from the historical simulations is retrieved for the period **1979-2005** whilst the future period under RCP scenario is covering the range **2022-2099**. It has been chosen to divide the future period into 3 periods greater than 20 years to cover possible climate change stimuli:

- Near future (**2022-2045**),
- Mid future (**2046-2074**),
- Far future (**2075-2099**).

RCP 4.5 and RCP 8.5 scenarios for the future periods respectively assume a reach of the radiative forcing to 4.5 Wm^{-2} and 8.5 Wm^{-2} by the end of the 21st century. The RCPs scenarios were used for the 5th phase of the assessment report from IPCC and are commonly used in the climate modelling community.

Table 7.2 RCM simulations from EURO-CORDEX project used in this study based on historical, RCP4.5 & RCP8.5 experiments

Simulation number	GCM	RCM	Institution
M1	IPSL-CM5A-MR	SMHI-RCA4	SMHI
M2	ICHEC-EC-EARTH	KNMI-RACMO22E	KNMI
M3	MPI-M-MPI-ESM-LR	SMHI-RCA4	SMHI
M4	NCC-NorESM1-M	SMHI-RCA4	SMHI
M5	NCC-NorESM1-M	DMI-HIRHAM5	DMI
M6	NCC-NorESM1-M	GERICS-REMO2015	GERICS
M7	CNRM-CERFACS	KNMI-RACMO22E	KNMI

The closest point of CORDEX grid to the points under study have been calculated. The distance of CORDEX grid nodes to measurement locations as well as the coordinates of the locations under study (IJVWFZ location) are summarised in the following Table 7.3 and Figure 7.2.

Table 7.3 Representative IJVWFZ location used in this study for climate change analysis

Location	Unified-WRF point		CORDEX point		
	Latitude [°]	Longitude [°]	Latitude [°]	Longitude [°]	Distance to measurement location [km]
IJV FLS	52.885556	3.710833	52.84	3.73	5.03

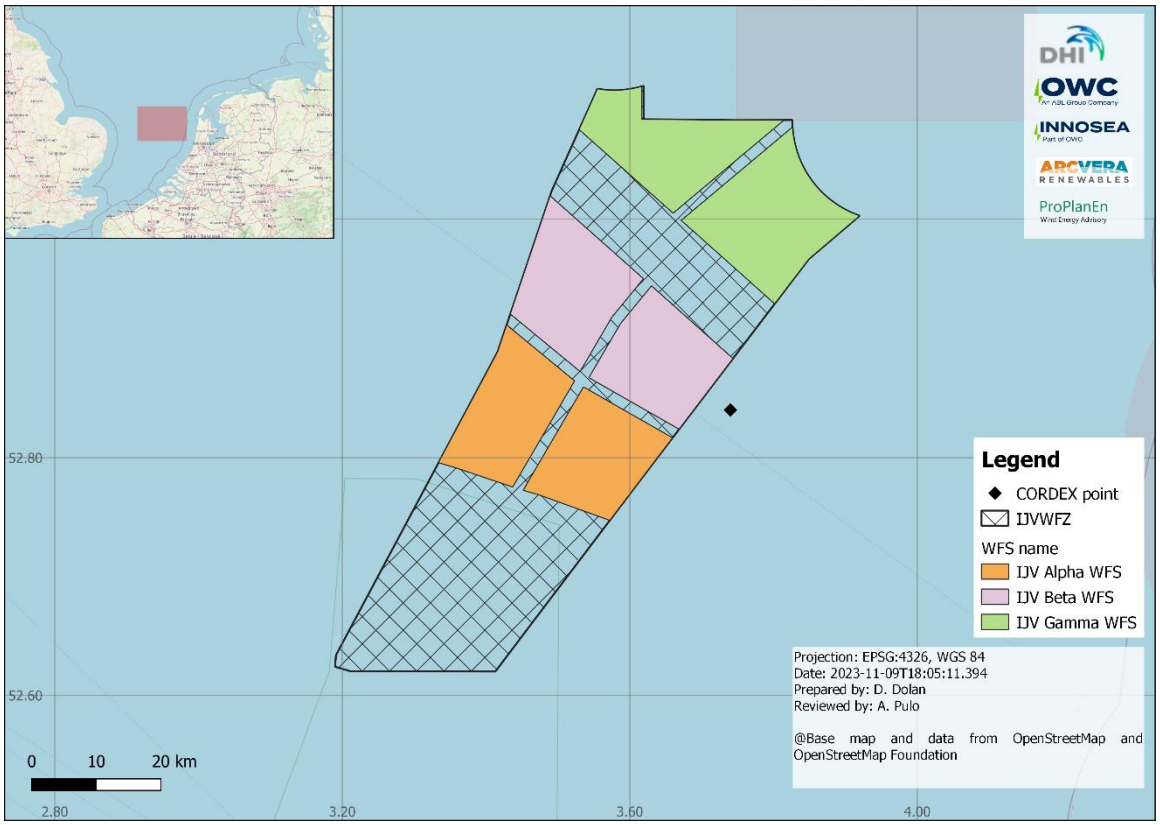

Figure 7.2 Location under study

7.2.2 Overview

According to the scientific community and the CORDEX guidelines, it is highly recommended to assess the reliability of climate models before handling future climate simulations. To do so, the climate models are run on a historical period (e.g.: from 1970 to 2005) to be compared with a reference dataset supposed to be representative of the past climate at the location of interest during the same time range. This reference dataset can be based on observations (buoys, wind mast, meteorology station, …) or reanalysis assumed to be a reasonable representation of the past climate. As the climate simulations are not synchronized with any observations of the climate [63], having good performance to reproduce the past climate is a good indicator for models' reliability. This method is widely used by the scientific community before performing a climate change analysis [61], [64]–[76].

To carry out a good assessment of this performance, it is recommended by the CORDEX community [63] and other climate scientists to use the widest common period available between the historical experiment from CORDEX and the reference dataset, which is obtained from the final Unified-WRF model output in this study. CORDEX simulations are Regional Climate Models (RCMs) forced with Global Climate Models (GCMs). The modelled climates represented by these simulations are not synchronized with the real climate, especially at hourly or daily scales, and a comparison day by day would not be accurate. On a small temporal scale, the climate simulation results primarily reflect mathematical randomness rather than the physical processes simulated by the climate models. Thus, the comparison between the dataset of reference and the climate simulations must be carried out by a statistical study spanning a **wide period** (over 10 years) that includes climate stimuli [63], [64]. Although

this study focuses on the wind resource evolution, the methodology presented in this report is also commonly used by climate scientists to analyse other variables (e.g.: temperature, sea level rise, humidity) [65], [67], [70], [72].

A multi-model approach is performed in this study to strengthen the confidence on the outcomes. It has been proved to be a good approach to deal with climate modelling limits (see references below). Indeed, each climate model simulation is an incomplete representation of reality [63], [77]:

- Not all temporal and spatial scales can be captured due to limitations in computational resources. Climate processes occur on time scales that range from centuries to hourly and spatial scales from tens of thousands of kilometres to below one (1) km.
- Not all climate processes and interactions (e.g.: turbulent exchanges under stable conditions, aerosol life cycles) are yet fully understood.
- Configuration of each climate model is based on assumptions that influence the result hence the interest of comparing and using different models in a climate change analysis.
- RCPs scenarios (forcing the climate simulations) are also based on assumptions for the future and internal climate variability.

A single model approach can therefore hides offsets errors and these are generally minimized by a multi-model approach [63], [71]–[73], [77]–[80]. [71] highlights that, by cancelling potential offsets errors, a multi-model approach reduces the effect of the natural climate variability. The multi-model approach of this study is based on a ranking of the climate models with the assessment of their individual performance to represent the past climate.

A careful step back should be taken when interpreting the future wind projections to study events occurring on short time period (such as **single storm events**) and spatial scale (**single grid point such as this study**). Although this study is using high-resolution downscaled simulations which add local detail to the simulation compared to GCM simulations, it remains forced by a GCM which is a large-scale field simulation and uncertainties of projected climate trends (due to natural climate variability) are not mitigated [63], [81].

Figure 7.3 exhibits an overview of the methodology applied in this study. It is noted that the analysis was be conducted at nearest grid point to the measurement location of FLS IJV A. This methodology has been developed by several climate scientists and a non-exhaustive list of references is available in [64], [67]–[71], [80], [82], [83].

The evaluation and multi-model methodology is explained in subsequent Section 7.2.3.

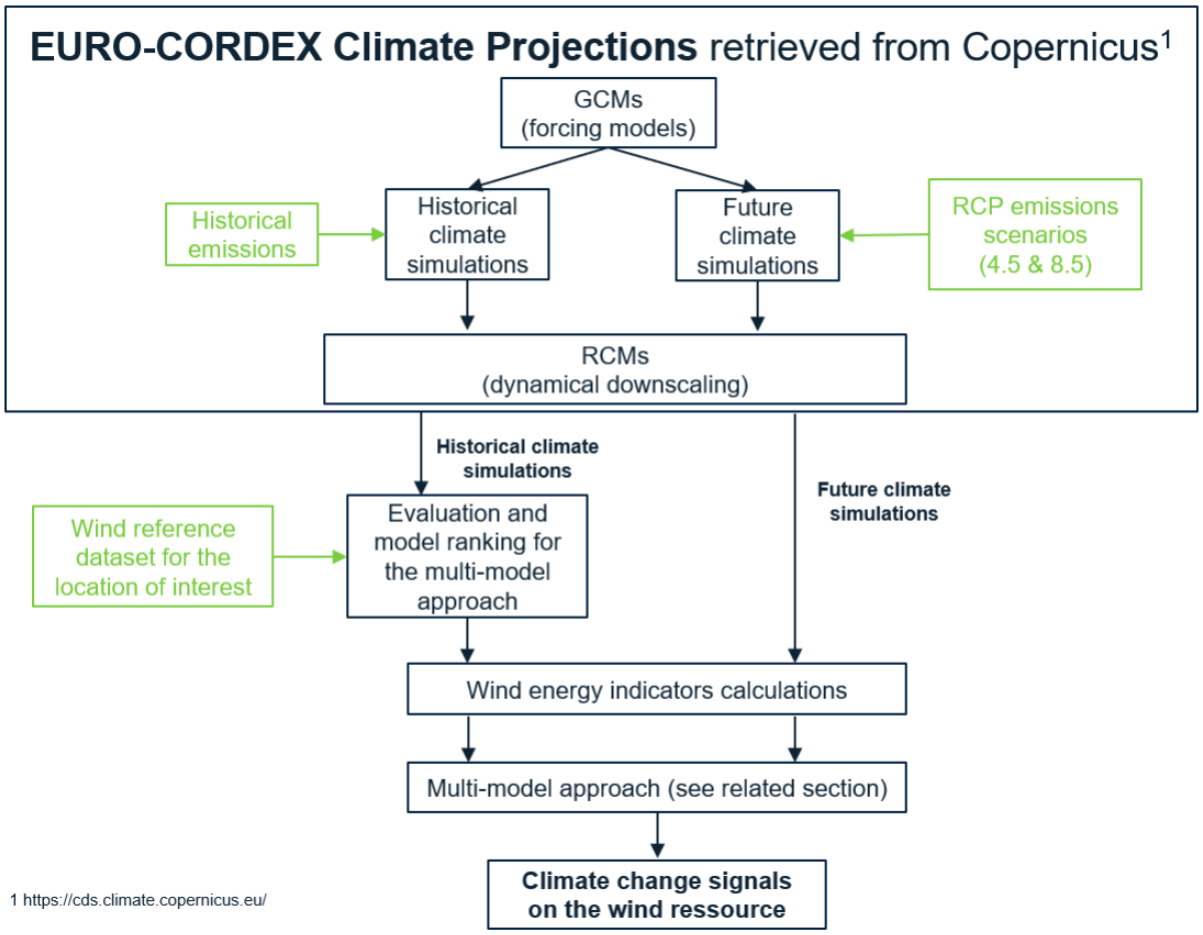

Figure 7.3 Climate change impact on WRA methodology

7.2.3 Model evaluation

As discussed before, the climate change assessment is performed after having assessed the historical climate simulations against the reference dataset assumed to be representative of the past wind climate at the representative location.

The skill of the historical simulations to reproduce the past climate is statistically analysed. This section details the statistical metrics used for the evaluation in this study. These metrics have been widely used by climate experts in recent climate change studies [64], [65], [67]–[70], [80].

Since the Unified-WRF wind speeds were available 10 m height and the climate simulations are at 10 m, the comparison between the datasets can be made directly without any vertical extrapolation.

This report defines and uses two metrics to evaluate climate model performance: Overlap Percentage (OP) and Percentage of Error (EP). OP measures how well modelled probability density functions (PDFs) of wind match observed data, with perfect overlap yielding 100%, while EP assesses the percentage error between modelled and observed mean wind speeds, with RMSE and bias calculations indicating the accuracy across multiple models. While EP focuses on mean wind speeds and may not capture all data characteristics such as extremes, it is a common initial step for comparing model performances and aligning with previous studies. This is further detailed and discussed in Appendix K, K.1.

7.2.4 Multi-model ensemble

A series of statistical methods applied in the atmospheric sciences have been used to process the multi-model approach. For each model, a 3-hourly Julian leap year composed of 366 days is calculated, for the modelled and measured dataset, to be able to process the metrics presented thereafter as the models are not synchronized on a 3-hourly basis with the reference climate. The wind speed of each 3-hourly timestep within a day of this “representative year” is the 3-hourly average of that 3-hourly timestep for all the years considered in the historical period set. For example, the 1st January 3 am timestep is the mean of all January first 3 am wind speed among all the retrieved historical years (1979 to 2005). The comparison between the reference and modelled temporal mean values from monthly to yearly scales allow the scrutiny of the non-synchronized present climate.

Standard statistical measures such as bias, MAE, MAPE, RMSE, and the Yule-Kendall skewness measure are calculated for wind speed at different time scales, aiming for the closest to zero (except for normalized standard deviation which targets one). These metrics are integral for ranking EURO-CORDEX simulation models, allowing for the creation of multi-model ensembles by averaging or multiplying individual model ranks, ensuring the sum of weights equals one for balanced representation. This is further detailed and discussed in Appendix K, K.2.

7.2.5 Wind resource and energy yield assessment indicators

The International Energy Agency (IEA) 15 MW offshore WTG was used as a reference to compute some wind energy indicators. This reference is relevant with the current generation of offshore WTGs developed lately within the industry [84].

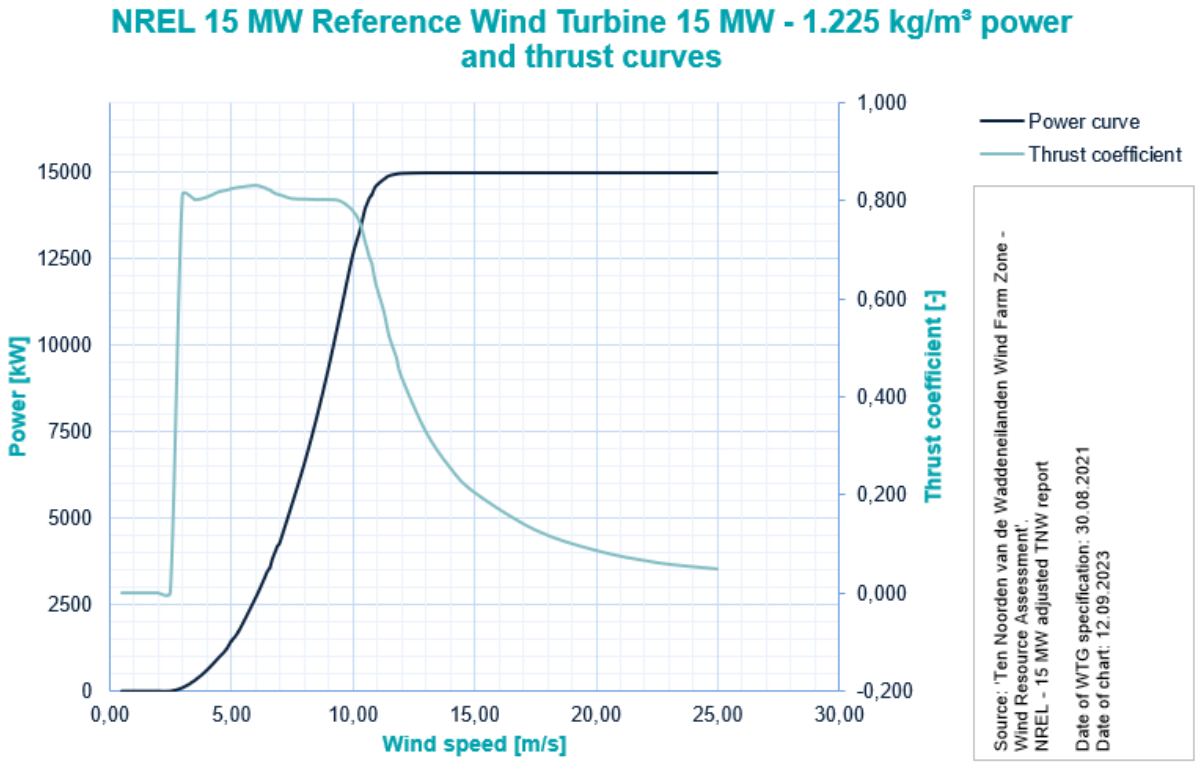

Figure 7.4 Power curve of the selected WTG

Before processing any analysis, the wind data from CORDEX simulations is extrapolated to the 140 m hub height of the reference WTG. Various methodologies for extrapolating wind speed data are available, each presenting varying degrees of accuracy. The most accurate ones consider the atmospheric stability which requires measurements regarding temperature, heat fluxes and friction velocity [67]. Such data is not available in CORDEX simulations thus the following power relationship was used to scale the 10 m values up to the hub height of the WTG:

$$V_{hub\ height} = V_{10m} \times \left(\frac{hub\ height}{10}\right)^{\alpha} \ [m.s^{-1}]$$

The exponent α depends on multiple factors such as elevation, time of day and temperature. Under neutral conditions and with a flat ground, α is equal to 0.14 [61] as recommended by the International Electronical Commission for offshore locations and used in several studies [61].

The wind energy resource was estimated in terms of wind power density (WPD). This metric only considers the wind energetic resource available on-site which is relevant to compare different locations or select the most wind energetic regions. It is calculated as follow:

$$WPD = \frac{1}{2}\rho_a V^3 \ [W.m^{-2}]$$

Where v is the wind speed at hub height and ρ_a is the air density calculated at hub height as follow to consider the reduction of the standard value ($\rho_0 = 1.225 \frac{kg}{m^3}$) due to the height effect [61]:

$$\rho = \rho_0 - 1.194 \times 10^{-4} \times hub\ height\ [kg.m^{-3}]$$

Mean wind speed was processed over the time series to give an overall information. The 99th percentile has also been computed as it provides extreme wind speed information straight from the distribution. Extreme wind speeds play a role in the dimensioning of the turbine support structure so looking at this percentile may provide information regarding trends of evolution for extreme values.

In order to provide WTG specific information, other quantities related to the WTG's characteristics were analysed. An operation time (OT) percentage was defined as the ratio between the number of hours in which the wind speed lies in the interval given by the cut-in and cut-out wind speed (n_{work}) and the total length of the time series (n_{tot}). This is based on heavy assumptions (no gusts, no maintenance phase, no WTG control, …) and should be seen as a means to provide indicative information only:

$$OT = \frac{n_{work}}{n_{tot}}\ [\%]$$

The gross energy yield (AEP_{gross}) is the annual energy output of a wind farm without wake or systematic operational losses. It has been evaluated through the relation given by the guidelines [61] of site-specific conditions and based on the assumption that the wind speed is not varying within the simulation periods of 3 hours:

$$AEP_{gross,i} = \sum_i P(w_i) \times H_i\ [kWh]$$

The AEP is calculated using the Weibull distribution of the ensemble of models calculated with the related formula in Section 7.2.4.

7.3 Results

7.3.1 Capabilities of CORDEX simulations to reproduce wind data

The reliability of the EURO-CORDEX simulations in representing the wind at 10 metres above sea level was evaluated at the IJWWFZ location by comparing the data from each RCM simulation to the reference dataset (Unified-WRF model output), with the OP and EP results shown in Table 7.4 and Table 7.5 respectively. The following Figure 7.5 below shows the Weibull distribution for the reference (thick grey curve) and each RCM simulation, using the Maximum Likelihood Estimation (MLE) method to fit the distribution. The parameters k, A and R^2 in the legend refer to the shape, the scale and the sum of the squares residual to fit the Weibull distribution. Based on the methodology and metrics defined in Section 7.2 the RCMs abilities to reproduce the past wind has been assessed in terms of:

- **Distribution:** OP values above than 90% were obtained for each RCM simulation with 1 simulation above 95% and an average of 93.5%. The

OP values shown in Table 7.4 are better or similar than those obtained in previous studies using the OP metric to validate CORDEX simulations using ERA reanalysis [64], [67]–[70], [80].

- **Mean:** EP values were calculated to assess the ability of the simulations to reproduce the mean trends of the reference. Low EP values (zero being the best) indicate that the RCM model has the same mean trend as the past climate information of the reference dataset. The EP, EPBIAS and EPRMSE values in Table 7.5 for the IJVWFZ are similar to the lowest values obtained in a study using the same methodology and EURO-CORDEX simulations for different sites in the Iberian Peninsula where the RCMs skills to reproduce the past wind was found to be high [64]. Even if the selected RCMs in this other study are not all the same, the fact that the EP values for the IJVWFZ are in the same range (and even lower) is reassuring. Table 7.5 also shows that the model 7 has a very low value (lowest EP value among the 7 RCMs models).

Table 7.4 OP values for each RCM for the IJVWFZ location

Model number	GCM	RCM	OP [%]
1	IPSL-CM5A-MR	SMHI-RCA4	95.4
2	ICHEC-EC-EARTH	KNMI-RACMO22E	94.6
3	MPI-M-MPI-ESM-LR	SMHI-RCA4	90.4
4	NCC-NorESM1-M	SMHI-RCA4	92.3
5	NCC-NorESM1-M	DMI-HIRHAM5	92.1
6	NCC-NorESM1-M	GERICS-REMO2015	94.8
7	CNRM-CERFACS-CM5	KNMI-RACMO22E	94.8
		OP Average	**93.5**
		Standard Deviation OP	**1.75**

Table 7.5 EP values for each RCM for the IJVWFZ location

Model Number	GCM	RCM	EP [%]
1	IPSL-CM5A-MR	SMHI-RCA4	1.2
2	ICHEC-EC-EARTH	KNMI-RACMO22E	2.2
3	MPI-M-MPI-ESM-LR	SMHI-RCA4	4.8
4	NCC-NorESM1-M	SMHI-RCA4	5.0
5	NCC-NorESM1-M	DMI-HIRHAM5	7.9
6	NCC-NorESM1-M	GERICS-REMO2015	3.6

Model Number	GCM	RCM	EP [%]
7	CNRM-CERFACS-CM5	KNMI-RACMO22E	-0.1
		EP RMSE	**4.30**
		EP Bias	**3.51**

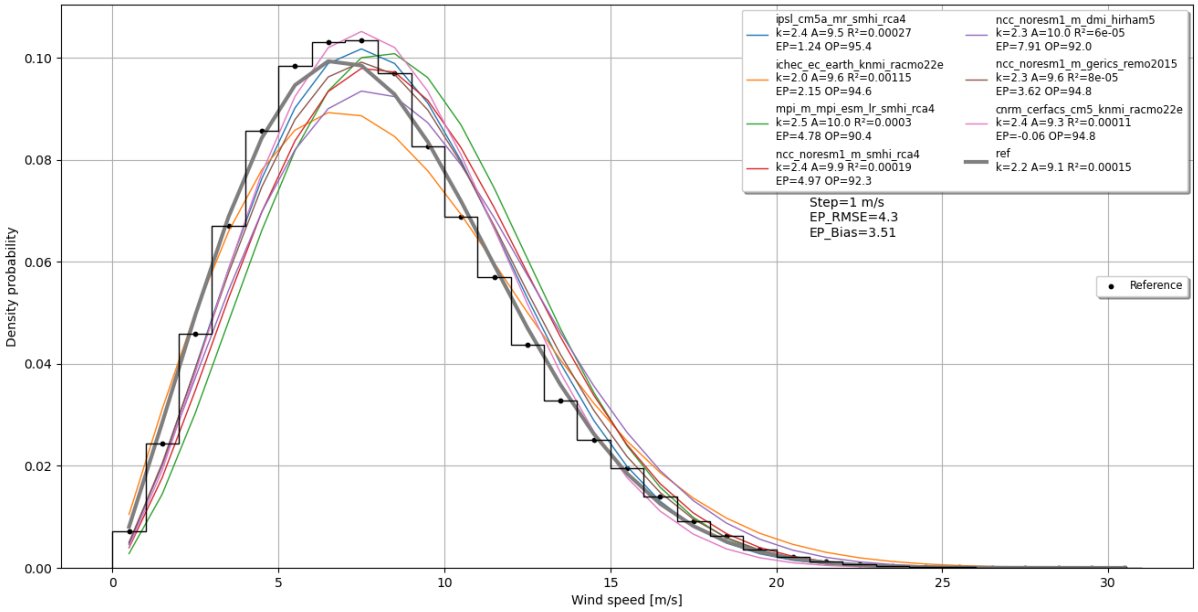

Figure 7.5 Weibull distributions of 7 RCM simulations and WRF (reference) for the IJVWFZ location

According to the EP and OP values, the seven (7) RCMs models have good capabilities to represent the past wind trends in terms of distribution and mean, when compared with previous studies performed with EURO-CORDEX wind projections [64], [67]–[70], [80]. The statistical metrics defined in 7.2.3 were computed to rank the seven models in terms of accuracy in representing the past wind in order to perform the multi-model ensemble methodology. The results in the different metrics are shown in Table 7.6. The weights shown in Table 7.7 were calculated based on the methodology described in Section 7.2.4. Table 7.7 shows the weights for each RCM to calculate the three (3) ensembles of this study: ENS_WM, ENS_WP and ENS_F.

Table 7.6 Results in the metrics allowing to build rank for the models

Model Number	Bias [m/s]	Bias [%]	MAE [m/s]	MAPE [%]	RMSE [m/s]	σ_n [m/s]	YK [-]
1	0.10	1.24	0.30	3.75	0.40	1.17	-0.07
2	0.17	2.14	0.29	3.62	0.33	1.04	-0.07
3	0.39	4.86	0.45	5.59	0.57	0.89	-0.11
4	0.42	5.14	0.42	5.23	0.55	1.13	-0.09
5	0.67	8.24	0.72	8.86	0.88	1.23	-0.05

Model Number	Bias [m/s]	Bias [%]	MAE [m/s]	MAPE [%]	RMSE [m/s]	σ_n [m/s]	YK [-]
6	0.30	3.69	0.36	4.44	0.48	1.10	-0.06
7	-0.01	-0.11	0.20	2.45	0.26	0.92	-0.08

Table 7.7 Weights for the ensemble WM, WP and F[17]

Model Number	Weight ENS_WM [-]	Weight ENS_WP [-]	Weight ENS_F [-]
1	0.122	0.001	0.143
2	0.153	0.002	0.143
3	0.083	0.000	0.143
4	0.084	0.000	0.143
5	0.072	0.000	0.143
6	0.108	0.000	0.143
7	0.378	0.996	0.143

Table 7.7 highlights the importance given to only one model (model number 7) within the WP ensemble. The WM ensemble is somewhat more balanced and gives credit to each model. However, for both ensembles, the model 7 is the considered to be the “best performing model” for this IJVWFZ location. The Overlap percentage (OP) was computed for the three (3) model ensembles as shown in Table 7.8. The three values are above 94%, which is similar to the values obtained in a study using an approach with ensembles [64]. The Weibull distributions of the three ensembles and the reference data set are shown in Figure 7.6.

Table 7.8 Overlap percentage for the three ensembles considered

Parameter	ENS_F [%]	ENS_WM [%]	ENS_WP [%]
Overlap	94.2	95.1	94.8

[17] For ENS_F the weights are equal as per definition in Section 7.2.4

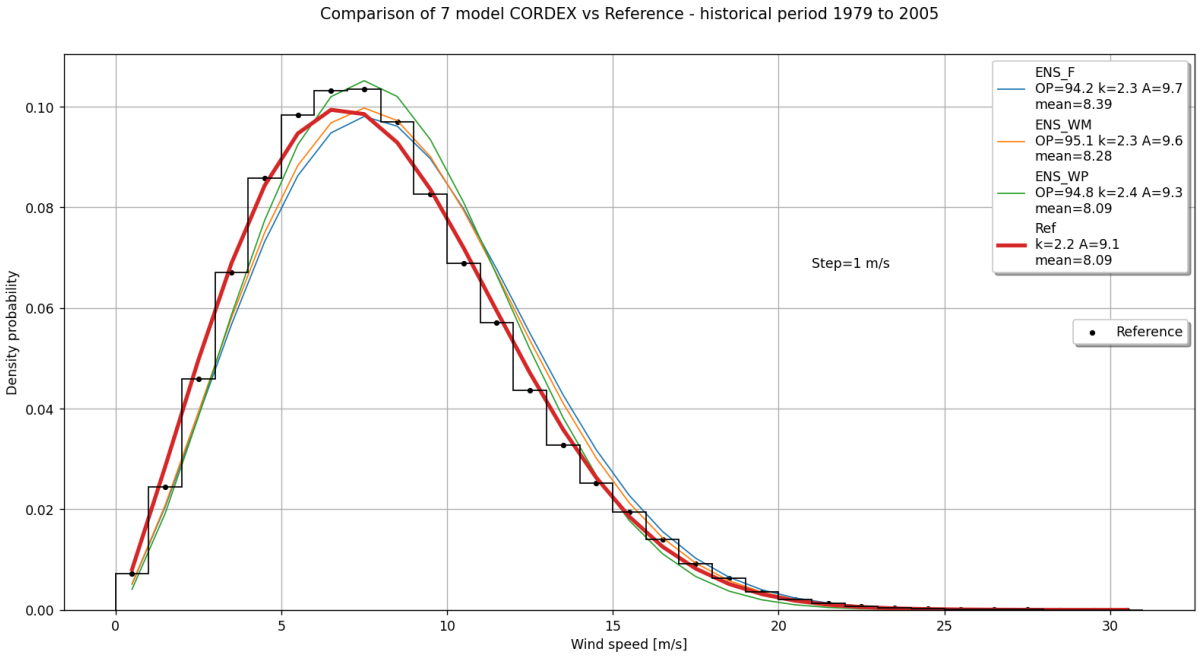

Figure 7.6 Weibull distribution of three ensembles at 10 m height

For the three ensembles the overlap percentage is better than the average overlap percentage of the seven models (Table 7.4) and ENS_WM is the best ensemble with respect to this criterion. In the context of the referenced study [85], it's pertinent to highlight that ensemble selection can be influenced by alternative criteria. Although such an approach was not employed during the current project, adopting diversified selection criteria is advisable to minimize uncertainties and address potential constraints inherent to opting for a singular ensemble.

Within this analysis, the exclusive selection of ENS_WP for wind resource assessment predominantly emphasizes one model, specifically model seven. While model seven presents commendable outcomes as seen in Table 7.6, its performance in terms of OP, as delineated in Table 7.4, is not the highest ranking one, albeit with very good results.

Notwithstanding the inherent constraints of this ensemble approach, leveraging three ensembles as opposed to seven discrete models offers an enhancement in global OP. A comparative review across these ensembles can provide insights into consistent trends and variances from one ensemble to another.

7.3.2 Wind energy resource indicators

The following Table 7.9, Table 7.10 and Table 7.11 summarise the changes to wind energy resource indicators (mean annual wind speed (wind speed), strongest wind percentile (P99 wind speed), wind power density, operation time (OT), annual energy production (AEP)), calculated for the three ensembles under the RCP8.5 scenario. The metrics are normalized to the historical period to show the relative magnitude of changes with the historical period. The same results under the RCP4.5 scenario are shown in the K.4. The RCP8.5 scenario is shown here because the magnitude of the changes are greater for this scenario so it can be considered the most critical in terms of potential impacts

on the offshore wind resource. In the context of the anticipated lifespan of the WTGs projected for installation in the IJVWFZ, values pertaining to the near-future scenarios merit particular emphasis given their immediate relevance.

Table 7.9 Results for ENS_F under the RCP 8.5 scenario

Parameter	Historical	Near-future	Mid-future	Far-future
Δ Wind speed	100.00%	**99.45%**	98.75%	99.14%
Δ P99[18] wind speed	100.00%	**100.30%**	100.41%	101.36%
Δ WPD	100.00%	**98.74%**	97.76%	99.93%
Δ OT	100.00%	**99.93%**	99.79%	99.41%
Δ AEP	100.00%	**98.50%**	96.57%	96.80%

Table 7.10 Results for ENS_WM under the RCP 8.5 scenario

Parameter	Historical	Near-future	Mid-future	Far-future
Δ Wind speed	100.00%	**99.62%**	98.94%	98.88%
Δ P99[18] wind speed	100.00%	**100.18%**	100.12%	100.74%
Δ WPD	100.00%	**98.85%**	97.62%	98.42%
Δ OT	100.00%	**100.00%**	99.94%	99.61%
Δ AEP	100.00%	**98.95%**	97.10%	96.78%

Table 7.11 Results for ENS_WP under the RCP 8.5 scenario

Parameter	Historical	Near-future	Mid-future	Far-future
Δ Wind speed	100.00%	**99.97%**	99.57%	98.55%
Δ P99[18] wind speed	100.00%	**100.58%**	100.04%	99.70%
Δ WPD	100.00%	**99.52%**	98.37%	95.67%
Δ OT	100.00%	**100.07%**	100.17%	99.97%
Δ AEP	100.00%	**99.64%**	98.51%	96.95%

All the ensembles project a decrease in the annual energy production and mean wind speed of about 3% and 1% respectively for the **far future (2075-2099)**. Mean wind power density and operation time are also projected to decrease over this period. However, no conclusion can be drawn for the 99th percentile as two ensembles (ENS F and ENS WM) predict an increase, i.e. higher extreme wind speeds, while one (ENS WP) shows a decrease, i.e. less extreme wind speeds, compared to historical values. This observation at the 99th percentile can also be made for the RCP4.5 climate scenario.

A similar observation can be made for the **near future (2022-2045)** period although the magnitude of changes are smaller: the three ensembles project a decrease of about 0.5% in mean wind speed and 1% in annual energy yield

[18] strongest wind percentile (P99 wind speed)

generation. A **very small increase in non-exceedance probability P99 wind speed is projected by the three ensembles for the near future**.

The observed AEP changes seem very sensitive to the changes in mean wind speed, compared to modern large WTGs and offshore wind speeds. However, this is a function of the power curve characteristic, and especially its rated wind speed and cut-out wind speed that are used to compute the AEP metric. It should be noted that the energy yield generation in this analysis depends only on the wind resource in this analysis and does not take into account possible changes (due to climate change) in, for example, the O&M weather windows. In particular, an increase in extreme wind speed (increase in P99) suggests more severe (and possibly more frequent, see Table 7.12) extreme weather events and thus a reduction in maintenance periods, additional asset losses or WTGs outages that would affect directly energy yield generation.

Table 7.12 below is a peak over threshold analysis assessing how often the WTG's cut-out is exceeded for each climate model under the RCP8.5 scenario. A wind speed above the WTG's cut-out (25m/s) is considered "extreme" in this analysis. Five models suggest that the extreme wind speed will be more frequent in the far future while two models (M2 and M7) suggest that the extreme wind speed are less frequent. This analysis is coarse and depends on the threshold value used but informs on the hypothesis of the more frequent severe events for the far future. Table K.5 in Appendix K shows the same result under the RCP4.5 scenario. The trends of evolution for more or less extreme wind speeds in the future under RCP4.5 scenario are more uncertain however. It is noted that the colour coding is done per climate model scenario in traffic light system.

Table 7.12 Percentage of values above WTG's cut-out for each climate model under RCP8.5 scenario

Parameter	M1	M2	M3	M4	M5	M6	M7
Historical	1.14%	1.50%	1.46%	1.74%	2.88%	1.73%	1.01%
Near-future	1.19%	1.21%	1.38%	1.86%	3.04%	1.95%	1.09%
Mid-future	1.29%	1.17%	1.41%	1.85%	3.12%	2.00%	1.01%
Far-future	1.43%	1.37%	2.00%	1.96%	3.40%	2.18%	0.97%

The following Figure 7.7, Figure 7.8 and Figure 7.9 show the monthly changes of normalised wind power density under the RCP8.5 scenario for the ensemble F, WM and WP respectively. The ensembles F (average of the seven climate models) and WM (weighted average) show a decrease of the wind power density in summer which becomes more significant in the far future. The **decrease during summer for the far future is about 20% compared to the historical values**. Lower wind power density during winter is also expected for the near and mid future periods but an increase is expected for the far future. The results for the ensemble WP (mainly considering climate model 7) are different: an increase in wind power density is expected in summer and a decrease in winter.

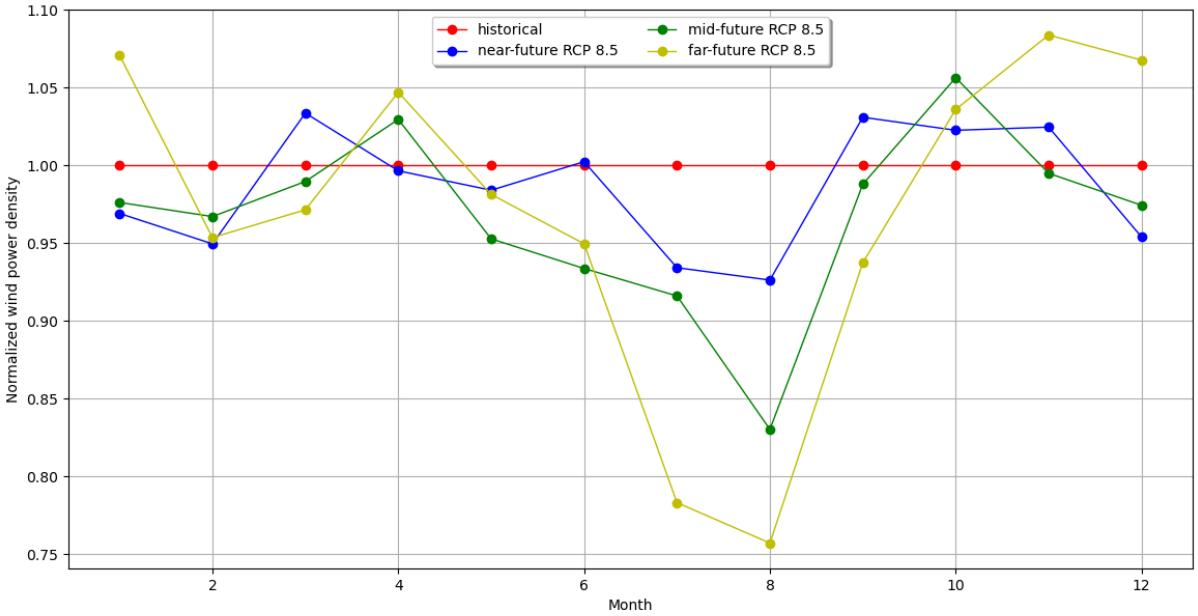

Figure 7.7 Projected changes of wind power density for each month under RCP8.5 scenario
Normalized wind power density on average months – ensemble F

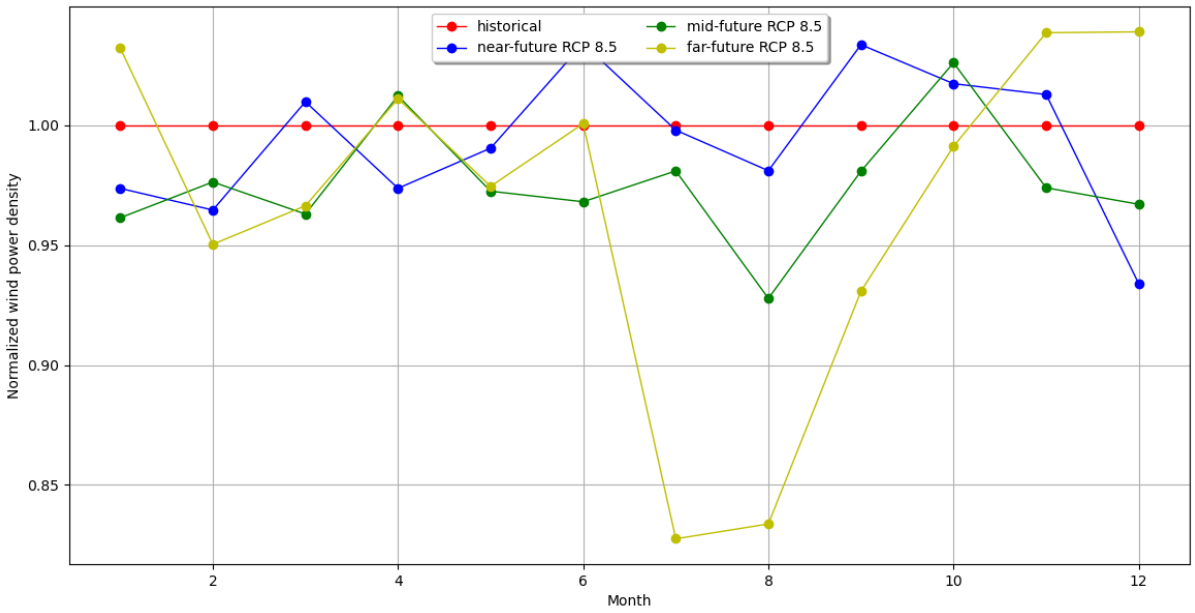

Figure 7.8 Projected changes of wind power density for each month under RCP8.5 scenario
Normalized wind power density on average months – ensemble WM

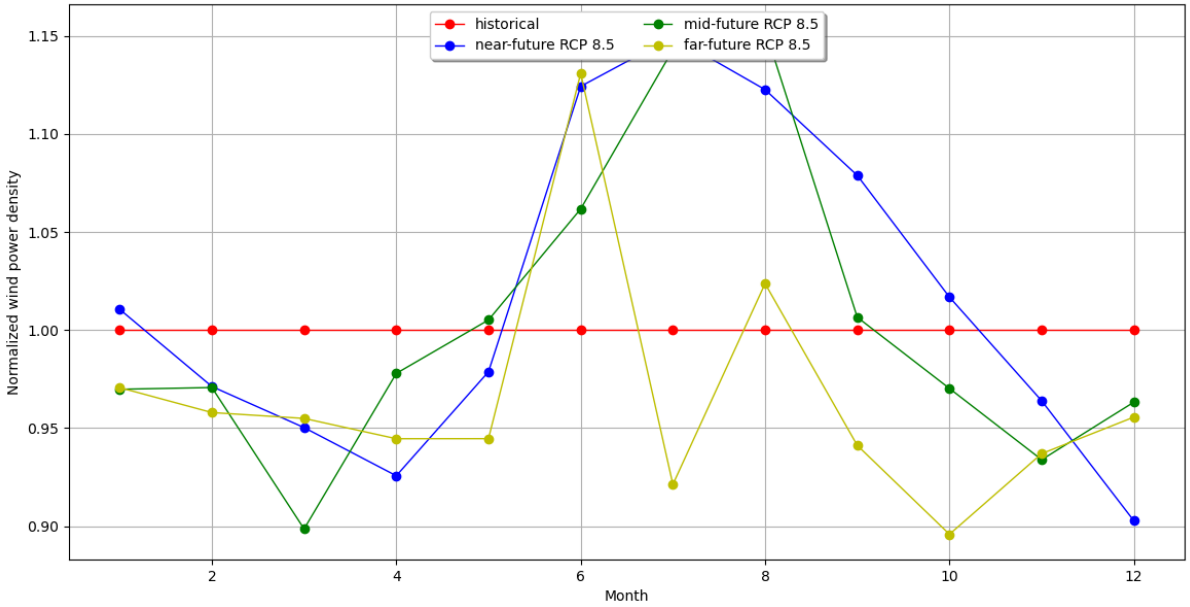

Figure 7.9 Projected changes of wind power density for each month under RCP8.5 scenario - ensemble WP

Normalized wind power density on average months – ensemble WP

Figure 7.10 shows the normalised energy yield generation of the future periods compared to the historical level for the three ensembles. As expected, the trends of change are similar to those observed for the wind power density, since energy yield generation is inherently related to the latter. A **decrease in summer energy yield generation** is projected by ensembles F and WM, gradually reaching 25% approximately by the end of the century. This trend is less straightforward for the WP ensemble as an increase in summer energy yield generation is projected for near and mid future, while a decrease is expected for the far future.

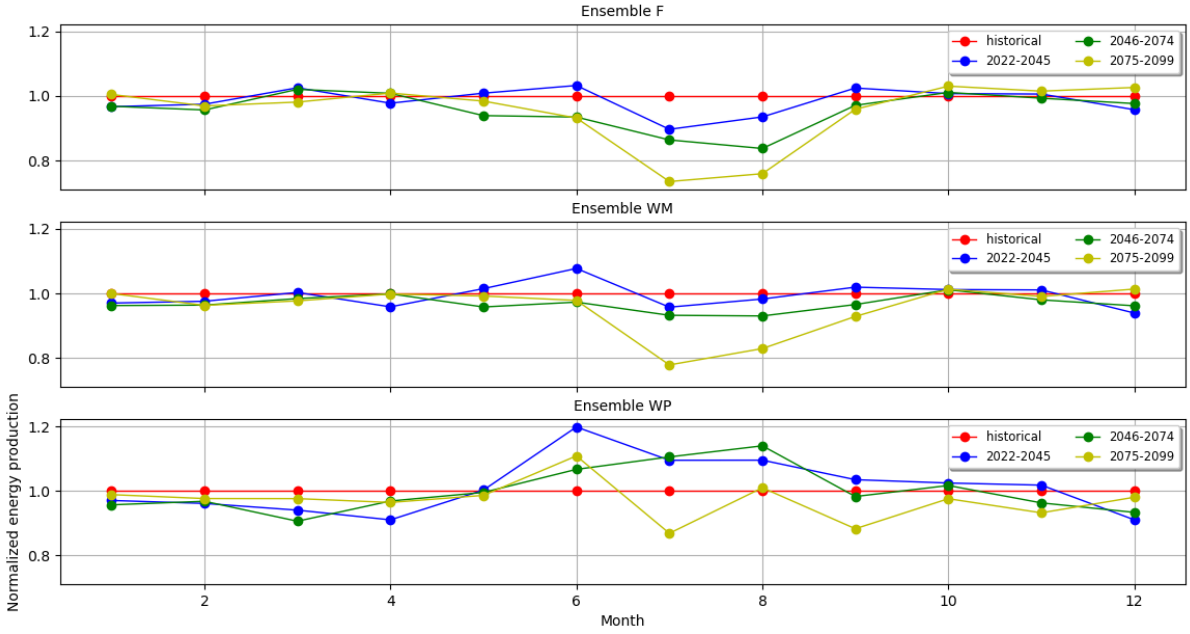

Figure 7.10 Projected changes of energy production for each month and all ensembles under RCP8.5 scenario

Figure 7.11 below shows the seasonal diurnal variability of the wind resource for the RCP8.5 scenario and ensemble F. Figure K.4 in Appendix K shows the same figure for the RCP4.5 scenario. The wind power density is normalised to the historical values to highlight the percentage of change. As shown in the Figure 7.11, a decrease in the wind resource is projected for summer days, with the magnitude of change reaching 5% and 20% for the near and far futures respectively. For autumn, a small increase of 1 to 4% can be expected for the future periods. For the spring season, the projections are similar to the historical values, with a small decrease of the resource during the night and an increase during the day. Concerning the winter season, as mentioned above, a decrease of the resource (about 5%) can be expected for the short and medium term but an increase is projected for the long future (also 5% change).

Figure K.4 in Appendix K shows that the percentage of changes in seasonal diurnal variability are different for the RCP4.5 scenario. In particular, the decrease in wind resource is less for summer days, which are around 95% of the historical levels throughout the 21st century. For winter, the three future periods are projected to be slightly below historical levels, at around 98% of historical levels.

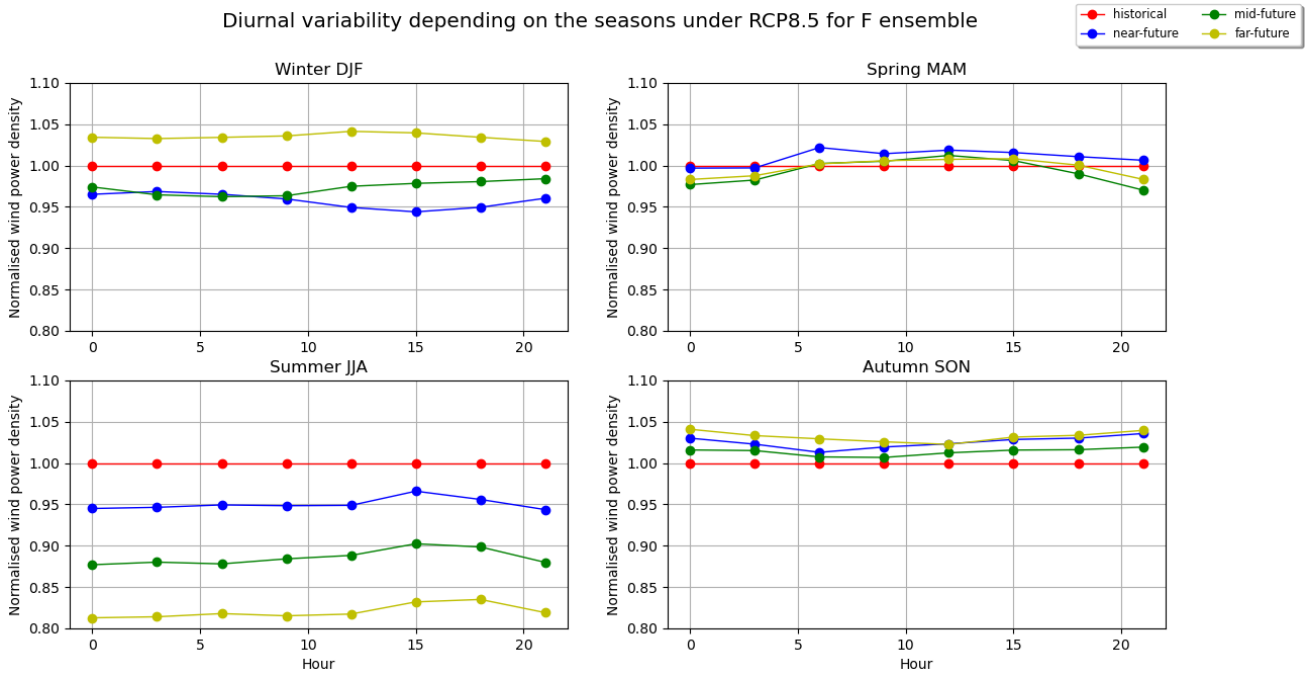

Figure 7.11 Seasonal diurnal variability of the wind resource under RCP8.5 scenario for the ensemble F

7.3.3 Weibull distribution

Figure 7.12 shows the Weibull distribution of the seven climate models (dashed line) used in this study and the 3 ensembles (full line) for the near future period (2022-2045) under the RCP8.5 scenario. The Weibull parameters for each climate model are given in the legend, where k and A stand for shape and scale, respectively, and the sum of the squares residual R^2 measures the bias between the Weibull fit and the associated histogram of the distribution. Table 7.13 shows the different Weibull parameters of each ensemble for all the periods under RCP8.5.

Table 7.13 Weibull parameters for the three ensembles under the RCP8.5 scenario at 10 metres height

Parameter		Historical	Near-future	Mid-future	Far-future
ENS F	**shape k**	2.43	2.39	2.13	2.34
	scale A	9.90	9.73	8.65	9.73
ENS WM	**shape k**	2.43	2.40	2.23	2.35
	scale A	9.72	9.59	8.88	9.49
ENS WP	**shape k**	2.44	2.42	2.39	2.38
	scale A	9.42	9.30	9.17	9.07

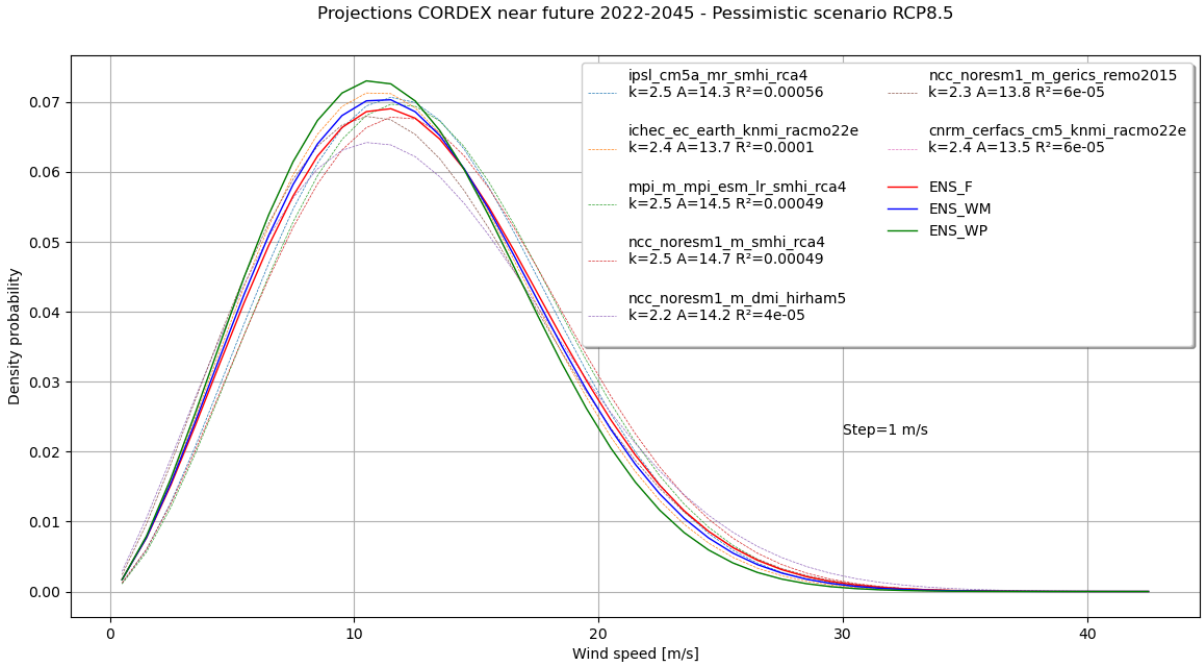

Figure 7.12 Weibull distributions for the near future period under RCP8.5 scenario

Figure 7.13, Figure 7.14 and Figure 7.15 show the cumulative distribution functions (CDF) of the wind speed at hub height for the ensemble F, WM and WP respectively under RCP8.5. Figure K.6, Figure K.7 and Figure K.8 in Appendix K show the same distribution for the three ensembles but under the RCP4.5 scenario.

Across all ensembles and scenarios, there's a discernible shift in the curves towards the left side when transitioning from the historical to the distant future period within the [cut-in; cut-out] range of the WTG. This observation is of particular importance, given that approximately 90% of the values reside within this specified range. Consequently, this shift suggests a potential reduction in the available wind resource for the WTG, underscoring an anticipated decrease in energy yield production in forthcoming periods.

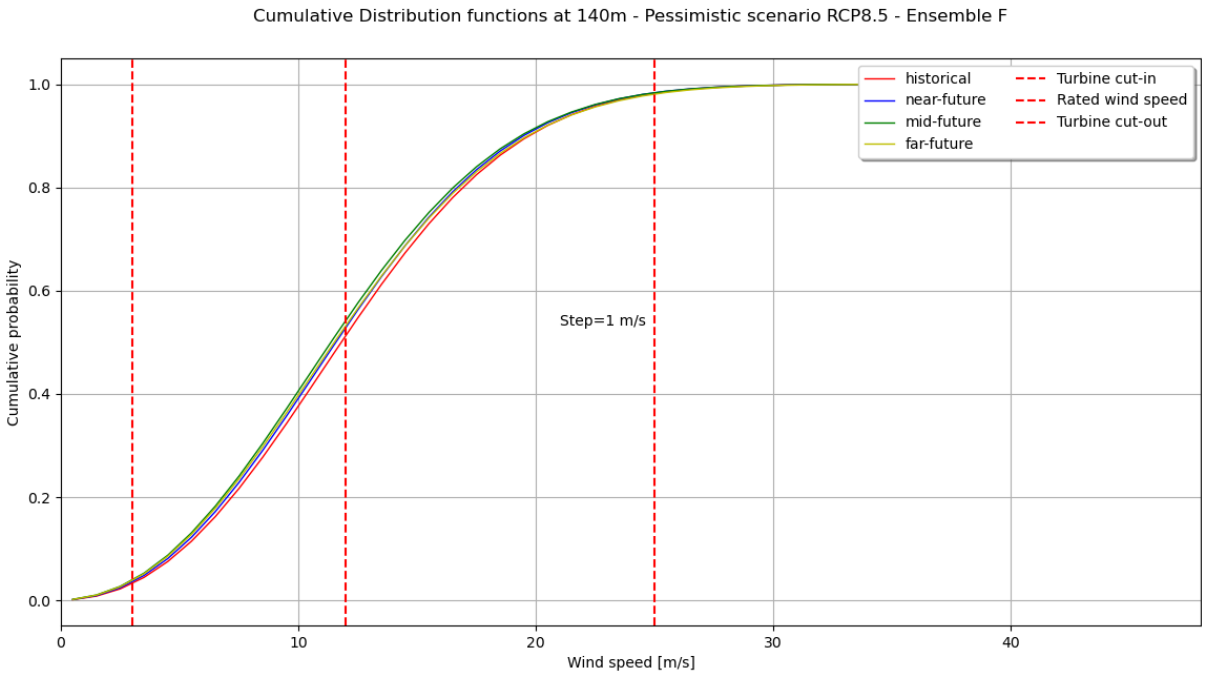

Figure 7.13 CDF at hub height for the ensemble F under RCP8.5

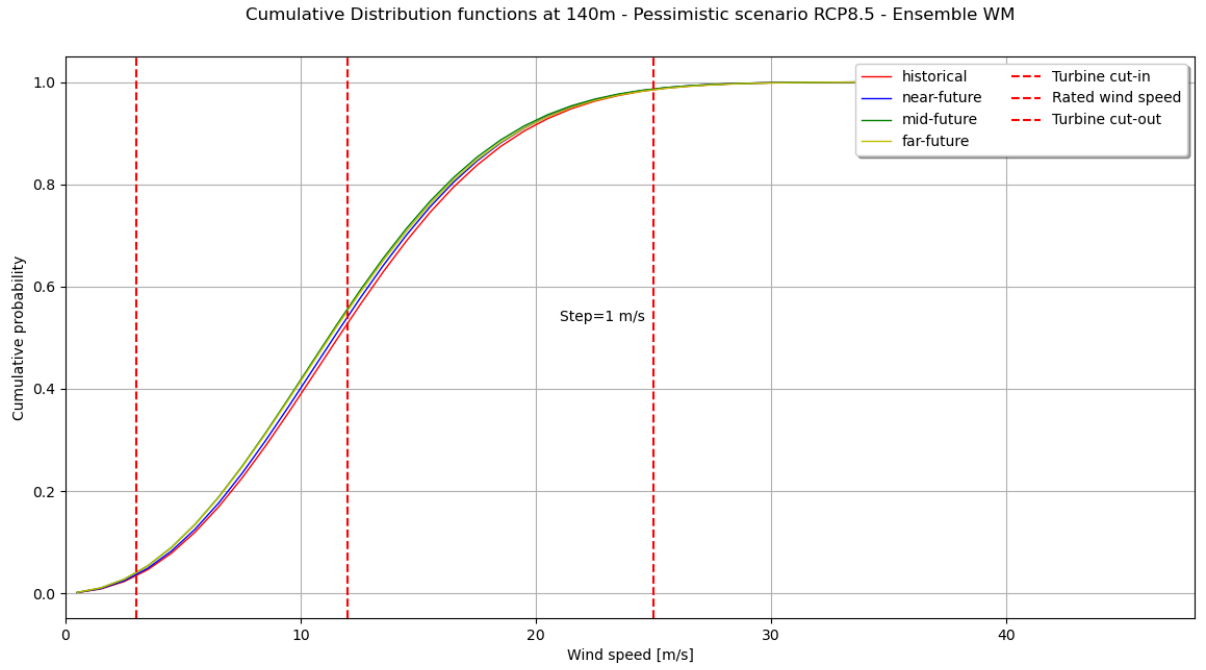

Figure 7.14 CDF at hub height for the ensemble WM under RCP8.5

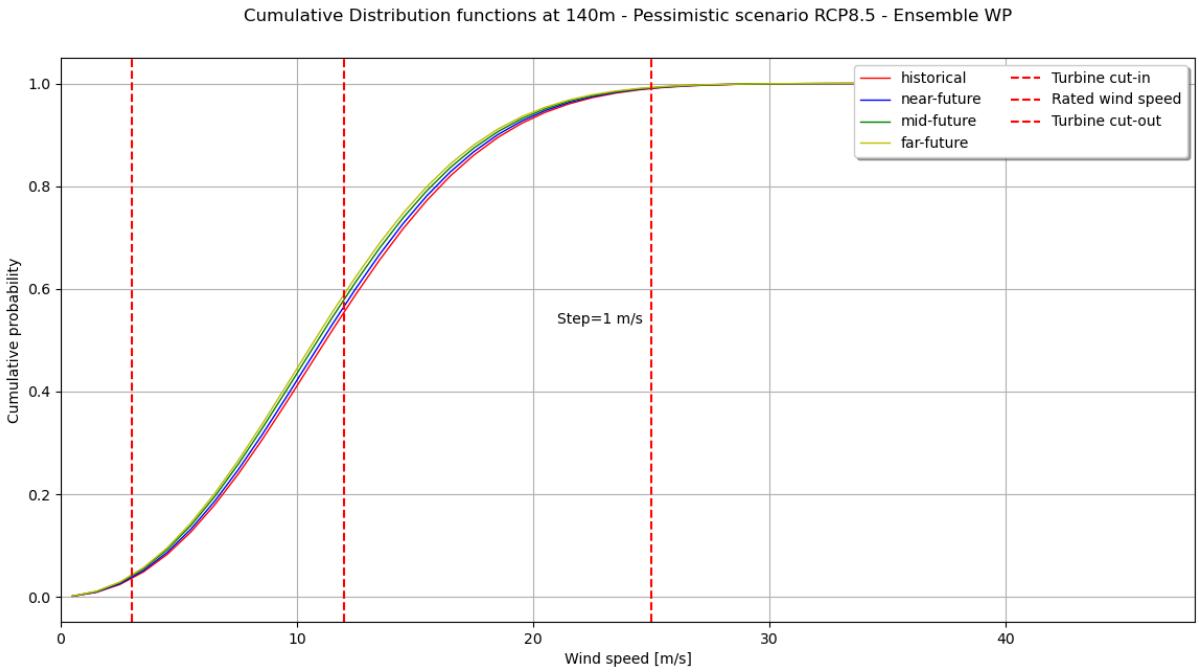

Figure 7.15 CDF at hub height for the ensemble WP under RCP8.5

7.3.4 Uncertainty in the climate change analysis

Climate change uncertainty for the FLS IJV location was assessed using near-future ensemble scenarios, including RCP45 - ENS F, RCP45 - ENS WM, RCP45 -ENW WP, RCP85 - ENS F, RCP85 - ENS WM, and RCP85 -ENW WP. These scenarios were developed based on various greenhouse gas emissions and socio-economic pathways. Given the limited information typically associated with Type B uncertainties, assumptions about upper and lower uncertainty bounds were obtained. Using a uniform distribution between these bounds, a standard uncertainty was determined. Consequently, a 0.2% uncertainty in wind speed for the FLS IJV location was calculated, and this value was assumed consistent for other primary dataset locations.

7.4 Conclusions on the climate change analysis

The impact of climate change on the wind resource at a site in the North Sea near the IJmuiden Ver measurement point was analysed using a EURO-CORDEX multi-model ensemble. The accuracy of the seven (7) CORDEX models used in this study to reproduce the historical wind speed was assessed by comparing them with a reference dataset of the location on a 26-year historical period. The main findings can be summarised as follows:

- The seven (7) climate models were used to perform the analysis as the ensemble was considered reliable by the validation methodology described in Section 3.1.
- Based on the validation methodology, three ensembles were constructed to **analyse the future wind resource between 2022 and 2099** in three (3) different time periods representing the short, medium and long term scenarios. Two representative concentration pathway scenarios were used for the study **(RCP4.5 and RCP8.5).**

- One of the ensemble analysed (ensemble F) **projects a decrease of 0.55% in mean wind speed and 1.5% in annual energy yield generation for the near future period (2022-2045) under the RCP8.5 scenario.** A similar study for the German North Sea based on the analysis of seven climate models has found similar results [61].
- In the far future (2075-2099), the decrease in wind resource and energy generation is **more pronounced,** reaching 1% and 3% for the mean wind speed and energy yield generation respectively, on average for the three ensembles analysed.
- The magnitude of the changes is smaller for the RCP4.5 scenario compared to RCP8.5. The mean change projected by the three ensembles analysed is a decrease of 0.7% in mean wind speed and 1.7% in annual energy produced for the far future period.
- Two ensembles project **a decrease in summer wind power density of about 5%, 10% and 20% under RCP8.5** for the near, mid and far future period respectively, compared to historical levels. This reduction in the wind resource leads to **a decrease in summer energy yield generation of around 25% in the long term**.
- **An overall decrease in energy yield generation and operation hours is expected**. The decrease in wind speed within the operating range of the WTG [cut-in; cut-out] and the trend towards more severe wind speeds are likely drivers of this overall decrease. There is a high confidence for increase of frequency for extreme wind speed events in the far future under the RCP8.5 scenario (5 models out of 7 projecting this trend) while the consensus is less certain under the RCP4.5 scenario.
- It is important to note that no bias correction has been made to the final long-term climates of the Unified-WRF based on the climate change analysis. This is considered outwith the scope of this analysis, and the reader is expected to evaluate and adapt any changes as necessary.

The primary constraint inherent in this study pertains to its utilization of a single grid point approach. Consideration of a larger region adjacent to the IJmuiden Ver site would increase the reliability of the results and include a broader view of the regional changes. The methodology applied in this study to assess CORDEX capabilities gives an understanding of the bias of climate models to perform such climate change analysis. Similar results for this region in the literature supports the findings [61], [62].

8 Uncertainty Assessment

The uncertainty associated with the long-term wind speed at each of the nodes is the total uncertainty of the wind speed measurement uncertainty (Section 2.4), the vertical extrapolation (Section 3.3.5), the correction to the long-term with MCP (Section 3.4.4) and the uncertainty associated with the horizontal extrapolation within the wind gradient model (Section 5.1.4) and the climate change uncertainty (Section 7.3.4).

The respective uncertainty components from four independent assessments are categorised and combined considering their nature as statistically independent, dependent (inter-dependent), and location specific. The total uncertainty associated with the long-term wind speed at the representative nodes at the height of 160 m are presented in Table 8.3 to Table 8.8 for the historical, projected 10-year and 25-year periods.

To derive the uncertainty of the project wind climate, four independent wind resource assessments at primary locations FLS IJV, MM IJmuiden, FLS HKW and lidar K13-A are combined using the reciprocal weighting of the variance of the independent sources of uncertainty. The combined approach considers that the overall uncertainty is reduced when for the composite results from the statistically independent elements of the four locations.

Table 8.1 Weighting of independent estimate of long-term wind climate

Designation	FLS IJV	MM IJmuiden	FLS HKW	Lidar K13-A
Wind speed uncertainty considering independent elements [%]	3.4	2.4	3.1	3.1
Variance of independent elements of wind speed uncertainty [(m/s)²]	0.12	0.06	0.10	0.10
Inverse variance weights [-]	0.18	0.36	0.23	0.23

For the horizontal extrapolation, in line with the methodology applied to derive the wind speeds for the final Unified-WRF across the IJVWFZ, the dependent uncertainties in wind speed were combined with an inverse distance weighting for the horizontal extrapolation in the model, where the weights were obtained with:

$$w_i = \frac{R^2}{(R^2 + d_i^2)}$$

where R is a constant, and d is the distance from the measurement site to the point of interest with R equal to 0.5 km. Each weight is then normalised by the sum of the weights for all the measurements sites being considered, so that the sum of all weights is equal to one.

The calculated weights for each node are presented in the below Table 8.2.

Dependent uncertainties, like for example the climate change uncertainty apply equally to all four locations and are not reduced by combination of the four assessments.

Table 8.2 Distance weights for modelling used in uncertainty assessment

Designation	FLS IJV	MM Ijmuiden	FLS HKW	Lidar K13-A
N1_Alpha1 [-]	0.35	0.55	0.08	0.02
N2_Alpha2 [-]	0.00	1.00	0.00	0.00
N3_Beta1 [-]	1.00	0.00	0.00	0.00
N4_Beta2 [-]	0.45	0.47	0.04	0.05
N5_Gamma1 [-]	0.72	0.15	0.06	0.06
N6_Gamma2 [-]	0.53	0.25	0.06	0.16

Within the evaluated dependent parameters, only horizontal variations were integrated using a distance-weighting method. For the other parameters, no weighting was considered necessary due to the presumption of uniformity across individual WRA sites.

The combined uncertainty in wind speed at a height of 160 m was determined to be 2.1%.

In the context of future projections, the combined uncertainty in long-term wind speed for 10-year was quantified at 2.7%. For 25-year projection, the uncertainty was ascertained to span from 2.3% to 2.4% for the delineated representative nodes: Alpha1, Alpha2, Beta1, Beta2, Gamma1, and Gamma2, situated within the IJVWFZ, as presented in Table 8.3 to Table 8.8 for the different projection periods.

.

Table 8.3 Total uncertainty in long-term wind speed at representative N1_Alpha1 location at 160 m

Uncertainty category	Uncertainty Description	Independence	Weight	FLS IJV	MM Ijmuiden	FLS HKW	Lidar K13-A
Site measurement	Total uncertainty in measured wind speed (wind statistics)	Independent	Inverse variance	3.2%	2.1%	2.9%	2.9%
Vertical extrapolation	Vertical extrapolation based on measured shear	Independent	Inverse variance	0.0%	0.4%	0.0%	0.0%
Historic wind resource	Long-term representation	Dependent	n/a	1.4%	1.4%	1.4%	1.4%
	MCP method uncertainty	Independent	Inverse variance	1.2%	1.1%	1.1%	1.1%
Spatial variation	Modelled horizontal extrapolation to node	Dependent	Distance	0.2%	0.1%	0.3%	0.4%
Climate change uncertainty	From climate change analysis, near-future ensemble	Dependent	n/a	0.2%	0.2%	0.2%	0.2%
Combined total uncertainty in long-term wind speed at N1_Alpha1 (historic)				**2.1%**			
Future wind variability	Inter-annual variability (10-year uncertainty)	Dependent	n/a	1.7%	1.7%	1.7%	1.7%
Future wind variability	Inter-annual variability (25-year uncertainty)	Dependent	n/a	1.1%	1.1%	1.1%	1.1%
Combined total uncertainty in long-term wind speed at N1_Alpha1 (10-year)				**2.7%**			
Combined total uncertainty in long-term wind speed at N1_Alpha1 (25-year)				**2.3%**			

Table 8.4 Total uncertainty in long-term wind speed at representative N2_Alpha2 location at 160 m

Uncertainty category	Uncertainty Description	Independence	Weight	FLS IJV	MM Ijmuiden	FLS HKW	Lidar K13-A
Site measurement	Total uncertainty in measured wind speed (wind statistics)	Independent	Inverse variance	3.2%	2.1%	2.9%	2.9%
Vertical extrapolation	Vertical extrapolation based on measured shear	Independent	Inverse variance	0.0%	0.4%	0.0%	0.0%
Historic wind resource	Long-term representation	Dependent	n/a	1.4%	1.4%	1.4%	1.4%
	MCP method uncertainty	Independent	Inverse variance	1.2%	1.1%	1.1%	1.1%
Spatial variation	Modelled horizontal extrapolation to node	Dependent	Distance	0.2%	0.1%	0.3%	0.4%
Climate change uncertainty	From climate change analysis, near-future ensemble	Dependent	n/a	0.2%	0.2%	0.2%	0.2%
Combined total uncertainty in long-term wind speed at N2_Alpha2 (historic)				**2.1%**			
Future wind variability	Inter-annual variability (10-year uncertainty)	Dependent	n/a	1.7%	1.7%	1.7%	1.7%
Future wind variability	Inter-annual variability (25-year uncertainty)	Dependent	n/a	1.1%	1.1%	1.1%	1.1%
Combined total uncertainty in long-term wind speed at N2_Alpha2 (10-year)				**2.7%**			
Combined total uncertainty in long-term wind speed at N2_Alpha2 (25-year)				**2.3%**			

Table 8.5 Total uncertainty in long-term wind speed at representative N3_Beta1 location at 160 m

Uncertainty category	Uncertainty Description	Independence	Weight	FLS IJV	MM Ijmuiden	FLS HKW	Lidar K13-A
Site measurement	Total uncertainty in measured wind speed (wind statistics)	Independent	Inverse variance	3.2%	2.1%	2.9%	2.9%
Vertical extrapolation	Vertical extrapolation based on measured shear	Independent	Inverse variance	0.0%	0.4%	0.0%	0.0%
Historic wind resource	Long-term representation	Dependent	n/a	1.4%	1.4%	1.4%	1.4%
	MCP method uncertainty	Independent	Inverse variance	1.2%	1.1%	1.1%	1.1%
Spatial variation	Modelled horizontal extrapolation to node	Dependent	Distance	0.2%	0.1%	0.3%	0.4%
Climate change uncertainty	From climate change analysis, near-future ensemble	Dependent	n/a	0.2%	0.2%	0.2%	0.2%
Combined total uncertainty in long-term wind speed at N3_Beta1 (historic)				**2.1%**			
Future wind variability	Inter-annual variability (10-year uncertainty)	Dependent	n/a	1.7%	1.7%	1.7%	1.7%
Future wind variability	Inter-annual variability (25-year uncertainty)	Dependent	n/a	1.1%	1.1%	1.1%	1.1%
Combined total uncertainty in long-term wind speed at N3_Beta1 (10-year)				**2.7%**			
Combined total uncertainty in long-term wind speed at N3_Beta1 (25-year)				**2.3%**			

Table 8.6 Total uncertainty in long-term wind speed at representative N4_Beta2 location at 160 m

Uncertainty category	Uncertainty Description	Independence	Weight	FLS IJV	MM Ijmuiden	FLS HKW	Lidar K13-A
Site measurement	Total uncertainty in measured wind speed (wind statistics)	Independent	Inverse variance	3.2%	2.1%	2.9%	2.9%
Vertical extrapolation	Vertical extrapolation based on measured shear	Independent	Inverse variance	0.0%	0.4%	0.0%	0.0%
Historic wind resource	Long-term representation	Dependent	n/a	1.4%	1.4%	1.4%	1.4%
	MCP method uncertainty	Independent	Inverse variance	1.2%	1.1%	1.1%	1.1%
Spatial variation	Modelled horizontal extrapolation to node	Dependent	Distance	0.2%	0.1%	0.3%	0.4%
Climate change uncertainty	From climate change analysis, near-future ensemble	Dependent	n/a	0.2%	0.2%	0.2%	0.2%
Combined total uncertainty in long-term wind speed at N4_Beta2 (historic)				**2.1%**			
Future wind variability	Inter-annual variability (10-year uncertainty)	Dependent	n/a	1.7%	1.7%	1.7%	1.7%
Future wind variability	Inter-annual variability (25-year uncertainty)	Dependent	n/a	1.1%	1.1%	1.1%	1.1%
Combined total uncertainty in long-term wind speed at N4_Beta2 (10-year)				**2.7%**			
Combined total uncertainty in long-term wind speed at N4_Beta2 (25-year)				**2.3%**			

Table 8.7 Total uncertainty in long-term wind speed at representative N5_Gamma1 location at 160 m

Uncertainty category	Uncertainty Description	Independence	Weight	FLS IJV	MM Ijmuiden	FLS HKW	Lidar K13-A
Site measurement	Total uncertainty in measured wind speed (wind statistics)	Independent	Inverse variance	3.2%	2.1%	2.9%	2.9%
Vertical extrapolation	Vertical extrapolation based on measured shear	Independent	Inverse variance	0.0%	0.4%	0.0%	0.0%
Historic wind resource	Long-term representation	Dependent	n/a	1.4%	1.4%	1.4%	1.4%
	MCP method uncertainty	Independent	Inverse variance	1.2%	1.1%	1.1%	1.1%
Spatial variation	Modelled horizontal extrapolation to node	Dependent	Distance	0.2%	0.1%	0.3%	0.4%
Climate change uncertainty	From climate change analysis, near-future ensemble	Dependent	n/a	0.2%	0.2%	0.2%	0.2%
Combined total uncertainty in long-term wind speed at N5_Gamma1 (historic)				**2.1%**			
Future wind variability	Inter-annual variability (10-year uncertainty)	Dependent	n/a	1.7%	1.7%	1.7%	1.7%
Future wind variability	Inter-annual variability (25-year uncertainty)	Dependent	n/a	1.1%	1.1%	1.1%	1.1%
Combined total uncertainty in long-term wind speed at N5_Gamma1 (10-year)				**2.7%**			
Combined total uncertainty in long-term wind speed at N5_Gamma1 (25-year)				**2.3%**			

Table 8.8 Total uncertainty in long-term wind speed at representative N6_Gamma2 location at 160 m

Uncertainty category	Uncertainty Description	Independence	Weight	FLS IJV	MM Ijmuiden	FLS HKW	Lidar K13-A
Site measurement	Total uncertainty in measured wind speed (wind statistics)	Independent	Inverse variance	3.2%	2.1%	2.9%	2.9%
Vertical extrapolation	Vertical extrapolation based on measured shear	Independent	Inverse variance	0.0%	0.4%	0.0%	0.0%
Historic wind resource	Long-term representation	Dependent	n/a	1.4%	1.4%	1.4%	1.4%
	MCP method uncertainty	Independent	Inverse variance	1.2%	1.1%	1.1%	1.1%
Spatial variation	Modelled horizontal extrapolation to node	Dependent	Distance	0.2%	0.1%	0.3%	0.4%
Climate change uncertainty	From climate change analysis, near-future ensemble	Dependent	n/a	0.2%	0.2%	0.2%	0.2%
Combined total uncertainty in long-term wind speed at N6_Gamma2 (historic)				**2.1%**			
Future wind variability	Inter-annual variability (10-year uncertainty)	Dependent	n/a	1.7%	1.7%	1.7%	1.7%
Future wind variability	Inter-annual variability (25-year uncertainty)	Dependent	n/a	1.1%	1.1%	1.1%	1.1%
Combined total uncertainty in long-term wind speed at N6_Gamma2 (10-year)				**2.7%**			
Combined total uncertainty in long-term wind speed at N6_Gamma2 (25-year)				**2.4%**			

9 Conclusion

The assessment of the wind resource across the IJmuiden Ver Wind Farm Zone (IJVWFZ, Project site) was performed, situated approximately 62 km from the west mainland coast of the Netherlands. This work was undertaken by OWC and partners, which included ProPlanEn, ArcVera, and Innosea.

The Ministry of Economic Affairs and Climate has assigned the IJVWFZ as a designated wind farm area. This site can be found in the Dutch Exclusive Economic Zone on the Dutch shelf in the North Sea.

The goal of the study was to evaluate the wind resource within the IJVWFZ, providing insight into potential future investments in offshore wind development. The work primarily focused on creating a unified wind dataset for both wind resource assessment and metocean analysis. The developed mesoscale model, Unified-WRF, served this purpose. Analysis of the long-term ambient wind conditions for the development area was conducted on behalf of RVO.

This study utilized both on-site and off-site wind measured data. In-depth analyses were conducted using 14 datasets from various offshore sites in the Dutch and German North Sea. Four of these measurement locations were categorized as primary. These included two on-site floating lidar systems (FLS IJV), an on-site offshore met mast (MM IJmuiden), two off-site FLS at the Hollandse Kust West WFZ (FLS HKW) and an off-site vertical profiling lidar at the K130A offshore platform (lidar K13-A). Beyond the creation and verification of the Unified-WRF, the primary datasets were instrumental in elucidating the long-term climate across the IJVWFZ and in the assessment of uncertainties associated with wind speed.

For the long-term climate calculations, the datasets at the four primary measurement locations were corrected and adjusted to a height of 160 m to showcase an independent statistical analysis of the primary measurements at the measurement locations. Long-term wind speeds at this height were found to be between 9.89 m/s and 10.17 m/s, with the prevailing wind direction being southwest.

Traditionally wind resource and met ocean assessments are conducted as independent assessments and cross-checked afterwards. A novel approach, the Unified WRF model, was taken in this study: The Weather Research and Forecasting (WRF) model driven by ERA5 reanalysis, was tailored to be used for both the wind resource and met ocean application in the IJVWFZ region.

Upon spatial analysis, the Unified-WRF model showcased outstanding performance when compared with other mesoscale models, emphasizing its ability to represent both short-term and long-term climate at the IJVWFZ. The overall long-term climate derived from the Unified-WRF indicates wind speeds ranging from 10.08 m/s to 10.20 m/s at a height of 160 m, with the southwest being the prevailing wind direction.

The potential effects of climate change on offshore wind energy at the FLS IJV measurement point were explored using seven climate projections from the CORDEX research project, which were considered under the RCP4.5 and RCP8.5 scenarios. A decrease in mean wind speed and subsequent energy yield generation was projected, with the reductions being more pronounced under the RCP8.5 scenario; additionally, significant reductions in summer wind

power density were observed, leading to a decrease in summer energy yield generation. These results were derived from a single grid point approach and were supported by findings in the broader scientific literature. The uncertainty in the wind speed for the near-future scenario was found to be 0.2%.

It is important to note that no bias correction has been made to the final long-term climates of the Unified-WRF based on the climate change analysis. This is considered outwith the scope of this analysis, and the reader is expected to evaluate and adapt any changes as necessary.

Through the integration of the primary measurement datasets, an enhanced calibration in uncertainty was achieved, leading to a more rigorous assessment of the wind climate. In the historical data, a combined uncertainty in wind speed at the height of 160 m was determined to be 2.1%. For future projections, the combined total uncertainty in long-term wind speed for the 10-year period was identified to be 2.7%. For the 25-year projection, the uncertainty was found to range between 2.3% and 2.4% for the designated representative nodes: Alpha1, Alpha2, Beta1, Beta2, Gamma1, and Gamma2, within the IJVWFZ. A comprehensive breakdown and supportive data were provided in the ensuing tables.

References

[1] RPS, 'TN328326 SUPPLY OF METOCEAN DATA FOR IJMUIDEN VER INVESTIGATION AREA, Monthly Measurement and Validation Report - May 2023', 100-CN-REP-2072 Rev 0, Jul. 2023.

[2] RPS, 'TN328326 SUPPLY OF METOCEAN DATA FOR IJMUIDEN VER INVESTIGATION AREA, Monthly Measurement and Validation Report - IJV May 2022', 100-CN-REP-2007 Rev 1, Aug. 2022.

[3] West wind, 'Validation of Floating Lidar Measurements from RPS Buoy FLB-103', C841/20/01, Feb. 2023.

[4] West wind, 'Validation of Floating Lidar Measurements from RPS Buoy FLB-104', C841/20/02, Feb. 2023.

[5] West wind, 'Validation of Floating Lidar Measurements from RPS Buoy FLB-105', C841/21/01, Feb. 2023.

[6] O. W. Accelerator, 'Carbon Trust Offshore Wind Accelerator roadmap for the commercial acceptance of floating LIDAR technology.', 2018.

[7] IEA Wind, 'Expert Group Report on Recommended Practices 18. Floating Lidar Systems', 2017.

[8] DNV, 'ZX888 Independent analysis and reporting of ZX Lidars performance verification executed by ZX Lidars at the UK Remote Sensing Test Site', DNV, 10284581-R-37-B, Jul. 2021.

[9] DNV, 'ZX874 Independent analysis and reporting of ZX Lidars performance verification executed by ZX Lidars at the UK Remote Sensing Test Site', DNV, 10332408-R-18-A, Feb. 2022.

[10] DNV, 'ZX914 Independent analysis and reporting of ZX Lidars performance verification executed by ZX Lidars at the UK Remote Sensing Test Site', DNV, 10332408-R-24-A, Mar. 2022.

[11] IEC, 'IEC 61400-12-1:2017 Edition 2.0 Wind energy generation systems – Power performance measurements of electricity producing wind turbines', *Int. Stand.*, 2017, [Online]. Available: https://webstore.iec.ch/publication/26603

[12] ECN, 'Offshore meteorological mast IJmuiden abstract of instrumentation report, ECN-Wind-Memo-12-010', 2012.

[13] Ecofys, 'Hollandse Kust (zuid) Offshore Wind Farm Zone Combined Wind Resource Assessment', 2017.

[14] Measnet, 'EVALUATION OF SITE-SPECIFIC WIND CONDITIONS, Version 3', Sep. 2022.

[15] ECN, 'Wind Measurements at Meteorological Mast IJmuiden', ECN-E–14-058, Feb. 2015.

[16] Fugro, 'Supply of Meteorological and Oceanographic data at Hollandse Kust (west) 24-month summary campaign report: 5 February 2019 - 11 February 2021', C75432_24M_F, Nov. 2021.

[17] DNV, 'FUGRO SEAWATCH WIND LIDAR BUOY WS 188 PRE-DEPLOYMENT VALIDATION Assessment of the Fugro Seawatch Wind LiDAR Buoy WS 188 Pre-Deployment Validation at Frøya, Norway', 10129033-R-7, Nov. 2021.

[18] DNV, 'FUGRO SEAWATCH WIND LIDAR BUOY WS 187 PRE-DEPLOYMENT VALIDATION Assessment of the Fugro Seawatch Wind

LiDAR Buoy WS 187 Pre-Deployment Validation at Frøya, Norway', 10129033-R-6, Nov. 2021.

[19] DNV, 'SEAWATCH WIND LIDAR BUOY WS170 OFFSHORE IN SITU VERIFICATION Quality assessment of the Fugro Seawatch Wind Lidar Buoy WS170', 10166838-R-1, Aug. 2019.

[20] Oldbaum, 'Verification of WS170 at Lichteiland Goeree (LEG) during May 2021', HKW_20210924_MC_Oldbaum_Post-deploy. WS170 at LEG using simplified verification_003-R-21-02-Rev2_F, Sep. 2021.

[21] DNV, 'ZX818 Independent analysis and reporting of ZX Lidars performance verification executed by Zephir Ltd. at the Pershore test site, including IEC compliant validation analysis', 10108274-R-0016, Oct. 2018.

[22] DNV, 'ZX802 Independent analysis and reporting of ZX Lidars performance verification executed by Zephir Ltd. at the Pershore test site, including IEC compliant validation analysis', 10108274-R-0015, Oct. 2018.

[23] DNV, 'ZP585 Independent analysis and reporting of ZephIR LiDAR performance verification executed by ZephIR Ltd. at Pershore test site, including IEC compliant validation analysis', GLGH-4270 17 14677 258-R-0025, May 2018.

[24] 'Our Assets - Wintershall Noordzee'. Accessed: Oct. 13, 2023. [Online]. Available: https://www.wintershall-noordzee.nl/our-assets.html

[25] TNO, 'Offshore wind energy deployment in the North Sea by 2030: long-term measurement campaign. K13a, 2016-2019', TNO 2020 R11058, Sep. 2020.

[26] TNO, 'Verification of ZephIR 300M unit563 at ECN part of TNO LiDAR Calibration Facility, for offshore measurements at K13-A production platform', TNO 2018 R10850, Apr. 2019.

[27] 'Technical Guidelines for Wind Turbines Part 6 (TG6) Determination of Wind Potential and Energy Yields - Revision 11', FGW e.V., 2020.

[28] TNO, 'K13-A LiDAR measurement campaign Instrumentation Report 2023', TNO 2023 R10159, Feb. 2023.

[29] TNO, 'Offshore wind energy deployment in the North Sea by 2030: long-term measurement campaign. K13A, 2016-2022', TNO 2023 R10580, Jun. 2023.

[30] TNO, 'Lichteiland Goeree LiDAR measurement campaign; Instrumentation Report 2022', TNO 2022 R10766, Jul. 2022.

[31] TNO, 'Offshore wind energy deployment in the North Sea by 2030: long-term measurement campaign. Lichteiland Goeree, 2014-2021', TNO 2022 R10649, Jul. 2022.

[32] TNO, 'Europlatform LiDAR measurement campaign; Instrumentation Report 2022', TNO 2022 R11776, Oct. 2022.

[33] TNO, 'Offshore wind energy deployment in the North Sea by 2030: long-term measurement campaign EPL 2016-2021', TNO 2022 R10909, Jul. 2022.

[34] Oldbaum, 'Wind Resource Assessment for Hollandse Kust (noord) Wind Farm Zone; Document No.: HKN_20190930_OBL_WRA-HKN_V6_0F', 2019.

[35] DNV GL, 'HOLLANDSE KUST (NOORD) WIND FARM ZONE Certification Report Site Conditions Wind CR-SC-DNVGL-SE-0190-02453-4_Wind (noord)'. Oct. 11, 2019.

[36] DNV GL, 'HOLLANDSE KUST (ZUID) WIND FARM ZONE, Certification Report Site Conditions Wind', CR-SC-DNVGL-SE-0190-02453-3_Wind, Oct. 2017.

[37] Pulo, Anna, Sargin, Okan, Schlez, Wolfgang, Stoelinga, Mark, and Schmidt, Sascha, 'Ten noorden van de Waddeneilanden Wind Farm Zone - Wind Resource Assessment', TNW_20220310_GHPC_WRA_Report_V6_F, Mar. 2022. [Online]. Available: https://offshorewind.rvo.nl/files/view/50c6a6f8-5f01-41a8-ad0a-702101e4aa49/tnw_22020706_guidehouse_wra_update-june-2022.pdf

[38] DNV, 'Ten Noorden van de Waddeneilanden (TNW) Wind Farm Zone Certification Report Site Conditions Wind CR-SC-DNV-SE-0190-06281-2_Wind'. Jun. 13, 2022.

[39] Ecofys, 'Strategic Advice about Floating LiDAR Campaigns Borssele offshore wind farm', 20160708_REP_Borssele LiDAR campaign advice_v3, Jul. 2016.

[40] Ecofys, 'Strategic advice floating LiDAR campaign BWFZ; Advice-on-Metocean-Campaign-BWFZ-Position-1', Mar. 2017.

[41] Ecofys, 'Borssele Offshore Wind Farm Zone Wind Resource Assessment', Sep. 2015.

[42] O. Sargin, S. Schmidt, W. Schlez, and A. Pulo, 'Site N-7.2 Comprehensive Report on the Wind Conditions Prepared for: Bundesamt für Seeschifffahrt und Hydrographie', 2022.

[43] Ecofys, 'Hollandse Kust (zuid) Offshore Wind Farm Zone Combined Wind Resource Assessment', 2017.

[44] Leiding, Tina *et al.*, 'Abschlussbericht - Standardisierung und vergleichende Analyse der meteorologischen FINO-Messdaten (FINO123)', Nov. 2016.

[45] 'IEC 61400-12-1:2022 | IEC Webstore'. Accessed: Oct. 17, 2023. [Online]. Available: https://webstore.iec.ch/publication/68499

[46] K. N. M. Instituut, 'TNO report - DOWA validation against offshore mast and LiDAR measurements - Report - Dutch Offshore Wind Atlas', TNO, rapport TNO report 2019 R10062, May 2019. Accessed: Oct. 13, 2023. [Online]. Available: https://www.dutchoffshorewindatlas.nl/publications/reports/2019/05/21/tno-report---dowa-validation-against-offshore-mast-and-lidar-measurements

[47] Tractabel Engineering S.A., 'Site Studies Hollandse Kust: Wind Resource Assessment Wind Farm Zone Hollandse Kust (west)', Ministrerie Economische Zaken & Klim Netherlands, 2020. [Online]. Available: https://offshorewind.rvo.nl/file/view/55040748/01

[48] K. Rohrig, *Windenergie Report Deutschland 2018*. 2019. [Online]. Available: http://scholar.google.com/scholar?hl=en&btnG=Search&q=intitle:windenergie+report+Deutschland+2013#0%5Cnhttp://scholar.google.com/scholar?hl=en&btnG=Search&q=intitle:Windenergie+Report+Deutschland+2012%230%5Cnhttp://windmonitor.iwes.fraunhofer.de/bilder/up

[49] W. (NREL) Musial, P. (NREL) Beiter, P. (DOE) Spitsen, J. (NREL) Nunemaker, and V. (NREL) Gevorgian, '2018 Offshore Wind Technologies Market Report', 2018. [Online]. Available:

https://www.energy.gov/sites/prod/files/2019/09/f66/2018 Offshore Wind Technologies Market Report.pdf

[50] E. Sloots, 'The North Seas Standard: enable growth with wind turbine standardization'. NWEA, Sep. 29, 2023. Accessed: Oct. 17, 2023. [Online]. Available: https://www.nwea.nl/the-north-seas-standard-enable-growth-with-wind-turbine-standardization/

[51] Copernicus Climate Change Service at ECMWF, 'ECMWF Reanalysis v5 (ERA5)'. [Online]. Available: https://www.ecmwf.int/en/forecasts/dataset/ecmwf-reanalysis-v5

[52] EMD International, 'EMD-WRF Europe+ MesoScale Data Set'. [Online]. Available: https://www.emd-international.com/data-services/mesoscale-time-series/pre-run-time-series/emd-wrf-europe-mesoscale-data-set/

[53] Global Modelling and Assimilation Office (GMAO), 'MERRA2', Modern-Era Retrospective analysis for Research and Applications, Version 2. [Online]. Available: https://gmao.gsfc.nasa.gov/reanalysis/MERRA-2/

[54] Sargin, Ahmet Okan, 'Analysis and Method Selection of a Measure-Correlate-Predict Methodology for a Digital Wind Buoy', Master's Thesis in MSc. Wind Energy Systems, University of Kassel, Kassel, Germany, 2022.

[55] H. Charnock, 'Wind Stress on a Water Surface', *Q. J. R. Meteorol. Soc.*, vol. 81, pp. 639–640, 1955.

[56] C. Davis *et al.*, 'Prediction of Landfalling Hurricanes with the Advanced Hurricane WRF Model', *Mon. Weather Rev.*, vol. 136, pp. 1990–2005, 2008.

[57] F.-N. Li, J.-B. Song, H.-L. He, S. Li, X. Li, and S. D. Guan, 'Assessment of Surface Drag Coefficient Parametrizations Based On Observations and Simulations Using the Weather Research and Forecasting Model', *Atmospheric Ocean. Sci. Lett.*, vol. 9, no. 4, pp. 327–336, 2016, doi: 10.1080/16742834.2016.1196105.

[58] Y. Rubner, C. Tomasi, and L. J. Guibas, 'The Earth Mover's Distance as a Metric for Image Retrieval', *Int. J. Comput. Vis. 2000 402*, vol. 40, no. 2, pp. 99–121, Nov. 2000, doi: 10.1023/A:1026543900054.

[59] A. Clerc, M. Anderson, P. Stuart, and G. Habenicht, 'A systematic method for quantifying wind flow modelling uncertainty in wind resource assessment', *J. Wind Eng. Ind. Aerodyn.*, vol. 111, pp. 85–94, Dec. 2012, doi: 10.1016/j.jweia.2012.08.006.

[60] B. Gribben, 'Lidar Uncertainty Standard Review Methodology Review and Recommendations Offshore Wind Accelerator – Wakes and Wind Resource LUSR – LiDAR Uncertainty Standard Review', Carbon Trust, 2018. doi: 55617/46883R.

[61] S. Susini, M. Menendez, P. Eguia, and J. M. Blanco, 'Climate Change Impact on the Offshore Wind Energy Over the North Sea and the Irish Sea', *Front. Energy Res.*, vol. 10, 2022, Accessed: May 23, 2023. [Online]. Available: https://www.frontiersin.org/articles/10.3389/fenrg.2022.881146

[62] JBA Consulting, 'Offshore Wind Farm Operations and Maintenance - Copernicus Knowledge Base - ECMWF Confluence Wiki'. Accessed: May 23, 2023. [Online]. Available: https://confluence.ecmwf.int/display/CKB/Offshore+Wind+Farm+Operations+and+Maintenance

[63] EURO-CORDEX community, 'Guidance for EURO-CORDEX climate projections data use', *Version 10*, p. 27, Aug. 2017.

[64] F. Santos *et al.*, 'On the accuracy of CORDEX RCMs to project future winds over the Iberian Peninsula and surrounding ocean', *Appl. Energy*, vol. 228, pp. 289–300, Oct. 2018, doi: 10.1016/j.apenergy.2018.06.086.

[65] S. E. Perkins, A. J. Pitman, N. J. Holbrook, and J. McAneney, 'Evaluation of the AR4 Climate Models' Simulated Daily Maximum Temperature, Minimum Temperature, and Precipitation over Australia Using Probability Density Functions', *J. Clim.*, vol. 20, no. 17, pp. 4356–4376, Sep. 2007, doi: 10.1175/JCLI4253.1.

[66] B. Jourdier, 'Ressource éolienne en France métropolitaine : méthodes d'évaluation du potentiel, variabilité et tendances', phdthesis, Ecole Doctorale Polytechnique, 2015. Accessed: May 23, 2023. [Online]. Available: https://hal-polytechnique.archives-ouvertes.fr/tel-01238226

[67] X. Costoya, M. deCastro, D. Carvalho, Z. Feng, and M. Gómez-Gesteira, 'Climate change impacts on the future offshore wind energy resource in China', *Renew. Energy*, vol. 175, pp. 731–747, Sep. 2021, doi: 10.1016/j.renene.2021.05.001.

[68] X. Costoya, M. deCastro, D. Carvalho, B. Arguilé-Pérez, and M. Gómez-Gesteira, 'Combining offshore wind and solar photovoltaic energy to stabilize energy supply under climate change scenarios: A case study on the western Iberian Peninsula', *Renew. Sustain. Energy Rev.*, vol. 157, p. 112037, Apr. 2022, doi: 10.1016/j.rser.2021.112037.

[69] X. Costoya, M. deCastro, D. Carvalho, and M. Gómez-Gesteira, 'On the suitability of offshore wind energy resource in the United States of America for the 21st century', *Appl. Energy*, vol. 262, p. 114537, Mar. 2020, doi: 10.1016/j.apenergy.2020.114537.

[70] X. Costoya, M. deCastro, F. Santos, M. C. Sousa, and M. Gómez-Gesteira, 'Projections of wind energy resources in the Caribbean for the 21st century', *Energy*, vol. 178, pp. 356–367, Jul. 2019, doi: 10.1016/j.energy.2019.04.121.

[71] D. W. Pierce, T. P. Barnett, B. D. Santer, and P. J. Gleckler, 'Selecting global climate models for regional climate change studies', *Proc. Natl. Acad. Sci.*, vol. 106, no. 21, pp. 8441–8446, May 2009, doi: 10.1073/pnas.0900094106.

[72] A. Cordeiro Pires, R. Nolasco, A. Rocha, A. M. Ramos, and J. Dubert, 'Climate change in the Iberian Upwelling System: a numerical study using GCM downscaling', *Clim. Dyn.*, vol. 47, no. 1, pp. 451–464, Jul. 2016, doi: 10.1007/s00382-015-2848-y.

[73] J. Najac, J. Boé, and L. Terray, 'A multi-model ensemble approach for assessment of climate change impact on surface winds in France', *Clim. Dyn.*, vol. 32, no. 5, pp. 615–634, Apr. 2009, doi: 10.1007/s00382-008-0440-4.

[74] J. Najac, C. Lac, and L. Terray, 'Impact of climate change on surface winds in France using a statistical-dynamical downscaling method with mesoscale modelling', *Int. J. Climatol.*, vol. 31, no. 3, pp. 415–430, 2011, doi: 10.1002/joc.2075.

[75] M. Reyers, J. Moemken, and J. G. Pinto, 'Future changes of wind energy potentials over Europe in a large CMIP5 multi-model ensemble', *Int. J. Climatol.*, vol. 36, no. 2, pp. 783–796, 2016, doi: 10.1002/joc.4382.

[76] J. Moemken, M. Reyers, H. Feldmann, and J. Pinto, 'Future changes of wind speed and wind energy potentials in EURO-CORDEX ensemble

simulations', *J. Geophys. Res. Atmospheres*, vol. 123, Jun. 2018, doi: 10.1029/2018JD028473.

[77] X. Costoya, A. Rocha, and D. Carvalho, 'Using bias-correction to improve future projections of offshore wind energy resource: A case study on the Iberian Peninsula', *Appl. Energy*, vol. 262, p. 114562, Mar. 2020, doi: 10.1016/j.apenergy.2020.114562.

[78] B. C. O'Neill *et al.*, 'The Scenario Model Intercomparison Project (ScenarioMIP) for CMIP6', *Geosci. Model Dev.*, vol. 9, no. 9, pp. 3461–3482, Sep. 2016, doi: 10.5194/gmd-9-3461-2016.

[79] K. Riahi *et al.*, 'The Shared Socioeconomic Pathways and their energy, land use, and greenhouse gas emissions implications: An overview', *Glob. Environ. Change*, vol. 42, pp. 153–168, Jan. 2017, doi: 10.1016/j.gloenvcha.2016.05.009.

[80] P. M. M. Soares, D. C. A. Lima, R. M. Cardoso, M. L. Nascimento, and A. Semedo, 'Western Iberian offshore wind resources: More or less in a global warming climate?', *Appl. Energy*, vol. 203, pp. 72–90, Oct. 2017, doi: 10.1016/j.apenergy.2017.06.004.

[81] C. Deser, R. Knutti, S. Solomon, and A. S. Phillips, 'Communication of the role of natural variability in future North American climate', *Nat. Clim. Change*, vol. 2, no. 11, Art. no. 11, Nov. 2012, doi: 10.1038/nclimate1562.

[82] 'An overview of offshore wind energy resources in Europe under present and future climate - PubMed'. Accessed: May 23, 2023. [Online]. Available: https://pubmed.ncbi.nlm.nih.gov/30008177/

[83] D. Carvalho, A. Rocha, M. Gómez-Gesteira, and C. Silva Santos, 'Potential impacts of climate change on European wind energy resource under the CMIP5 future climate projections', *Renew. Energy*, vol. 101, pp. 29–40, Feb. 2017, doi: 10.1016/j.renene.2016.08.036.

[84] E. Gaertner *et al.*, 'Definition of the IEA Wind 15-Megawatt Offshore Reference Wind Turbine Technical Report', 2020. [Online]. Available: www.nrel.gov/publications.

[85] 'The surface processes of the Rossby Centreregional atmospheric climate model (RCA4) | SMHI'. Accessed: May 23, 2023. [Online]. Available: https://www.smhi.se/en/publications/the-surface-processes-of-the-rossby-centreregional-atmospheric-climate-model-rca4-1.89801

[86] Fugro, 'Supply of Meteorological and Oceanographic data at Hollandse Kust (west) Monthly Data Report: 01 January - 11 February 2021', C75432_MDR24_F, Jun. 2021.

[87] I. L. Wijnant *et al.*, 'The Dutch Offshore Wind Atlas (DOWA): description of the dataset', Royal Netherlands Meteorological Institute, 2019.

[88] I. L. Wijnant, A. Stepek, M. Savenije, and H. W. van den Brink, 'User manual of the (KNMI North Sea Wind) KNW-atlas', 2016.

[89] 'EURO-CORDEX: new high-resolution climate change projections for European impact research | SpringerLink'. Accessed: May 23, 2023. [Online]. Available: https://link.springer.com/article/10.1007/s10113-013-0499-2

[90] D. P. van Vuuren *et al.*, 'The representative concentration pathways: an overview', *Clim. Change*, vol. 109, no. 1, p. 5, Aug. 2011, doi: 10.1007/s10584-011-0148-z.

[91] K. L. Ebi *et al.*, 'A new scenario framework for climate change research: background, process, and future directions', *Clim. Change*, vol. 122, no. 3, pp. 363–372, Feb. 2014, doi: 10.1007/s10584-013-0912-3.

[92] A. Busuioc, 'Empirical-Statistical Downscaling: Nonlinear Statistical Downscaling', in *Oxford Research Encyclopedia of Climate Science*, 2021. doi: 10.1093/acrefore/9780190228620.013.770.

Acknowledgements

The authors of this study would like to thank the following people for reviewing this report and providing valuable feedback throughout the Project.

The entire DHI team, led by Jacob Berg as director, Ameya Sathe as project manager, with Sara Johnson serving as the lead analyst and Daniel Caichac as the main analyst throughout the project, deserves our heartfelt appreciation for their unwavering professionalism, outstanding collaboration, and invaluable contributions to the success of our endeavour.

OWC and its partners extend heartfelt thanks to RVO, with particular recognition for Frank van Erp, whose insights and dedication have not only propelled the unified-WRF model and the Dutch offshore market but have also set an inspiring example for European sustainability goals. Daniëlle, in her role as project manager, has consistently displayed a commendable dedication to ensuring the project's success through her unwavering management efforts.

Immense gratitude is expressed to Maziar Golestani for his valuable insights and invitation, Hendrik Wrenger for his meticulous project organization at the start of the project, and Rodolfo Sanchez for his exceptional project management skills as previous members of the DHI project team. Their contributions have proven to be invaluable.

The expert team from RVO, featuring Erik Holtslag, Gus Jeans, Marco Westra, and Wouter Pustjens, has consistently provided invaluable support by offering crucial insights, constructive criticism, and expert advice to OWC and its partners.

We would also like to extend our appreciation to the diligent contributions of C2Wind analysts Dager Borvaran Baez and Jorge Leonel Garza Cantú during the quality assurance process, whose expertise greatly enriched our project.

Finally, OWC and its partners must acknowledge the invaluable contributions of the DNV certification team, represented by Helena Hunt and Erik Asp, whose early involvement brought us invaluable insights that significantly contributed to the project's success.

Appendix A OWC and Partners

A.1 OWC

OWC, an ABL Group company, is a specialised independent consultancy offering project development services, owner's engineering, and technical due diligence to the offshore wind industry, developing, and realising projects across the globe.

OWC's core team possesses strong industry expertise which dates to the first offshore wind farm development in the UK. Since then, OWC has been involved in the majority of the major offshore wind projects in Europe, Asia, and the US.

OWC wind & site team supports clients with early conceptual design, site screening and pre-feasibility assessments, ensemble wake modelling, layout and turbine optimization, mesoscale modelling, wind resource assessments, post-construction operational yield assessments, and third-party energy yield reviews.

OWC offices are located in Hamburg, London, Edinburgh, New York, Boston, Seoul, Taipei, Tokyo, and Warsaw.

OWC is active in the markets: fixed and floating offshore wind, ocean energy, subsea cables, and energy storage.

A.2 ArcVera Renewables

ArcVera Renewables provides expert insights, targeted analysis and reporting for renewable energy prospecting, development, sponsor financing, portfolio transactions, post-construction operational analysis, and repowering. ArcVera's wind energy resource assessment service is anchored in principles of atmospheric science and wind engineering and uses mesoscale numerical weather prediction as the foundation of its wind resource assessment methods. The company's experienced team of atmospheric scientists, data analysts, and engineers are known for their expertise, precision, responsiveness, and reliability. Services in measurement and analysis comprise resource measurement, measurement campaign strategy, instrument specification, design, IEC standards and placement of meteorological station(s) and remote sensors.

A.3 ProPlanEn

ProPlanEn was founded as an independent wind energy consultancy in 2015 by Dr Wolfgang Schlez, and the ProPlanEn team has since delivered a wide range of independent advice and specialist tools to the wind energy industry.

ProPlanEn is well connected in the industry. It is member of the industry associations WindEurope and the German Wind Energy Association (BWE), and it actively contributes to national and international expert working groups including Wind Resource Group (UK), Wind Resource Assessment Group (EU), Vindkraftnet (DK), IEA-Task 31 Wakebench, and BWE Windgutachterbeirat.

ProPlanEn has carried out confidential industrial research (strategic studies, literature research summarizing the state of the art for specific topics, and product and methodology development) for major clients in the industry, including for major global developers, utilities, and manufacturers.

ProPlanEn has delivered commercial assessments of wind farm wake losses, and effective turbulences for many offshore wind farms in German, French, English, and Taiwanese waters. It has also assessed the operational performance of over 20 operational wind farms, based on SCADA data.

ProPlanEn holds commercial licences for the wind farm design software tools, WindPRO, WindFarmer, WAsP, and OpenWind and it employs consultants who are experienced in operating these tools. ProPlanEn operates at a high level of quality, and environmental, social, and corporate responsibility.

In 2016/7 ProPlanEn attracted co-funding from Innovate UK to develop WakeBlaster - a new 3D RANS wake model, suited to accurately modelling the yield of very large wind farms with up to, and exceeding, 10,000 wind turbines.

The model has been validated against production data from onshore and offshore wind farms, it recently achieved very good results in the OWA wake model blind test for 5 offshore wind farms. After intensive testing, WakeBlaster was recently integrated into WindPRO and Openwind, two of the worldwide leading software packages for designing wind farms.

WakeBlaster is not an adaptation of a general purpose CFD toolbox. Instead, it was developed as a flexible tool and from scratch. As its developer, ProPlanEn has full access to all details regarding WakeBlaster, as well as the in-depth know-how and capability to implement any modifications that prove necessary.

A.4 Innosea

INNOSEA, Part of OWC, is an independent specialist Marine Renewable Energies (MRE) multidisciplinary engineering, strategy advisory and R&D consultancy. INNOSEA support clients throughout the full development cycle of an MRE project or technology, to help unlock its commercial potential, scalability, and enhanced performance.

100% dedicated to MRE, this commitment keeps INNOSEA at the cutting-edge of green technology. Its wide range of specialised services covers concept studies, basic engineering, detailed engineering, testing, and pre-certification amongst others. It conducts detailed studies to support clients in delivering technology with enhanced profitability, performance, and future viability across its lifecycle.

INNOSEA has a large project portfolio covering a range of expert services, and the marine renewable energy sectors, in which it works: offshore wind fixed and floating, floating solar PV, wave and tidal energy, OTEC / SWAC and deep-water tech, hydrogen, as well as integrated engineering for green technology solutions or renewable energy clustering.

INNOSEA offices are located in Nantes, Paris, Marseille, and Edinburgh.

Appendix B Measurement Campaign Documentation (Primary Datasets)

B.1 FLS IJV

The following measurement campaign description is an excerpt from [2] and is applicable to the buoys installed at FLS IJV. It is noted that [2] is the first monthly report issued by RPS. The information presented below can be found in any of the monthly reports issued by RPS.

The two measurement locations, IJV A and IJV B, were positioned 1000 m apart, approximately 40 Nm to the West of Den Helder. To allow the spare buoy to be deployed before recovering the existing buoy, both measurement locations consist of 2 sites 1000m apart.

The RPS LiDAR 4.5 Buoy follows the ocean surface to position sensors at:

- ZX 300M lidar sensor at 3.3 m MSL
- Anemometers at 3.7 m MSL
- Air Temperature and Barometric Pressure at 3.6 m MSL
- RPS Tide Sensor at 3.6m MSL
- MRU at 0.0 m AMSL
- ADCP at 1.8 m BMSL

All reported parameters are logged and stored by individual instruments with subsets transferred to the two, independent onboard RPS M200 data loggers for near real-time transmission.

M200 data logger

Each buoy contains a pair of independent RPS M200 data loggers. The recorded data is stored to a 64 Gigabyte compact flash card at a sampling rate of 2 Hz, which provides a two-year storage capacity. The recorded 10-minute averaged data are also transmitted via iridium modem from the M200 data logger to RPS servers. Raw data can be collected via 4G (or Iridium Broadband) as required.

The buoy GPS information and buoy health status is also transmitted in the data, allowing the monitoring of the buoys' positions and health for proactive intervention if required.

The following data is logged by the M200:

- 10-minute data from the ZX 300M LiDAR.
- Raw and processed wave data from the MRU 5.
- Raw and processed data on buoy heading and water levels.
- 10-minute data from the Nortek Signature current profiler.

ZX 300M lidar

RPS uses the ZX 300M lidar. The buoy provides power for the lidar, plus backup memory and real-time data transmission.

The ZX 300M lidar measures wind from 10 to 300 m above sensor height in 10 user selectable height bins (with a fixed 11th reference bin measured at 38 m above sensor height), along with data from an AirMar 150WX at 3.7 m AMSL measuring barometric pressure, air temperature, and wind.

Measured parameters from the lidar are:

- Wind data measured at each of the 11 heights:
- Horizontal wind speed (m s-1).
- Horizontal wind speed min (m s-1).
- Horizontal wind speed max (m s-1).
- Horizontal wind speed std. dev. (m s-1).
- Vertical wind speed (m s-1).
- Turbulence intensity.
- Met. parameters (air temperature, barometric pressure, near-surface wind).

The data comes direct from the ZX 300M lidar, with buoy heading measured separately by GPS to correct directions. There is no motion compensation required and the lidar unit quality flags the data automatically during measurements based on algorithms applied internally.

RPS does not filter the data further, other than in post processing to check for potential 180-degree ambiguity in the wind directions.

B.2 MM IJmuiden and lidar IJmuiden

The following measurement campaign description is an excerpt from [12] which is the associated measurement campaign instrumentation report for both MM IJmuiden and lidar IJmuiden.

On the authority of the Ministry of Economic Affairs, Agriculture and Innovation of The Netherlands, ECN is performing measurements on the offshore meteorological station IJmuiden (in the following denoted as MMIJ), situated 85 km from the coast of IJmuiden. These measurements will run for 4 years, and all measured data will be made publicly available.

The station consists of a platform with a control room, a meteorological mast (Met mast), and a wave buoy that has been deployed close to the mast.

Platform

On a monopile, a platform has been built with a size of approximately 12 x 10.5 meters. On the platform a control room and the meteorological mast are present. The platform height is 18 meter above LAT. The top of the met mast is 92 meters above LAT.

On the container and in the mast 10 solar panels and 8 small wind turbine generators (WTGs) are installed to provide power for the measurement system and all safety lights / communication systems. In the container two diesel generators are installed to provide power in case the solar panels and the small WTGs do not provide enough power to keep all systems running. The platform is accessible by means of a ladder from the boat-landing provision. Above the ladder a hatch provides access to the platform. The hatch is locked to prevent unauthorized access to the platform.

Met mast

The met-mast is placed on top of the platform, next to the container. A picture of the offshore meteorological station can be seen in Figure B.1. The orientation of the platform, the mast and the container can be seen in Figure B.2.

Figure B.1 The offshore meteorological station

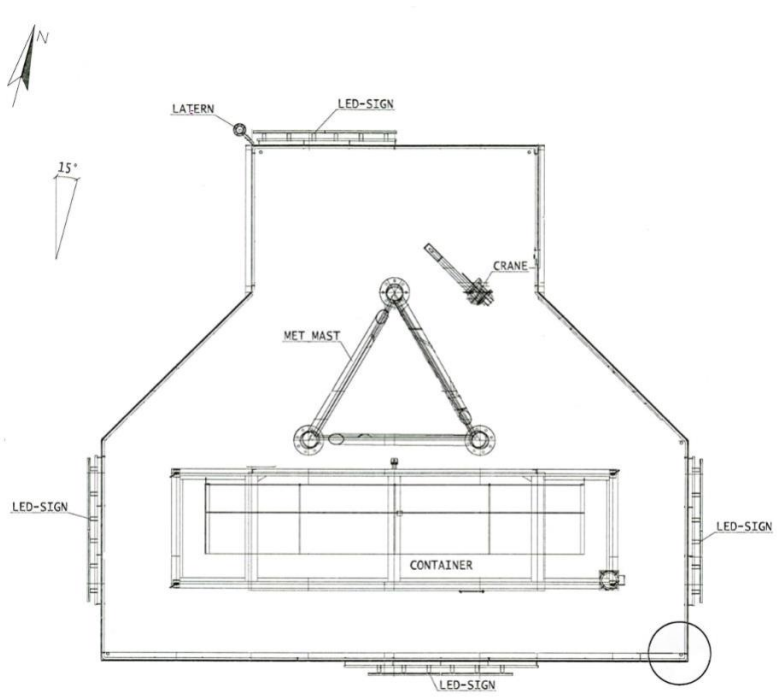

Figure B.2 Platform and mast orientation

Met mast booms

On heights of 25.5 m, 57 m and 86.5 m, booms have been installed on the mast in three directions, pointing outward from each face of the mast. In the signal list (listed in Appendix A in [12]), we call the booms the 0, 120 and 240 degree booms, although this is not quite right. The platform is oriented almost according Figure B.2, in reality the 15 degree angle is 13.5 degrees. So the 0 degree boom points in a 46.5 degree direction, the 120 degree boom points in a 166.5 degree direction, and the 240 degree boom points in a 286.5 degree direction. All measurement data will be corrected for this, so that the delivered data will contain true wind directions.

Met mast sensor locations

In the met mast and on the container roof sensors have been installed to measure wind speed, wind direction, air pressure, air temperature and relative humidity. Figure B.3 shows the location of all installed sensors, together with their output signals, working down from the top of the mast.

Installed sensors met-mast				
Sensor	**level**	**Location**	**Signal(s)**	**unit**
Thies First Class Advanced anemometer	92 m	150 cm above North-East leg of mast	MMIJ_H92B180_Ws_Q1	m/s
Thies First Class Advanced anemometer	92 m	150 cm above South-West leg of mast	MMIJ_H92B300_Ws_Q1	m/s
Vaisala PTB210 air pressure sensor	90 m	North-East side of top platform	MMIJ_H90_Pair_Q1	hPa
Vaisala HMP155D	90 m	North-West side of top platform	MMIJ_H90_Tair_Q1	deg C
			MMIJ_H90_Rh_Q1	%
Thies First Class wind vane	87 m	70 cm above end of 86.5 m boom, 46.5 deg	MMIJ_H87B0_Wd_Q1	deg
Thies First Class wind vane	87 m	70 cm above end of 86.5 m boom, 166.5 deg	MMIJ_H87B120_Wd_Q1	deg
Thies First Class wind vane	87 m	70 cm above end of 86.5 m boom, 286.5 deg	MMIJ_H87B240_Wd_Q1	deg
Metek USA-1 sonic anemometer	85 m	150 cm below end of 86.5 m boom, 46.5 deg	MMIJ_H85B0_WsXSon_Q1	m/s
			MMIJ_H85B0_WsYSon_Q1	m/s
			MMIJ_H85B0_WsZSon_Q1	m/s
			MMIJ_H85B0_SSon_Q1	-
			MMIJ_H85B0_WsHor_Q1	m/s
			MMIJ_H85B0_WsMag_Q1	m/s
Metek USA-1 sonic anemometer	85 m	150 cm below end of 86.5 m boom, 166.5 deg	MMIJ_H85B120_WsXSon_Q1	m/s
			MMIJ_H85B120_WsYSon_Q1	m/s
			MMIJ_H85B120_WsZSon_Q1	m/s
			MMIJ_H85B120_SSon_Q1	-
			MMIJ_H85B120_WsHor_Q1	m/s
			MMIJ_H85B120_WsMag_Q1	m/s
Metek USA-1 sonic anemometer	85 m	150 cm below end of 86.5 m boom, 286.5 deg	MMIJ_H85B240_WsXSon_Q1	m/s
			MMIJ_H85B240_WsYSon_Q1	m/s
			MMIJ_H85B240_WsZSon_Q1	m/s
			MMIJ_H85B240_SSon_Q1	-
			MMIJ_H85B240_WsHor_Q1	m/s
			MMIJ_H85B240_WsMag_Q1	m/s
Thies First Class Advanced anemometer	58,5 m	150 cm above end of 57 m boom, 46.5 deg	MMIJ_H58B0_Ws_Q1	m/s
Thies First Class Advanced anemometer	58,5 m	150 cm above end of 57 m boom, 166.5 deg	MMIJ_H58B120_Ws_Q1	m/s
Thies First Class Advanced anemometer	58,5 m	150 cm above end of 57 m boom, 286.5 deg	MMIJ_H58B240_Ws_Q1	m/s
Thies First Class wind vane	58 m	70 cm above 57 m boom, 46.5 deg	MMIJ_H58B0_Wd_Q1	deg
Thies First Class wind vane	58 m	70 cm above 57 m boom, 166.5 deg	MMIJ_H58B120_Wd_Q1	deg
Thies First Class wind vane	58 m	70 cm above 57 m boom, 286.5 deg	MMIJ_H58B240_Wd_Q1	deg
Thies First Class Advanced anemometer	27 m	150 cm above end of 25.5 m boom, 46.5 deg	MMIJ_H27B0_Ws_Q1	m/s
Thies First Class Advanced anemometer	27 m	150 cm above end of 25.5 m boom, 166.5 deg	MMIJ_H27B120_Ws_Q1	m/s
Thies First Class Advanced anemometer	27 m	150 cm above end of 25.557 m boom, 286.5 deg	MMIJ_H27B240_Ws_Q1	m/s
Thies First Class wind vane	26 m	70 cm above 25.5 m boom, 46.5 deg	MMIJ_H27B0_Wd_Q1	deg
Thies First Class wind vane	26 m	70 cm above 25.5 m boom, 166.5 deg	MMIJ_H27B120_Wd_Q1	deg
Thies First Class wind vane	26 m	70 cm above 25.5 m boom, 286.5 deg	MMIJ_H27B240_Wd_Q1	deg
Thies Disdro laser precipitation sensor	21 m	Railing of container, South side	MMIJ_H21_Prec_l_Q5	%
			MMIJ_H21_Synop_l_Q5	-
			MMIJ_H21_amount_l_Q5	mm
			MMIJ_H21_intens_l_Q5	mm/min
			MMIJ_H21_OK_l_Q5	%
			MMIJ_H21_qual_l_Q5	%
			MMIJ_H21_visib_l_Q5	m
Thies Disdro laser precipitation sensor	21 m	Railing of container, South side	MMIJ_H21_Prec_r_Q5	%
			MMIJ_H21_Synop_r_Q5	-
			MMIJ_H21_amount_r_Q5	mm
			MMIJ_H21_intens_r_Q5	mm/min
			MMIJ_H21_OK_r_Q5	%
			MMIJ_H21_qual_r_Q5	%
			MMIJ_H21_visib_r_Q5	m
Vaisala HMP155D	21 m	Railing of container, North side	MMIJ_H21_Tair_Q1	deg C
			MMIJ_H21_Rh_Q1	%
Vaisala PTB210 air pressure sensor	21 m	Railing of container, North side	mmij_pair21	hPa

Figure B.3 Screenshot of Table 1 Sensory locations and signals in [12]

Met mast sensor mounting

To minimize mast influence on the measurements, the wind speed and wind direction sensors have been mounted on vertical spigots mounted on the booms. Figure B.4 shows the distance of the sensor to the mast and the length of the vertical spigot each sensor has been mounted on. The boom lengths on the anemometer locations is about 3 times the face width of the mast at that position.

The top level anemometers have been mounted on vertical spigots so that the anemometers are 1.5 m above the top of the mast.

The air pressure, air temperature and relative humidity sensors have been mounted close to the mast so that they can be reached easily for maintenance.

The 21 meter level sensors (2 x Thies laser precipitation sensor, air temperature sensor, relative humidity sensor, air pressure sensor) have been mounted on the railing of the container roof.

Sensor mounting		
Sensor	**Distance from mast [m]**	**Spigot length [cm]**
Wind vane 87 m	4.60	70
Sonic anemometer 85 m	4.60	150
Cup anemometer 58.5 meter	7.00	150
Wind vane 57.7 meter	4.35	70
Cup anemometer 27 m	9.20	150
Wind vane 26.2 meter	5.60	70

Figure B.4 Screenshot of Table 2 Sensor mounting data in [12]

Lidar wind speed measurement

On a height of 20.88 above LAT, a Lidar system has been installed on a platform in the met mast. The Lidar has been installed in the South-West corner of the mast, with its North mark in the 46.5 degree direction. A picture of the installed Lidar is shown in Figure B.6. The Lidar has been installed in a way that it has enough free sight to perform wind speed measurements, and measures the wind speed and wind direction on heights of 90, 115, 140, 165, 190, 215, 240, 265, 290 and 315 meter above LAT. The Lidar provides some general signals and a list of measuring signals for each measuring height. The total list of signals coming from the Lidar is shown in Figure B.5.

Measured signals Lidar			
Level	Signal	Signal short name	Unit
21	Battery Voltage	MMIJ_Li_BatVoltage_m	V
21	Max temperature inside Lidar	MMIJ_Li_TempMax_m	deg C
21	Min temperature inside Lidar	MMIJ_Li_TempMin_m	deg C
21	CPU temperature in Lidar	MMIJ_Li_TempCPU_m	deg C
21	Relative humidity inside Lidar	MMIJ_Li_HumPod_m	%
21	Lidar bearing	MMIJ_Li_Bearing_m	deg
21	Lidar tilt angle	MMIJ_Li_Tilt_m	deg
21	Air temperature at Lidar position	MMIJ_Li_H21_Tair_m	deg C
21	Air pressure at Lidar position	MMIJ_Li_H21_Pair_m	hPa
21	Relative humidity at Lidar position	MMIJ_Li_H21_RH_m	%
21	Wind speed measured by Lidar meteo station	MMIJ_Li_H21_WsMet_m	m/s
21	Wind direction measured by Lidar meteo station	MMIJ_Li_H21_WdMet_m	deg
21	Precipitation measured by Lidar meteo station	MMIJ_Li_Rain_m	%
	For every measuring height :	xxx : measuring height	
xxx	# measuring points	MMIJ_Li_Hxxx_npts_m	-
xxx	# missed points	MMIJ_Li_Hxxx_missed_m	-
xxx	# packets in fit	MMIJ_Li_Hxxx_npackets_m	-
xxx	Wind direction	MMIJ_Li_Hxxx_Wd_m	deg
xxx	Horizontal wind speed average	MMIJ_Li_Hxxx_WsHor_avg_m	m/s
xxx	Horizontal wind speed std deviation	MMIJ_Li_Hxxx_WsHor_std_m	m/s
xxx	Horizontal wind speed minimum	MMIJ_Li_Hxxx_WsHor_min_m	m/s
xxx	Horizontal wind speed maximum	MMIJ_Li_Hxxx_WsHor_max_m	m/s
xxx	Vertical wind speed average	MMIJ_Li_Hxxx_WsVer_m	m/s
xxx	Spatial variation	MMIJ_Li_Hxxx_SpVar_m	-
xxx	CS	MMIJ_li_Hxxx_CS_m	-
xxx	Backscatter	MMIJ_Li_Hxxx_BS_m	-
xxx	Horizontal confidence	MMIJ_Li_Hxxx_Hconf_m	-
xxx	Turbulence intensity	MMIJ_Li_Hxxx_TI_m	%

Figure B.5 Screenshot of Table 5 List of Lidar signals in [12]

Figure B.6 Top view of lidar system installed in met mast

B.3 FLS HKW

The following measurement campaign description is an excerpt from [86] and is applicable to all the buoys installed at FLS HKW. It is noted that [86] is the last monthly report issued by Fugro. The information presented below can be found in any of the monthly reports issued by Fugro.

Two independent Seawatch Wind LiDAR buoys (SWLB) with were deployed in February 2019 at the Hollandse Kust (west) stations HKWA and HKWB, respectively. A 3rd location, HKWC, was temporarily added in June 2019 to facilitate concurrent in-situ validation of a 3rd SWLB. Data from HKWC were used for the campaign from August 2019. On 9th May 2020 an additional station HKWA-2 (150 m distance from HKWA) was added after the mooring at HKWA became unusable.

The two SWLBs provide a redundant arrangement of instrumentation for the measurement campaign in particular in order to safeguard against data loss. Data measured at each buoy is packed into a digital package that is simultaneously stored on the buoy and transmitted via satellite to allow for near real-time operations checks, maintenance scheduling and monthly reporting. The SWLBs transmit data in near real-time to Fugro for continuous monitoring of the performance as well as monthly reporting. The transmitted data is used as the primary dataset for the monthly report. If the transmitted data is of lower availability (e.g. due to missed satellite transmissions) and a visit is performed at a later time, a recovered data set is provided at the end of the campaign.

Instrumentation

Each buoy is a Seawatch Wind LiDAR Buoy based on the original Seawatch Wavescan buoy design with the following sensors and main equipment:

- Wavesense 3 3-directional wave sensor
- ZephIR ZX300 CW lidar
- Gill Windsonic M acoustic wind sensor
- Nortek Aquadopp 600kHz current profiler
- Vaisala PTB330A air pressure sensor
- Vaisala HMP155 air temperature and humidity sensor
- Dual GPS Septentrio position tracking
- Acoustic receiver for Thelma TBR700 water pressure sensor.

The LiDARs used in this project are marinized versions of the ZX300 LiDAR type.

An independent Thelma (TBR 700) water pressure/level sensor (WLS) is located on the sea floor connected to the buoy mooring via a line. The pressure sensor transmits data to the buoy via an acoustic link.

The LiDAR is equipped with a met station that also measures air temperature and pressure. These measurements are given in the dataset as supporting data only (calibration not verified).

Figure B.7 shows the basic shape of the buoy illustrating the principle for wind and current profile measurements. The drawing shows the location of the sensors, and illustrates the LiDAR and current profiler beams.

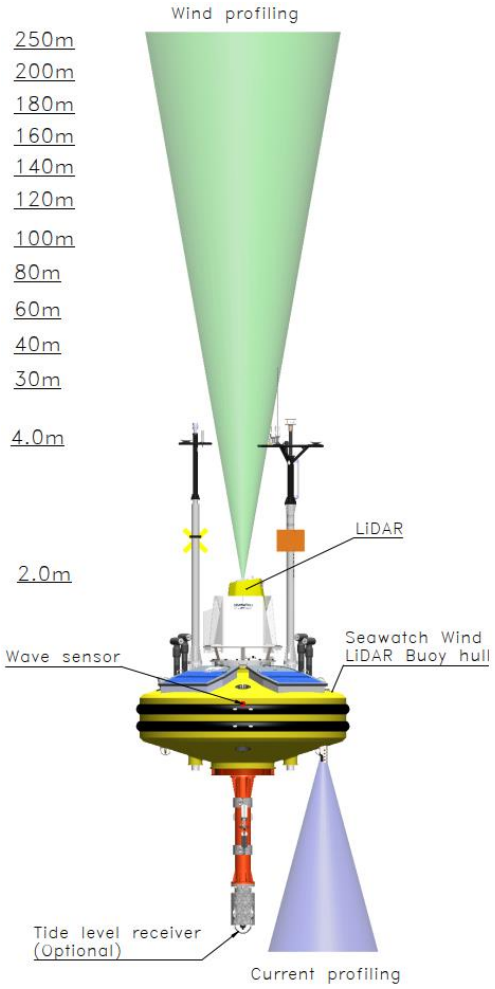

Figure B.7 Illustration of the wind and current profile measurements from the lidar buoy. Heights with reference to the sea surface.

B.4 Lidar K-13A

The following is an excerpt from [28] which is the measurement campaign instrumentation report. .

The K13-a offshore platform owned by Wintershall Noordzee B.V. is located northwest of Den Helder, 101 kilometres from the coast, see Figure B.8. The platform serves as a production platform for natural gas. Since November 2016 wind measurements are carried out by TNO using a platform-mounted ZX 300M wind LiDAR Figure 6 (~35 m above MSL). The platform is part of the North Sea Monitoring Network consisting of several permanent monitoring locations.

The platform serves as a measurement station for oceanographic (Rijkswaterstaat) and meteorological (KNMI) measurements.

Figure B.8 Aerial view of K13-A platform

ZX lidars ZX300M

The ZX Lidars Z300M LiDAR consists of a tripod-shaped housing, with dimensions of ca. 90 x 90 x 90 cm. The inclined top of the housing contains the lens through which the laser beam is projected upwards.

The laser beam of this LiDAR points up with an angle of 30 degrees with respect to the vertical, and sweeps to describe full circles, as can be seen in [28].

Installation and limitation

The installation of the LiDAR is limited by the fact that the top of the platform is a helicopter landing area, which makes it impossible to install the LiDAR on top of the platform, as no objects are allowed to protrude above the helicopter deck.

Mechanical installation

The LiDAR is mounted on top of the accommodation building with six bolts on three hard plastic mounting blocks. The three blocks are mounted to the platform with three bolts and made watertight using Sikaflex, see Figure B.9.

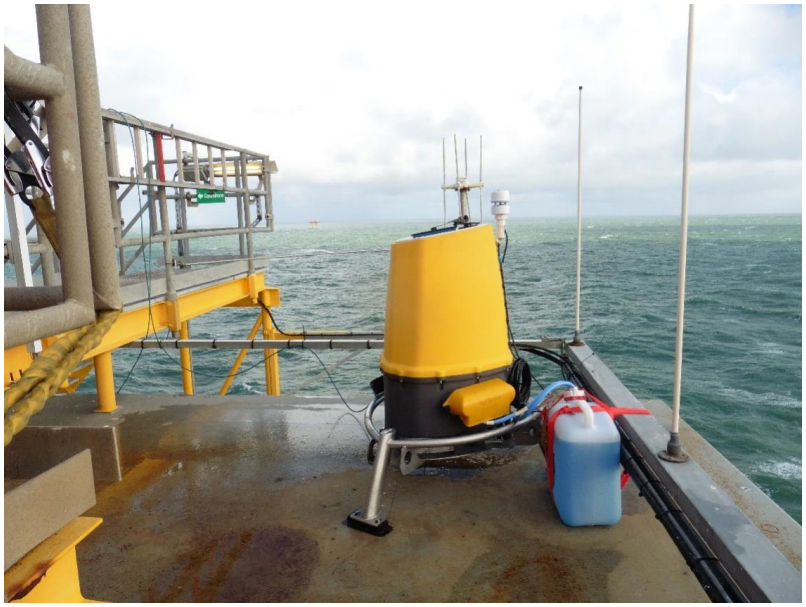

Figure B.9 ZX300M mounted on top of the accommodation building at K13-A [ref]

Electrical installation

Power supply

To be able to operate, the LiDAR needs a 12VDC power supply. The power requirements of the LiDAR in standard climate conditions is 69 Watt, see Appendix B in [28].

From the Lidar a power cable is guided to the computer room, where the LiDAR power AC(230V)-DC(12V) transformer is located and plugged into an 230VAC socket.

Communication

To be able to transfer the data measured by the LiDAR to TNO, a laptop is installed in the computer room, located close to the LiDAR. The laptop is connected to the internet by local wireless network and satellite connection, see Figure B.10.

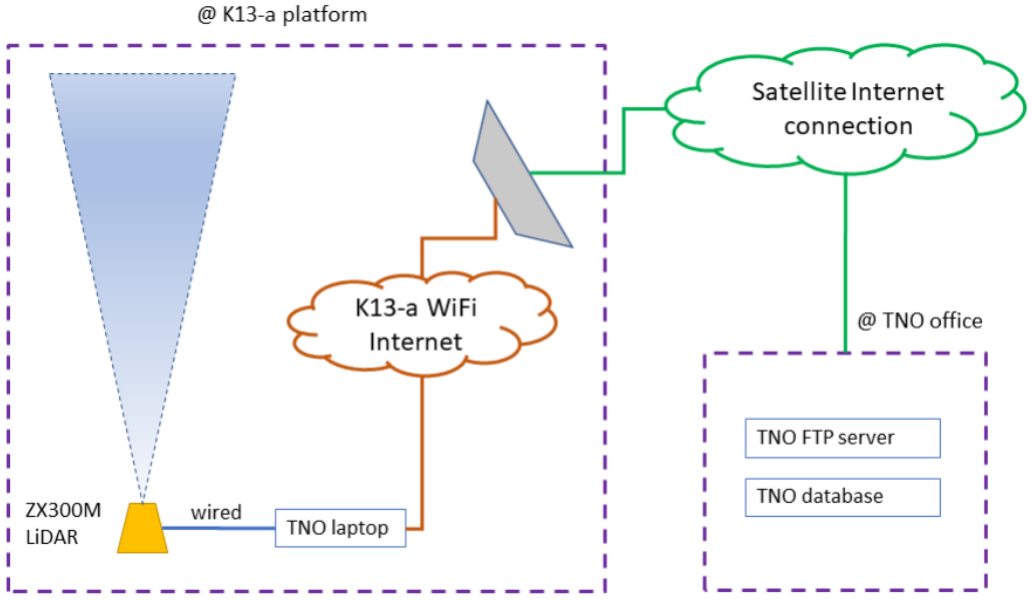

Figure B.10 K13-A lidar campaign network layout

Orientation of the lidar

The LiDAR has been installed with the 'North' marker of the LiDAR pointing towards the platform North. As seen in Figure 4 the platform North is orientated 35 degrees west of true north. Therefore a 360-35=325 degrees bearing is configured in the LiDAR settings, see Figure B.11.

Obstacles

The ZX300M LiDAR is installed just below the helicopter deck on a platform to the side of the helicopter deck, see Figure B.8, therefore the LiDAR experiences free sight for the complete scan circle of the LiDAR beam with an opening angle of 30 degree to the vertical. The meteo station of the LiDAR however experiences the blockage effect of the platform. This results in periods with a 180 degrees offset as explained in Chapter 5.5 in [28].

Lidar settings – measuring heights

We have chosen to configure the measurement heights (MSL) at the K13-a platform the same as the heights measured at the Lichteiland Goeree platform, which in turn are based on the meteorological mast (MMIJ) measurement height configuration, mentioned in chapter 1.

The lens of the LiDAR is around 36 meters above sea level (MSL). The measuring heights as configured in the LiDAR can be seen in Figure B.11 and Table B.1 gives the corresponding measurement heights above MSL as well.

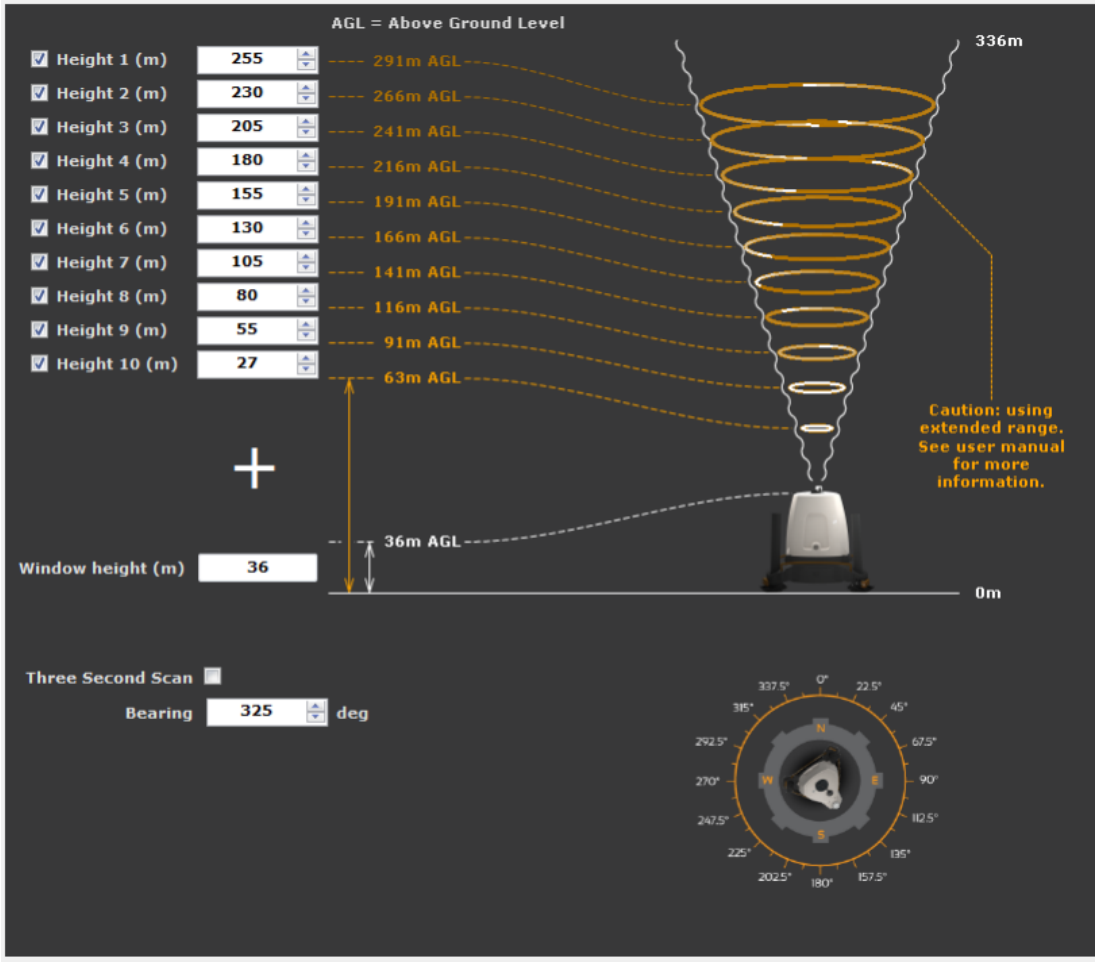

Figure B.11 Height configuration of the ZX300MW lidar

Table B.1 Lidar configuration and measurement height to MSL

No	Lidar height configuration [m]	Measurement height to MSL [m]
1	27	63
2	55	91
3	80	116
4	105	141
5	130	166
6	155	191
7	180	216
8	205	241
9	230	266
10	255	291

Appendix C Primary Datasets' Measurement Campaign Monthly Values

C.1 FLS IJV A

Table C.2 FLS IJV A monthly mean wind speed and wind direction

Height [m]	300		250		200		180		160		140		120		100		70		41		30	
Month/ Variable	WS [m/s]	WD [°]	WS [m/s]	WD [°]	WS [m/s]	WD [°]	WS [m/s]	WD [°]	WS [m/s]	WD [°]	WS [m/s]	WD [°]	WS [m/s]	WD [°]	WS [m/s]	WD [°]	WS [m/s]	WD [°]	WS [m/s]	WD [°]	WS [m/s]	WD [°]
May 2022	8.62	252	8.65	250	8.66	247	8.64	246	8.58	245	8.48	243	8.35	242	8.14	240	7.71	238	7.00	237	6.68	237
Jun 2022	8.11	243	8.07	241	8.03	239	8.01	238	7.97	236	7.90	235	7.80	234	7.64	231	7.30	229	6.78	229	6.50	231
Jul 2022	8.30	266	8.26	265	8.18	262	8.14	262	8.08	260	8.00	259	7.91	257	7.78	257	7.52	257	7.10	259	6.86	261
Aug 2022	7.16	64	7.20	64	7.24	66	7.26	67	7.25	67	7.25	67	7.22	66	7.16	65	6.98	60	6.58	52	6.35	48
Sep 2022	8.65	314	8.57	316	8.47	320	8.42	321	8.37	322	8.32	323	8.24	325	8.17	326	8.03	328	7.80	329	7.67	329
Oct 2022	11.24	225	11.08	224	10.86	222	10.77	222	10.66	221	10.54	220	10.41	220	10.23	219	9.93	218	9.47	218	9.23	218
Nov 2022	12.61	206	12.47	205	12.30	204	12.24	204	12.16	203	12.09	203	12.00	203	11.89	202	11.72	202	11.40	201	11.23	201
Dec 2022	11.96	231	11.77	228	11.49	225	11.35	224	11.23	223	11.08	222	10.91	221	10.72	220	10.44	219	10.06	218	9.88	218
Jan 2023	13.93	251	14.07	250	13.38	248	13.18	248	12.97	248	12.77	247	12.55	247	12.46	247	11.98	247	11.47	247	11.23	247
Feb 2023	10.65	286	10.51	282	10.33	277	10.23	276	10.10	274	9.95	273	9.78	271	9.58	271	9.15	268	8.56	267	8.33	267
Mar 2023	13.02	239	12.81	236	12.49	233	12.35	232	12.16	230	11.93	229	11.67	227	11.36	227	10.82	225	10.08	224	9.79	224
Apr 2023	11.06	102	10.92	100	10.71	97	10.62	95	10.50	92	10.37	90	10.20	85	9.96	77	9.64	72	9.17	68	8.96	66
May 2023	8.52	35	8.49	34	8.52	33	8.53	32	8.52	32	8.49	31	8.42	30	8.35	30	8.05	29	7.51	28	7.31	28

Table C.3 FLS IJV A monthly wind speed and wind direction data coverage

Height [m]	300		250		200		180		160		140		120		100		70		41		30	
Month/ Data coverage	WS [m/s]	WD [°]	WS [m/s]	WD [°]	WS [m/s]	WD [°]	WS [m/s]	WD [°]	WS [m/s]	WD [°]	WS [m/s]	WD [°]	WS [m/s]	WD [°]	WS [m/s]	WD [°]	WS [m/s]	WD [°]	WS [m/s]	WD [°]	WS [m/s]	WD [°]
May 2022	87.5	86.7	88.6	87.7	90.3	89.6	90.9	90.1	91.3	90.3	91.8	91.3	92.0	91.6	92.7	92.3	93.4	93.0	95.3	94.7	95.3	94.9
Jun 2022	92.0	92.6	94.3	94.2	96.0	95.5	96.7	96.1	97.0	95.7	97.3	96.6	97.6	97.0	98.2	97.6	98.4	97.6	98.3	97.5	98.4	97.7
Jul 2022	94.6	94.5	95.8	95.2	96.7	96.0	96.9	96.4	97.0	96.1	97.2	96.6	97.3	96.6	97.7	97.1	97.7	97.1	97.9	97.3	97.8	97.2
Aug 2022	92.8	92.1	94.4	93.5	95.2	94.5	95.4	94.6	95.6	94.7	95.6	94.8	95.7	94.9	96.3	95.5	96.3	95.5	96.6	95.9	96.5	95.8
Sep 2022	95.1	95.2	95.8	95.7	96.6	96.2	96.9	96.5	97.0	95.9	97.3	96.7	97.7	97.2	97.9	97.5	98.2	97.7	98.2	97.7	98.2	97.8
Oct 2022	97.6	97.2	97.9	97.4	98.4	97.9	98.5	97.9	98.6	98.1	98.7	98.2	98.8	98.1	98.8	98.2	98.8	98.2	98.8	98.2	98.8	98.1
Nov 2022	94.0	93.1	94.3	93.7	95.0	94.5	95.0	94.6	95.1	94.6	95.4	94.9	95.4	94.9	95.5	95.1	95.6	95.1	95.6	95.1	95.6	95.1
Dec 2022	96.4	96.3	96.9	96.7	97.6	97.4	98.0	97.7	98.0	97.3	98.3	98.1	98.7	98.4	99.2	98.9	99.2	98.9	99.2	99.0	99.2	98.9
Jan 2023	96.4	96.4	93.0	92.9	96.8	96.8	97.4	97.3	98.1	98.1	98.3	98.3	98.7	98.6	97.0	97.0	98.8	98.8	98.8	98.8	98.8	98.8
Feb 2023	91.2	91.1	92.5	92.3	94.2	93.9	94.4	94.3	94.6	94.4	94.7	94.6	95.3	95.1	94.1	93.8	96.6	96.4	98.3	97.9	98.1	98.0
Mar 2023	88.0	87.2	89.3	88.6	91.1	90.3	91.8	90.8	92.3	91.5	93.1	92.2	93.9	93.0	95.9	95.0	97.1	96.0	97.4	96.6	97.8	96.8
Apr 2023	63.2	63.0	63.8	63.6	64.4	64.3	64.6	64.4	64.8	64.7	65.1	64.8	65.7	65.5	67.8	67.6	68.2	67.9	68.4	68.0	68.4	68.2
May 2023	71.9	71.0	72.8	72.1	75.7	74.9	76.4	76.0	77.3	76.7	78.2	77.7	79.3	79.0	82.4	81.9	84.9	84.4	89.7	89.2	89.6	89.3

C.2 FLS IJV B

Table C.4 FLS IJV B monthly mean wind speed and wind direction

Height [m]	300		250		200		180		160		140		120		100		70		41		30	
Month/ Variable	WS [m/s]	WD [°]	WS [m/s]	WD [°]	WS [m/s]	WD [°]	WS [m/s]	WD [°]	WS [m/s]	WD [°]	WS [m/s]	WD [°]	WS [m/s]	WD [°]	WS [m/s]	WD [°]	WS [m/s]	WD [°]	WS [m/s]	WD [°]	WS [m/s]	WD [°]
May 2022	8.71	252	8.76	250	8.78	248	8.75	246	8.69	245	8.60	244	8.45	242	8.25	240	7.82	238	7.09	237	6.77	237
Jun 2022	8.11	242	8.09	240	8.05	238	8.03	237	7.99	235	7.91	234	7.80	232	7.65	230	7.32	227	6.78	226	6.51	228
Jul 2022	8.32	267	8.27	265	8.20	262	8.16	261	8.10	260	8.02	259	7.93	257	7.80	256	7.54	256	7.11	258	6.88	259
Aug 2022	7.12	66	7.18	66	7.23	68	7.24	69	7.24	69	7.23	69	7.20	69	7.15	67	6.96	62	6.56	54	6.33	50
Sep 2022	8.69	312	8.59	315	8.47	318	8.43	320	8.38	321	8.32	322	8.25	323	8.17	325	8.04	327	7.80	328	7.67	328
Oct 2022	11.26	224	11.08	223	10.88	222	10.78	221	10.68	220	10.57	220	10.43	219	10.26	218	9.95	218	9.49	217	9.25	217
Nov 2022	12.50	205	12.39	205	12.19	204	12.14	203	12.07	203	11.99	202	11.89	202	11.80	202	11.63	201	11.32	201	11.13	201
Dec 2022	11.92	230	11.74	227	11.44	225	11.32	224	11.19	222	11.05	221	10.89	221	10.71	219	10.44	219	10.07	218	9.87	218
Jan 2023	13.81	250	13.86	249	13.24	248	13.08	248	12.89	247	12.70	247	12.50	247	12.36	247	11.94	247	11.45	247	11.20	247
Feb 2023	10.77	283	10.62	279	10.41	276	10.29	274	10.16	273	10.02	271	9.83	270	9.62	270	9.20	268	8.60	266	8.36	267
Mar 2023	12.98	238	12.75	236	12.48	233	12.34	232	12.15	230	11.93	229	11.67	228	11.35	227	10.80	225	10.09	224	9.79	225
Apr 2023	9.99	107	9.88	106	9.70	102	9.61	100	9.51	98	9.39	95	9.24	91	9.06	83	8.78	78	8.34	73	8.15	71
May 2023	8.23	32	8.25	32	8.26	31	8.24	30	8.23	30	8.19	29	8.13	28	8.06	28	7.81	27	7.31	27	7.11	27

Table C.5 FLS IJV B monthly wind speed and wind direction data coverage

Height [m]	300		250		200		180		160		140		120		100		70		41		30	
Month/ Data coverage	WS [%]	WD [%]	WS [%]	WD [%]	WS [%]	WD [%]	WS [%]	WD [%]	WS [%]	WD [%]	WS [%]	WD [%]	WS [%]	WD [%]	WS [%]	WD [%]	WS [%]	WD [%]	WS [%]	WD [%]	WS [%]	WD [%]
May 2022	86.0	85.0	87.5	86.5	89.0	88.0	89.5	88.6	90.1	88.9	90.4	89.9	91.0	90.6	91.7	91.3	92.2	91.9	94.0	93.6	93.9	93.6
Jun 2022	90.9	91.5	93.7	93.7	95.8	95.4	96.2	95.8	96.6	95.6	97.0	96.5	97.4	97.0	97.9	97.4	97.9	97.5	98.0	97.4	98.0	97.5
Jul 2022	94.7	94.4	96.0	95.3	97.2	96.3	97.3	96.6	97.6	96.5	97.7	97.0	97.9	97.1	98.0	97.2	98.1	97.3	98.0	97.4	97.8	96.8
Aug 2022	92.7	91.9	94.5	93.8	95.7	95.0	95.8	95.1	96.0	95.1	96.2	95.4	96.3	95.5	96.7	96.1	96.8	96.2	96.8	96.2	96.8	96.1
Sep 2022	94.6	94.8	95.7	95.4	96.5	95.9	96.7	96.1	97.0	96.1	97.3	96.6	97.5	96.7	97.6	97.1	97.8	97.2	97.9	97.3	97.9	97.3
Oct 2022	97.9	97.9	98.1	98.1	98.2	98.1	98.3	98.1	98.4	98.1	98.5	98.2	98.5	98.3	98.5	98.2	98.5	98.2	98.5	98.2	98.5	98.2
Nov 2022	97.0	96.4	97.0	96.9	97.7	97.5	97.7	97.4	97.8	97.5	97.9	97.6	97.9	97.6	98.0	97.7	98.0	97.7	98.0	97.7	98.0	97.7
Dec 2022	96.6	96.3	96.8	96.6	97.6	97.3	97.8	97.5	98.0	97.5	98.2	97.8	98.4	98.1	98.9	98.5	98.8	98.4	98.8	98.3	98.8	98.3
Jan 2023	96.7	96.6	93.9	93.9	97.1	97.1	97.4	97.4	97.6	97.4	97.9	97.8	98.0	98.0	97.1	97.0	98.1	98.1	98.1	98.1	98.1	98.0
Feb 2023	90.4	90.2	91.5	91.3	92.2	92.1	92.4	92.2	92.5	92.2	92.7	92.6	92.9	92.8	92.2	92.2	93.9	93.8	95.6	95.4	95.6	95.4
Mar 2023	88.0	87.3	89.0	88.2	90.3	89.5	90.8	90.0	91.3	90.4	91.7	90.8	92.2	91.5	93.9	93.1	95.1	94.3	95.4	94.5	95.7	94.7
Apr 2023	87.9	87.7	88.5	88.2	89.0	88.7	89.4	89.2	89.6	89.2	90.1	89.8	90.8	90.4	92.7	92.4	93.3	92.9	94.1	93.5	94.0	93.6
May 2023	79.9	79.2	82.1	81.3	83.6	83.0	84.5	84.1	85.2	84.7	86.0	85.5	86.9	86.5	89.6	89.1	91.8	91.2	96.5	95.8	96.5	96.0

C.3 MM IJmuiden and lidar IJmuiden

Table C.6 MMIJ monthly mean wind speed and wind direction

Height [m] Variable/ Month	92 m WS [m/s]	85 m WS [m/s]	58 m WS [m/s]	27 m WS [m/s]	87 m WD [°]	58 m WD [°]	27 m WD [°]
Jan 2012	12.25	11.59	11.82	11.24	255	265	265
Feb 2012	11.07	10.95	10.44	9.67	270	265	260
Mar 2012	7.98	7.91	7.39	6.39	292	291	284
Apr 2012	9.54	9.49	9.11	8.54	191	187	184
May 2012	9.37	9.24	8.72	7.63	29	24	14
Jun 2012	9.92	9.82	9.27	8.37	211	213	209
Jul 2012	7.76	7.68	7.42	6.91	231	232	233
Aug 2012	7.92	7.81	7.50	6.86	205	203	203
Sep 2012	9.72	9.65	9.49	9.12	250	249	250
Oct 2012	9.74	9.68	9.53	9.22	242	242	243
Nov 2012	10.64	10.60	10.45	10.15	225	224	223
Dec 2012	12.28	12.20	11.88	11.32	235	235	235
Jan 2013	10.28	10.20	9.88	9.41	226	212	208
Feb 2013	10.06	10.01	9.86	9.57	40	36	38
Mar 2013	11.03	10.88	10.60	10.12	77	79	77
Apr 2013	10.03	9.89	9.32	8.41	194	173	138
May 2013	9.56	9.43	8.87	7.96	275	279	282
Jun 2013	9.54	9.40	8.86	7.97	279	284	291
Jul 2013	7.04	6.93	6.65	5.75	3	53	38
Aug 2013	7.65	7.55	7.19	6.46	208	224	226
Sep 2013	8.67	8.65	8.45	8.10	278	277	278
Oct 2013	12.13	12.10	11.68	11.09	205	203	202
Nov 2013	10.30	10.33	10.14	9.82	297	295	213
Dec 2013	13.28	13.25	12.85	12.26	220	218	207
Jan 2014	12.99	12.99	12.58	12.06	199	197	196
Feb 2014	14.41	14.39	13.85	13.10	205	204	201
Mar 2014	10.08	9.96	9.52	8.66	200	205	177
Apr 2014	8.60	8.16	8.05	7.28	182	305	327
May 2014	8.06	7.82	7.59	6.86	184	182	182
Jun 2014	6.21	5.85	5.96	5.54	331	332	331
Jul 2014	8.12	7.79	7.59	6.78	357	352	343
Aug 2014	9.35	9.15	9.11	8.75	233	242	243
Sep 2014	6.47	5.92	6.34	6.08	19	3	358
Oct 2014	10.71	10.47	10.39	9.97	220	219	218
Nov 2014	9.58	9.41	9.40	9.19	162	162	162
Dec 2014	13.17	12.54	12.82	12.28	272	265	265
Jan 2015	12.80	12.16	12.40	11.81	254	251	251
Feb 2015	10.00	9.73	9.68	9.29	245	252	252
Mar 2015	11.19	11.02	10.64	9.92	263	262	263
Apr 2015	7.71	7.63	7.30	6.77	286	286	291

Height [m] Variable/ Month	92 m WS [m/s]	85 m WS [m/s]	58 m WS [m/s]	27 m WS [m/s]	87 m WD [°]	58 m WD [°]	27 m WD [°]
May 2015	9.45	9.30	8.80	7.98	235	233	233
Jun 2015	8.79	8.64	8.30	7.43	256	255	259
Jul 2015	9.04	8.88	8.45	7.65	242	242	243
Aug 2015	8.79	8.65	8.28	7.56	189	187	187
Sep 2015	8.96	8.83	8.75	8.45	296	296	297
Oct 2015	8.19	8.09	7.96	7.69	108	106	105
Nov 2015	13.72	13.64	13.16	12.40	248	247	247
Dec 2015	14.77	14.57	13.96	12.90	215	214	213

Table C.7 MMIJ monthly wind speed and wind direction data coverage

Height [m]/ Data coverage Month	92 m WS [%]	85 m WS [%]	58 m WS [%]	27 m WS [%]	87 m WD [%]	58 m WD [%]	27 m WD [%]
Jan 2012	100.0	78.9	100.0	100.0	100.0	100.0	99.4
Feb 2012	82.7	82.7	82.7	82.7	82.7	82.7	82.7
Mar 2012	85.5	85.8	85.5	85.6	85.7	85.5	83.9
Apr 2012	99.9	99.9	99.9	99.9	100.0	100.0	99.9
May 2012	100.0	100.0	100.0	100.0	100.0	100.0	100.0
Jun 2012	99.9	99.9	99.9	99.9	99.9	93.8	99.9
Jul 2012	96.1	96.1	96.1	96.1	96.0	92.0	96.1
Aug 2012	99.9	100.0	100.0	100.0	100.0	100.0	100.0
Sep 2012	99.9	99.9	99.9	99.9	99.9	99.9	99.9
Oct 2012	99.8	99.9	99.8	99.9	99.9	99.8	99.9
Nov 2012	99.9	100.0	100.0	99.9	100.0	100.0	99.9
Dec 2012	100.0	100.0	100.0	100.0	100.0	100.0	100.0
Jan 2013	100.0	99.1	100.0	100.0	82.3	99.9	100.0
Feb 2013	99.9	99.9	100.0	100.0	93.8	100.0	100.0
Mar 2013	99.9	99.9	99.9	100.0	80.2	99.9	100.0
Apr 2013	100.0	100.0	100.0	100.0	88.0	100.0	100.0
May 2013	99.9	99.9	99.9	99.9	91.4	99.9	99.9
Jun 2013	99.9	99.9	100.0	100.0	85.2	100.0	100.0
Jul 2013	99.9	99.9	100.0	99.9	87.4	100.0	99.9
Aug 2013	96.7	96.7	96.9	96.9	83.3	94.8	96.9
Sep 2013	99.9	100.0	100.0	100.0	100.0	100.0	100.0
Oct 2013	99.8	99.8	99.8	99.8	99.8	99.8	99.8
Nov 2013	100.0	100.0	100.0	100.0	100.0	100.0	11.1
Dec 2013	99.9	99.9	99.9	99.9	94.4	94.4	70.8
Jan 2014	99.9	100.0	100.0	100.0	100.0	100.0	100.0
Feb 2014	100.0	100.0	100.0	100.0	100.0	99.9	99.6
Mar 2014	100.0	93.8	100.0	100.0	99.9	100.0	32.6
Apr 2014	99.9	87.5	99.9	100.0	100.0	99.9	98.8
May 2014	99.8	93.9	99.8	99.8	99.8	99.8	99.8

Height [m]/ Data coverage Month	92 m WS [%]	85 m WS [%]	58 m WS [%]	27 m WS [%]	87 m WD [%]	58 m WD [%]	27 m WD [%]
Jun 2014	100.0	92.3	100.0	100.0	100.0	100.0	99.9
Jul 2014	100.0	91.8	100.0	100.0	100.0	100.0	100.0
Aug 2014	100.0	88.5	100.0	100.0	100.0	100.0	100.0
Sep 2014	97.9	86.5	97.9	97.9	97.9	97.9	97.9
Oct 2014	98.4	90.2	98.4	98.4	98.5	98.4	98.4
Nov 2014	100.0	95.3	99.9	99.9	99.9	99.9	99.9
Dec 2014	100.0	87.3	99.9	99.9	99.9	99.9	99.9
Jan 2015	100.0	90.4	99.9	100.0	99.9	99.9	99.9
Feb 2015	99.9	92.7	100.0	99.9	100.0	99.9	99.9
Mar 2015	99.6	98.2	99.6	99.6	99.6	99.6	99.6
Apr 2015	100.0	100.0	100.0	100.0	99.9	99.9	99.9
May 2015	99.9	99.8	99.8	99.8	99.7	99.8	99.8
Jun 2015	100.0	100.0	100.0	100.0	100.0	99.9	99.9
Jul 2015	99.8	99.8	99.8	99.8	99.8	99.8	99.8
Aug 2015	100.0	99.9	99.9	99.9	99.9	99.9	99.9
Sep 2015	100.0	99.9	99.9	99.9	99.9	99.9	99.9
Oct 2015	99.9	99.9	99.9	99.9	99.8	99.9	99.9
Nov 2015	99.9	99.9	99.9	99.9	99.8	99.9	99.9
Dec 2015	99.8	99.8	99.8	99.8	99.8	99.8	99.8

Table C.8 IJlidar monthly mean wind speed and wind direction

Height [m]	315		240		190		165		140	
Month/ Variable	WS [m/s]	WD [°]	WS [m/s]	WD [°]	WS [m/s]	WD [°]	WS [m/s]	WD [°]	WS [m/s]	WD [°]
Nov 2011	10.81	210	10.69	208	10.54	206	10.45	205	10.36	205
Dec 2011	15.68	263	15.57	262	15.43	261	15.33	261	15.16	260
Jan 2012	14.09	275	13.83	272	13.59	272	13.43	270	13.23	269
Feb 2012	11.95	297	11.90	290	11.77	283	11.63	278	11.43	274
Mar 2012	8.05	293	8.07	293	8.08	291	8.08	289	8.07	288
Apr 2012	10.49	207	10.37	203	10.20	200	10.08	198	9.93	196
May 2012	9.51	309	9.59	1	9.62	36	9.62	35	9.60	34
Jun 2012	11.09	222	10.95	220	10.75	217	10.61	216	10.42	215
Jul 2012	8.27	238	8.23	237	8.15	236	8.08	235	7.99	234
Aug 2012	8.61	212	8.52	211	8.42	210	8.34	209	8.25	208
Sep 2012	10.22	251	10.15	251	10.07	250	10.01	250	9.95	250
Oct 2012	10.30	245	10.25	245	10.17	245	10.12	245	10.06	245
Nov 2012	10.68	237	10.62	237	10.55	237	10.50	237	10.43	236

Height [m]	315		240		190		165		140	
Month/ Variable	WS [m/s]	WD [°]	WS [m/s]	WD [°]	WS [m/s]	WD [°]	WS [m/s]	WD [°]	WS [m/s]	WD [°]
Dec 2012	13.42	241	13.27	239	13.07	238	12.91	237	12.74	236
Jan 2013	11.07	237	11.02	232	10.94	228	10.85	225	10.72	223
Feb 2013	10.64	28	10.55	30	10.44	35	10.37	36	10.29	36
Mar 2013	11.42	85	11.42	85	11.38	84	11.33	84	11.25	83
Apr 2013	10.73	232	10.71	228	10.67	220	10.63	214	10.52	208
May 2013	10.12	270	10.23	268	10.21	273	10.14	272	10.02	272
Jun 2013	10.11	294	10.11	291	10.02	291	9.93	290	9.80	290
Jul 2013	6.91	225	6.95	223	7.04	300	7.10	296	7.12	295
Aug 2013	8.24	229	8.23	227	8.18	231	8.12	230	8.00	228
Sep 2013	8.97	254	8.91	252	8.86	281	8.87	280	8.88	279
Oct 2013	13.44	218	13.21	214	12.93	206	12.77	206	12.59	205
Nov 2013	10.76	318	10.72	316	10.64	306	10.60	305	10.54	303
Dec 2013	14.99	222	14.72	220	14.39	222	14.17	221	13.92	221
Jan 2014	14.33	199	14.14	197	13.86	196	13.68	195	13.48	194
Feb 2014	16.12	206	15.84	204	15.49	203	15.27	202	15.03	202
Mar 2014	11.08	221	11.02	217	10.92	212	10.81	209	10.61	206
Apr 2014	9.31	254	9.21	252	9.14	246	9.09	244	9.01	244
May 2014	8.71	216	8.66	212	8.61	199	8.55	196	8.45	193
Jun 2014	6.56	321	6.50	322	6.46	324	6.43	325	6.39	326
Jul 2014	8.04	294	8.09	298	8.18	311	8.28	319	8.30	326
Aug 2014	9.89	238	9.84	238	9.77	238	9.71	238	9.63	238
Sep 2014	6.65	290	6.55	290	6.52	292	6.51	293	6.45	293
Oct 2014	11.45	219	11.36	218	11.25	217	11.17	217	11.06	216
Nov 2014	9.95	164	9.92	163	9.86	162	9.83	161	9.78	161
Dec 2014	14.31	265	14.15	263	13.89	262	13.73	261	13.58	260
Jan 2015	14.16	251	13.97	249	13.72	248	13.54	247	13.36	247
Feb 2015	10.31	352	10.15	351	9.98	351	9.90	350	9.82	350
Mar 2015	12.19	286	12.09	284	11.94	288	11.79	287	11.61	287
Apr 2015	8.71	276	8.63	273	8.54	282	8.47	281	8.36	279
May 2015	10.49	247	10.36	245	10.19	243	10.07	241	9.90	240
Jun 2015	9.06	262	9.07	261	9.03	262	8.99	262	8.91	261
Jul 2015	9.40	249	9.43	248	9.41	247	9.37	246	9.28	246
Aug 2015	9.23	200	9.26	199	9.23	196	9.18	195	9.08	194
Sep 2015	9.24	288	9.16	291	9.08	293	9.03	294	8.98	296
Oct 2015	8.50	127	8.42	127	8.35	114	8.30	114	8.23	113

Height [m]	315		240		190		165		140	
Month/ Variable	WS [m/s]	WD [°]	WS [m/s]	WD [°]	WS [m/s]	WD [°]	WS [m/s]	WD [°]	WS [m/s]	WD [°]
Nov 2015	15.15	253	14.94	252	14.65	250	14.43	249	14.17	249
Dec 2015	16.89	224	16.64	222	16.24	220	15.94	219	15.57	219
Jan 2016	14.13	229	14.02	227	13.86	225	13.72	224	13.53	223
Feb 2016	13.10	257	12.91	255	12.67	252	12.49	250	12.28	249
Mar 2016	10.18	244	10.14	244	10.09	243	10.04	242	9.96	242

Table C.9 IJlidar monthly wind speed and wind direction data coverage

Height [m]	315		240		190		165		140	
Month/ Data coverage	WS [%]	WD [%]	WS [%]	WD [%]	WS [%]	WD [%]	WS [%]	WD [%]	WS [%]	WD [%]
Nov 2011	76.1	74.3	76.1	74.2	76.1	76.0	76.1	76.0	76.1	76.1
Dec 2011	99.8	98.5	99.8	98.5	99.8	99.8	99.8	99.8	99.8	99.8
Jan 2012	86.1	81.9	87.4	83.2	87.7	87.7	87.9	87.9	88.1	88.1
Feb 2012	79.2	78.9	79.6	79.3	79.6	79.6	79.6	79.6	79.6	79.5
Mar 2012	88.4	86.7	89.0	87.4	89.3	89.1	89.5	89.4	89.6	89.4
Apr 2012	100.0	99.7	99.9	99.7	100.0	99.9	100.0	99.9	100.0	99.8
May 2012	99.6	92.3	100.0	92.7	100.0	99.7	100.0	99.7	100.0	99.8
Jun 2012	99.8	96.7	99.8	97.0	99.9	99.8	99.9	99.8	99.9	99.8
Jul 2012	96.6	94.0	96.6	94.0	96.6	96.5	96.6	96.4	96.6	96.4
Aug 2012	99.7	98.8	99.7	98.8	99.7	99.6	99.7	99.5	99.7	99.6
Sep 2012	99.6	99.2	99.8	99.4	99.8	99.8	99.9	99.7	99.9	99.6
Oct 2012	92.7	92.4	92.8	92.6	92.8	92.8	92.8	92.8	92.8	92.7
Nov 2012	83.4	82.6	83.4	82.7	83.4	83.2	83.4	83.3	83.4	83.3
Dec 2012	99.5	99.4	99.5	99.4	99.5	99.4	99.5	99.4	99.5	99.4
Jan 2013	97.7	97.3	97.7	97.3	97.7	97.6	97.7	97.6	97.7	97.6
Feb 2013	99.0	98.2	99.0	98.2	99.0	99.0	99.0	99.0	99.0	99.0
Mar 2013	100.0	99.2	100.0	99.2	100.0	99.6	100.0	99.9	100.0	99.8
Apr 2013	95.4	94.8	96.2	95.5	97.5	97.3	98.2	98.0	98.6	98.4
May 2013	97.3	94.0	97.3	94.0	97.3	97.2	97.3	97.2	97.3	97.2
Jun 2013	94.4	92.1	94.4	92.1	94.5	94.0	94.5	94.1	94.5	94.2
Jul 2013	96.4	71.9	97.0	72.1	97.5	96.8	98.0	97.2	98.6	97.6
Aug 2013	99.9	89.1	100.0	89.1	99.9	99.2	100.0	99.2	100.0	99.5

Height [m]	315		240		190		165		140	
Month/ Data coverage	WS [%]	WD [%]	WS [%]	WD [%]	WS [%]	WD [%]	WS [%]	WD [%]	WS [%]	WD [%]
Sep 2013	100.0	85.1	100.0	85.2	100.0	99.5	100.0	99.5	100.0	99.4
Oct 2013	100.0	69.0	100.0	69.1	100.0	83.0	100.0	86.1	100.0	88.8
Nov 2013	99.3	64.8	99.4	66.1	99.3	83.5	99.3	83.7	99.2	84.2
Dec 2013	98.3	88.2	98.3	88.3	98.3	94.3	98.3	94.8	98.3	94.8
Jan 2014	97.0	94.2	97.0	94.2	97.0	96.8	97.0	97.0	97.0	97.0
Feb 2014	99.6	99.1	99.7	99.2	99.7	99.6	99.7	99.6	99.6	99.5
Mar 2014	99.6	96.0	99.7	96.0	99.7	99.6	99.7	99.7	99.7	99.6
Apr 2014	99.2	94.6	99.3	94.6	99.4	99.1	99.5	99.3	99.4	99.3
May 2014	99.5	86.4	99.7	86.2	99.6	99.2	99.6	99.3	99.6	99.2
Jun 2014	99.5	97.6	99.5	97.5	99.6	99.4	99.5	99.4	99.6	99.4
Jul 2014	87.8	85.2	89.4	86.3	91.6	91.3	93.9	92.7	95.5	93.8
Aug 2014	98.7	98.0	98.8	98.0	98.8	98.6	98.8	98.7	98.9	98.8
Sep 2014	61.5	59.8	61.3	59.5	61.0	60.5	60.8	60.5	61.0	60.9
Oct 2014	99.3	98.8	99.3	98.7	99.3	99.3	99.3	99.3	99.3	99.3
Nov 2014	99.3	97.3	99.4	97.4	99.4	99.3	99.4	99.3	99.3	99.1
Dec 2014	99.6	96.9	99.6	96.8	99.6	99.4	99.6	99.5	99.6	99.4
Jan 2015	99.3	97.6	99.2	97.6	99.1	98.9	99.1	99.0	99.1	99.0
Feb 2015	34.9	34.6	34.9	34.7	34.9	34.8	34.9	34.7	34.8	34.6
Mar 2015	46.7	42.2	46.7	42.3	46.7	46.6	46.7	46.6	46.7	46.6
Apr 2015	81.2	73.5	81.2	73.5	81.2	80.9	81.2	81.1	81.2	81.1
May 2015	100.0	99.6	100.0	99.7	100.0	99.9	100.0	99.9	100.0	99.9
Jun 2015	99.8	98.1	99.8	98.2	99.9	99.8	100.0	100.0	100.0	99.9
Jul 2015	94.5	93.8	94.5	93.7	94.5	94.2	94.5	94.4	94.5	94.4
Aug 2015	100.0	99.5	100.0	99.3	100.0	99.9	100.0	99.9	100.0	99.8
Sep 2015	100.0	98.3	100.0	98.3	100.0	100.0	100.0	100.0	100.0	100.0
Oct 2015	100.0	94.9	100.0	95.0	100.0	99.9	100.0	100.0	100.0	100.0
Nov 2015	100.0	100.0	100.0	99.9	100.0	100.0	100.0	100.0	100.0	100.0
Dec 2015	100.0	99.6	100.0	99.6	100.0	99.8	100.0	99.9	100.0	99.8
Jan 2016	100.0	98.5	100.0	98.4	100.0	100.0	100.0	99.9	100.0	99.8
Feb 2016	100.0	98.9	100.0	98.9	100.0	100.0	100.0	100.0	100.0	100.0
Mar 2016	29.1	29.1	29.1	29.1	29.1	29.1	29.1	29.1	29.1	29.1

C.4 FLS HKW

Table C.10 FLS HKW A monthly mean wind speed and wind direction

Height [m]	250		200		160		120		100		60		30	
Month/ Variable	WS [m/s]	WD [°]	WS [m/s]	WD [°]	WS [m/s]	WD [°]	WS [m/s]	WD [°]	WS [m/s]	WD [°]	WS [m/s]	WD [°]	WS [m/s]	WD [°]
Feb 2019	11.38	233	11.21	232	11.00	230	10.64	227	10.36	226	9.69	223	8.81	221
Mar 2019	13.04	264	12.70	262	12.33	262	11.92	261	11.62	260	10.88	259	10.14	259
Apr 2019	9.79	102	9.74	100	9.66	97	9.53	95	9.43	93	8.96	87	8.06	81
May 2019	8.01	323	7.98	320	7.89	318	7.72	317	7.61	316	7.26	326	6.83	334
Jun 2019	8.97	202	8.84	199	8.65	197	8.38	194	8.21	192	7.69	182	6.99	176
Jul 2019	7.83	266	7.75	264	7.66	262	7.48	261	7.35	261	6.98	264	6.46	268
Aug 2019	9.27	238	9.15	237	9.03	236	8.90	236	8.80	236	8.52	236	8.15	237
Sep 2019	10.30	255	10.16	254	10.01	254	9.81	254	9.71	254	9.42	255	9.07	255
Oct 2019	11.47	227	11.27	226	11.08	225	10.86	224	10.74	224	10.42	223	10.01	223
Nov 2019	10.88	217	10.74	215	10.57	213	10.32	210	10.18	209	9.86	207	9.49	207
Dec 2019	13.18	229	12.94	228	12.68	227	12.36	226	12.17	226	11.67	226	11.11	226
Jan 2020	13.47	236	13.16	234	12.86	233	12.43	232	12.17	232	11.41	231	10.71	230
Feb 2020	17.49	245	16.96	244	16.44	243	15.82	242	15.47	242	14.63	242	13.68	242
Mar 2020	12.84	222	12.59	218	12.30	215	11.93	211	11.71	209	11.17	204	10.55	199
Apr 2020	9.44	79	9.43	78	9.37	77	9.19	73	9.01	71	8.41	65	7.51	60

Table C.11 FLS HKW A monthly wind speed and wind direction data coverage

Height [m]	250		200		160		120		100		60		30	
Month/ Data coverage	WS [%]	WD [%]	WS [%]	WD [%]	WS [%]	WD [%]	WS [%]	WD [%]	WS [%]	WD [%]	WS [%]	WD [%]	WS [%]	WD [%]
Feb 2019	70.0	70.0	70.6	70.6	70.9	70.9	71.2	71.2	71.5	71.5	74.1	74.1	74.0	74.0
Mar 2019	79.8	79.8	80.3	80.3	81.5	81.5	81.9	81.9	82.6	82.6	84.2	84.2	84.1	84.1
Apr 2019	90.3	90.3	90.7	90.7	91.1	91.1	91.2	91.2	91.2	91.2	93.1	93.1	93.1	93.1
May 2019	76.2	76.2	76.9	76.9	77.5	77.5	78.0	78.0	78.4	78.4	79.7	79.7	79.8	79.8
Jun 2019	82.9	82.9	83.5	83.5	84.1	84.1	84.8	84.8	84.9	84.9	87.3	87.3	88.1	88.1
Jul 2019	81.3	81.3	81.9	81.9	82.4	82.4	82.9	82.9	83.1	83.1	86.4	86.4	86.4	86.4
Aug 2019	84.4	84.4	84.4	84.4	84.4	84.4	84.5	84.5	84.4	84.4	84.8	84.8	84.9	84.9
Sep 2019	87.9	87.9	88.2	88.2	88.1	88.1	88.2	88.2	88.2	88.2	88.7	88.7	88.8	88.8
Oct 2019	93.6	93.6	93.9	93.9	94.1	94.1	94.1	94.1	94.1	94.1	95.2	95.2	95.2	95.2
Nov 2019	22.6	22.6	22.7	22.7	22.7	22.7	22.7	22.7	22.7	22.7	22.9	22.9	22.9	22.9
Dec 2019	97.8	97.8	97.9	97.9	98.0	98.0	98.0	98.0	98.1	98.1	99.0	99.0	99.0	99.0
Jan 2020	95.6	95.6	96.2	96.2	96.2	96.2	96.5	96.5	96.7	96.7	99.5	99.5	99.7	99.7
Feb 2020	99.3	99.3	99.4	99.4	99.5	99.5	99.5	99.5	99.5	99.5	99.8	99.8	99.8	99.8
Mar 2020	98.9	98.9	99.0	99.0	99.1	99.1	99.2	99.2	99.1	99.1	99.9	99.9	99.8	99.8
Apr 2020	77.6	77.6	78.0	78.0	78.1	78.1	78.1	78.1	78.1	78.1	78.2	78.2	78.1	78.1

Table C.12 FLS HKW A-2 monthly mean wind speed and wind direction

Height [m]	250		200		160		120		100		60		30	
Month/ Variable	WS [m/s]	WD [°]	WS [m/s]	WD [°]	WS [m/s]	WD [°]	WS [m/s]	WD [°]	WS [m/s]	WD [°]	WS [m/s]	WD [°]	WS [m/s]	WD [°]
May 2020	9.35	346	9.25	347	9.11	347	8.88	348	8.71	349	8.22	353	7.52	355
Jun 2020	9.29	230	9.22	229	9.12	228	8.97	227	8.84	228	8.37	236	7.55	253
Jul 2020	8.68	248	8.54	246	8.38	245	8.15	244	8.00	244	7.64	244	7.23	245
Aug 2020	8.98	226	8.90	224	8.83	224	8.71	223	8.61	224	8.32	228	7.68	236
Sep 2020	9.30	276	9.18	276	9.07	277	8.93	278	8.85	278	8.68	276	8.38	278
Oct 2020	12.56	225	12.28	223	12.04	223	11.79	222	11.64	222	11.32	221	10.86	221
Nov 2020	12.11	229	11.90	228	11.64	227	11.31	226	11.14	226	10.70	226	10.14	225
Dec 2020	12.33	219	12.09	219	11.94	218	11.54	218	11.37	216	10.80	210	10.21	210
Jan 2021	20.40	214	19.51	214	18.67	214	17.73	213	17.22	213	16.07	212	14.89	212
Feb 2021	11.65	105	11.59	120	9.48	138	10.01	195	9.96	154	16.25	73	11.76	74

Table C.13 FLS HKW A-2 monthly wind speed and wind direction data coverage

Height [m]	250		200		160		120		100		60		30	
Month/ Data coverage	WS [%]	WD [%]	WS [%]	WD [%]	WS [%]	WD [%]	WS [%]	WD [°]	WS [m/s]	WD [°]	WS [m/s]	WD [°]	WS [m/s]	WD [°]
May 2020	72.7	72.7	72.7	72.7	72.8	72.8	72.7	72.7	72.7	72.7	72.7	72.7	72.8	72.8
Jun 2020	92.9	92.9	93.3	93.3	94.0	94.0	94.5	94.5	95.0	95.0	97.0	97.0	98.7	98.7
Jul 2020	99.3	99.3	99.5	99.5	99.7	99.7	99.8	99.8	99.8	99.8	99.9	99.9	99.9	99.9

Height [m]	250		200		160		120		100		60		30	
Month/ Data coverage	WS [%]	WD [%]	WS [%]	WD [%]	WS [%]	WD [%]	WS [%]	WD [°]	WS [m/s]	WD [°]	WS [m/s]	WD [°]	WS [m/s]	WD [°]
Aug 2020	95.3	95.3	95.8	95.8	95.9	95.9	96.1	96.1	96.5	96.5	98.4	98.4	99.1	99.1
Sep 2020	96.1	96.1	96.1	96.1	96.2	96.2	96.4	96.4	96.3	96.3	99.1	99.1	99.0	99.0
Oct 2020	99.7	99.7	99.8	99.8	99.8	99.8	99.9	99.9	99.9	99.9	99.9	99.9	99.9	99.9
Nov 2020	66.9	66.9	67.0	67.0	67.1	67.1	67.0	67.0	66.9	66.9	67.2	67.2	67.1	67.1
Dec 2020	14.3	14.3	14.4	14.4	14.5	14.5	14.4	14.4	14.6	14.6	15.8	15.8	15.8	15.8
Jan 2021	6.7	6.7	6.7	6.7	6.8	6.8	6.8	6.8	6.7	6.7	6.9	6.9	7.0	7.0
Feb 2021	0.3	0.3	0.3	0.3	0.2	0.2	0.2	0.2	0.3	0.3	0.7	0.7	0.4	0.4

Table C.14 FLS HKW B monthly mean wind speed and wind direction

Height [m]	250		200		160		120		100		60		30	
Month/ Variable	WS [m/s]	WD [°]	WS [m/s]	WD [°]	WS [m/s]	WD [°]	WS [m/s]	WD [°]	WS [m/s]	WD [°]	WS [m/s]	WD [°]	WS [m/s]	WD [°]
Feb 2019	9.42	237	9.40	234	9.36	232	9.14	227	8.94	226	8.25	221	7.28	219
Mar 2019	13.17	261	12.82	260	12.47	259	12.03	258	11.77	258	10.92	256	10.14	256
Apr 2019	9.89	106	9.84	104	9.76	102	9.62	98	9.51	96	8.93	89	8.05	83
May 2019	8.10	314	8.06	313	7.97	313	7.79	313	7.65	314	7.35	325	6.94	331
Jun 2019	9.01	204	8.87	202	8.69	200	8.42	197	8.24	196	7.81	187	7.13	183
Jul 2019	7.70	260	7.61	259	7.52	257	7.35	255	7.23	255	6.87	262	6.37	266
Aug 2019	11.58	235	11.38	234	11.17	233	10.88	232	10.71	232	10.21	233	9.69	234
Sep 2019	-	-	-	-	-	-	-	-	-	-	-	-	-	-

Height [m]	250		200		160		120		100		60		30	
Month/ Variable	WS [m/s]	WD [°]	WS [m/s]	WD [°]	WS [m/s]	WD [°]	WS [m/s]	WD [°]	WS [m/s]	WD [°]	WS [m/s]	WD [°]	WS [m/s]	WD [°]
Oct 2019	-	-	-	-	-	-	-	-	-	-	-	-	-	-
Nov 2019	-	-	-	-	-	-	-	-	-	-	-	-	-	-
Dec 2019	-	-	-	-	-	-	-	-	-	-	-	-	-	-
Jan 2020	-	-	-	-	-	-	-	-	-	-	-	-	-	-
Feb 2020	-	-	-	-	-	-	-	-	-	-	-	-	-	-
Mar 2020	-	-	-	-	-	-	-	-	-	-	-	-	-	-
Apr 2020	-	-	-	-	-	-	-	-	-	-	-	-	-	-
May 2020	9.41	347	9.30	346	9.18	346	8.95	348	8.77	349	8.27	353	7.56	355
Jun 2020	9.27	229	9.22	230	9.12	231	8.98	230	8.86	230	8.38	236	7.56	252
Jul 2020	8.70	248	8.56	247	8.40	246	8.17	245	8.03	245	7.68	245	7.26	246
Aug 2020	9.03	229	8.96	227	8.87	227	8.74	228	8.65	228	8.34	231	7.70	238
Sep 2020	9.11	267	8.99	267	8.88	268	8.74	267	8.67	267	8.48	268	8.18	269
Oct 2020	12.38	227	12.11	226	11.90	225	11.67	225	11.53	225	11.21	224	10.76	224
Nov 2020	11.73	230	11.50	228	11.26	227	10.94	226	10.77	226	10.37	225	9.87	225
Dec 2020	11.20	206	11.02	204	10.82	202	10.62	200	10.47	199	10.17	197	9.76	196
Jan 2021	11.33	287	11.09	286	10.87	285	10.62	284	10.48	284	10.27	286	9.87	287
Feb 2021	9.90	101	9.80	103	9.66	103	9.49	103	9.32	103	10.01	93	9.52	92

Table C.15 FLS HKW B monthly wind speed and wind direction data coverage

Height [m]	250		200		160		120		100		60		30	
Month/ Data coverage	WS [%]	WD [%]	WS [%]	WD [%]	WS [%]	WD [%]	WS [%]	WD [%]	WS [%]	WD [%]	WS [%]	WD [%]	WS [%]	WD [%]
Feb 2019	64.3	64.3	65.0	65.0	65.4	65.4	65.6	65.6	65.7	65.7	66.4	66.4	66.3	66.3
Mar 2019	95.1	95.1	95.6	95.6	96.1	96.1	96.2	96.2	96.2	96.2	99.7	99.7	99.8	99.8
Apr 2019	94.8	94.8	94.9	94.9	95.0	95.0	95.1	95.1	95.0	95.0	99.8	99.8	99.7	99.7
May 2019	91.6	91.6	92.1	92.1	92.5	92.5	93.4	93.4	93.6	93.6	99.8	99.8	99.5	99.5
Jun 2019	91.0	91.0	91.7	91.7	92.7	92.7	92.8	92.8	92.9	92.9	99.6	99.6	99.5	99.5
Jul 2019	90.6	90.6	91.7	91.7	92.3	92.3	92.8	92.8	92.9	92.9	99.5	99.5	99.5	99.5
Aug 2019	34.1	34.1	34.3	34.3	34.3	34.3	34.3	34.3	34.3	34.3	35.1	35.1	35.1	35.1
Sep 2019	0.0	0.0	0.0	0.0	0.0	0.0	0.0	0.0	0.0	0.0	0.0	0.0	0.0	0.0
Oct 2019	0.0	0.0	0.0	0.0	0.0	0.0	0.0	0.0	0.0	0.0	0.0	0.0	0.0	0.0
Nov 2019	0.0	0.0	0.0	0.0	0.0	0.0	0.0	0.0	0.0	0.0	0.0	0.0	0.0	0.0
Dec 2019	0.0	0.0	0.0	0.0	0.0	0.0	0.0	0.0	0.0	0.0	0.0	0.0	0.0	0.0
Jan 2020	0.0	0.0	0.0	0.0	0.0	0.0	0.0	0.0	0.0	0.0	0.0	0.0	0.0	0.0
Feb 2020	0.0	0.0	0.0	0.0	0.0	0.0	0.0	0.0	0.0	0.0	0.0	0.0	0.0	0.0
Mar 2020	0.0	0.0	0.0	0.0	0.0	0.0	0.0	0.0	0.0	0.0	0.0	0.0	0.0	0.0
Apr 2020	0.0	0.0	0.0	0.0	0.0	0.0	0.0	0.0	0.0	0.0	0.0	0.0	0.0	0.0
May 2020	71.9	71.9	72.1	72.1	72.3	72.3	72.3	72.3	72.3	72.3	72.3	72.3	72.3	72.3
Jun 2020	93.4	93.4	93.9	93.9	94.7	94.7	95.4	95.4	95.6	95.6	97.7	97.7	99.5	99.5
Jul 2020	98.8	98.8	99.2	99.2	99.4	99.4	99.5	99.5	99.5	99.5	99.5	99.5	99.5	99.5
Aug 2020	95.7	95.7	95.8	95.8	96.2	96.2	96.4	96.4	96.7	96.7	97.9	97.9	98.8	98.8
Sep 2020	87.3	87.3	87.6	87.6	87.7	87.7	88.0	88.0	88.0	88.0	88.0	88.0	88.0	88.0

Height [m]	250		200		160		120		100		60		30	
Month/ Data coverage	WS [%]	WD [%]	WS [%]	WD [%]	WS [%]	WD [%]	WS [%]	WD [%]	WS [%]	WD [%]	WS [%]	WD [%]	WS [%]	WD [%]
Oct 2020	92.8	92.8	92.9	92.9	92.9	92.9	92.8	92.8	92.8	92.8	92.9	92.9	92.9	92.9
Nov 2020	86.6	86.6	86.8	86.8	86.9	86.9	87.2	87.2	87.3	87.3	87.7	87.7	87.6	87.6
Dec 2020	88.8	88.8	88.7	88.7	89.1	89.1	89.8	89.8	90.2	90.2	92.0	92.0	91.9	91.9
Jan 2021	85.4	85.4	85.6	85.6	85.9	85.9	86.0	86.0	86.1	86.1	99.1	99.1	99.2	99.2
Feb 2021	28.2	28.2	28.1	28.1	28.2	28.2	28.3	28.3	28.2	28.2	38.5	38.5	38.5	38.5

Table C.16 FLS HKW C monthly mean wind speed and wind direction

Height [m]	250		200		160		120		100		60		30	
Month/ Variable	WS [m/s]	WD [°]	WS [m/s]	WD [°]	WS [m/s]	WD [°]	WS [m/s]	WD [°]	WS [m/s]	WD [°]	WS [m/s]	WD [°]	WS [m/s]	WD [°]
Aug 2019	9.31	234	9.20	233	9.08	233	8.93	232	8.83	232	8.56	232	8.15	233
Sep 2019	10.16	254	10.02	253	9.86	253	9.66	253	9.55	254	9.29	254	8.92	254
Oct 2019	11.43	226	11.23	225	11.05	224	10.83	223	10.70	223	10.41	222	9.99	222
Nov 2019	9.91	207	9.85	206	9.78	205	9.68	203	9.61	203	9.44	202	9.14	201
Dec 2019	12.31	210	12.10	208	11.81	206	11.44	205	11.21	204	10.66	203	10.06	203
Jan 2020	8.95	195	8.97	194	8.99	195	8.81	195	8.70	193	8.49	189	8.07	188
Feb 2020	-	-	-	-	-	-	-	-	-	-	-	-	-	-

Table C.17 FLS HKW C monthly wind speed and wind direction data coverage

Height [m]	250	200	160	120	100	60	30

Month/ Data coverage	WS [%]	WD [%]	WS [%]	WD [%]	WS [%]	WD [%]	WS [%]	WD [%]	WS [%]	WD [%]	WS [%]	WD [%]	WS [%]	WD [%]
Aug 2019	99.3	99.3	99.4	99.4	99.4	99.4	99.4	99.4	99.4	99.4	99.4	99.4	99.4	99.4
Sep 2019	98.2	98.2	98.4	98.4	98.5	98.5	98.6	98.6	98.5	98.5	98.7	98.7	98.7	98.7
Oct 2019	98.9	98.9	99.1	99.1	99.2	99.2	99.2	99.2	99.3	99.3	99.5	99.5	99.5	99.5
Nov 2019	71.9	71.9	72.0	72.0	72.0	72.0	72.1	72.1	72.1	72.1	72.3	72.3	72.3	72.3
Dec 2019	39.9	39.9	40.1	40.1	40.1	40.1	40.1	40.1	40.1	40.1	40.8	40.8	40.8	40.8
Jan 2020	2.5	2.5	2.6	2.6	2.6	2.6	2.6	2.6	2.7	2.7	3.0	3.0	3.0	3.0
Feb 2020	0.0	0.0	0.0	0.0	0.0	0.0	0.0	0.0	0.0	0.0	0.0	0.0	0.0	0.0

C.5 Lidar K13-A

Table C.18 Lidar K13-A monthly mean wind speed and wind direction

Height [m]	291		216		191		166		141	
Month/ Variable	WS [m/s]	WD [°]	WS [m/s]	WD [°]	WS [m/s]	WD [°]	WS [m/s]	WD [°]	WS [m/s]	WD [°]
Nov 2016	10.53	246	10.46	246	10.43	245	10.37	245	10.30	245
Dec 2016	10.79	243	10.60	241	10.48	239	10.34	237	10.17	236
Jan 2017	9.83	270	9.67	267	9.59	266	9.50	266	9.40	265
Feb 2017	13.41	217	13.30	212	13.18	209	13.01	206	12.76	203
Mar 2017	11.15	244	11.09	240	11.02	238	10.91	235	10.72	233
Apr 2017	9.13	298	9.03	295	9.00	295	8.94	294	8.84	293
May 2017	9.12	172	9.13	162	9.13	159	9.11	155	9.06	152
Jun 2017	10.08	239	9.98	236	9.93	234	9.84	233	9.69	231
Jul 2017	8.40	244	8.25	240	8.19	239	8.11	238	8.01	237
Aug 2017	7.72	241	7.60	241	7.54	240	7.47	240	7.38	239
Sep 2017	8.71	242	8.66	241	8.62	240	8.57	240	8.51	240
Oct 2017	13.60	259	13.32	258	13.22	257	13.09	256	12.93	256
Nov 2017	11.63	279	11.48	278	11.40	278	11.30	278	11.19	278
Dec 2017	12.62	271	12.44	270	12.33	269	12.19	268	12.03	268
Jan 2018	13.75	248	13.50	245	13.34	244	13.13	242	12.88	241
Feb 2018	10.69	173	10.62	169	10.56	168	10.49	167	10.37	169
Mar 2018	11.40	124	11.41	122	11.36	121	11.30	120	11.18	119
Apr 2018	10.86	205	10.97	200	10.99	198	10.98	195	10.89	192
May 2018	9.10	63	9.25	64	9.32	64	9.38	64	9.44	63
Jun 2018	7.58	326	7.62	327	7.64	327	7.65	326	7.63	326
Jul 2018	7.42	170	7.39	156	7.39	153	7.39	148	7.37	140
Aug 2018	8.10	247	8.06	245	8.02	244	7.97	243	7.91	242
Sep 2018	10.24	255	10.13	255	10.07	254	9.97	254	9.86	254
Oct 2018	10.83	260	10.71	258	10.64	258	10.55	258	10.43	258
Nov 2018	12.23	167	12.08	166	12.01	165	11.91	164	11.80	163
Dec 2018	11.85	249	11.71	248	11.64	247	11.54	246	11.40	245
Jan 2019	12.07	300	11.87	298	11.75	297	11.60	296	11.43	296
Feb 2019	11.47	235	11.39	233	11.32	231	11.22	229	11.05	227
Mar 2019	13.55	260	13.11	258	12.96	258	12.76	257	12.51	256
Apr 2019	9.72	108	9.79	106	9.80	105	9.81	104	9.78	102
May 2019	8.20	312	8.13	312	8.09	310	8.04	309	7.95	308
Jun 2019	9.30	202	9.29	197	9.28	196	9.24	194	9.16	191

Height [m]	291		216		191		166		141	
Month/ Variable	WS [m/s]	WD [°]	WS [m/s]	WD [°]	WS [m/s]	WD [°]	WS [m/s]	WD [°]	WS [m/s]	WD [°]
Jul 2019	8.20	252	8.20	249	8.20	247	8.17	246	8.09	244
Aug 2019	9.46	230	9.34	229	9.27	228	9.19	227	9.09	226
Sep 2019	9.92	256	9.83	255	9.77	255	9.70	255	9.60	255
Oct 2019	11.26	227	11.12	227	11.05	227	10.98	226	10.89	226
Nov 2019	9.54	196	9.48	196	9.45	195	9.41	194	9.36	193
Dec 2019	12.96	234	12.74	233	12.61	232	12.47	232	12.32	231
Jan 2020	13.54	241	13.16	240	12.99	239	12.78	238	12.54	237
Feb 2020	17.61	246	16.97	244	16.69	244	16.38	243	16.04	243
Mar 2020	12.33	232	12.12	226	12.01	224	11.86	222	11.69	220
Apr 2020	9.34	94	9.36	95	9.32	94	9.27	94	9.17	93
May 2020	8.08	316	7.98	316	7.97	315	7.93	315	7.88	314
Jun 2020	8.91	209	8.97	201	8.98	199	8.97	196	8.94	191
Jul 2020	8.76	252	8.64	248	8.58	247	8.50	246	8.40	245
Aug 2020	9.37	215	9.40	212	9.39	210	9.37	207	9.33	205
Sep 2020	9.59	284	9.55	283	9.52	283	9.46	283	9.38	283
Oct 2020	12.09	230	11.83	228	11.72	228	11.61	227	11.47	227
Nov 2020	11.79	228	11.54	227	11.43	226	11.30	226	11.16	225
Dec 2020	11.59	208	11.43	207	11.36	206	11.27	205	11.17	204
Jan 2021	11.33	288	11.18	287	11.09	286	10.97	286	10.84	286
Feb 2021	13.13	176	13.04	173	12.95	171	12.80	169	12.58	167
Mar 2021	11.24	268	10.98	265	10.84	263	10.67	262	10.46	260
Apr 2021	9.05	349	8.96	350	8.91	349	8.84	349	8.76	349
May 2021	9.72	241	9.49	239	9.41	238	9.30	238	9.18	236
Jun 2021	7.08	25	7.20	29	7.25	29	7.32	29	7.37	29
Jul 2021	7.64	252	7.72	249	7.72	249	7.70	248	7.62	246
Aug 2021	8.69	299	8.63	299	8.61	298	8.57	298	8.50	299
Sep 2021	8.24	228	8.26	225	8.25	224	8.22	223	8.18	221
Oct 2021	12.18	236	11.98	235	11.90	235	11.81	235	11.70	234
Nov 2021	10.26	293	10.19	292	10.14	292	10.09	291	10.03	291
Dec 2021	11.14	246	11.15	243	11.12	241	11.03	240	10.89	238
Jan 2022	13.82	256	13.90	251	14.11	249	14.43	247	14.60	245

Table C.19 Lidar K13-A monthly wind speed and wind direction data coverage

Height [m]	291		216		191		166		141	
Month/ Data coverage	WS [%]	WD [%]	WS [%]	WD [%]	WS [%]	WD [%]	WS [%]	WD [%]	WS [%]	WD [%]
Nov 2016	96.5	96.5	96.5	96.5	96.5	96.5	96.5	96.5	96.5	96.5
Dec 2016	98.0	97.9	98.1	98.2	98.1	98.2	98.1	98.2	98.1	98.1
Jan 2017	99.1	98.9	99.1	99.1	99.1	99.1	99.1	99.1	99.1	98.8
Feb 2017	100.0	100.0	100.0	100.0	100.0	100.0	100.0	100.0	100.0	100.0
Mar 2017	99.4	99.8	99.7	99.8	99.7	99.8	100.0	100.0	100.0	100.0
Apr 2017	99.1	100.0	100.0	100.0	100.0	100.0	100.0	100.0	100.0	100.0
May 2017	100.0	100.0	100.0	100.0	100.0	100.0	100.0	100.0	100.0	100.0
Jun 2017	100.0	100.0	100.0	100.0	100.0	100.0	100.0	100.0	100.0	100.0
Jul 2017	99.1	99.0	100.0	99.7	100.0	99.7	100.0	99.9	100.0	99.9
Aug 2017	99.9	99.9	99.9	99.9	99.9	99.9	99.9	99.9	100.0	100.0
Sep 2017	100.0	100.0	100.0	100.0	100.0	100.0	100.0	100.0	100.0	100.0
Oct 2017	99.2	100.0	100.0	100.0	100.0	100.0	100.0	100.0	100.0	100.0
Nov 2017	100.0	100.0	100.0	100.0	100.0	100.0	100.0	100.0	100.0	100.0
Dec 2017	100.0	100.0	100.0	100.0	100.0	100.0	100.0	100.0	100.0	100.0
Jan 2018	97.7	97.7	97.7	97.7	97.7	97.7	97.7	97.7	97.7	97.7
Feb 2018	98.9	98.9	99.8	99.8	99.7	99.7	99.7	99.7	98.8	98.8
Mar 2018	99.5	99.4	99.9	99.9	99.8	99.8	99.8	99.8	99.9	99.9
Apr 2018	99.5	99.7	99.9	99.8	99.9	99.8	99.9	99.9	99.9	99.9
May 2018	100.0	100.0	100.0	100.0	100.0	100.0	100.0	100.0	100.0	100.0
Jun 2018	98.9	98.8	98.9	98.8	98.9	98.8	99.0	98.7	98.9	98.8
Jul 2018	99.5	98.9	99.5	99.2	99.5	99.2	99.5	99.3	99.5	99.4
Aug 2018	99.2	99.2	99.2	99.2	99.2	99.2	99.2	99.2	99.2	99.2
Sep 2018	99.2	99.2	99.2	99.2	99.2	99.2	99.1	99.1	99.1	99.1
Oct 2018	99.3	99.2	99.3	99.3	99.3	99.3	99.3	99.3	99.3	99.3
Nov 2018	99.6	99.6	99.6	99.6	99.6	99.6	99.6	99.6	99.6	99.6
Dec 2018	99.4	99.4	99.4	99.4	99.4	99.4	99.4	99.4	99.4	99.4
Jan 2019	99.4	99.3	99.4	99.4	99.4	99.4	99.4	99.4	99.4	99.4
Feb 2019	99.6	99.6	99.6	99.6	99.6	99.6	99.6	99.6	99.6	99.6
Mar 2019	98.1	99.4	99.6	99.6	99.6	99.6	99.6	99.6	99.6	99.6
Apr 2019	99.4	99.4	99.4	99.4	99.4	99.4	99.4	99.4	99.4	99.4
May 2019	99.2	99.1	99.3	99.2	99.2	99.1	99.2	99.1	99.2	99.2
Jun 2019	99.4	99.0	99.4	99.4	99.4	99.4	99.4	99.4	99.4	99.4
Jul 2019	99.4	99.2	99.4	99.4	99.4	99.4	99.4	99.4	99.4	99.4
Aug 2019	99.6	99.5	99.6	99.4	99.6	99.5	99.6	99.5	99.6	99.5

Height [m]	291		216		191		166		141	
Month/ Data coverage	WS [%]	WD [%]	WS [%]	WD [%]	WS [%]	WD [%]	WS [%]	WD [%]	WS [%]	WD [%]
Sep 2019	99.5	99.5	99.5	99.5	99.5	99.5	99.5	99.5	99.5	99.5
Oct 2019	99.5	99.5	99.5	99.5	99.5	99.5	99.5	99.5	99.5	99.5
Nov 2019	99.5	99.5	99.5	99.5	99.5	99.5	99.5	99.5	99.5	99.5
Dec 2019	99.7	99.7	99.7	99.6	99.7	99.6	99.7	99.6	99.6	99.6
Jan 2020	99.4	99.4	99.4	99.4	99.4	99.4	99.4	99.4	99.4	99.4
Feb 2020	99.3	99.3	99.4	99.4	99.4	99.4	99.4	99.4	99.4	99.4
Mar 2020	98.3	98.3	98.4	98.4	98.4	98.4	98.4	98.4	98.5	98.5
Apr 2020	95.1	95.1	95.6	95.4	95.7	95.7	95.9	95.9	96.1	96.1
May 2020	95.7	96.2	97.0	96.9	97.0	96.9	97.3	97.2	97.5	97.4
Jun 2020	99.0	99.0	99.1	99.1	99.1	99.1	99.2	99.1	99.3	99.3
Jul 2020	99.3	99.3	99.3	99.3	99.3	99.2	99.4	99.3	99.4	99.3
Aug 2020	99.2	99.2	99.3	99.2	99.3	99.2	99.3	99.3	99.3	99.2
Sep 2020	99.3	99.3	99.2	99.2	99.2	99.2	99.2	99.2	99.2	99.2
Oct 2020	99.1	99.1	99.1	99.1	99.1	99.1	99.1	99.1	99.1	99.1
Nov 2020	99.1	99.1	99.1	99.1	99.1	99.1	99.1	99.1	99.1	99.1
Dec 2020	99.2	99.2	99.2	99.2	99.2	99.2	99.2	99.2	99.2	99.2
Jan 2021	99.2	99.2	99.2	99.2	99.2	99.2	99.2	99.2	99.2	99.2
Feb 2021	98.3	98.3	98.3	98.3	98.3	98.3	98.4	98.4	98.7	98.7
Mar 2021	95.3	95.3	95.4	95.4	95.7	95.6	95.9	95.9	96.1	96.1
Apr 2021	86.8	86.7	87.2	87.2	87.3	87.3	87.3	87.3	87.4	87.3
May 2021	90.5	90.1	91.3	91.2	91.6	91.5	91.9	91.9	91.8	91.7
Jun 2021	96.3	96.3	96.6	96.6	96.8	96.8	96.8	96.8	96.9	96.9
Jul 2021	98.5	98.1	98.8	98.8	99.0	99.0	99.0	99.0	99.2	99.2
Aug 2021	99.3	99.3	99.3	99.3	99.3	99.3	99.3	99.3	99.3	99.3
Sep 2021	99.4	99.4	99.4	99.4	99.4	99.4	99.4	99.4	99.4	99.4
Oct 2021	99.2	99.2	99.2	99.2	99.2	99.2	99.2	99.2	99.2	99.2
Nov 2021	99.4	99.4	99.4	99.4	99.4	99.4	99.4	99.3	99.4	99.4
Dec 2021	99.5	99.5	99.5	99.5	99.5	99.5	99.5	99.5	99.5	99.5
Jan 2022	0.1	0.1	0.1	0.1	0.1	0.1	0.1	0.1	0.1	0.1

Appendix D Secondary Datasets' Overview

D.1 Lidar LEG

The table below presents an overview of the setup at the lidar LEG.

Table D.1 Lidar LEG measurement campaign overview [30], [31]

Parameter	Lidar LEG
Measurement type	Leosphere (now Vaisala) WindCube v2
Measurement period considered in the analysis	17 November 2024 to 31 December 2021
Location (latitude, longitude) [°]	51°55.502' N 3°40.106' E
Measurement averaging temporal interval [min]	10
Measurement heights (MSL) [m]	291, 266, 241, 216, 191, 166, 141, 116, 91, 63

D.2 Lidar EPL

The table below presents an overview of the setup at the lidar EPL.

Table D.2 Lidar EPL measurement campaign overview [26] [33]

Parameter	Lidar EPL
Measurement type	ZephIR ZX 300
Measurement period considered in the analysis	01 July 2016 to 01 January 2022
Location (latitude, longitude) [°]	51°59.875' N 3°16.489' E
Measurement averaging temporal interval [min]	10
Measurement heights (MSL) [m]	291, 266, 241, 216, 191, 166, 141, 116, 91, 63

D.3 FLS HKN

The table below presents an overview of the setup at the FLS HKN. The measurement campaign at this location consisted of two FLS (FLS HKN A, FLS HKN B), deployed a small distance apart (< 2km) for redundancy purposes. They were considered as two separate datasets in the mesoscale validation.

Table D.3 FLS HKN measurement campaign overview [34] [35]

Parameter	FLS HKN A	FLS HKN B
Measurement type	ZephIR 300s	ZephIR 300s
Measurement period considered in the analysis	10 April 2017 to 11 April 2019	10 April 2017 to 11 April 2019

Parameter	FLS HKN A	FLS HKN B
Location (latitude, longitude) [°]	52°41.239' N 4°14.532' E	52°40.98' N 4°14.52' E
Measurement averaging temporal interval [min]	10	10
Measurement heights (MSL) [m]	200, 180, 160, 140, 120, 100, 80, 60, 40 and 30	200, 180, 160, 140, 120, 100, 80, 60, 40 and 30

D.4 FLS HKZ

The table below presents an overview of the setup at the FLS HKZ. The measurement campaign at this location consisted of two FLS (FLS HKZ A, FLS HKZ B), deployed a small distance apart (< 2km) for redundancy purposes. They were considered as two separate datasets in the mesoscale validation.

Table D.4 FLS HKZ measurement campaign overview [13], [36]

Parameter	FLS HKZ A	FLS HKZ B
Measurement type	ZephIR 300s	ZephIR 300s
Measurement period considered in the analysis	05 June 2016 to 05 June 2018	05 June 2016 to 05 June 2018
Location (latitude, longitude) [°]	52°18.42' N 4°0.541' E	52°17.346' N 4°0.516' E
Measurement averaging temporal interval [min]	10	10
Measurement heights (MSL) [m]*	200, 180, 160, 140, 120, 100, 80, 60, 40 and 30	200, 180, 160, 140, 120, 100, 80, 60, 40 and 30

* It is unclear from the documentation whether the reference height is MSL or LAT. It is assumed to be MSL for the purpose of this study.

D.5 FLS TNW

The table below presents an overview of the setup at the FLS HKZ. The measurement campaign at this location consisted of two FLS (FLS TNW A, FLS TNW B), deployed a small distance apart (< 2km) for redundancy purposes. One of the measurement locations was relocated a short distance away from the original position during the measurement campaign (FLS TNW A-2), effectively resulting in three measurement locations. The datasets were combined into a single dataset to maximise data coverage. The singular combined dataset was applied in the mesoscale validation.

Table D.5 FLS TNW measurement campaign overview [37], [38]

Parameter	FLS TNW A	FLS TNW A-2	FLS TNW B
Measurement type	ZephIR ZX 300 CW	ZephIR ZX 300 CW	ZephIR ZX 300 CW
Measurement period considered in the analysis	19 June 2019 to 31 December 2020	16 January 2021 to 20 June 2021	19 June 2019 to 20 June 2021
Location (latitude, longitude) [°]	54°1.09' N 5°33.015' E	54°1.094' N 5°33.831' E	54°1.305' N 5°32.994' E

Parameter	FLS TNW A	FLS TNW A-2	FLS TNW B
Measurement averaging temporal interval [min]	10	10	10
Measurement heights (LAT) [m]	250, 200, 180, 160, 140, 120, 100, 80, 60, 40 and 30	250, 200, 180, 160, 140, 120, 100, 80, 60, 40 and 30	250, 200, 180, 160, 140, 120, 100, 80, 60, 40 and 30

D.6 MM OWEZ

The table below presents an overview of the setup at the MM OWEZ.

Table D.6 MM OWEZ measurement campaign overview [11], [36]

Parameter	MM OWEZ
Measurement type	Lattice met mast
Measurement period considered in the analysis	01 July 2005 to 02 July 2006
Location (latitude, longitude) [°]	52°36.381' N 4°23.378' E
Measurement averaging temporal interval [min]	10
Measurement heights cup anemometers (MSL) [m]	116, 70 and 21

D.7 FLS Borssele

The table below presents an overview of the setup at the FLS Borssele. The measurement campaign at this location consisted of two FLS (FLS Borssele 1, FLS Borssele 2), deployed some distance apart. Only one of the datasets was applied in the mesoscale validation, FLS Borssele 1.

Table D.7 FLS Borssele measurement campaign overview [37], [39]

Parameter	FLS Borssele 1
Measurement type	ZephIR 300s
Measurement period considered in the analysis	12 February 2016 to 27 February 2017
Location (latitude, longitude) [°]	51°42.414' N 3°2.077' E
Measurement averaging temporal interval [min]	10
Measurement heights (MSL) [m]*	250, 200, 180, 160, 140, 120, 100, 80, 60, 40 and 30

* It is unclear from the documentation whether the reference height is MSL or LAT. It is assumed to be MSL for the purpose of this study.

D.8 FLS N-7.2

The table below presents an overview of the setup at the FLS N-7.2.

Table D.8 FLS N-7.2 measurement campaign overview [40]

Parameter	FLS N-7.2
Measurement type	ZephIR 300 M
Measurement period considered in the analysis	20 May 2020 to 04 May 2021
Location (latitude, longitude) [°]	54°17.34' N 6°13.321' E
Measurement averaging temporal interval [min]	10
Measurement heights (LAT) [m]	250, 200, 160, 140, 120, 100, 80, 60 and 42

D.9 MM FINO1

The table below presents an overview of the setup at the MM FINO1.

Table D.9 MM FINO1 measurement campaign overview [41]

Parameter	MM FINO1
Measurement type	Lattice met mast
Measurement period considered in the analysis	01 February 2004 to 31 December 2008
Location (latitude, longitude) [°]	54°0.892' N 6°35.259' E
Measurement averaging temporal interval [min]	10
Measurement heights with cup anemometers (LAT) [m]	102.5, 91.6, 81.6, 71.6, 61.6, 51.6, 41.6 and 34.1

Appendix E Trend Analysis for MCP ERA5 Long-Term Period

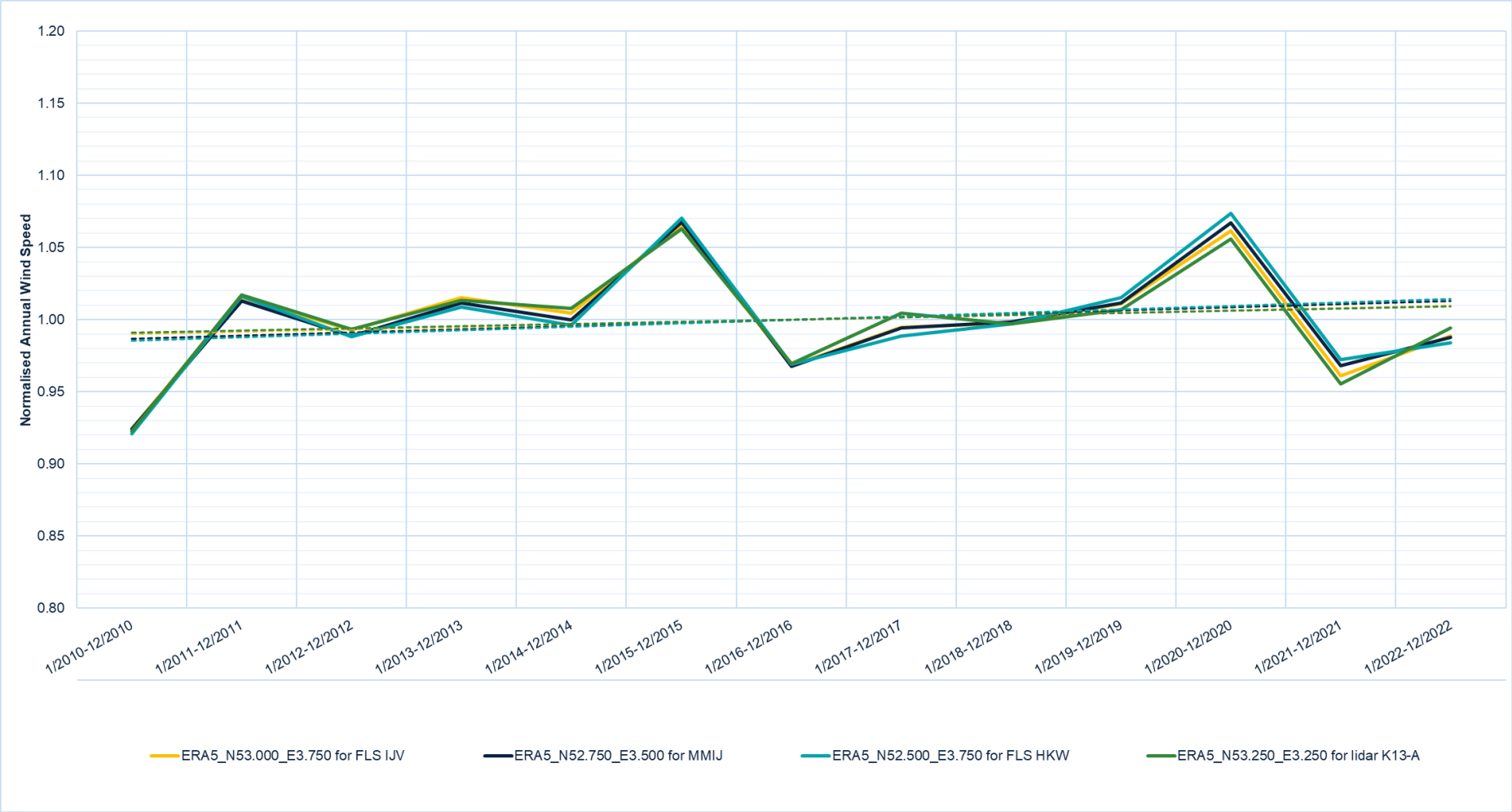

Figure E.12 Long-term trend analysis

Appendix F Long-Term Correction Plots

F.1 Sector-wise wind speed correlations

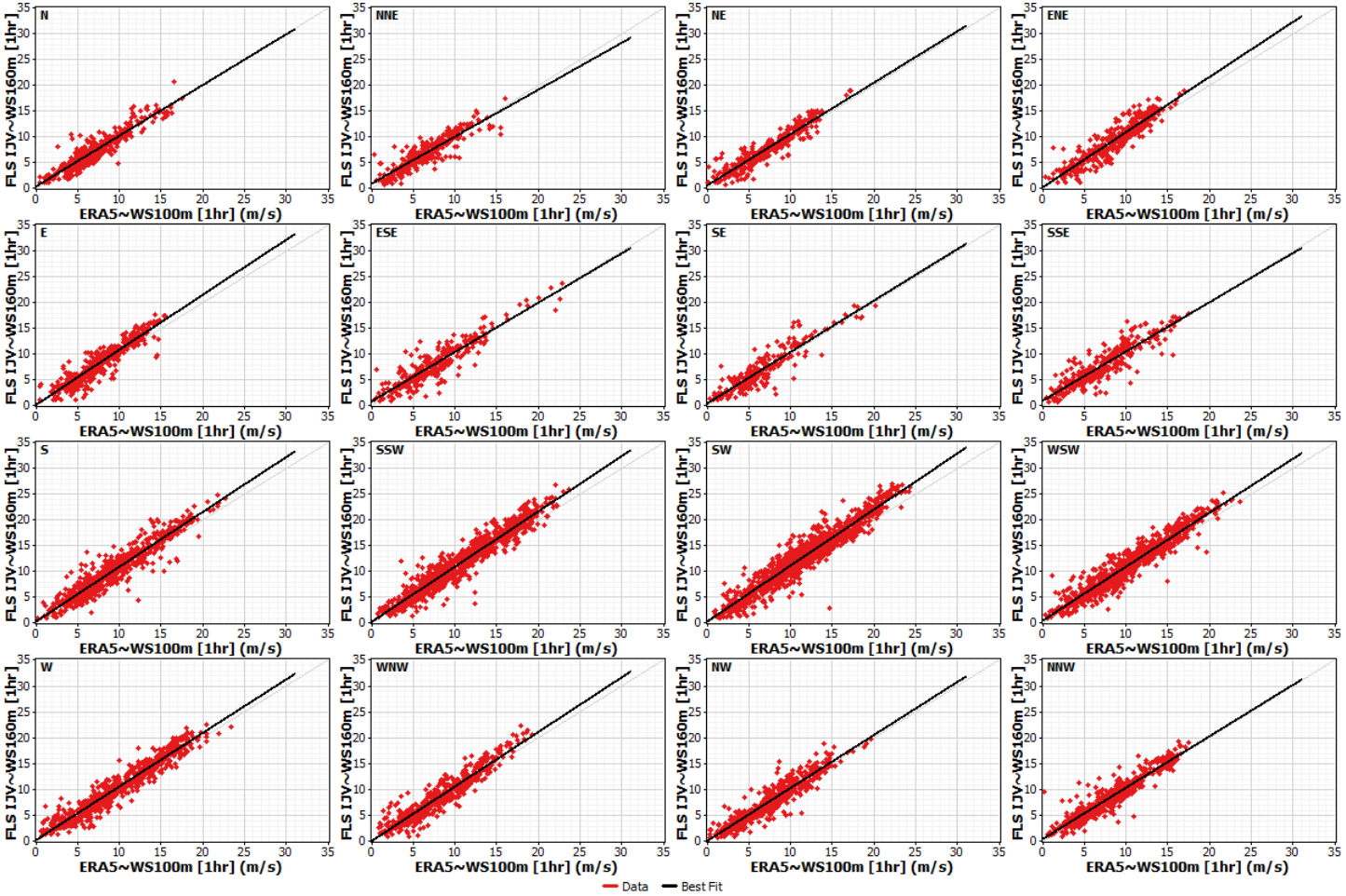

Figure F.1 FLS IJV: long-term correction wind speed scatter plots

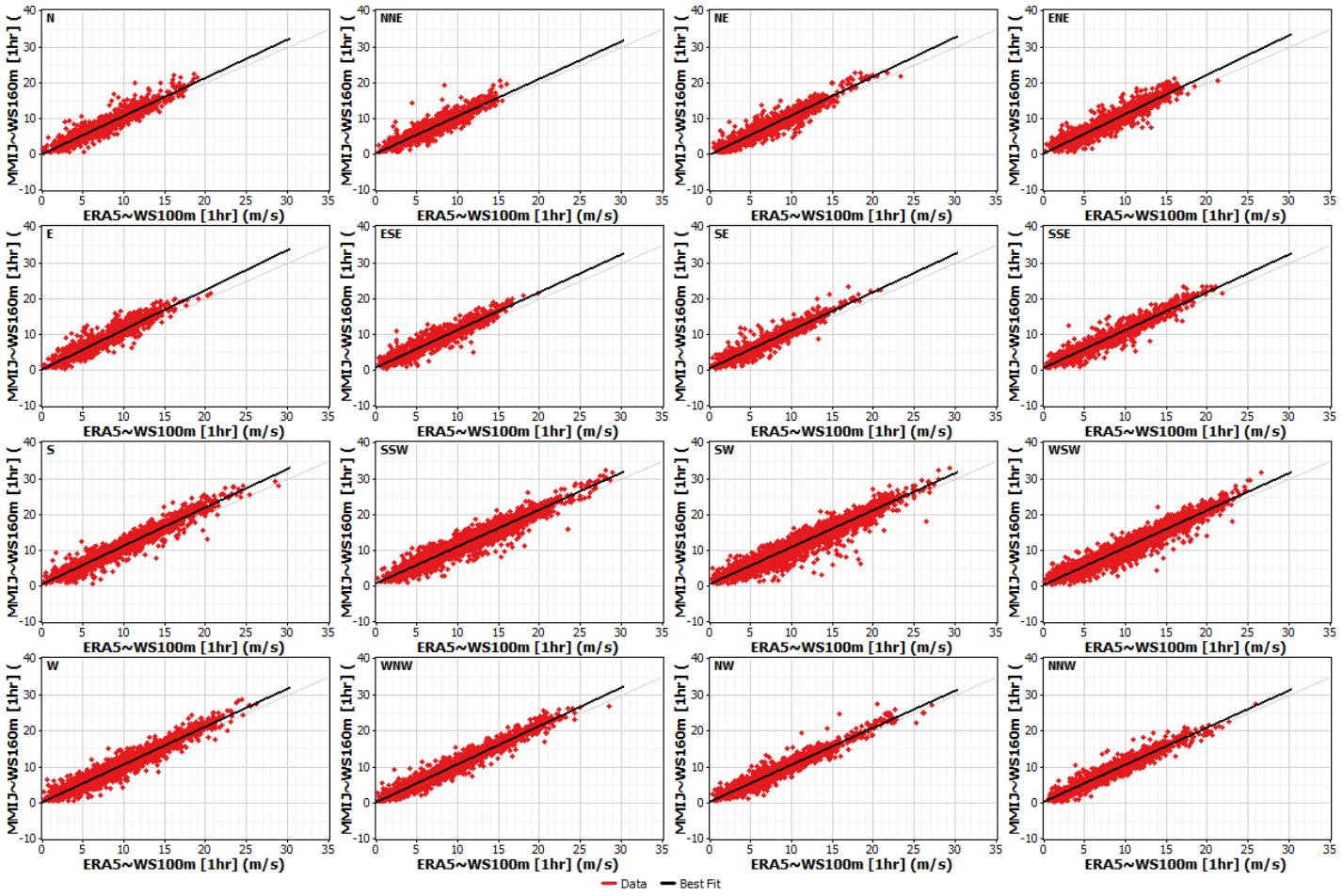

Figure F.2 MMIJ: long-term correction wind speed scatter plots

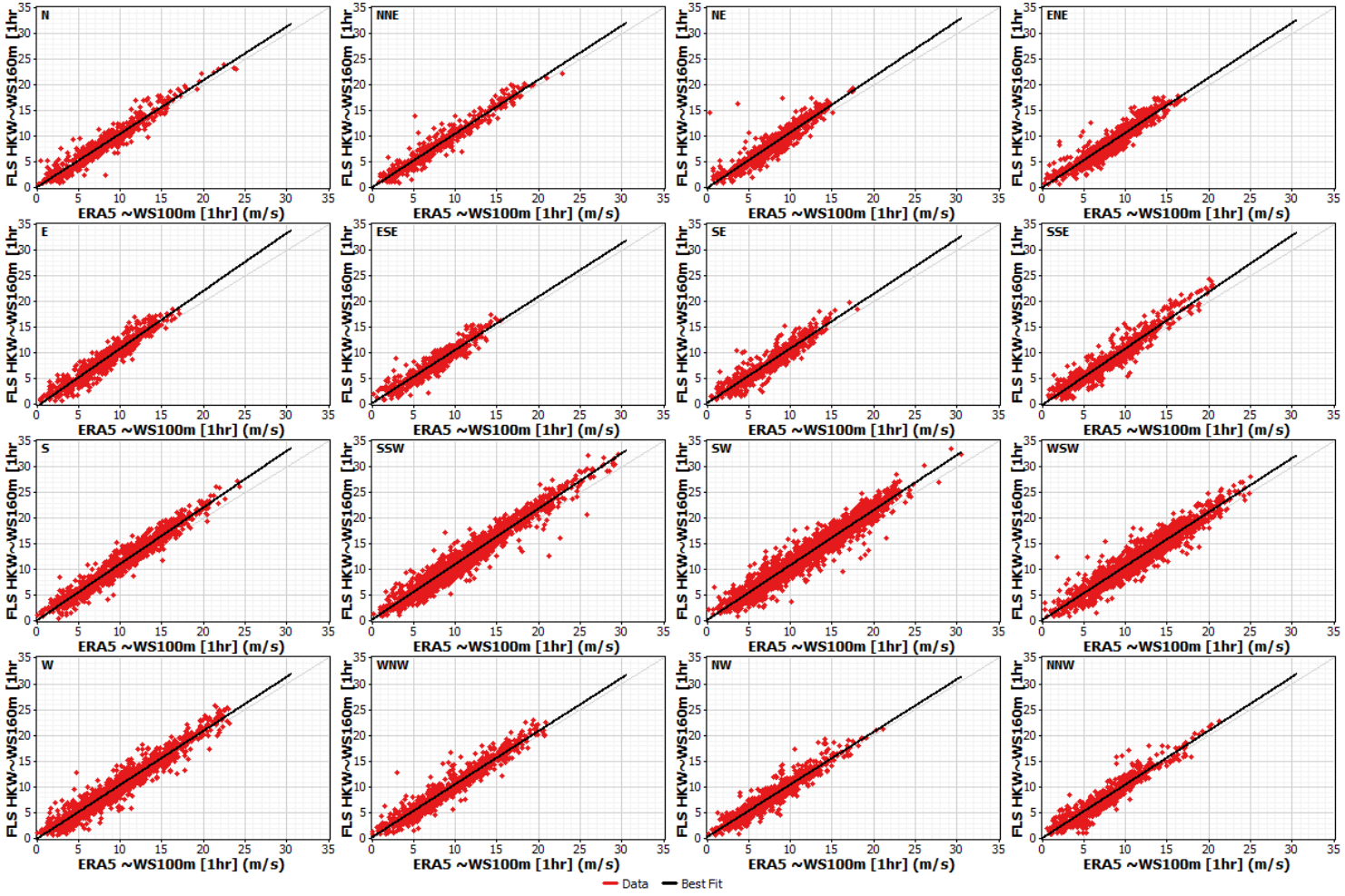

Figure F.3 FLS HKW: long-term correction wind speed scatter plots

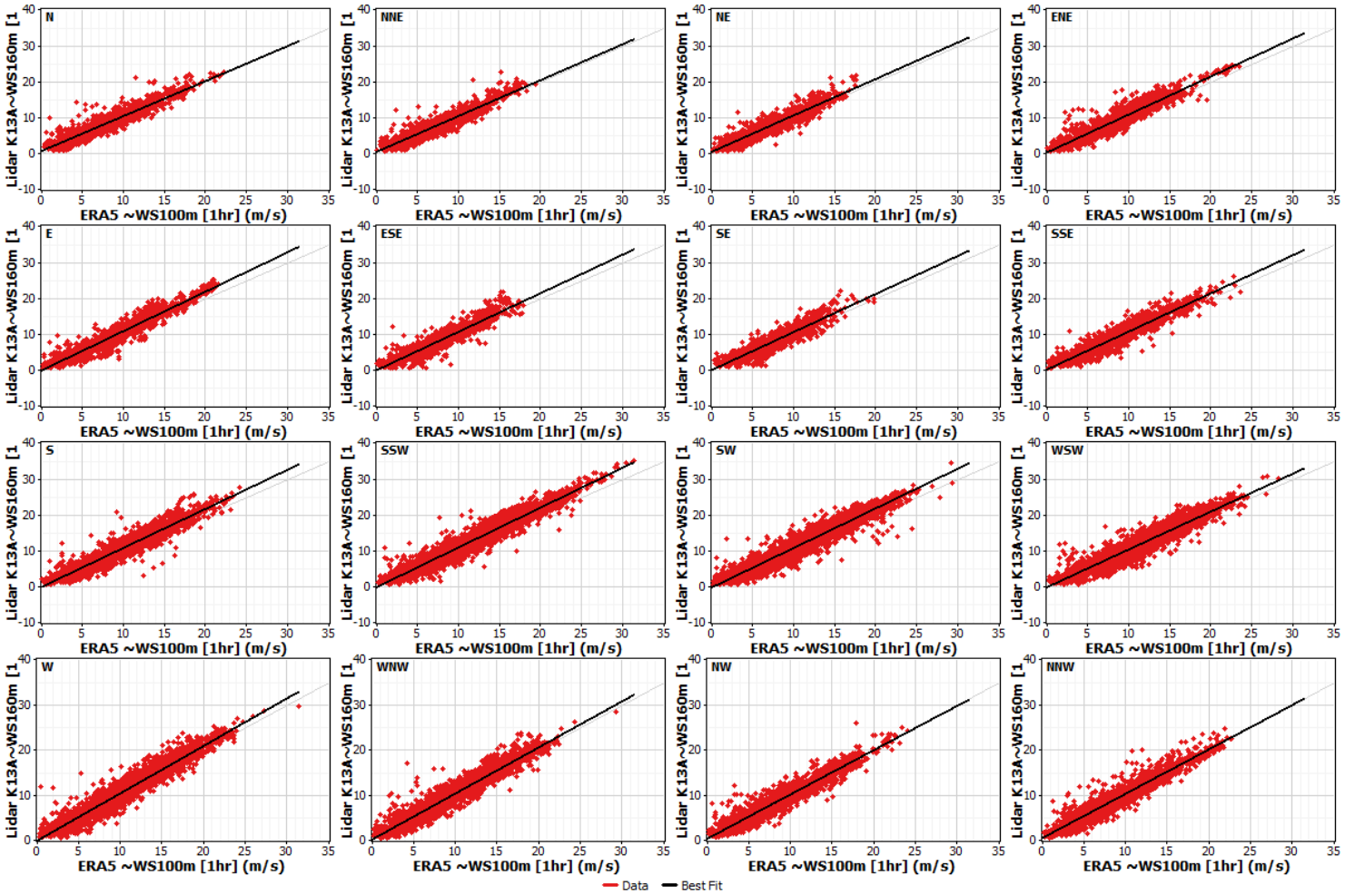

Figure F.4 Lidar K13-A: long-term correction wind speed scatter plots

F.2 Wind direction scatter plots

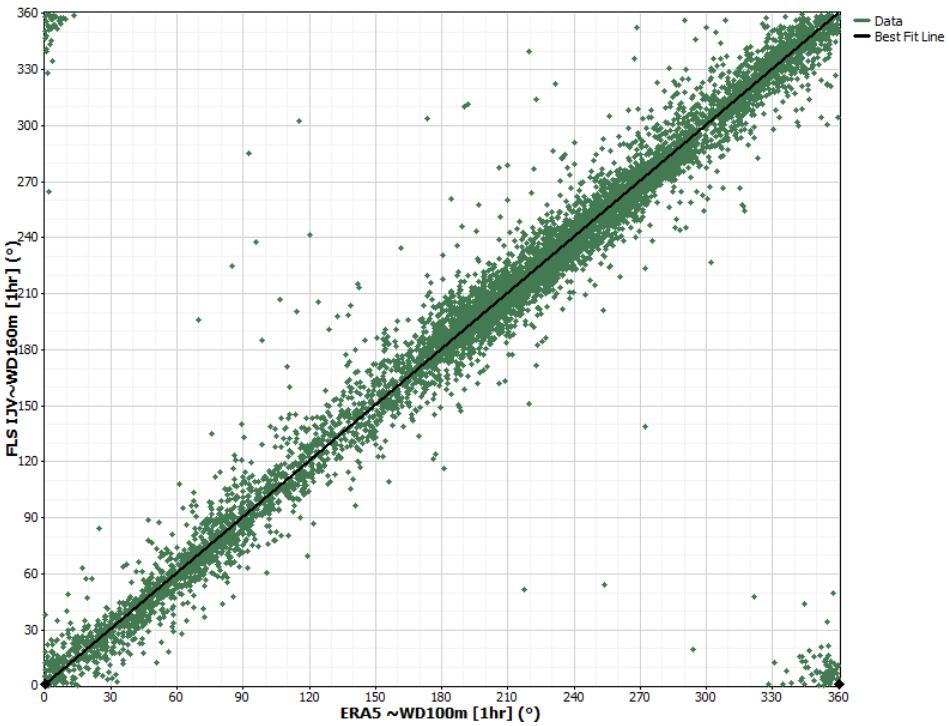

Figure F.5 FLS HKW: long-term correction wind speed scatter plots

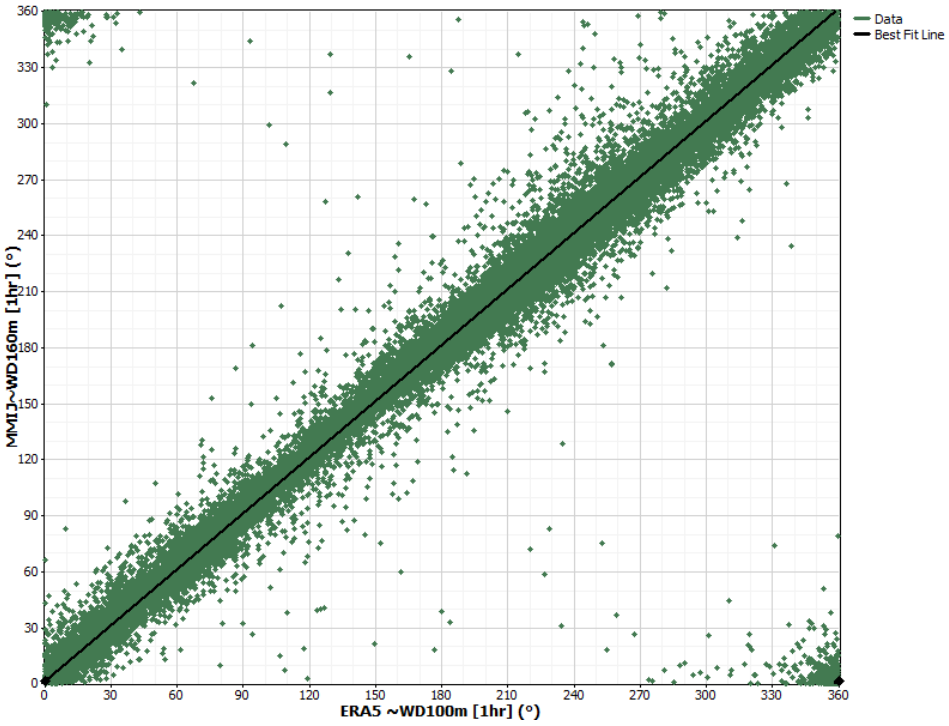

Figure F.6 MMIJ: long-term correction wind speed scatter plots

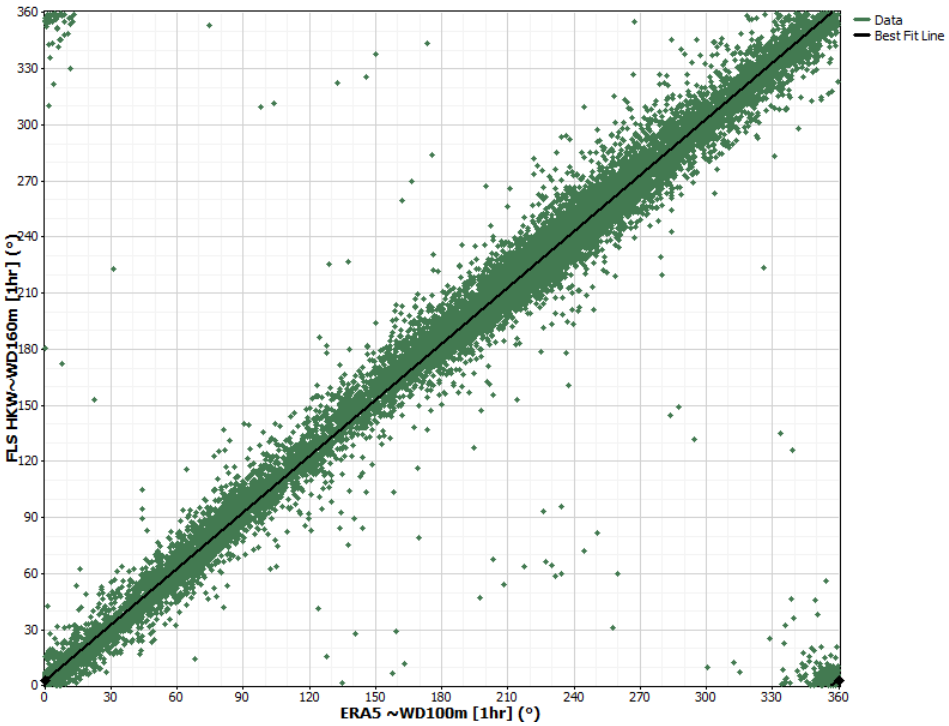

Figure F.7 FLS HKW: long-term correction wind speed scatter plots

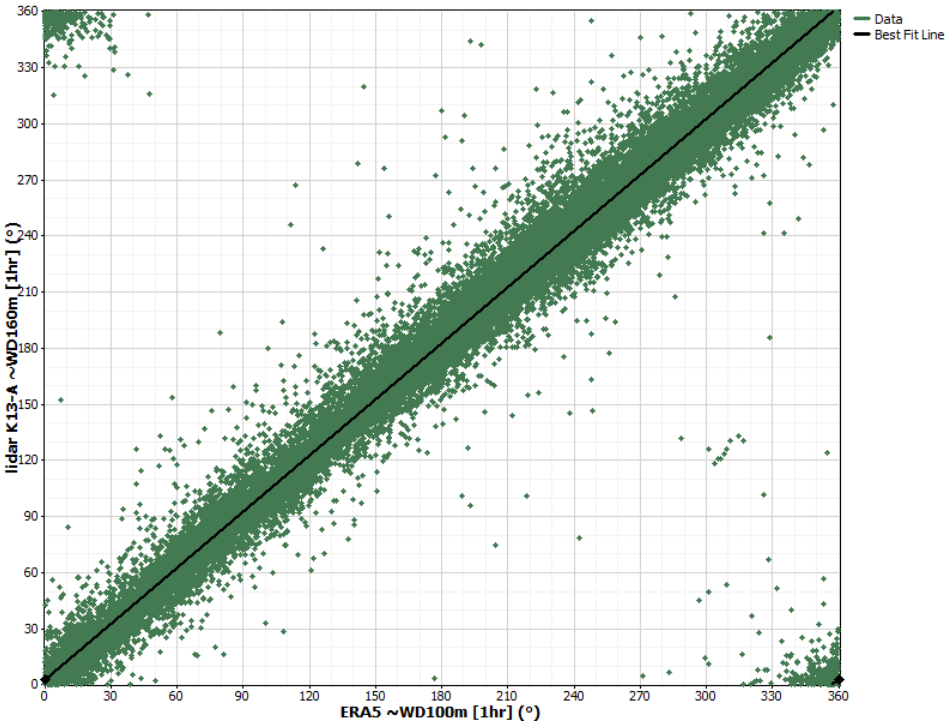

Figure F.8 Lidar K13-A: long-term correction wind speed scatter plots

Appendix G Overview of the Mesoscale/Global Datasets

G.1 EMD-WRF Europe+

The EMD-WRF Europe+ (ERA5) dataset (or short, 'EMD-EUR+') is the high-resolution mesoscale dataset covering Europe. The mesoscale dataset is based upon ECMWF (http:/www.ecmwf.int) reanalysis data from ERA5 as its boundary conditions. 'EMD-WRF Europe+ (ERA5)' is provided by EMD. The model domain of EMD-WRF Europe+ is shown in Figure G.1.

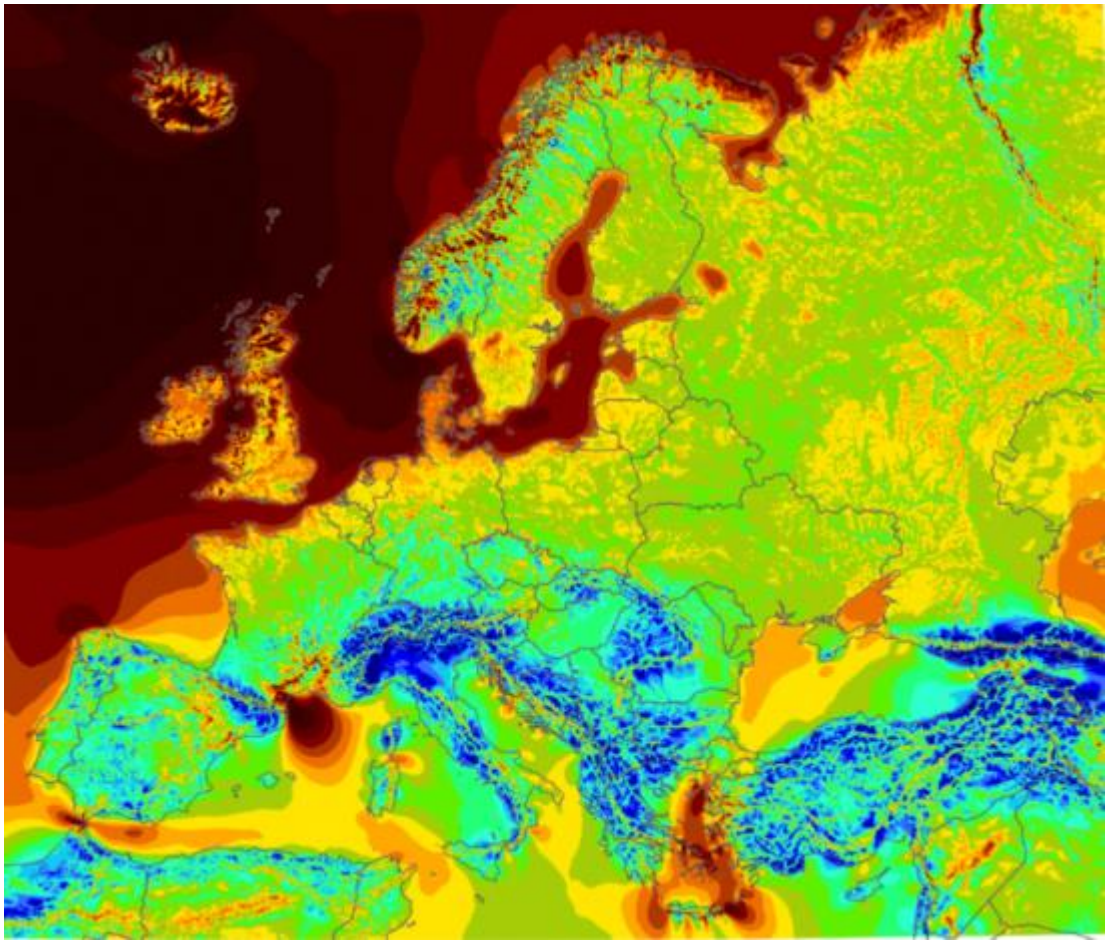

Figure G.1 EMD-WRF Europe+ Model Domain [48]

EMD-EUR+ is based on the global reanalysis model ERA5 and a WRF modelling system that is significantly improved and optimized compared to the one used for EMD ConWx. A detailed validated study conducted by EMD gives an overview of the EMD-EUR+ dataset (Section 1) and a comprehensive analysis of the EMD-EUR+ data as opposed to alternative data sets (Section 2) [52].

G.2 DOWA

The Dutch Offshore Wind Atlas (DOWA) is a wind atlas covering a period of 11 years, from 2008 until and including 2018. Regional numerical weather model HARMONIE and additional satellite and aircraft measurements were used to downscale the global re-analysis ERA5 to a dataset of hourly information on a 2.5 by 2.5 km grid spacing and up to 600 m height [87].

The DOWA is the successor of the KNMI North Sea Wind (KNW) atlas. Both the DOWA and the KNW-atlas are a “downscaled” global re-analysis, but they are made with improved versions of the models and in a fundamentally different way.

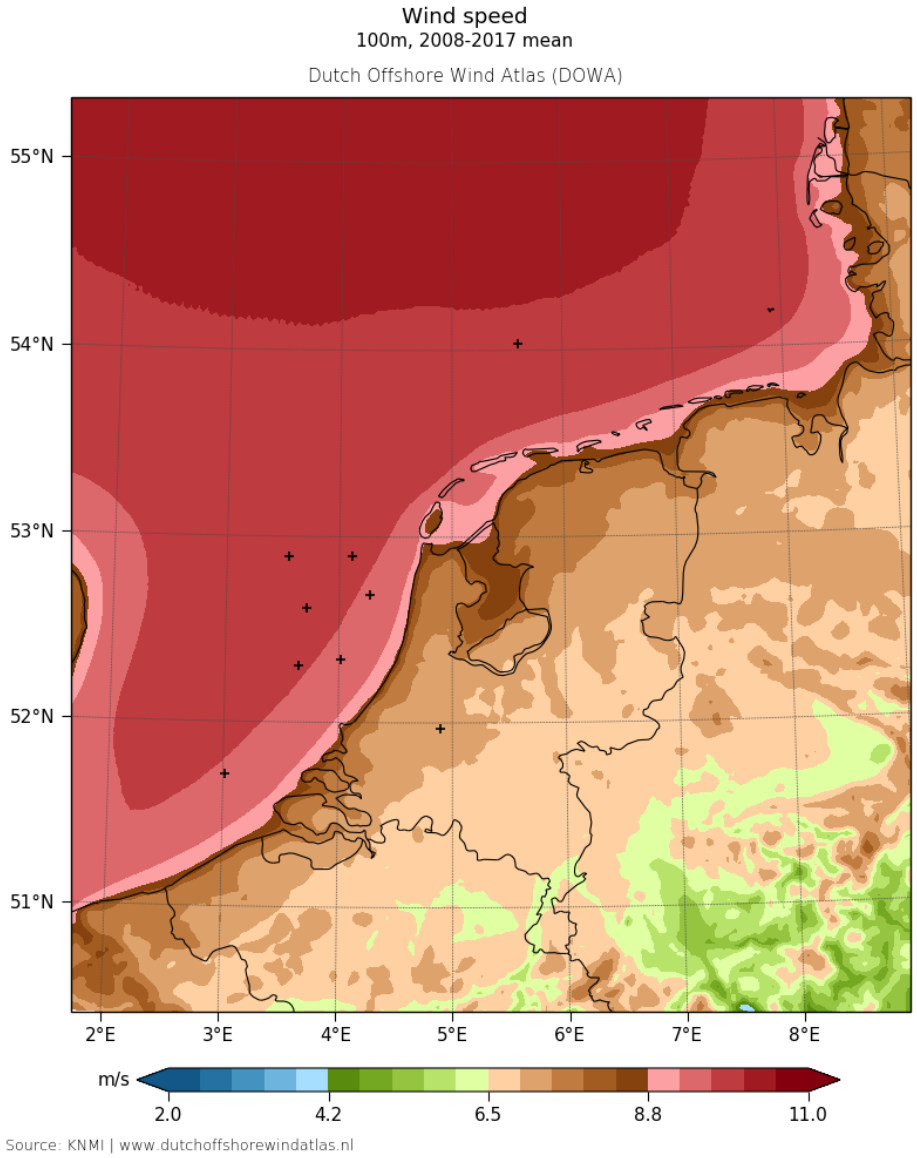

Figure G.2 10-year (2008 – 2017) average wind speed at 100 m height [87]

Making the Dutch Offshore Wind Atlas (DOWA) was part of the DOWA-project. The DOWA project is executed by the project partners ECN part of TNO, Whiffle and KNMI and supported by Topsector Energy subsidy from the Ministry of Economic Affairs and Climate Policy (SDE+ Hernieuwbare Energie Call). Information on the project can be found on the DOWA website: (https://www.dutchoffshorewindatlas.nl/about-the-atlas).

G.3 KNW

The KNW-atlas is a 4D wind atlas based on the ERA-Interim reanalyses dataset which captures 35 years (1979-2013) of meteorological measurements and generates every 6 hours 3D fields on a horizontal grid of 80 km which are consistent with these measurements and the laws of physics. This dataset is "downscaled" using the state-of-the-art weather forecasting model HARMONIE which generates hourly data on a horizontal grid of 2.5 km. The wind speeds were then tuned to match the measurements made at KNMI's 200 m tall meteorological mast at Cabauw by increasing the vertical shear of the horizontal wind speed by 15%. The same wind shear correction factor was applied uniformly throughout the whole KNW-atlas domain and period. The result is a high-resolution dataset of 35 years: the KNW-atlas [88].

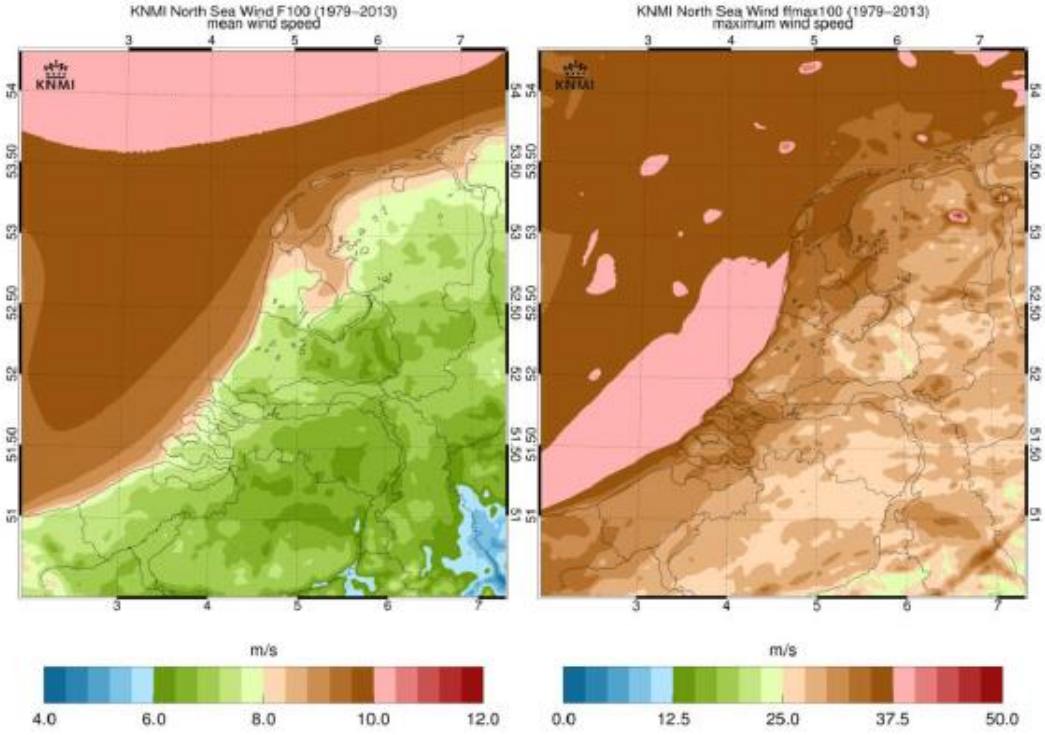

Figure G.3 Example of the average (left) and maximum (right) wind speed at 100 m for the whole KNW domain and the whole 35-year period [88]

G.4 ERA5

ERA5 was generated using 4D-Var data assimilation in CY41R2 of ECMWF's Integrated Forecast System (IFS), with a vertical level of 137 hybrid sigma/pressure (model) and a top level of 0.01 hPa. At these levels, atmospheric data are available, and they are also interpolated to 37 pressure levels, 16 potential temperature levels, and 1 potential vorticity level. Both satellite and in-situ observations are used as input into ERA5. ERA5 benefits from a decade of developments related to ERA-Interim in model physics, core dynamics, and data assimilation. An assimilation diagram for ERA5 is shown in Figure G.4 [51].

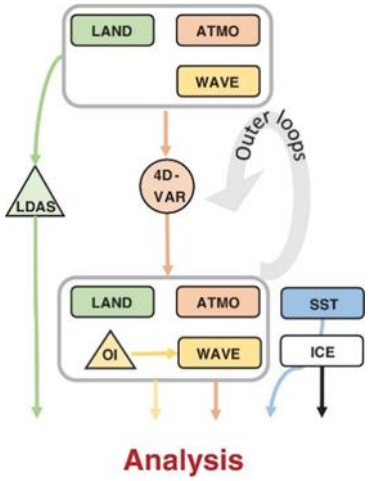

Figure G.4 Assimilation diagram for ERA5 [51]

ERA5 superseded ERA-I with a better capacity to use several important types of observational data. An overview of the conventional observations for ERA5 is shown in Figure G.5 [51].

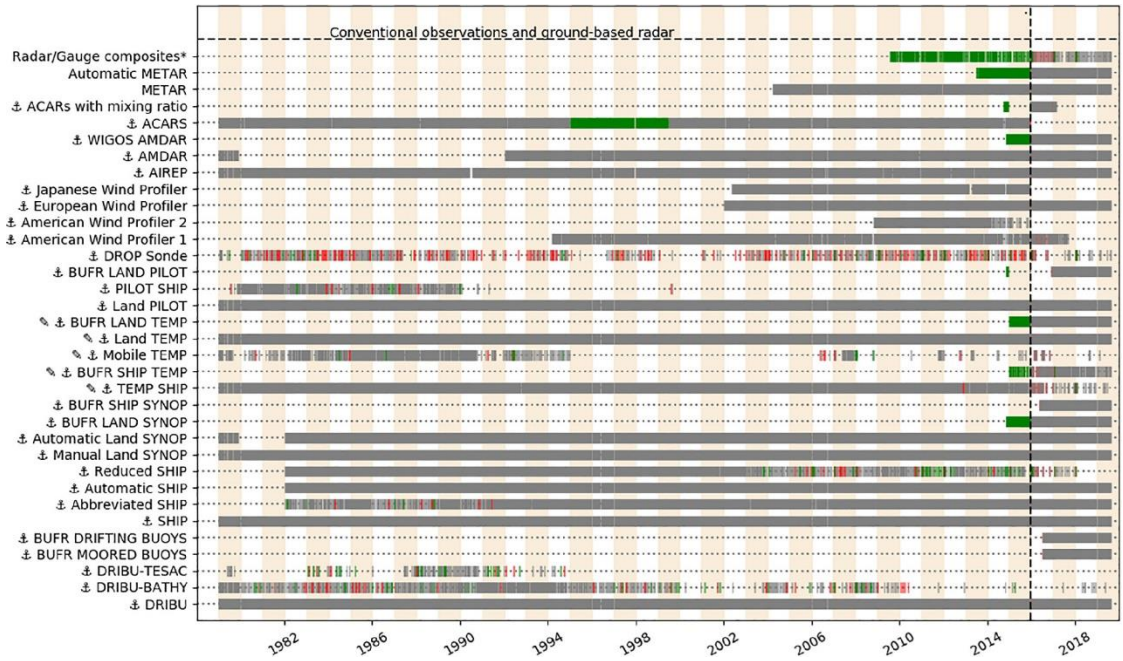

Figure G.5 Conventional observations ERA5

G.5 MERRA2

The Research and Applications Modern-Era Retrospective Analysis, Version 2 (MERRA-2) provides data that began in 1980. MERRA-2 was introduced to supersede the original MERRA dataset due to the advances made in the assimilation system that allow the assimilation of modern hyperspectral radiance and microwave observations together with GPS-Radio Occultation data sets. [53]

MERRA-2 assimilates observation forms which are not applicable to its predecessor, MERRA, and provides improvements to the Goddard Earth Observing System (GEOS) model and analysis scheme to provide a viable ongoing climate study beyond the terminus of MERRA. An overview of the observations for MERRA-2 is shown in Figure G.6.

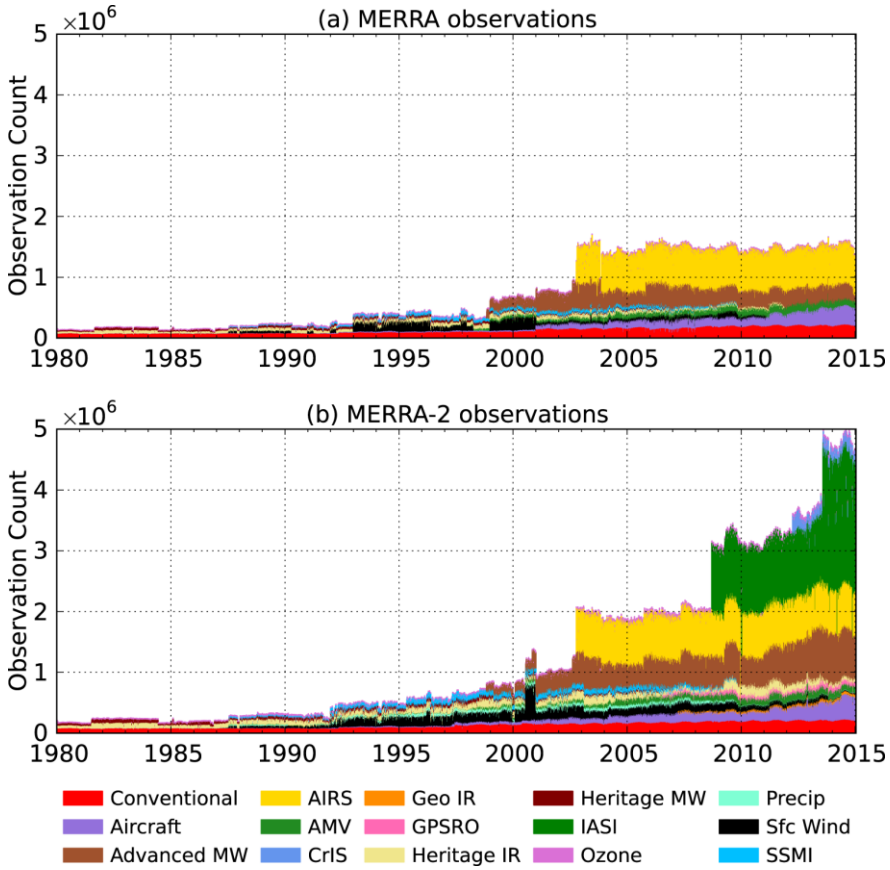

Figure G.6 MERRA-2 observations [53]

Appendix H Nodal Locations of Modelled Datasets

Table H.1 Nodal locations of modelled datasets closest to each primary measurement location

Modelled data source	Node closest to: [Latitude, Longitude]			
	FLS IJV	MMIJ	FLS HKW	Lidar K13-A
EMD-WRF Europe+	52.883°N, 3.683°E	52.851°N, 3.418°E	52.557°N, 3.743°E	53.213°N, 3.204°E
KNW	52.887°N, 3.677°E	52.845°N, 3.452°E	52.571°N, 3.738°E	53.207°N, 3.201°E
DOWA	52.956°N, 3.703°E	52.897°N, 3.437°E	52.617°N, 3.749°E	53.263°N, 3.203°E
Unified-WRF	52.894°N, 3.685°E	52.848°N, 3.436°E	52.57°N, 3.727°E	53.218°N, 3.219°E

Appendix I Trend Analysis for Unified-WRF Long-Term Period

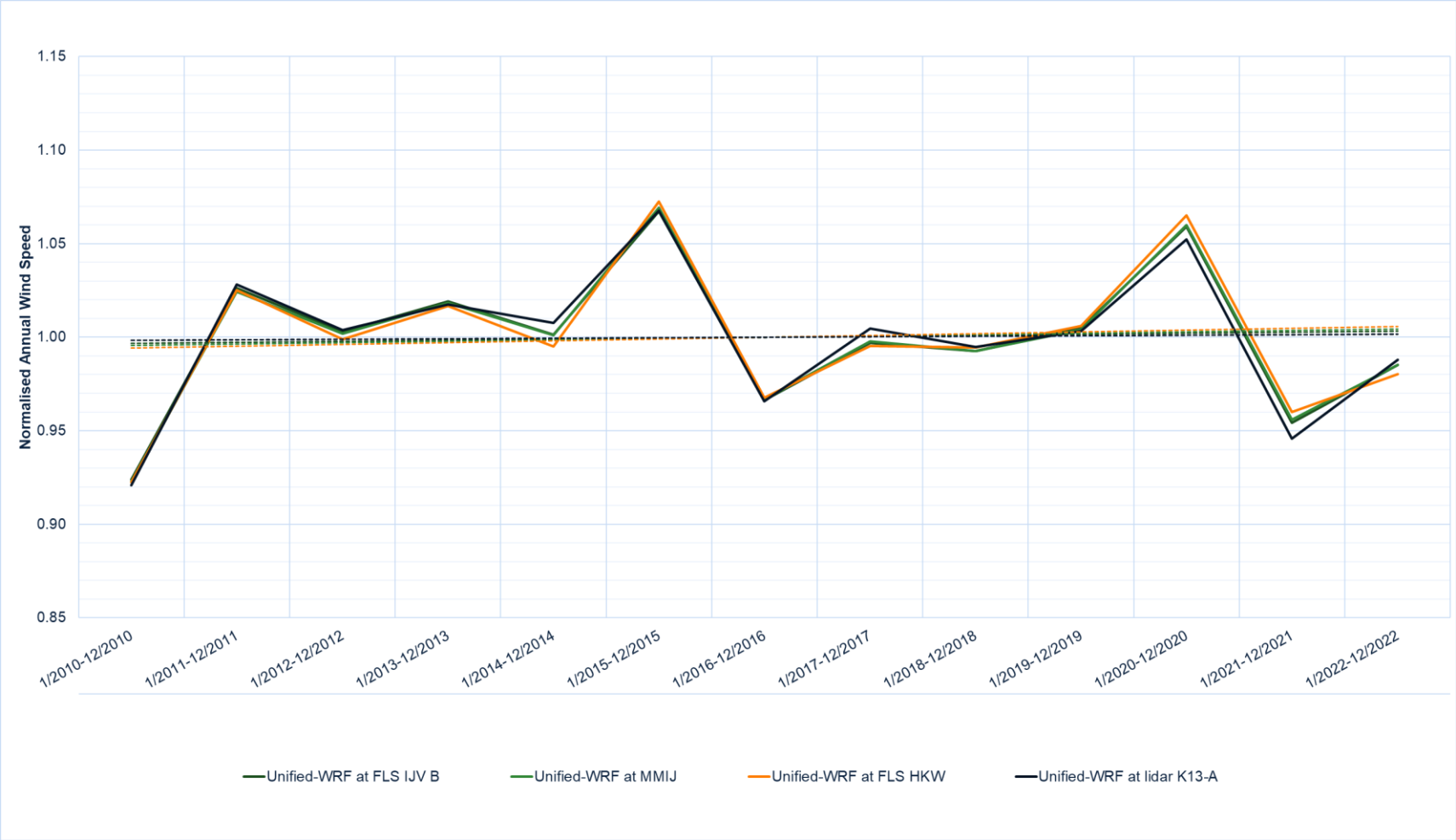

Figure I.1 Unified-WRF long-term trend analysis

Appendix J Long-Term Sectorwise Weibull Parameters

J.1 N1_Alpha1 sectorwise Weibull parameters

Table J.1 N1 sectorwise Weibull A at various heights

Height [m] / Sector	300	250	200	160	140	120	100	60	30	10
N	9.71	9.76	9.72	9.63	9.61	9.56	9.45	9.11	8.66	8.00
NNE	9.08	9.06	9.01	8.96	8.91	8.84	8.72	8.43	8.01	7.40
NE	9.26	9.33	9.41	9.41	9.41	9.37	9.36	9.11	8.59	7.84
ENE	10.04	10.17	10.20	10.13	10.05	9.95	9.82	9.38	8.76	7.95
E	10.57	10.57	10.51	10.42	10.42	10.30	10.13	9.62	9.03	8.23
ESE	9.86	9.88	9.87	9.74	9.65	9.53	9.35	8.86	8.34	7.61
SE	9.70	9.58	9.60	9.61	9.55	9.48	9.38	8.96	8.40	7.62
SSE	10.09	10.21	10.17	10.01	9.93	9.81	9.69	9.30	8.75	7.94
S	11.82	11.80	11.69	11.57	11.48	11.35	11.19	10.66	10.01	9.06
SSW	13.58	13.50	13.32	13.11	12.96	12.77	12.53	11.88	11.12	10.03
SW	14.74	14.54	14.28	13.93	13.73	13.47	13.14	12.40	11.56	10.43
WSW	13.76	13.57	13.27	12.96	12.77	12.57	12.32	11.73	11.08	10.08
W	12.85	12.68	12.43	12.25	12.15	12.03	11.85	11.43	10.83	9.91
WNW	11.64	11.50	11.31	11.12	11.03	10.92	10.76	10.32	9.83	9.04
NW	10.65	10.58	10.49	10.41	10.35	10.26	10.16	9.88	9.41	8.70
NNW	10.41	10.35	10.28	10.18	10.12	10.05	9.91	9.56	9.11	8.41

Table J.2 N1 sectorwise Weibull k at various heights

Height [m] / Sector	300	250	200	160	140	120	100	60	30	10
N	2.190	2.211	2.238	2.259	2.278	2.298	2.317	2.352	2.380	2.453
NNE	2.164	2.206	2.258	2.292	2.306	2.312	2.313	2.312	2.339	2.389
NE	2.174	2.216	2.266	2.297	2.312	2.327	2.358	2.425	2.471	2.517
ENE	2.237	2.270	2.293	2.321	2.331	2.356	2.377	2.431	2.422	2.426
E	2.128	2.146	2.170	2.180	2.203	2.209	2.223	2.208	2.196	2.199
ESE	2.113	2.113	2.145	2.183	2.207	2.249	2.266	2.289	2.282	2.270
SE	1.976	2.009	2.077	2.142	2.143	2.154	2.177	2.219	2.222	2.210
SSE	1.960	1.994	2.027	2.037	2.059	2.077	2.089	2.099	2.078	2.069
S	1.897	1.944	1.990	2.039	2.064	2.083	2.103	2.114	2.108	2.129
SSW	1.966	2.020	2.081	2.141	2.168	2.192	2.214	2.241	2.241	2.267
SW	2.212	2.265	2.327	2.361	2.380	2.382	2.382	2.368	2.369	2.418
WSW	2.141	2.183	2.220	2.245	2.253	2.262	2.271	2.280	2.298	2.355
W	2.127	2.148	2.148	2.156	2.162	2.166	2.155	2.164	2.170	2.224
WNW	2.069	2.084	2.087	2.084	2.090	2.094	2.102	2.113	2.147	2.209
NW	2.096	2.114	2.131	2.144	2.144	2.142	2.142	2.152	2.161	2.230
NNW	2.114	2.126	2.144	2.151	2.158	2.160	2.166	2.175	2.206	2.279

J.2 N2_Alpha2 sectorwise Weibull parameters

Table J.3 N2 sectorwise Weibull A at various heights

Height [m] / Sector	300	250	200	160	140	120	100	60	30	10
N	9.73	9.75	9.75	9.69	9.67	9.59	9.45	9.10	8.62	7.97
NNE	9.10	9.11	9.07	9.02	8.96	8.89	8.75	8.40	7.98	7.38
NE	9.20	9.28	9.38	9.41	9.42	9.38	9.38	9.21	8.69	7.93
ENE	10.20	10.36	10.40	10.36	10.30	10.21	10.10	9.60	8.93	8.07
E	10.52	10.54	10.50	10.50	10.45	10.34	10.14	9.56	8.95	8.13
ESE	9.97	10.04	9.98	9.83	9.74	9.61	9.43	8.95	8.33	7.54
SE	9.79	9.74	9.77	9.74	9.74	9.69	9.58	9.10	8.52	7.67
SSE	10.21	10.32	10.31	10.18	10.09	9.94	9.79	9.31	8.65	7.81
S	11.91	11.93	11.84	11.69	11.59	11.43	11.21	10.64	9.93	8.93
SSW	13.46	13.44	13.35	13.12	12.97	12.74	12.47	11.75	10.93	9.85
SW	14.80	14.68	14.45	14.13	13.94	13.68	13.33	12.53	11.69	10.56
WSW	13.83	13.67	13.38	13.06	12.87	12.66	12.41	11.78	11.14	10.16
W	12.88	12.68	12.48	12.28	12.15	12.00	11.81	11.30	10.71	9.81
WNW	11.64	11.52	11.31	11.11	11.00	10.89	10.65	10.16	9.68	8.91
NW	10.54	10.48	10.40	10.31	10.26	10.18	10.08	9.80	9.35	8.64
NNW	10.45	10.37	10.31	10.19	10.13	10.05	9.90	9.54	9.08	8.40

Table J.4 N2 sectorwise Weibull k at various heights

Height [m] / Sector	300	250	200	160	140	120	100	60	30	10
N	2.136	2.147	2.176	2.188	2.204	2.203	2.214	2.235	2.250	2.325
NNE	2.104	2.171	2.230	2.287	2.291	2.286	2.276	2.228	2.255	2.328
NE	2.138	2.194	2.260	2.318	2.344	2.373	2.428	2.543	2.580	2.590
ENE	2.284	2.325	2.368	2.442	2.464	2.499	2.533	2.587	2.539	2.488
E	2.066	2.097	2.121	2.166	2.170	2.171	2.171	2.129	2.087	2.071
ESE	2.151	2.167	2.177	2.206	2.239	2.291	2.318	2.364	2.243	2.168
SE	2.008	2.096	2.203	2.277	2.303	2.324	2.352	2.358	2.328	2.249
SSE	2.048	2.078	2.115	2.136	2.145	2.149	2.144	2.090	1.986	1.954
S	1.913	1.989	2.046	2.085	2.101	2.106	2.095	2.068	2.021	2.000
SSW	1.929	2.003	2.094	2.151	2.179	2.180	2.182	2.161	2.112	2.134
SW	2.224	2.311	2.398	2.441	2.463	2.456	2.445	2.405	2.399	2.459
WSW	2.175	2.244	2.293	2.314	2.316	2.311	2.321	2.307	2.336	2.407
W	2.147	2.160	2.168	2.169	2.161	2.149	2.130	2.092	2.086	2.149
WNW	2.039	2.060	2.069	2.059	2.056	2.052	2.031	2.025	2.048	2.120
NW	1.996	2.016	2.029	2.041	2.048	2.043	2.043	2.055	2.070	2.140
NNW	2.076	2.087	2.111	2.109	2.104	2.105	2.100	2.129	2.142	2.221

J.3 N3_Beta1 sectorwise Weibull parameters

Table J.5 N3 sectorwise Weibull A at various heights

Height [m] / Sector	300	250	200	160	140	120	100	60	30	10
N	9.67	9.69	9.65	9.56	9.50	9.43	9.32	9.05	8.59	7.96
NNE	8.91	8.92	8.92	8.91	8.87	8.80	8.63	8.30	7.88	7.29
NE	9.20	9.29	9.37	9.37	9.39	9.39	9.40	9.21	8.71	7.94
ENE	10.13	10.24	10.31	10.25	10.21	10.12	10.00	9.55	8.88	8.02
E	10.49	10.51	10.43	10.35	10.33	10.22	10.05	9.52	8.90	8.13
ESE	10.00	10.03	9.96	9.89	9.81	9.69	9.52	9.04	8.48	7.72
SE	9.87	9.92	9.93	9.87	9.82	9.73	9.64	9.21	8.60	7.74
SSE	10.21	10.38	10.36	10.22	10.13	10.01	9.84	9.37	8.72	7.89
S	11.81	11.83	11.74	11.60	11.50	11.35	11.19	10.57	9.87	8.89
SSW	13.55	13.48	13.33	13.09	12.92	12.72	12.41	11.71	10.89	9.82
SW	14.68	14.56	14.32	14.00	13.79	13.53	13.20	12.41	11.59	10.47
WSW	13.77	13.59	13.31	12.99	12.79	12.58	12.31	11.71	11.06	10.07
W	12.87	12.69	12.48	12.28	12.18	12.04	11.86	11.34	10.74	9.81
WNW	11.60	11.49	11.29	11.14	11.04	10.91	10.71	10.25	9.75	8.98
NW	10.56	10.50	10.44	10.34	10.27	10.20	10.08	9.80	9.36	8.65
NNW	10.35	10.29	10.21	10.11	10.06	9.98	9.83	9.52	9.06	8.37

Table J.6 N3 sectorwise Weibull k at various heights

Height [m] / Sector	300	250	200	160	140	120	100	60	30	10
N	2.171	2.174	2.196	2.201	2.206	2.202	2.218	2.272	2.284	2.377
NNE	2.069	2.148	2.225	2.279	2.298	2.290	2.250	2.214	2.236	2.300
NE	2.117	2.179	2.255	2.304	2.344	2.391	2.456	2.561	2.617	2.632
ENE	2.288	2.329	2.392	2.453	2.486	2.514	2.545	2.601	2.529	2.475
E	2.092	2.122	2.139	2.149	2.161	2.167	2.163	2.119	2.083	2.095
ESE	2.141	2.154	2.163	2.238	2.285	2.322	2.350	2.380	2.325	2.277
SE	2.051	2.176	2.279	2.320	2.321	2.340	2.380	2.411	2.372	2.278
SSE	2.045	2.105	2.135	2.157	2.179	2.193	2.179	2.122	2.022	2.001
S	1.903	1.978	2.044	2.080	2.101	2.111	2.121	2.090	2.057	2.044
SSW	1.951	2.014	2.091	2.144	2.162	2.172	2.162	2.140	2.094	2.115
SW	2.195	2.282	2.371	2.416	2.439	2.431	2.424	2.391	2.402	2.460
WSW	2.155	2.218	2.268	2.294	2.296	2.299	2.291	2.281	2.310	2.369
W	2.139	2.158	2.163	2.160	2.159	2.152	2.132	2.102	2.108	2.158
WNW	2.014	2.042	2.054	2.066	2.074	2.066	2.060	2.060	2.085	2.161
NW	1.991	2.015	2.043	2.045	2.045	2.048	2.040	2.060	2.084	2.155
NNW	2.047	2.059	2.074	2.080	2.085	2.084	2.078	2.099	2.122	2.191

J.4 N4_Beta2 sectorwise Weibull parameters

Table J.7 N4 sectorwise Weibull A at various heights

Height [m] Sector	300	250	200	160	140	120	100	60	30	10
N	9.77	9.82	9.80	9.72	9.70	9.63	9.51	9.13	8.69	8.03
NNE	8.99	8.97	8.93	8.90	8.86	8.80	8.68	8.38	7.95	7.34
NE	9.14	9.18	9.25	9.27	9.25	9.22	9.18	8.94	8.46	7.74
ENE	10.06	10.18	10.24	10.14	10.10	10.01	9.89	9.45	8.85	8.03
E	10.69	10.71	10.68	10.65	10.62	10.51	10.33	9.73	9.12	8.30
ESE	10.09	10.18	10.15	10.02	9.91	9.75	9.56	9.09	8.55	7.81
SE	9.86	9.75	9.74	9.69	9.66	9.60	9.51	9.06	8.52	7.74
SSE	10.21	10.34	10.30	10.16	10.10	9.99	9.86	9.45	8.89	8.05
S	12.02	11.98	11.83	11.70	11.59	11.47	11.29	10.72	10.02	9.06
SSW	13.65	13.54	13.41	13.17	13.01	12.79	12.53	11.86	11.11	10.01
SW	14.81	14.64	14.38	14.04	13.85	13.60	13.29	12.53	11.70	10.56
WSW	13.79	13.59	13.29	13.00	12.82	12.63	12.37	11.74	11.09	10.09
W	12.98	12.80	12.60	12.40	12.29	12.17	12.01	11.55	10.93	9.99
WNW	11.66	11.51	11.29	11.11	11.00	10.88	10.68	10.22	9.74	8.95
NW	10.67	10.60	10.49	10.38	10.34	10.27	10.16	9.86	9.38	8.66
NNW	10.48	10.40	10.35	10.25	10.19	10.11	9.98	9.62	9.16	8.45

Table J.8 N4 sectorwise Weibull k at various heights

Height [m] Sector	300	250	200	160	140	120	100	60	30	10
N	2.184	2.213	2.250	2.265	2.287	2.301	2.314	2.336	2.364	2.442
NNE	2.108	2.172	2.214	2.262	2.271	2.278	2.283	2.276	2.289	2.337
NE	2.146	2.168	2.217	2.262	2.282	2.292	2.314	2.359	2.410	2.456
ENE	2.192	2.232	2.261	2.274	2.290	2.318	2.348	2.409	2.420	2.421
E	2.163	2.185	2.220	2.247	2.255	2.263	2.258	2.226	2.203	2.200
ESE	2.146	2.182	2.195	2.227	2.252	2.267	2.280	2.325	2.307	2.300
SE	1.996	2.030	2.092	2.128	2.137	2.144	2.191	2.224	2.232	2.240
SSE	1.999	2.023	2.047	2.071	2.092	2.116	2.132	2.147	2.119	2.112
S	1.944	1.987	2.018	2.058	2.077	2.109	2.129	2.141	2.128	2.142
SSW	1.985	2.025	2.103	2.163	2.191	2.210	2.230	2.243	2.246	2.272
SW	2.212	2.274	2.336	2.371	2.391	2.396	2.402	2.401	2.402	2.451
WSW	2.160	2.203	2.246	2.279	2.294	2.305	2.315	2.306	2.318	2.378
W	2.158	2.178	2.180	2.179	2.180	2.182	2.180	2.182	2.190	2.246
WNW	2.063	2.075	2.082	2.099	2.102	2.105	2.109	2.129	2.158	2.219
NW	2.098	2.113	2.119	2.124	2.132	2.138	2.134	2.135	2.145	2.214
NNW	2.132	2.139	2.162	2.166	2.167	2.166	2.176	2.198	2.220	2.284

J.5 N5_Gamma1 sectorwise Weibull parameters

Table J.9 N5 sectorwise Weibull A at various heights

Height [m] / Sector	300	250	200	160	140	120	100	60	30	10
N	9.73	9.77	9.75	9.66	9.62	9.56	9.44	9.10	8.67	8.03
NNE	8.81	8.80	8.74	8.71	8.68	8.61	8.53	8.26	7.84	7.25
NE	9.08	9.16	9.26	9.25	9.24	9.21	9.16	8.96	8.50	7.78
ENE	10.01	10.06	10.07	10.00	9.97	9.89	9.80	9.36	8.74	7.93
E	10.55	10.58	10.52	10.47	10.45	10.37	10.22	9.73	9.14	8.35
ESE	10.19	10.19	10.18	10.07	9.96	9.82	9.66	9.17	8.65	7.90
SE	9.85	9.88	9.80	9.71	9.70	9.61	9.52	9.09	8.50	7.72
SSE	10.26	10.34	10.33	10.27	10.19	10.08	9.93	9.45	8.90	8.09
S	12.01	11.95	11.83	11.67	11.56	11.42	11.25	10.71	10.05	9.11
SSW	13.65	13.55	13.35	13.10	12.93	12.72	12.46	11.81	11.04	9.97
SW	14.70	14.51	14.25	13.90	13.70	13.45	13.14	12.39	11.57	10.44
WSW	13.74	13.54	13.23	12.91	12.73	12.56	12.32	11.73	11.06	10.08
W	12.97	12.77	12.57	12.41	12.31	12.17	11.97	11.49	10.88	9.95
WNW	11.60	11.46	11.26	11.07	10.96	10.86	10.71	10.30	9.78	9.00
NW	10.72	10.62	10.50	10.41	10.35	10.27	10.16	9.86	9.39	8.67
NNW	10.50	10.43	10.34	10.24	10.19	10.12	10.01	9.68	9.20	8.50

Table J.10 N5 sectorwise Weibull k at various heights

Height [m] / Sector	300	250	200	160	140	120	100	60	30	10
N	2.228	2.245	2.276	2.289	2.312	2.329	2.341	2.352	2.398	2.484
NNE	2.090	2.148	2.199	2.237	2.254	2.251	2.264	2.276	2.294	2.345
NE	2.144	2.184	2.259	2.289	2.304	2.322	2.345	2.403	2.465	2.516
ENE	2.191	2.210	2.223	2.265	2.291	2.319	2.346	2.420	2.423	2.434
E	2.154	2.183	2.203	2.219	2.231	2.247	2.256	2.252	2.238	2.245
ESE	2.163	2.179	2.221	2.277	2.303	2.320	2.334	2.342	2.346	2.339
SE	2.009	2.087	2.147	2.178	2.189	2.205	2.240	2.270	2.252	2.242
SSE	2.009	2.017	2.041	2.085	2.108	2.135	2.141	2.126	2.116	2.116
S	1.947	1.983	2.026	2.064	2.079	2.095	2.121	2.143	2.148	2.165
SSW	1.982	2.032	2.086	2.142	2.170	2.190	2.205	2.228	2.227	2.258
SW	2.192	2.249	2.323	2.359	2.373	2.376	2.379	2.379	2.391	2.442
WSW	2.152	2.195	2.232	2.250	2.268	2.287	2.301	2.307	2.328	2.391
W	2.140	2.152	2.158	2.168	2.171	2.171	2.158	2.154	2.166	2.222
WNW	2.066	2.084	2.099	2.112	2.114	2.121	2.128	2.158	2.188	2.255
NW	2.100	2.115	2.119	2.127	2.129	2.128	2.131	2.137	2.156	2.221
NNW	2.151	2.161	2.172	2.176	2.178	2.182	2.188	2.213	2.234	2.305

J.6 N6_Gamma2 sectorwise Weibull parameters

Table J.11 N6 sectorwise Weibull A at various heights

Height [m] / Sector	300	250	200	160	140	120	100	60	30	10
N	9.80	9.84	9.82	9.75	9.74	9.68	9.57	9.19	8.75	8.10
NNE	8.90	8.87	8.82	8.77	8.73	8.68	8.60	8.31	7.91	7.31
NE	9.06	9.12	9.20	9.21	9.20	9.16	9.12	8.86	8.41	7.72
ENE	9.98	10.12	10.17	10.10	10.05	9.97	9.87	9.45	8.82	7.99
E	10.63	10.63	10.61	10.58	10.56	10.47	10.28	9.70	9.13	8.32
ESE	10.25	10.29	10.28	10.15	10.04	9.92	9.78	9.27	8.72	7.96
SE	9.82	9.75	9.70	9.62	9.61	9.50	9.42	8.98	8.42	7.66
SSE	10.18	10.33	10.35	10.27	10.19	10.10	9.94	9.50	8.94	8.10
S	11.98	11.93	11.83	11.69	11.60	11.46	11.25	10.65	9.97	9.02
SSW	13.60	13.51	13.34	13.09	12.92	12.70	12.45	11.75	10.99	9.91
SW	14.73	14.55	14.31	13.97	13.77	13.51	13.21	12.47	11.66	10.53
WSW	13.80	13.59	13.29	12.99	12.80	12.63	12.37	11.72	11.04	10.05
W	13.05	12.88	12.66	12.47	12.35	12.22	12.03	11.54	10.92	9.99
WNW	11.64	11.47	11.26	11.08	11.00	10.88	10.72	10.23	9.74	8.95
NW	10.73	10.66	10.55	10.43	10.36	10.28	10.18	9.89	9.43	8.70
NNW	10.58	10.48	10.41	10.32	10.25	10.19	10.07	9.71	9.25	8.54

Table J.12 N6 sectorwise Weibull k at various heights

Height [m] / Sector	300	250	200	160	140	120	100	60	30	10
N	2.224	2.252	2.282	2.306	2.330	2.345	2.365	2.394	2.416	2.499
NNE	2.108	2.161	2.204	2.236	2.253	2.263	2.276	2.274	2.299	2.350
NE	2.143	2.178	2.230	2.272	2.296	2.308	2.335	2.371	2.416	2.468
ENE	2.173	2.211	2.256	2.292	2.314	2.341	2.363	2.427	2.439	2.452
E	2.143	2.156	2.178	2.201	2.214	2.224	2.230	2.227	2.213	2.211
ESE	2.172	2.180	2.202	2.232	2.252	2.287	2.318	2.327	2.321	2.310
SE	1.978	2.040	2.090	2.110	2.119	2.132	2.164	2.210	2.201	2.212
SSE	1.982	2.013	2.043	2.081	2.108	2.139	2.148	2.163	2.146	2.136
S	1.937	1.977	2.023	2.073	2.098	2.114	2.129	2.140	2.142	2.156
SSW	1.980	2.030	2.095	2.150	2.176	2.195	2.214	2.223	2.227	2.256
SW	2.189	2.246	2.317	2.363	2.380	2.379	2.386	2.398	2.408	2.464
WSW	2.177	2.225	2.262	2.282	2.293	2.310	2.325	2.317	2.330	2.389
W	2.157	2.177	2.180	2.186	2.188	2.191	2.178	2.183	2.189	2.248
WNW	2.079	2.086	2.101	2.116	2.129	2.136	2.146	2.156	2.186	2.251
NW	2.110	2.139	2.145	2.140	2.137	2.139	2.141	2.147	2.167	2.230
NNW	2.155	2.150	2.168	2.181	2.178	2.184	2.185	2.215	2.244	2.316

Appendix K Climate Change Analysis

K.1 Model evaluation

Parameters used in the model evaluation are detailed in the subsequent paragraphs.

Overlap percentage (OP)

Although traditionally most of the analyses evaluate the skill of climate models in terms of means and standard deviations (see next sections), the approach does not allow to understand how the data is distributed. Indeed, a good simulation of the mean does not ensure that the main features of the data, generally shown by the data distribution – for example extreme values, are satisfactorily captured by the models [65], [80]. Besides, a metric based on mean values alone can mask biases or systematic errors that would be observable at daily scale. A metric to compare probability density functions (PDFs) of modelled and in-situ dataset is defined here.

This metric called Overlap Percentage (OP thereafter) is applied within several scientific papers evaluating the reliability of climate models to simulate the future climate [64], [65], [67]–[70], [77], [80]. This criterion is also an approach used in the weather forecasting field to assess whether the reanalysis show good representation of the observed climate or not, for example.

OP allows to identify the percentage of overlapping between measured and modelled PDFs of wind. This metric is computed for each climate simulation. This comparison is based on the representation of the probabilities which is sensitive to the ranges (bins) used. The bin size used in this report for the wind speed is 1 m/s.

The OP is calculated as follows:

$$OP = \sum_{i=1}^{N} minimum(Z_m, Z_0) \times 100$$

where N refer to the number of bins used to calculate PDFs, Z_m and Z_0 are the probability of values in a given bin from the model and the reference dataset respectively. A model perfectly reproducing the reference dataset makes both PDFs coincident with an OP equal to 100%.

Percentage of error (EP)

Mean wind speed of each model $(\bar{V}_{M_i})$ is computed with the standard deviation (σ_{M_i}) and then compared with the mean wind speed $(\bar{V}_{in-situ})$ and standard deviation $(\sigma_{in-situ})$ of the reference. Comparing the mean and standard deviation with the reference is probably the most common practice to evaluate the models [64], [65]. The percentage of error (EP) between modelled and in-situ dataset is calculated for each model M_i:

$$EP_{M_i} = 100 \times \frac{\bar{V}_{M_i} - \bar{V}_{in-situ}}{\bar{V}_{ref}}$$

where $\bar{V}_{M_i}$ refers to the mean wind speed of the model i, $\bar{V}_{in-situ}$ the mean wind speed of the in-situ dataset and $\bar{V}_{ref}$ to a reference value that is calculated as the average between measured and modelled means.

$$\bar{V}_{ref} = \frac{\bar{V}_{M_i} + \bar{V}_{in-situ}}{2}$$

Considering the multi-model approach, EP is calculated over all the models to compute the root mean square error (RMSE) and the bias of EP through the following equations.

$$EP_{RMSE} = \sqrt{\frac{1}{N}\sum_{i=1}^{N}\left(EP_{M_i}\right)^2}$$

$$EP_{Bias} = \frac{1}{N}\sum_{i=1}^{N} EP_{M_i}$$

where N refers to the total number of models.

EP is a criterion embodying the percentage of error of a model in reproducing the past climate statistic compared to the reference dataset. This criterion is only based on the mean wind speed thus not representative for all the features of the time series. However, this is a first step to compare errors over different models and observe whether some series are significantly different or not. In addition, this metric has been used in several studies assessing the quality of climate models [64], [77], [80] thus it is possible to compare the results with the literature. The RMSE (Bias) measures the deviation (raw difference) of the EP for a given location (only one location is studied in this project). When these criteria are used on a single location with several models, they observe the difference between the models to represent a single sample of the past climate. A low value of these criteria (the best expected result is zero) would suggest that the models head towards a similar representation of the past climate in term of mean [64], [80].

K.2 Multi-model ensemble

The following standard statistics for wind speed are computed for each time scale of interest (monthly, seasonally, yearly): bias, percentual bias (bias%), mean absolute error (MAE), mean absolute percentage error (MAPE), root mean square error (RMSE), standard deviation (σ), normalized standard deviation (σ_n) and the Yule-Kendall skewness measure (YK) [19].

1) $Bias = \frac{1}{M}\sum_{k=1}^{M}(p_k - o_k)$

2) $Bias\% = \frac{\sum_{k=1}^{M}(p_k - o_k)}{\sum_{k=1}^{M} o_k} \times 100$

3) $MAE = \frac{1}{M}\sum_{k=1}^{M}|p_k - o_k|$

4) $MAPE = \frac{\sum_{k=1}^{M}|p_k - o_k|}{\sum_{k=1}^{M} o_k} \times 100$

5) $RMSE = \sqrt{\frac{1}{M}\sum_{k=1}^{M}(p_k - o_k)^2}$

$$6)\quad \sigma = \sqrt{\frac{1}{M}\sum_{k=1}^{M}(p_k - \bar{p})^2} \text{ or } \sqrt{\frac{1}{M}\sum_{k=1}^{M}(o_k - \bar{o})^2}$$

$$7)\quad \sigma_n = \frac{\sigma_p}{\sigma_o} = \frac{\sqrt{\frac{1}{M}\sum_{k=1}^{M}(p_k-\bar{p})^2}}{\sqrt{\frac{1}{M}\sum_{k=1}^{M}(o_k-\bar{o})^2}}$$

Where M represents the number of observed/modelled events (at a monthly scale the number of modelled events is twelve), o_k the observed values, p_k the projected values from models, $\bar{o}$ the mean of observed values, $\bar{p}$ the mean of projected values and P the percentiles. These metrics were used by climate experts to study the distributions of atmospheric variables [80]. The best expected result for these metrics is zero (except for the normalized standard deviation which is one). Following the work from Soares et al. [80], the Yule-Kendall skewness measure (YK) is also computed based on the PDFs such as the OP metric (best expected result is zero).

$$8)\quad YK = \left[\frac{(P_{95}-P_{50})-(P_{50}-P_5)}{(P_{90}-P_5)}\right]_{model} - \left[\frac{(P_{95}-P_{50})-(P_{50}-P_5)}{(P_{90}-P_5)}\right]_{obs}$$

Following the literature, a ranking of the EURO-CORDEX simulations is performed to select the best models and build multi-model ensembles based on individual model's quality. The following steps describe the approach to build the multi-model ensembles:

1) For metrics in which the best expected result is zero (bias, bias%, MAE, MAPE, RMSE, Yule-Kendall) the inverse of its absolute value is calculated.
2) The previous method is also applied to the normalized standard deviation after its subtraction by 1, since the best expected value is 1.
3) The individual model ranks, for each metric, are obtained by dividing each value by the sum of all values from all the models. In this way, the sum of the ranks is equal to 1.
4) Weights are constructed by either averaging the ranks of all the metrics or by multiplying the ranks.
5) Finally, each weight is divided by the sum of the weights so that the total sum of the weights is equal to 1.

This procedure allows the construction of two multi-model ensembles: the ENS_WM where the ranks are averaged, and the ENS_WP where the ranks are multiplied. Another ensemble, is considered, ENS_F, in which the weights are equal for all models (in our case 1/7). Then, for all ensembles, the mean measures are averaged, and the PDFs are obtained by the following equation:

$$PDF(x) = \sum_{i=1}^{N} PDF(x)_i \times wg_i$$

Where N is the number of models and wg_i the model weight.

K.3 Analysis datasets

K.3.1 Climate scenarios

Climate scenarios (or climate projections) are representations of various possible future states of the climate system, based on numerical model simulations. These models are tools to describe the complex processes and interactions affecting the climate system, which also use the climate forcing induced by the anthropogenic activities. Different factors of anthropogenic activities can be considered like the socio-economic, technological, or environmental activities. They are characterized inside the climate models with an equivalent level of greenhouse gases forcing and consider the land use and

land cover [63]. Since the future evolution of the anthropogenic activities cannot be known, different scenarios describing different socioeconomic choices are produced, thus driving future possible emission pathways. When a simulation is performed, the chosen emission scenario provides forcing information for the climate model which result in a physical reaction with the climate system to reach the anthropogenic forcing. This is shown in Figure K.1 [79].

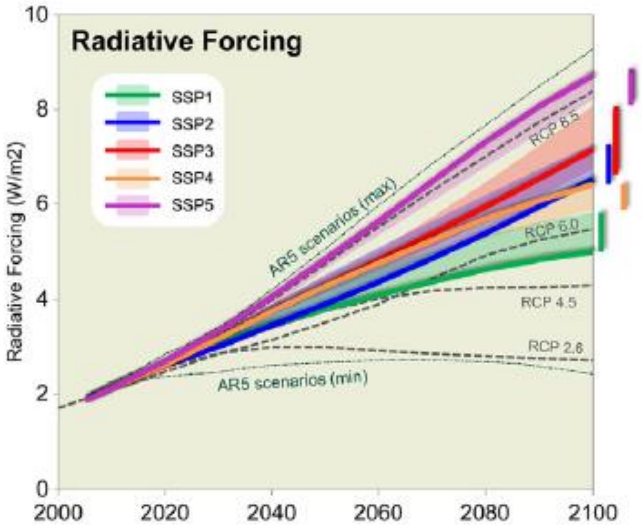

Figure K.1 Latest climate scenarios used within the AR6 of IPCC

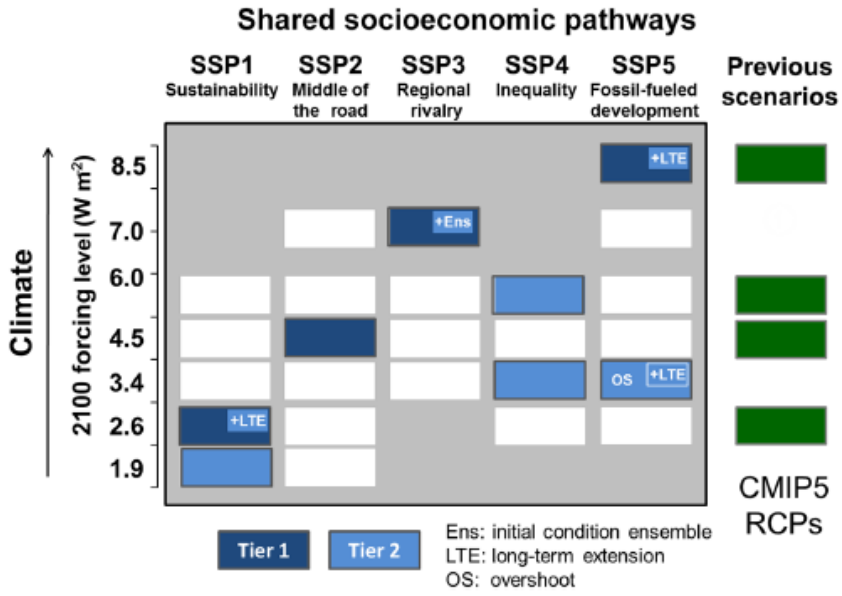

Figure K.2 Equivalence between SSP and RCP scenarios

In contrast to the SRES or SSP scenarios, RCP scenarios do not specify socioeconomic scenarios but assumes pathways that target different radiative forcing for 2100. There are four specific RCP scenarios which are RCP2.6, RCP4.5, RCP6.0 and RCP8.5 with the figure in each name that stand for the radiative forcing assumed by the scenario for 2100. For example, RCP8.5 assumes an increase of 8.5 Wm^{-2} by the end of the century, relative to pre-industrial conditions [89], [90]. SSP scenarios are the latest scenarios developed by the ScenarioMIP and include five socio-economic alternatives, from SSP1 to SSP5, which lead to different levels of radiative forcing (Figure K.2) [79]. More information related to the ScenarioMIP project, RCPs scenarios and SSPs scenarios can be respectively found in O'Neill et al., van Vuuren et al. and Riahi et al. [89]–[91].

K.3.2 CORDEX dataset

The climate simulations carried out in this study are retrieved from the Climate Data Store, the open-source climate database developed within the European Copernicus project.

The Coordinated Regional Climate Downscaling Experiment (CORDEX) is a project launched by the World Climate Research Project (WCRP) which uses as forcings the state-of-the-art GCMs from CMIP5 (the fifth phase of CMIP) to provide climate projections for different regions worldwide through a dynamical downscaling approach with a wide range of RCMs. CORDEX is therefore supposed to provide a significant improvement in the representation of regional climates given its increased spatial resolution [63], [67]–[70], [73], [77].

Impact applications, such as energy models, need high-resolution information on various climate variables on different scale such as the scale of a wind farm, scale that are not available from the usual GCMs. Downscaling is a method providing climate information on a finer scale than the GCMs, based on the assumption that there is a link between large-scale and local climates [92]. There are two types of downscaling approaches: dynamical downscaling which is based on RCMs forced by a GCMs and statical downscaling which develops statistical relationships between large-scale atmospheric variables from GCMs and observed local-scale variables of interest. The two downscaling approaches are complementary as each downscaling technique has its own strengths and weaknesses. Busuioc highlights for example that the combination of different downscaling techniques maximizes the performance and reliability of the data for climate change studies [92]. The interested reader can refer to the following references for more information on the different downscaling technique widely used in climate sciences and impact study [63], [66], [73], [74], [92].

CORDEX has therefore developed a downscaling technique to provide high-resolution data for the climate scientists. All the CORDEX datasets used within this study are obtained by a dynamical downscaling technique provided by RCMs. The RCMs used to process this downscaling technique are also called limited area models (LAMs). They use the GCMs as boundary conditions to provide detailed climate information at an inner scale, typically 10 to 50km. The quality of a simulation depends on the quality of the RCM and the GCM involved in this simulation. However, according to CORDEX experts, the RCMs used in CORDEX simulation have a stronger impact on local variables than their driving GCMs, although it also depends on the location and the season [63].

CORDEX activities are divided in regions worldwide, called domains. This study has been made on Europe, thus the European EURO-CORDEX domain was used. This domain has the highest temporal (up to hourly) and spatial (up to 0.11°x0.11° grid) resolution, comparing with other CORDEX domains. Shows the domain covered by the EURO-CORDEX simulations.

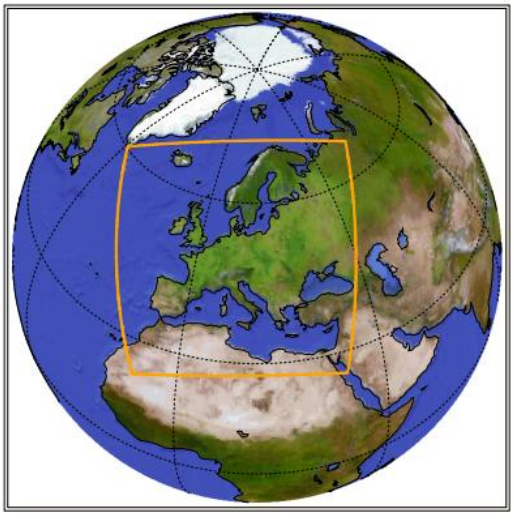

Figure K.3 EURO-CORDEX domain

K.4 Future wind resource analysis – additional figures

Table K.1 Results for ENS_F under the RCP 4.5 scenario

Parameter	Historical	Near-future	Mid-future	Far-future
Δ Wind speed	100.00%	**99.54%**	99.53%	99.27%
Δ P99 wind speed	100.00%	**100.12%**	99.98%	100.19%
Δ WPD	100.00%	**99.00%**	98.85%	98.40%
Δ OT	100.00%	**99.88%**	99.97%	99.96%
Δ AEP	100.00%	**98.83%**	98.87%	98.11%

Table K.2 Results for ENS_WM under the RCP 4.5 scenario

Parameter	Historical	Near-future	Mid-future	Far-future
Δ Wind speed	100.00%	**99.49%**	99.34%	99.23%
Δ P99 wind speed	100.00%	**99.79%**	99.92%	99.81%
Δ WPD	100.00%	**98.24%**	98.31%	97.88%
Δ OT	100.00%	**100.01%**	100.01%	100.04%
Δ AEP	100.00%	**98.89%**	98.50%	98.13%

Table K.3 Results for ENS_WP under the RCP 4.5 scenario

Parameter	Historical	Near-future	Mid-future	Far-future
Δ Wind speed	100.00%	**99.40%**	98.90%	99.46%
Δ P99 wind speed	100.00%	**99.05%**	99.90%	99.30%
Δ WPD	100.00%	**96.28%**	97.31%	97.65%
Δ OT	100.00%	**100.30%**	100.01%	100.19%
Δ AEP	100.00%	**99.03%**	97.46%	98.61%

Table K.4 Weibull parameters for the three ensembles under the RCP4.5 scenario at 10 metres height

Parameter		Historical	Near-future	Mid-future	Far-future
ENS F	**shape k**	2.43	2.41	2.42	2.18
	scale A	9.90	9.80	9.86	8.81
ENS WM	**shape k**	2.43	2.42	2.40	2.18
	scale A	9.72	9.58	9.57	8.56
ENS WP	**shape k**	2.44	2.44	2.36	2.40
	scale A	9.42	9.14	9.09	9.15

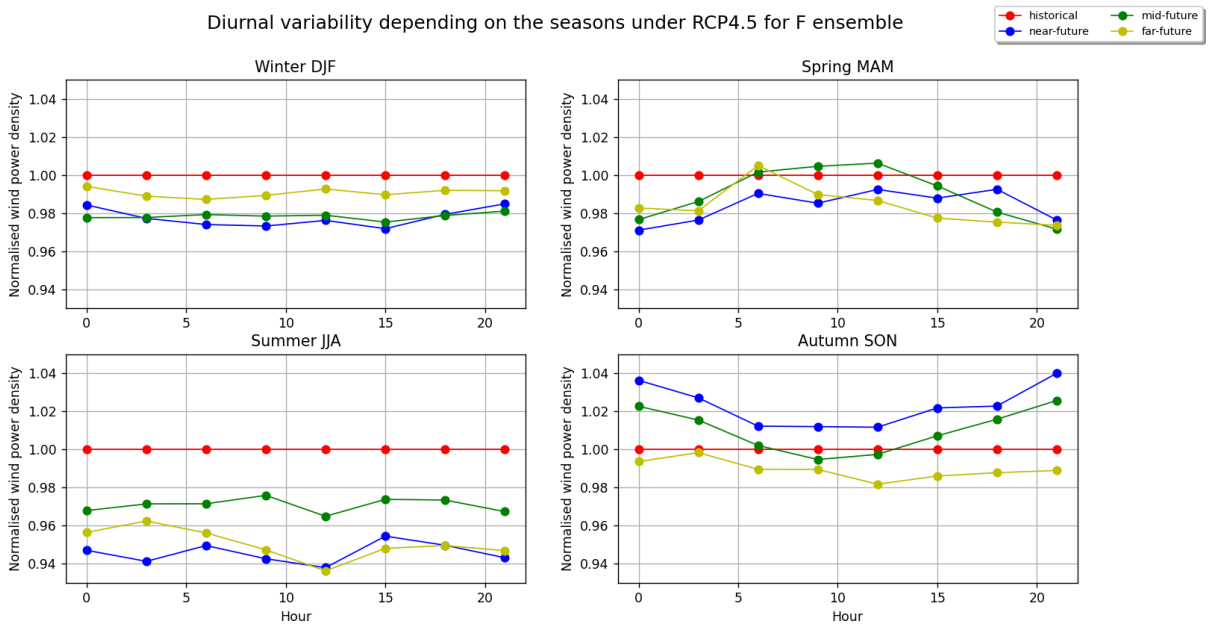

Figure K.4 **Seasonal diurnal variability of the wind resource under RCP4.5 scenario for the ensemble F**

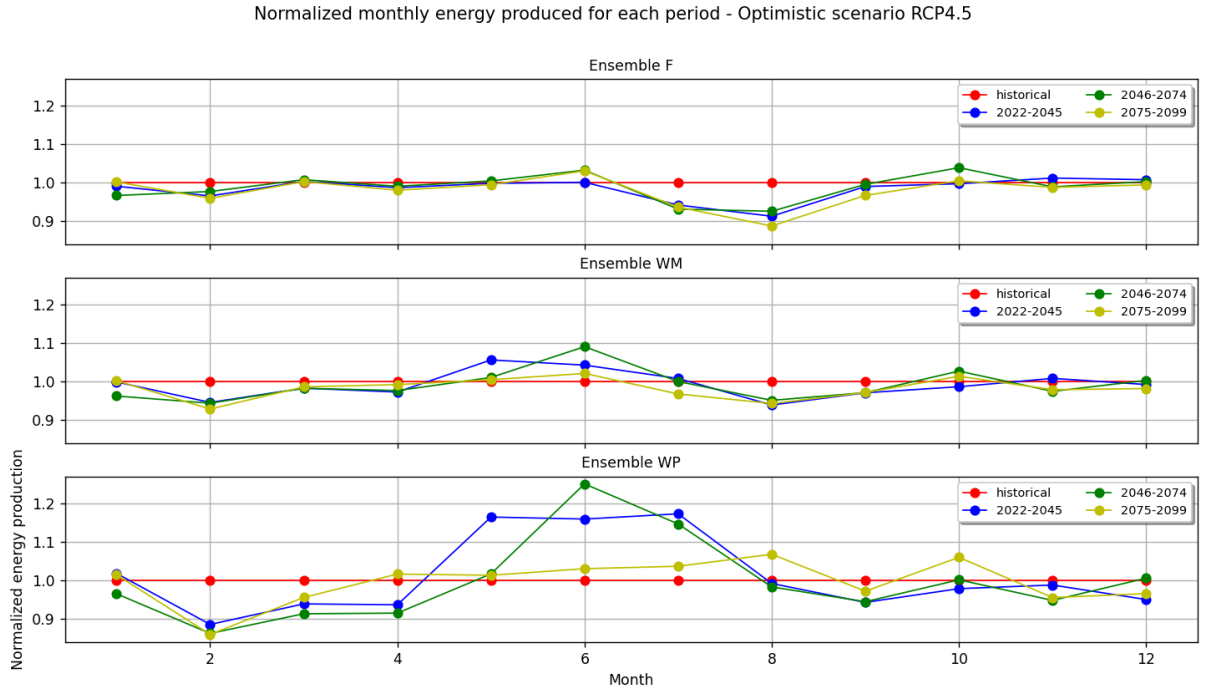

Figure K.5 **Projected changes of energy production for each month and all ensembles under RCP4.5 scenario**

Table K.5 **Percentage of values above WTG's cut-out for each climate model under RCP4.5 scenario**

Parameter	M1	M2	M3	M4	M5	M6	M7
Historical	1.14%	1.50%	1.46%	1.74%	2.88%	1.73%	1.01%
Near-future	1.11%	1.49%	1.51%	1.86%	3.11%	1.80%	0.91%
Mid-future	1.02%	1.50%	1.27%	1.80%	3.00%	1.85%	1.00%
Far-future	1.09%	1.37%	1.49%	1.79%	3.12%	1.92%	0.94%

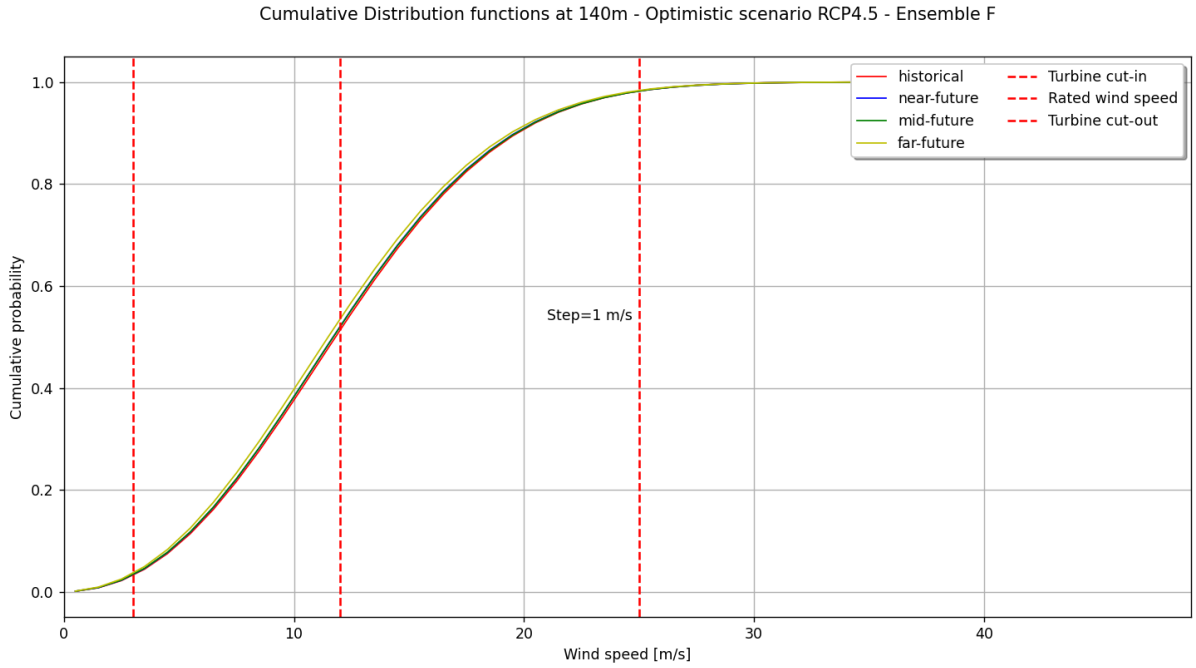

Figure K.6 CDF at hub height for the ensemble F under RCP4.5

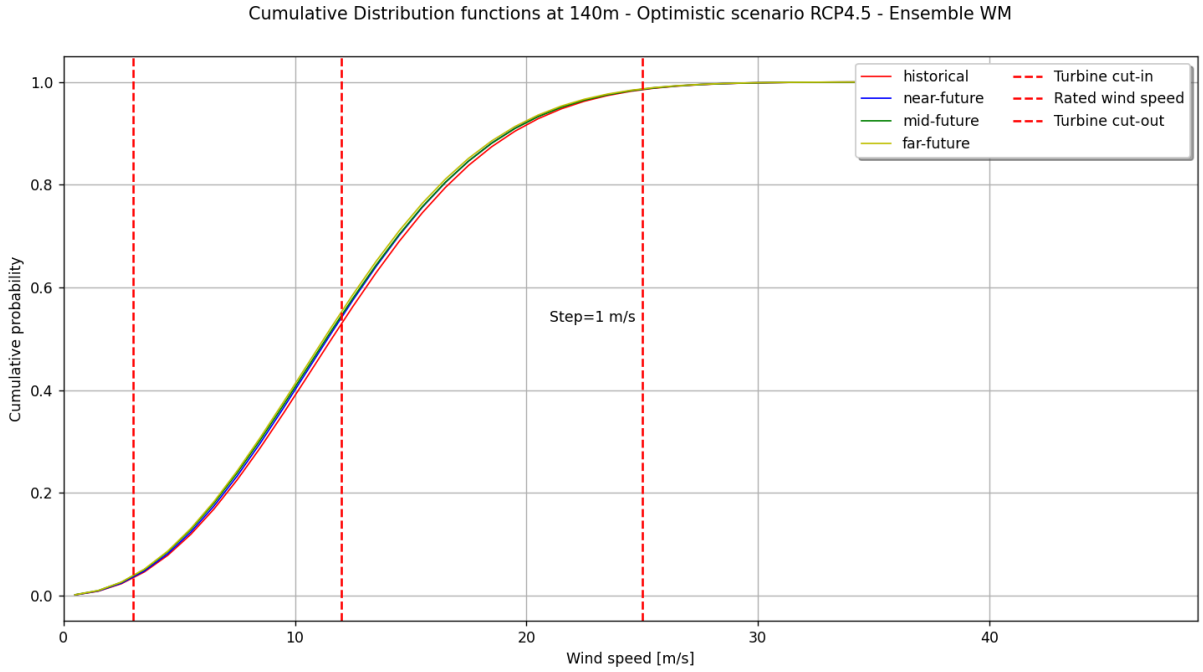

Figure K.7 CDF at hub height for the ensemble WM under RCP4.5

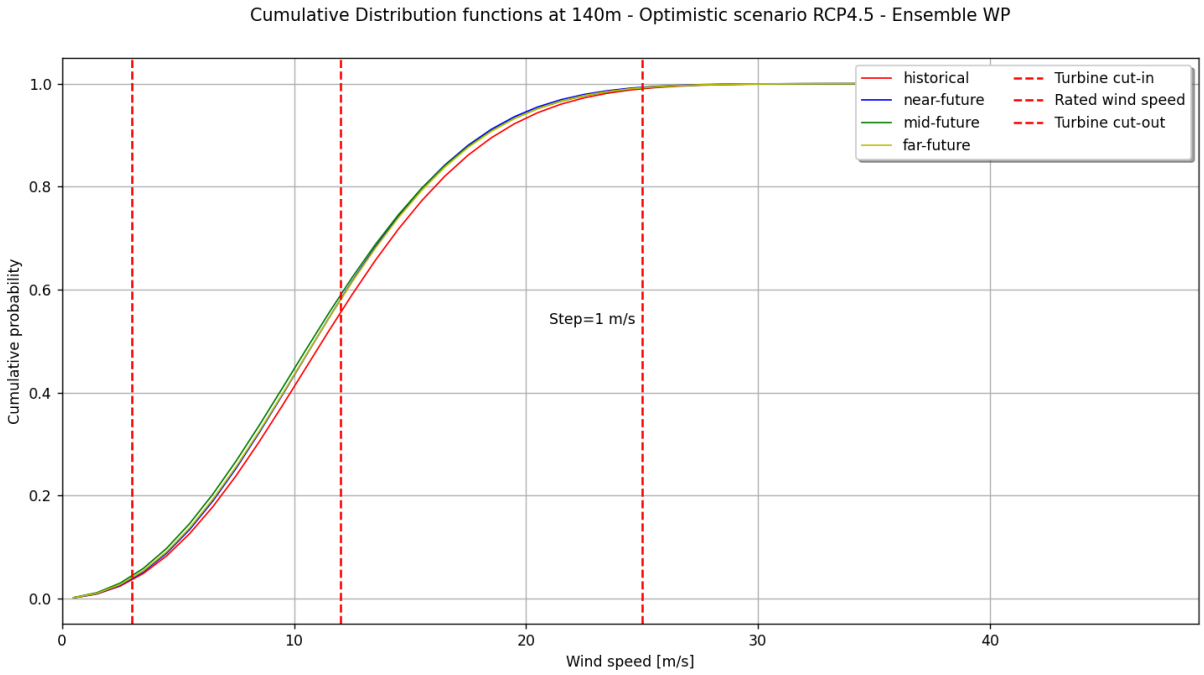

Figure K.8 CDF at hub height for the ensemble WP under RCP4.5

This investigation was carried out by a consortium, consisting of DHI (main lead), OWC, Arcvera, ProPlanEn, Innosea and C2wind, commissioned by RVO, an agency of the Ministry of Economic Affairs and Climate Policy.

The information in this document is valid at the time of publishing (see month/year). Updates will be published on the website https://offshorewind.rvo.nl, at the relevant sitemap, General Information, submap Revision Log and Q&A. In the Revision Log is indicated which versions are the latest and what the changes are in relation to previous versions. The documents can be found at the relevant sites, indicated in the List of all reports and deliverables.

Contacts
Netherlands Enterprise Agency (RVO)
Graadt van Roggenweg 200 | 3531 AH | Utrecht
P.O. Box 8242 | 3503 RE | Utrecht
www.rvo.nl / https://english.rvo.nl

Netherlands Enterprise Agency (RVO) | November 2023